8-9-2014

ROLE OF CHRONIC INFLAMMATION ON LIVER FUNCTION DURING CACHEXIA PROGRESSION IN THE APC$^{MIN/+}$ MOUSE MODEL

Aditi Narsale
University of South Carolina - Columbia

ROLE OF CHRONIC INFLAMMATION ON LIVER FUNCTION DURING CACHEXIA PROGRESSION IN THE *APC*$^{MIN/+}$ MOUSE MODEL

by

Aditi Narsale

Bachelor of Science,
Mumbai University, 2005

Master of Science,
Mumbai University, 2007

Submitted in Partial Fulfillment of the Requirements

For the Degree of Doctor of Philosophy in

Exercise Science

The Norman J. Arnold School of Public Health

University of South Carolina

2014

Accepted by:

James Carson, Major Professor

Raja Fayad, Committee Member

Larry Durstine, Committee Member

Marjorette Pena, Committee Member

Lacy Ford, Vice Provost and Dean of Graduate Studies

DEDICATION

To my family

`

ABSTRACT

Cachexia is a multifactorial syndrome that manifests during the advanced stage of chronic diseases and is characterized by a progressive loss of body mass sustained by underlying inflammation. The *Apc*$^{Min/+}$ mouse is an established model of cachexia that exhibits a gradual loss of body mass correlating with increasing tumor burden and plasma IL – 6 levels. Moreover it also mimics other secondary characteristics observed in cachectic patients like splenomegaly, elevated plasma endotoxin levels, gut barrier dysfunction, hypogonadism and an overall hypermetabolic state. Liver controls the energy metabolism in the body by regulating glucose and lipid metabolism, glycogen storage, filtration of toxins from the portal blood, secretion of essential plasma protein like albumin and other acute phase proteins. As cachexia development results from sustained elevated energy demands, it can be speculated that liver might play a role in development of cachexia progression. The purpose of this study thus was to examine the role of chronic inflammation on liver function in the *Apc*$^{Min/+}$ model of cancer cachexia. For this study liver function was studied using hepatic metabolic markers, inflammatory markers and markers of anabolic signaling. Specific Aim1 examined if liver function is altered with cachexia progression in the *Apc*$^{Min/+}$ mouse. We report that liver function is altered by upregulation ER stress protein in non – cachectic mice. Non – cachectic mice also upregulate liver STAT- 3 phosphorylation along and suppression of liver gluconeogenic enzyme transcription.

`

However, the liver maintains stores glycogen stores, Akt/mTOR/S6 signaling expression and does not initiate a NF - κB or acute phase dependent immune response. However cachexia progression, sustains activation of ER stress pathways leading to inhibition of protein synthesis marker S6 phosphorylation and activation of the apoptotic marker CHOP. Severely cachectic mice exhibit inhibition of proteins associated with cell survival like Akt, ERK and NF - κB. This is accompanied by an elevated STAT-3 and haptaglobin levels, but suppressed JNK expression in the liver. However, histological analysis of the cachectic liver shows a regenerative and inflammatory pathology post injury. Severely cachectic mice also show depleted liver glycogen reserves along with upregulation of enzymes regulating gluconeogeneic and glycolytic process. These results indicate the cachexia progression leads to liver dysfunction by elevating transcription of enzymes regulating glucose flux, acute phase protein response and inhibition of anabolic and survival pathways in the IL – 6 dependent $Apc^{Min/+}$ model. Specific Aim 2 was targeted towards the inhibition of IL – 6 signaling to attenuate chronic inflammation in the $Apc^{Min/+}$ mouse. Aim 2.1 used pyrrolidine dithiocarbamate (PDTC), an antioxidant and inhibitor for NF-κB and STAT-3 phosphorylation, to suppress systemic inhibition in the $Apc^{Min/+}$ mouse. PDTC administration attenuated body weight loss, fat loss and liver lipid content in the cachectic mouse. Though PDTC did not attenuate total polyp counts, it did suppress polyp growth by suppressing total number of large polyps in the intestine. There was an attenuation of liver metabolic markers by suppression of PEPCK mRNA and sparing of liver glycogen stores in the PDTC treated mice. Interestingly though liver PFK expression increased further with PDTC administration in the cachectic $Apc^{Min/+.}$ Attenuation of metabolic markers was seen independent of liver inflammation as liver STAT- 3 and haptaglobin

`

expression remained elevated post treatment. PDTC treatment also did not affect the dysregulated Akt/mTOR/S6 signaling in the liver. Aim 2.2 used the trans – IL – 6 inhibitor sFcgp130 to attenuate liver dysfunction in the $Apc^{Min/+}$. sFcgp130 administration attenuated body weight loss and fat loss in the severely cachectic $Apc^{Min/+}$ mouse, but had no effect on total lean mass. sFcgp130 treated $Apc^{Min/+}$ did not attenuate percentage of large tumors in the intestine but it did inhibit plasma IL – 6 levels. However, liver STAT-3 and haptaglobin levels were sustained independent of IL – 6. There was an increase in the mRNA levels of hepatic PEPCK indicating an upregulation of liver gluconeogenic response which could be possible reason for depleted liver glycogen stores in the sFcgp130 treated mice. Inhibition of trans – signaling did not attenuate hepatic suppression of the Akt, NF-κB or S6 phosphorylation. Overall these results indicate that liver dysfunction during cachexia progression is independent of the IL – 6 signaling pathway. Aim 3 of this study examined the role of antibiotic treatment on cachexia progression in the $Apc^{Min/+}$ mouse. The purpose of the antibiotic treatment was to suppress endotoxin mediated inflammatory response in the severely cachectic $Apc^{Min/+}$ mouse. Administration of the antibiotic treatment attenuated splenomegaly and mesenteric lymph node swelling the $Apc^{Min/+}$ mouse, indicating suppression of immune proliferation. However, this suppression of immune cell proliferation was not sufficient to suppress hepatic STAT-3 or haptaglobin levels. Surprisingly even plasma endotoxin levels remained elevated in the antibiotic treated $Apc^{Min/+}$ mouse. Antibiotic treatment had no effect of hepatic NF-κB/MMP2 or Akt/S6 pathway. Overall these results demonstrate that liver dysfunction is observed with cachexia progression in the $Apc^{Min/+}$ mouse and this dysfunction is independent of plasma IL – 6 and factors affecting splenomegaly.

`

TABLE OF CONTENTS

`

LIST OF TABLES

`

LIST OF FIGURES

`

List of Abbreviations

AIDS ..... Acquired Immunodeficiency Syndrome

AKT ..... Protein Kinase B

B6 ..... C57BL/6

BW ..... Body Weight

C – 26 ..... C26 colon adenocarcinoma

COPD ..... Chronic Obstructive Pulmonary Disorder

EDL ..... Extensor Digitorum Longus

ELISA ..... Enzyme Linked Immunosorbent Assay

ERK ..... Extracelluar signal regulated kinases

GAPDH ..... Glyceraldehyde 3-phosphate dehydrogenase

Gas/Gastroc ..... Gastrocnemius

IL – 6 ..... Interleukin 6

JNK ..... c-Jun N-terminal Kinases

LLC ..... Lewis Lung Cell Carcinoma

LPS ..... Lipopolysaccharide

MAPK ..... Mitogen Activated Protein Kinases

MCP – 1 ..... Macrophage Chemotactic Protein 1

Min ..... $Apc^{Min/+}$

`

mTOR ..... mechanistic target of rapamycin

NF – κB..... Nuclear factor Kappa B

Nor/Amp .....Norfloxacin/Ampicillin

PBS ..... Phosphate buffered saline

PDTC .....Pyrrolidine dithiocarbamate

PEPCK .....Phosphoenolpyruvate carboxylase

PFK ..... Phosphofructokinase

Pla .....Plantaris

PVDF .....Polyvinylidene fluoride

Quad..... Quadriceps

RNA .....Ribonucleic acid

SDS .....Sodium dodecyl sulfate

sFcgp130 ..... soluble glycoprotein 130 fusion protein

sIL-6R ..... soluble IL-6 receptor

Skmgp130KO ..... skeletal muscle gp130 knockout mice

Skm-gp130r..... skeletal muscle specific glycoprotein 130r knockout

Sol ..... Soleus

STAT3.....Signal Transducer and Activator of Transcription 3

TA .....Tibialis Anterior

TBST..... Tris Buffered Saline and Tween

TNFα.....Tumor Necrosis Factor alpha

`

V..... Volts

WT ..... Wild Type

`

CHAPTER 1

INTRODUCTION AND LITERATURE REVIEW

1.1 INTRODUCTION

Cachexia is a multifactorial syndrome diagnosed in patients with chronic diseases like AIDS, COPD and cancer via the unintentional loss of body weight[1-3]. No treatment is currently approved for cachexia due to its multifactorial nature caused by various chronic diseases[3, 4]. However, chronic systemic inflammation persists in all patients that exhibit cachectic symptoms even though the components of the immune response may vary. Recent studies with cancer cachexia have shown that degradation of muscle and fat loss during cachexia is a result of a hypermetabolic state that needs a constant supply of energy[5]. This energy is obtained from the breakdown of fat and muscle in the body and used to feed the elevated basal metabolic rate (due to the tumors) and a highly stimulated immune system (activated to fight the chronic disease)[1, 5]. Cachectic patients thus also display an enlargement of the visceral organs like spleen and liver, the organs responsible for immune activation and maintenance of homeostasis respectively[6,7]. The observed hepatosplenomegaly not only induces a hypermetabolic state but also leads to activation of the innate acute phase response by the liver. Production of acute phase proteins is extremely energy expensive but is essential to sustain the hypermetabolic state by breaking down muscle for metabolic and immune functions[8]. Many anti – inflammatory therapies being tested in clinical trials study its effect on attenuation of fat mass, and endpoint variable,

`

but not many studies look at the effect of these treatments on the liver, which governs the metabolic responses in the body. There is clearly a need to study liver function during cachexia progression and develop therapies that can act on the liver to alleviate its hypermetabolic and immune responses and to see if these responses would translate into attenuation of muscle and fat loss with cachexia.

The liver is known to perform over 500 physiological functions including the regulation of glucose and lipid mechanism, glycogen storage, production of acute phase proteins, cholesterol synthesis, filtration of toxins from the portal blood and metabolism of drugs in the system amongst other things[9, 10]. It also has a tremendous capacity to regenerate and making it one of the more resistant organs in the body. However a disruption of liver function due to diseases like cancer or chronic alcohol intake can lead to a severe systemic effect with fatigue, disruption in glucose homeostasis, bilirubin accumulation, anemia etc[11]. Hepatocarcinomas lead to hepatocyte proliferation, hepatic inflammation and liver fibrosis compromising liver functions, making it one of the diseases with lowest prognosis rates. If not detected and treated in time the disease is usually fatal in 3 - 6 months[12, 13]. Hepatocellular carcinomas are hence aggressively researched for therapies. However, very little is known about the secondary effect of tumor on liver function. A few recent studies have established that liver plays a role in cachexia development alteration in lipid metabolism and production of acute phase proteins due the systemic effect of tumor related pro – inflammatory and hypermetabolic response on the liver[14, 15]. However, these studies are performed in severely cachectic mice that already have substantial weight loss. The model system used for the studies is the C26 model of cancer cachexia that develops an IL – 6 dependent cachexia over a period of two weeks, limiting our ability to track the liver

`

during cachexia progression[15, 16]. Establishing a time course in the liver with cachexia progression is very important for development of effective therapies with minimal side effects.

The *Apc*$^{Min/+}$ model of cancer cachexia is an excellent model to develop cachexia progression as it transitions from a cancerous but non – cachectic state (12 weeks of age) to a pre – cachectic state (14 weeks of age) to a severely cachectic stage (20 weeks of age). The *Apc*$^{Min/+}$ a colon cancer mouse model that mimics a various symptoms of cancer cachexia like gradual and progressive weight loss, splenomegaly, endotoxemia and an IL-6 dependent loss of muscle mass[16, 17]. The *Apc*$^{Min/+}$ mouse starts tumor development at around 4 -5 week of age and have the maximum tumor number by the time it becomes 12 week old. However cachexia development is only seen once the tumors start to grow in size post 12 weeks of ages and by 20 weeks of age the *Apc*$^{Min/+}$ intestine is riddled with approximately 80 tumors and a majority of these being more than 2mm in diameter[16]. The mouse elicits a systemic response to fight these tumors as we see elevated levels of plasma MCP – 1 in the mice starting 12 weeks of age and an increase in plasma IL – 6 levels from 14 weeks of age. Plasma concentration of both these cytokines is highly elevated in the severely cachectic mice[18, 19]. Loss of fat and muscle mass is induced by IL – 6 with muscle mass loss corresponding to serum IL – 6 in the male *Apc*$^{Min/+}$ mouse.

Inhibition of plasma IL – 6 by administration of an IL – 6 receptor antibody is attenuates muscle mass loss by inhibiting pathways inhibition of protein degradation in the *Apc*$^{Min/+}$ muscle. This effect of IL – 6 on muscle wasting was duplicated in the skm – gp130 knockout mouse that attenuated muscle mass loss in the LLC model of cancer cachexia[20]. However muscle protein content is the ratio of protein synthesis to degradation and loss of

`

protein synthesis rates are suppressed in the cachectic muscle and are not attenuated by inhibition of IL – 6. However recent studies have shown that cachexia induced muscle protein synthesis inhibition can be attenuated by administration of PDTC, a drug known to inhibit both NF – kB and STAT - 3[21]. Exercise and anti – inflammatory supplements like quercetin have also been implicated in inhibition of muscle mass loss, but interestingly quercetin combined with exercise is detrimental to the cachectic $Apc^{Min/+}$ mice (unpublished data) [22]. Suppression of immune response through inhibitors can thus interact with and impede normal physiological responses. There is therefore a need to specifically inhibit the detrimental immune response and preserve the beneficial arm of any immune response. For example, complete inhibition of the acute phase response protein in the liver, or systemic inhibition of haptaglobin in the $Apc^{Min/+}$ mouse are detrimental and reduce survival rate[23]. Similarly complete inhibition of IL – 6 responses could blunt the beneficial effects of exercise on cachexia progression. Hence apart from establishing a time course for cachexia development this study also look at specific anti – inflammatory therapies that can modulate specific arms of the immune response mounted in the $Apc^{Min/+}$ mouse in response to tumor growth. We thus use the IL – 6 trans – signaling inhibitor, a fusion protein for the soluble IL – 6 receptor (sFcgp130), that can specifically block the pro – inflammatory effects of IL – 6 leaving the classical signaling intact and an antibiotic treatment[24], to block the endotoxin mediated arm of systemic inflammation in the severely cachectic $Apc^{Min/+}$ mouse.

IL – 6 is classically defined as pleiotropic cytokine, which can have both beneficial and detrimental effects. Acute IL – 6 exposure is been shown to be beneficial for regeneration and growth. However, chronic IL – 6 is often detrimental leading to muscle mass and fat

`

loss and insulin resistance with cachexia. Fortunately it recent studies have shown that the source of chronic IL – 6 as seen during cachexia as well as its functional mechanism is different from the classical IL – 6 signaling that aids regeneration and growth[25, 26]. Classical IL – 6 signaling as seen with exercise attached to the IL – 6 receptor in the muscle and dimerizes with its beta receptor gp130 to initiate signaling. IL – 6 trans – signaling however is secreted by immune cells or the tumor microenvironment and can bind to the soluble IL – 6 receptor present in the serum. The soluble IL – 6 – IL 6R complex and then bind to any organ as the beta receptor gp130 is expressed ubiquitously in all tissues. The soluble IL – 6 signaling thus has more far reaching effects on organs that are generally protected for IL – 6. The trans – signaling response has been recently identified as the pro – inflammatory arm for IL – 6 signaling and the liver is known to be a major contributor of the soluble IL – 6 receptor in response to systemic inflammation. It would thus be interesting to study if inhibition of the trans – IL – 6 signaling attenuates liver function with cachexia progression[27].

Cachectic patients sometimes show elevated levels of plasma endotoxin during the late stages of cancer. $Apc^{Min/+}$ mouse mimics this effect as severely cachectic mice show elevated levels of plasma endotoxin corresponding with an increase in gut permeability, implicating gut bacteria as the primary cause of elevated endotoxin levels[16]. We thus hypothesize that increased gut permeability in the $Apc^{Min/+}$ mouse allows the bacterial endotoxin to leak in to the body cavity and plasma. Upregulation of endotoxin in a chronically elevated system is detrimental and hence we hypothesize that inhibition of this adjunct arm of inflammation in the $Apc^{Min/+}$, could improve survival and attenuate cachexia

`

progression. Furthermore, the liver is implicated in endotoxin clearance from the blood and but if elevated endotoxin levels in the $Apc^{Min/+}$ blood alter liver function is not known.

In summary, the liver governs the metabolic process in the body and can also be implicated in sustenance of the muscle degrading acute phase response in a hypermetabolic state. But it is unclear if liver signaling in terms of metabolic, inflammatory and protein synthesis is affected during cachexia progression in the $Apc^{Min/+}$ mouse. Further it is known that inhibition of partial inhibition of plasma IL-6 attenuates muscle mass loss in the $Apc^{Min/+}$ by inhibition of muscle degradation pathways, without rescuing the protein synthesis arm. However, PDTC, a global inhibitor of STAT-3 and NF – kB is known to attenuate muscle protein synthesis inhibition in the skeletal muscle but its effect on liver function are yet unknown[21]. It would thus be interesting to see if PDTC can enhance liver protein turnover in the $Apc^{Min/+}$ mouse, and if this would be beneficial in a chronic hypermetabolic state. Lastly, this study recognizes the complexity and necessity of immune response elicited during cachexia and aims to target specific arms of the immune system to manage the exacerbated immune response seen the severely cachectic $Apc^{Min/+}$ mice. We thus propose to inhibit IL – 6 trans signaling and endotoxin signaling during cachexia progression and study its role on liver function in the cachectic mouse. $Apc^{Min/+}$ mice will be introduced into the study during their non – cachectic state and monitored till sacrifice at the severely cachectic stage. Drug targeting the IL – 6 pathway would administered in moderately cachectic mice, while antibiotic administration for the endotoxin levels will be initiated in non – cachectic mice. Apart from liver function markers, body weight loss, muscle/fat mass loss and attenuation of visceral organ hypertrophy will be used as evaluate the effective of the treatment.

`

1.2 REVIEW OF LITERATURE

1.2.1 WHAT IS CACHEXIA?

Derived from the Greek word kachexia (kakos = bad; hexis = state), Cachexia in terms of modern medicinal terms stands for a malnourished state leading to the loss of peripheral organs like fat and muscle and hypertrophy of internal organs like spleen and the liver accompanied by edema. Cachexia is often the result of chronic inflammatory diseases like cancer, AIDS, congestive heart failure, end stage renal failure, rheumatoid arthritis, COPD and other conditions[28].

Chronic diseases like cancer at their end stage are often "autocannibalistic" meaning that the underlying condition, in this case the tumor, leads to the degradation of peripheral organs like fat and skeletal muscle. The tumor also elicits systemic effects on visceral organs with increased gut permeability[16], splenomegaly, and hepatomegaly [6, 29], hyperlipidemia, enlarged mesenteric lymph nodes[16] and an ever increasing tumor burden. Hypertrophy of the visceral organs along with increasing tumor burden creates a hypermetabolic state in the patient. The Resting Energy Expenditure (REE) in cancer patients is heightened both because of the tumor and the hypertrophy of the visceral organs[6]. Peripheral tissues like adipose and skeletal muscle are broken down to sustain this hypermetabolic state, often compounded by a simultaneous onset of anorexia[30].

Cancer cachexia is a multifactorial syndrome, which can be attributed to a sustained immune response mounted by the body to fight of the tumor. But as the tumor burden increases, the sustained chronic inflammation alters signaling in all the major tissues in the body, creating a secondary condition that is as detrimental as the disease itself. Chronic

`

inflammation manifests itself in the form of a sustained inflammatory response with elevated levels of cytokines like IL – 6, TNF – alpha, IL -1 beta, MCP-1, IFN-γ , IL -12 These cytokines trigger an inflammatory cascade which affects function in most organs, like the synthesis of acute phase response proteins in the liver and skeletal muscle, suppression of protein synthesis in skeletal muscle while upregulation of the same in the liver, activation and proliferation of immune cells in the spleen, protein degradation in the muscle, suppression of appetite by manipulation of leptin levels etc[2, 31].

Therapeutic interventions like hypercaloric diets, exercise and treatment with anti – inflammatory antibodies often curtail protein degradation, but rarely rescue protein synthesis. Treatment of with anabolic steroids or growth hormones have been shown to redirect the excess amino acid to the protein synthesis pathway, but this is often increases the mortality rate in cachexia patients as it cuts off the amino acid supply to immune response leading to proliferation of the underlying disease. [28]

With the advent of modern medicine to treat cancer, efforts need to be made to develop potent techniques to deal with cachexia, to ensure better quality of life for cancer patients and survivors. Modern advances like chemotherapy, radiation and surgery combined with immunotherapies and nutrition supplementation, have significantly prolonged life expectancy of cancer patients. Surviving with cancer is now a reality, but is often riddled with poor quality of life due to severe loss of fat and skeletal muscle in patients. Treating cachexia ensures quality of life and thus it's essential to explore therapies that could treat this multifactorial systemic syndrome.

`

1.2. II LIVER DURING CACHEXIA

Liver is located in the abdominal cavity, below the diaphragm on the right hand side. The liver is has two main lobes, which are further divided into thousands of lobules. The liver receives blood supply from two main sources: 1) hepatic artery, 2) hepatic portal vein. Filtering of this blood is one of the main functions of the liver. The liver at any given point contains 13% of the body's blood supply. The liver thus functions as a major detoxifying organ of the body and is the first site to intercept pathogen in the blood[15, 32]. The liver is lined with resident macrophages known as Kupffer cells, which get activated in response to an invading pathogen, preparing the liver and the body to fight infection, mainly by the production of cytokines, reactive oxygen species, acute phase proteins and their secretion in the blood stream. Acute phase proteins activate the immune system to fight the invading pathogens. The liver also produces bile which helps breakdown of ingested fats in the small intestine for further utilization by the body. The liver also monitors the breakdown of various drugs and nutrients in the body. It also converts excess glucose blood glucose to glycogen for further storage, and stores iron by processing hemoglobin and regulate blood clotting by production of prothrombin.

During cancer cachexia, the tumors are known to proliferate under pro – inflammatory conditions leading to wasting seen as a result of skeletal muscle and fat degradation. This loss of muscle indicates a hypermetabolic state, wherein the energy demands of the body at rest increase tremendously. One of the reasons for this increase in energy demand can be attributed to gluconeogenesis by activation of Cori's cycle. The tumor is known to produce lactic acid which accumulates in the blood stream. As the liver filters all the blood from the body, lactic acid from the blood is converted to glucose by the

`

consumption of ATP, via the Cori's cycle. Chronic activation of Cori's cycle could thus alter liver function during cachexia[33],[15]. Chronic inflammation is also responsible for production of acute phase proteins (APR) in the liver. Production of APPs requires free amino acid for its production. APPs are known to trigger and sustain an inflammatory response in the by activation of STAT3 and further activation of muscle and fat. The liver thus is a site of extensive energy consumption during cancer cachexia, by aiding the sustenance of inefficient energy cycles[8].

1.2.III LIVER AND THE PRO – INFLAMMATORY CYTOKINE IL-6

IL – 6 is a pleiotropic cytokine and is implicated in a number of process like muscle growth and hypertrophy[34], muscle atrophy [35, 36], activation and stimulation of immune system[37], production of acute phase proteins[8], wound healing and repair, gut permeability[16], insulin resistance[38], dysregulation of serum triglyceride levels[15] etc. IL – 6 signaling proceeds via the IL – 6 receptor (IL – 6R) which upon binding to IL – 6 binds and dimerizes the gp130 receptor. The gp130 receptor is an ubiquitously expressed secondary receptor that can be activated by the entire IL – 6 family of cytokines like LIF, OSM, CNTF and also by IL -27 [39, 40]. Once activated the receptor can activate Janus Kinase (JAKs) finally leading to the activation of STAT3. STAT 3 activation by IL – 6 can lead to the secretion of acute phase proteins in both skeletal muscle and liver. STAT3 is measured as a marker for inflammation and inhibition of STAT 3 can lower inflammation [36, 37],[8]. Other than STAT 3, IL – 6 signaling is also known to activate ERK via gp130 dependent activation of the Ras, Raf pathway. Gp130 via activation of Gab1 can also activate PI3K leading to activation of mTOR and Akt[41]. The varied functions of IL – 6 thus can be explained by the multiple signaling cascades it can activate, but there also exists

`

evidence that acute IL – 6 stimulation is beneficial as opposed to chronic IL – 6 stimulation which proves to be atrophic[36]. The pleiotropic nature of IL – 6 can also be attributed to the classical vs trans IL – 6 response. IL – 6 receptor is not abundantly found on all tissues, but cases of infection and chronic diseases like cancer, the IL – 6 receptor on immune cells and visceral tissues like liver is shed into the blood stream as soluble IL – 6 receptor (sIL-6R). sIL -6 receptor can bind IL – 6 in plasma and then aid the dimerization of the gp130 receptor on various cell types. As discussed earlier, since the gp130 receptor is ubiquitously expressed, the extent of IL – 6 signaling is broadened and are more damaging. Recent studies conducted on the topic indicate that the IL – 6 trans-signaling is pro – inflammatory in nature, while the classical signaling pathway is anti – inflammatory in nature. Due to such pleiotropic nature, the effects of IL – 6 in cancer, cachexia and on liver have proved to be often contradictory and interesting.

Secretion of IL – 6 in response to infection or tumor is known to elicit an Acute Phase Response by the liver. Chronic IL – 6 stimulation suppresses the production of normal liver proteins like albumin and increase the production of acute phase proteins alike α2 – macroglobulin, fibrinogen, haptaglobin etc. [31]Acute phase proteins are additive to systemic inflammation seen with chronic inflammatory diseases[8].

IL – 6 can upregulate muscle expression of TLR 4 and TLR2 leading to insulin resistance in human subjects[42]. Insulin resistance is observed in severely cachectic *Apc* $^{Min/+}$ mice and is attributed to inhibition of glucose uptake by skeletal muscle, as the body tries to divert the energy source to more metabolic active tissues like the liver, spleen and tumor itself. Indeed IL – 6 stimulation of hepatocytes has been shown to upregulate glucose production in hepatocytes[43]. IL – 6 treatment is mice can also reduce lipid to glycogen

`

ratio, indicating either increased lipid synthesis or depleted glycogen content. Considering lipolysis is elevated during cachexia, IL – 6 induced cachexia probably increases lipolysis rather than depleting glycogen levels[44]. Level of mitochondrial transport protein CPT I and II is downregulated with cancer. But the data on IL – 6 induced insulin resistance is contradictory with certain studies indicating that IL 6 null mice are similar to WT mice in terms of plasma glucose, NEFA, and hepatic glycogen content.[43]

IL – 6 is known to have differential atrophic effects in males and females with female mice being obtuse to the deleterious effects of muscle wasting as compared to men. This is often attributed to the presence of to the interaction of estrogen receptor and the cytochrome P 450 system in the liver [45, 46].

Various inhibitor, overexpression and knockout studies have been performed in both humans and mice to understand the role of IL – 6 during chronic diseases. Inhibition of chronic inflammatory response has been shown to be beneficial in at the signaling levels, with IL – 6 RA attenuating muscle weight loss by inhibition of muscle protein degradation in the $Apc^{Min/+}$ mouse, but complete loss of IL 6 from the Min mouse lead to insulin resistance in older mice. IL – 6 has been shown to have both pro –survival and inflammatory effects due to activation of Akt and STAT3 respectively. Also its role in liver appears to be crucial with production of acute phase proteins, interaction with the CYP system to affect sex dependent atrophic signaling and its influence on hepatic glucose and lipid metabolism. Thus it would be interesting to study the effect of IL – 6 on liver function with cachexia progression.

`

1.2.IV ENDOTOXIN AND LIVER:

Endotoxin levels in the blood are often seen to be increased in a number of diseases like alcoholic liver disease, sepsis, or CCL4 induced liver injury. LPS can further exacerbate the injury by stimulation of Kupffer cells in the liver. Increased endotoxin levels can be leaked into the plasma from the gut due to increased gut permeability and via the portal vein. Kupffer cells in the liver are derived from the monocytic lineage and express the TLR 4 receptor on the surface[47] . Activation of Kupffer cells is known to trigger ROS production leading to liver injury of the parenchymal cells. Alcohol induced liver injury, leads to a hypermetabolic state with increased oxygen consumption but decreased liver glucose production due to activation of PGE2 by Kupffer cells. Endotoxin due to increased gut permeability has been shown to be the primary cause for Kupffer cell activation in the liver. Pretreatment with antibiotics protects endotoxin induced Kupffer cell activation and prevents liver injury[48]. Destruction of Kupffer cells by $GdCL_3$ treatment protects the hepatocyte from LPS induced injury. Kupffer cells thus play a paradoxical role in LPS regulation in the liver. They are responsible for clearing out the endotoxin entering the liver via the portal blood supply, but high concentration of LPS in the blood leads to ROS production in these cells leading to liver injury[49]. Increased endotoxin levels and endotoxin mediated injury can inhibit bile secretion [50] and affect hepatocyte blood flow .

TLR 4 levels are increased in response to endotoxin on hepatic tissue. All cell types in the liver – hepatocytes, Kupffer cells and Hepatic Stellate cells are known to express TLR 4 but in very low levels as compared to other tissue. The expression of TLR 4 on these tissues rises with exposure to LPS, sensitizing the liver to foreign antigens. The co – receptors for TLR 4 like MD2 and CD14 follow a similar trend as TLR 4. Once activated

`

TLR 4 can lead to activation of NF – kB and AP – 1 downstream. LPS uptake via hepatocytes leads to secretion of acute phase proteins, but this upregulation is weak as compared to acute phase production by IL – 6. LPS can also lead to secretion of IL – 6, MCP – 1 and TNF – alpha in hepatocytes. Kupffer cells are the resident macrophages in the liver and activation of Kupffer cells leads to production of IL -6, TNF – alpha, IL – 1 and ROS. Kupffer cells are the primary mediators of pro – inflammatory cytokine and chemokine secretion following LPS exposure. Activation of Kupffer cell can also prime the allogenic T cell activation. HSC are known to be sensitive to very low levels of LPS leading to secretion of a host of pro – inflammatory cytokines and chemokines. TLR4 dependent activation of HSC activates pro – survival signals making these cells apoptosis resistant. As HSC are ECM producing cells in the liver, this can lead to liver fibrosis[51].

1.2.v Antibiotic Treatment and Liver:

Antibiotics are known for their ability to specifically target bacterial proliferation and survival. All antibiotics use specific enzymes and proteins synthesized by the bacterial genome. This allows for specific targeting of the infectious species and spares the mammalian cells. Most antibiotics thus can target a group of similar bacterial species. Broadly, bacteria can be divided in to 2 classes – Gram positive and Gram negative bacteria. The Gram negative bacteria have a thick coat of LPS surrounding their outer cell wall. Endotoxin or LPS is toxic when found introduced into the blood stream and elicits a host of pro – inflammatory processes. Gram positive bacteria on the other hand have a very thin or no LPS coat around them. Such bacteria are still toxic and are recognized as foreign antigen by the body. Antibiotics have been developed against both gram positive and gram negative bacteria, while some antibiotics can target both gram positive and gram negative

`

bacteria together. Polymyxin is an example of an antibiotic targeting the Gram negative bacteria. Polymyxin structure allows it to bind to the Lipid A component of LPS and puncturing holes in the bacterial cell wall [52, 53]. Norfloxacin on the other hand targets both Gram positive and Gram negative bacteria by inhibiting the activity of DNA replication enzyme DNA gyrase and is known as a broad-spectrum antibiotic[54]. Ampicillin is another common example of broad spectrum antibiotic and acts a substrate for one of the key cell wall forming enzyme in bacteria.

Antibiotic treatment to prevent alcohol induced liver injury have proved to be beneficial in lowering serum markers of liver injury like AST and in restoring oxygen tension on surface of the liver[55]. Antibiotic treatment is also known to suppress Kupffer cell activation the phenotype responsible for inducing liver injury[51].

`

CHAPTER 2

ROLE OF CACHEXIA PROGRESSION DURING LIVER FUNCTION IN THE *Apc*$^{Min/+}$ MICE[1]

[1] Narsale, A. et. al. 2014 Role of Cachexia Progression During Liver Function in the *Apc*$^{Min/+}$ mice, To be submitted to Biochemica et Biophysica Acta

`

2.1 ABSTRACT

The *Apc*$^{Min/+}$ (Min) mouse exhibits a gradual loss of muscle and fat due to a chronic inflammatory, hypermetabolic and energy deficient state. Since liver governs the systemic energy demands by regulating glucose and lipid metabolism, it is likely that liver function is altered in the Min during cancer and subsequent cachexia progression (CP). The purpose of this study was to examine if cancer and the progression of cachexia alters liver function related to ER stress, inflammatory, metabolic and protein synthesis signaling. The effect of cancer without weight loss was examined in wild type and weight stable Min. CP was examined in weight-stable, pre-cachectic and severely cachectic *Min mice*. Livers were analyzed for morphology, glycogen content, ER stress, inflammation, and metabolic changes. Cancer induced the expression of ER stress markers Bip and IRE-1α, and inflammatory intermediate p-STAT3. While gluconeogenic enzyme PEPCKmRNA expression was suppressed by cancer, there was no effect on glycogen content or Akt/mTOR signaling. CP depleted liver glycogen content and increased mRNA expression of glycolytic enzyme PFK and gluconeogenic enzyme PEPCK. Related to inflammation, CP further increased STAT3 phosphorylation but suppressed p-65 and JNK activation. Interestingly, CP suppressed upstream ER Stress markers Bip and IRE-1 α, while upregulating the downstream target CHOP. Cachectic mice exhibit a dysregulation of protein synthesis signaling, with an induction of p-mTOR, despite a suppression of Akt and S6 phosphorylation. Our results demonstrate liver dysfunction with CP is a result of chronic ER stress, disrupted protein synthesis signaling and suppressed hepatic inflammation in the Min mouse.

Keywords: Liver, IL – 6, acute phase response, protein synthesis, ER stress

`

2.2. INTRODUCTION

Cachexia is a wasting syndrome observed during the later stages of chronic diseases like cancer, AIDS, COPD [1], and greatly hampers quality of life in patients undergoing remission. No pharmacological treatments are currently approved for cachexia[56] primarily because of its multifactorial and systemic nature, which limits the effectiveness of a single drug or therapy. It is therefore important to study the effect of cachexia progression not only in terms of loss of body mass, evident only in advanced stages of the disease, but also on systemic events that initiate and lead to wasting. Cachectic patients, along with an evident but gradual loss fat and muscle mass, also suffer from a host of underlying ailments such as chronic systemic inflammation, insulin resistance, increased gut permeability, anemia, anorexia, splenomegaly, hypermetabolism[5, 57-61]. Interestingly, tough characterized as a wasting syndrome, the visceral organs such as heart, spleen, liver maintain mass or even hypertrophy with cachexia[1].

Liver hypertrophy seen during cachexia[57] is particularly intriguing since nutrient depletion and increased energy demands as observed during fasting[62] and infection depletes liver glycogen stores causing a decrease in liver mass[63, 64]. In fact, liver hypertrophy is speculated to contribute towards cachexia progression and severity by contributing to elevated resting energy expenditure in cancer patients [57, 65]. Liver governs the systemic metabolic rate by regulating pathways regulating glucose and fat utilization, transport, storage and breakdown. Liver is also known to produce the acute phase proteins (APPs) in response to an inflammatory stimulus that can lead to degradation of muscle into amino acids [14, 66]. Thus alteration in liver function can potentially trigger a host of ailments

`

associated with cachexia including loss of muscle mass. It would therefore be advantageous to study the role of liver in cachexia progression.

Elevated pro – inflammatory cytokines during cachexia are known to initiate lipolysis [67], muscle wasting[19] and affect glucose metabolism [17, 58]. Thus, chronic inflammation induced cachexia progression, increases metabolic demands placed by the tumors and coupled with inadequate nutrition triggers rapid wasting and alters several liver functions. The secondary effect of tumor on liver function has been recently examined and it has been shown to affect metabolic functions in terms of glucose and lipid metabolism in the liver [68]. A novel molecule TSC22D4 has been implicated in cachexia related body weight loss in the C-26 adenocarcinoma model [69]. However the effect of cachexia progression on liver function is not well understood and could impact patient survival [1, 70]. The liver is known to perform around 500 physiological functions; but since cachexia is primarily characterized by chronic inflammation, loss of body mass, altered regulation of protein turnover, metabolic disorders and elevated levels of cellular stress, liver function was defined by these markers, for the purpose of this study.

Current animal models for cachexia mimic varied subsets of cachectic conditions to study the effect of cachexia and efficacy of treatments on attenuation of muscle and fat loss in these animals. Recent studies with the C-26 tumor implant model of cachexia, have shown that cachexia induces an alteration in liver VLDL profile [69] and an induction of acute phase response (APR) in the muscle and the liver leading to muscle loss[14]. Tumor implantation models induce a rapid rate of weight loss; with mice losing close more than

`

20% of their body weight in over a one week period[71], making it difficult to study mechanisms involved in cachexia progression. The *Apc*$^{Min/+}$ mouse on the other hand, displays a gradual weight loss spanning approximately 6 weeks. While tumor development is initiated at 4 weeks of age[72], cachexia initiation is not seen until after 13 weeks of age and a severely cachectic phenotype is seen only at 18 – 20 weeks of age[59]. The gradual transition from a weight stable cancer state via a pre – cachectic to a severely cachectic state, correlates with plasma IL – 6 and total tumor burden[73], making the *Apc*$^{Min/+}$ mouse an ideal model to study cachexia progression. Increasing tumor burden corresponds to increased levels of MCP-1 and IL – 6 in the male *Apc*$^{Min/+}$ mouse [19, 59, 72, 74]. IL – 6 levels correspond to muscle mass loss in the *Apc*$^{Min/+}$ [19].

IL – 6 is also known to activate an acute phase response in the liver and muscle, leading to secretion of acute phase proteins like haptaglobin, CRP, which further exacerbates the inflammation [14, 60, 75]. Severely cachectic mice also have elevated levels of endotoxin in the serum, with increased gut permeability in the *Apc*$^{Min/+}$ [59], which can also affect liver function. The purpose of this study was to examine if cancer and the progression of cachexia alters liver function related to inflammatory, metabolic and protein synthesis signaling. We hypothesized that cachexia progression would increase liver inflammation leading to disruption in liver metabolic functions and inhibit liver protein synthesis. The effect of cancer without weight loss was examined in wild type and weight stable *Apc*$^{Min/+}$ mice. Cachexia progression was examined in weight-stable, pre-cachectic and severely cachectic *Apc*$^{Min/+}$ *mice*. Livers were analyzed for morphology, glycogen content, inflammation, and metabolic changes.

`

2.3 MATERIALS AND METHODS:

2.3. I ANIMALS:

All animal procedures were approved by the University of South Carolina's Institutional Animal Care and Use Committee. The mice were housed in a room kept at a 12:12hr light: dark cycle, with the light cycle starting at 07:00 hrs. The mice were had ad libitum access to food (standard chow – Harlan Teklad Rodent Diet, #8604) and water. 8 week old C57BL/6 and *Apc*$^{Min/+}$ mice were introduced into the study and monitored for Body weight loss, Food intake and body temperature, throughout the course of the study. Following an overnight fast, mice were sacrificed at 12 weeks (non – cachectic, N = 6), 14 weeks (pre – cachectic N = 6) and 18 – 20 weeks (severely cachectic, N=6). Comparison between the WT and non – cachectic group highlights the effect of cancer, while comparisons between the *Apc*$^{Min/+}$ groups teases out the effect of cachexia progression from effect of cancer in these mice.

2.3. II TISSUE COLLECTION:

Mice were anesthetized using the ketamine cocktail. Plasma was collected prior to tissue collection via blood draws through the retro-orbital sinus. Liver tissue was collected during the sacrifice and was snap frozen in liquid nitrogen and stored at - 80^{0}C[19]. Intestine segments were isolated, cleaned and cut into 4 equal segments of the small intestine and a segment for the colon. These were used to account for tumor burden in the cachectic *Apc* $^{Min/+}$ mice [19, 59].

`

2.3.III RNA ISOLATION/PCR:

RNA extraction, cDNA preparation and real – time PCR was performed as described previously [76]. Briefly, RNA was isolated by homogenizing the liver tissue in Trizol (Invitrogen, Cat # 15596), followed by a chloroform/isopropyl alcohol extraction. cDNA and RT-PCR assays were performed using reagents purchased from (ABI, Foster City, USA). Primers for SOCS-3[14], Haptaglobin[14], PFK[77] and PEPCK[77] primers purchased from IDT (Coralville, IA, USA). Data was analyzed using the comparative cycle threshold [Ct] method calculated by the ABI software.

2.3. IV WESTERN BLOT:

Western blots were performed as described previously [78]. Briefly, a piece of the liver was cut, weighed and placed in 10 times the volume of Muller Buffer. The tissue was homogenized in the buffer using a glass or glass homogenizer. The resultant homogenate was quantified for protein concentration using the Bradford assay. All protein samples were diluted to 3ug/µl concentration to aid equal loading on the gel. Homogenates were fractionated on SDS – PAGE acrylamide gels (6% - 15%) and transferred overnight onto a PVDF membrane. The membrane was Ponceaued following the transfer to ensure equal loading. The PVDF membrane was then probed for STAT-3, mTOR, S6, Akt, MMP-2, p-p65, GAPDH (Cell Signaling Technology, Danvers, MA, USA) gp130 and Albumin (Santa Cruz Biotechnology). A corresponding secondary antibody was used along with the chemiluminescent agent Quantum ECL (BioExpress, Kaysville, UT, USA) to visualize the protein bands. ImageJ (NIH, Bethesda, MD, USA) software was used for quantification of the integrated optical density (IOD) for Western blot bands.

`

2.3. v PERIODIC ACID SCHIFF'S (PAS) STAINING:

Glycogen was stained by using cryosections of the liver tissue and staining them with PAS stain[79]. Briefly, a small piece of liver tissue was mounted on an OCT block and sectioned at -16^{0}C. The slides were fixed in Carnoy's fixative for 10 minutes followed by 30 minute incubation in the Periodic Acid. Slides were then washed with water and exposed to Schiff's reagent for 30 minutes. The slides were counter stained with Hematoxylin, dehydrated through alcohol grades and mounted using Permount. The slides were imaged the next day using the DP70 Olympus microscope.

2.3. VI HEMATOXYLIN AND EOSIN STAINING:

A subset of severely cachectic *Apc*$^{Min/+}$ mice were perfused with 4% PFA in PBS. Liver was stored in 4% PFA overnight and transferred to a 30% sucrose solution. The perfused liver was mounted in a wax block and cut using a microtome. The sections were deprafinized and stained with Hematoxylin and Eosin stained, dehydrated using alcohol grades. Slides were mounted in the Permount media and imaged using the DP-70 camera.

2.3. VII STATISTICAL ANALYSIS:

All statistical analysis was performed using the GraphPad Prism software. A One – Way ANOVA was performed to calculate the effect of cachexia with time on the *Apc*$^{Min/+}$ mice. A Two – Way ANOVA was performed to examine the effect of genotype and treatment. Post – Hoc Analysis was performed using the Student-Newman-Keuls test. Pre-planned test were performed to determine the effect of *Apc*$^{Min/+}$ as compared to WT animals. Liver glycogen content, as determined by PAS staining, was analyzed using the non – parametric Krushal – Wallis test. Significance was set at $p<0.05$.

`

2.4 RESULTS

2.4. I TUMOR BURDEN AND BODY WEIGHT IN APCMIN/+ MICE

Our lab has worked extensively with the *Apc*$^{Min/+}$ model and time course studies with the model have established that increased tumor burden correlates to plasma IL – 6 levels, leading to a IL – 6 dependent body weight loss in these mice[73]. As previously reported, the initiation of weight loss in the *Apc*$^{Min/+}$ mouse occurs at 13 weeks of age. 12 week old *Apc*$^{Min/+}$ mice weigh 23 – 24grams which is comparable to a healthy age – matched C57BL/6 control [59]. Cachexia is initiated at 13 – 14 weeks of age with pre – cachectic mice exhibiting a small but significant, less than 5%, weight loss compared to the WT animals. 20 week *Apc*$^{Min/+}$ are severely cachectic with a loss of 20% body mass in the form of fat and muscle. Cachexia progression is can also be determined by the progressive increase in tumor size. It has been reported that, the tumor number does not increase significantly from the non – cachectic to severely – cachectic state, but there is a distinctive increase in tumor size with increase in cachexia severity [59]. Previous studies have also reported an increase in tumor diameter from the non – cachectic (<1mm diameter) to pre – cachectic (1-2mm in diameter) to severely cachectic wherein majority of the tumors are >2mm in diameter [59]. The *Apc*$^{Min/+}$ liver function is examined using these previously classified non – cachectic, pre – cachectic and severely cachectic mice.

2.4. II LIVER MORPHOLOGY DURING CACHEXIA PROGRESSION

A subset of WT, non – cachectic and severely - cachectic mice were perfused using a fixative and stained with the hematoxylin and eosin stain to determine cachexia progression leads to liver pathology. Severely cachectic mice displayed signs of mild liver injury with signs of liver regeneration, and infiltrating liver leukocytes especially in the

`

sinusoids as compared to the C57BL/6 mice. Protein expression of the mitotic marker ERK showed no significant difference during the early stages of cachexia but was inhibited in severely cachectic mice. On the other hand, the inflammatory and stress marker JNK showed no change with cachexia progression in the *Apc*$^{Min/+}$ mouse.

2.4.III LIVER ER STRESS SIGNALING WITH CANCER

ER stress signaling in the liver was examined in the WT and non – cachectic *Apc*$^{Min/+}$mice, by probing for the unfolded protein chaperone - Bip/GRP78, and the ER stress transducers IRE-1, ATF6 and PERK induced phosphorylation of eIF2α. We report that Bip/GRP78 and IRE1α was upregulated in the non – cachectic *Apc*$^{Min/+}$ mice with cancer. Moreover, ATF6 was suppressed while eIF2 and CHOP showed no change in the cancer mice with without cachexia (Figure 2).

2.4. IV LIVER GLYCOGEN CONTENT WITH CANCER

Liver glycogen content was determined using PAS staining and quantified using morphometry. Non – cachectic mice did not show any decrease in liver glycogen content with the cancer (Figure 3).

2.4. V LIVER METABOLIC AND PROTEIN SYNTHESIS SIGNALING WITH CANCER.

We examined the expression liver metabolic genes regulating glycolysis (PFK mRNA) and gluconeogenesis (PEPCK mRNA) in the non – cachectic *Apc*$^{Min/+}$. We found no effect of cancer on PFK mRNA expression (Fig 4a). However, PEPCK mRNA expression was significantly reduced by 45% with cancer (Fig 4a). Signaling intermediates regulating the protein synthesis signaling were not affected by cancer in the non – cachectic mice as measured by phosphorylation of Akt, mTOR and S6.

`

2.4. VI LIVER INFLAMMATORY SIGNALING WITH CANCER

The mRNA expression of inflammation related signaling was examined. Liver IL – 6 and TLR 4mRNA expression was not affected by cancer (data not shown), however, there was considerable variability in baseline control measurements with these genes. Liver SOCS3 mRNA expression was induced by cancer in non-cachectic mice (Fig 5A). The mRNA expression of acute phase proteins haptaglobin and serum amyloid A (SAA) was not altered by cancer (Fig 5A). Cancer increased liver STAT3 phosphorylation approximately 2-fold (Fig 5B), which coincided with a significant 20% reduction ($p=0.002$) in liver albumin protein concentration. There was a small, but significant change in liver MMP2 protein expression (Fig 5B).Cancer did not change liver gp130 protein expression, phosphorylated p65 protein expression (Fig 5B), These results demonstrate that cancer induces liver STAT3 signaling with a corresponding increase in SOCS3 mRNA expression, and a suppression of PEPCK mRNA expression.

2.4. VII LIVER ER STRESS WITH CACHEXIA PROGRESSION

To examine the effect of cancer cachexia progression we examined non-cachectic, pre-cachectic, and severely cachectic $Apc^{Min/+}$ mice. We show that cachexia progression downregulates expression of Bip/GRP78 and IRE-1α, but does not further affect the expression of ATF6p50. Expression of the apoptotic marker CHOP is severely upregulated in the severely cachectic mice coinciding with the suppression of Bip/GRP78 and IRE1α (Figure 6).

`

2.4.VIII LIVER GLYCOGEN CONTENT WITH CACHEXIA PROGRESSION

Liver glycogen content was determined using PAS staining and quantified using morphometry. Glycogen stores were severely depleted in the severely cachectic $Apc^{Min/+}$ mice as compared to the non – cachectic and the pre – cachectic mice (Figure 7).

2.4.IX LIVER METABOLIC AND PROTEIN SYNTHESIS SIGNALING WITH CACHEXIA PROGRESSION

We examined the expression of liver mRNA's with cachexia progression in the $Apc^{Min/+}$ mice (Fig 8A). The progression of cachexia induced liver PFK mRNA expression 11-fold and PEPCK mRNA expression 2-fold (Fig 8A). No difference in either PFK or PEPCK gene expression was observed early in cachexia, as pre – cachectic mice were not different from non – cachectic mice. A significant inhibition of Akt and S6 phosphorylation was observed in the liver with cachexia progression. Interestingly, mTOR phosphorylation was upregulated both in the pre – cachectic and severely cachectic $Apc^{Min/+}$ mice (Fig 8C).

2.4.X LIVER INFLAMMATORY SIGNALING WITH CACHEXIA PROGRESSION

IL – 6 and TLR4 mRNA expression was not different from the non – cachectic $Apc^{Min/+}$ mice, but severely cachectic $Apc^{Min/+}$ mice significantly upregulated TLR4 mRNA expression in liver as compared to the WT mice (data not shown). SOCS3 expression did not increase further with cachexia progression (Fig 9a). Acute phase gene expression for haptaglobin was elevated ~7 fold but expression of serum amyloid A (SAA) was not significantly different from the non – cachectic $Apc^{Min/+}$ mice (Fig 9A). IL – 6/STAT3 signaling is a powerful trigger for haptaglobin transcription and upregulation of haptaglobin is seen only in severely cachectic, but not in pre – cachectic $Apc^{Min/+}$ mice. Cachexia progression further increased STAT3 phosphorylation, though we did not see a change with gp130 and liver albumin protein content with cachexia progression (Fig 9B).

`

Interestingly, cachexia progression suppressed phosphorylation of NF-kB ~ 50% as compared to non – cachectic mice and ~25% as compared to pre – cachectic mice, in the severely cachectic mice (Fig 9A); this was mimicked by p65's downstream target MMP-2, an angiogenic and fibrotic marker, which showed an approximate 90% inhibition in the severely cachectic mice (Fig. 9B).

In summary, ER stress markers are upregulated early with cancer along with an IL – 6 independent activation of STAT3 and its downstream target SOCS-3 expression. This activation of ER stress markers affects the protein synthesis pathway by inhibiting Akt and S6 phosphorylation in the pre – cachectic mice, along with an increase in phosphorylated mTOR. Severely cachectic $Apc^{Min/+}$ mice completely depleted glycogen stores and increased transcription of PFK and PEPCK. Cachexia progression increases liver inflammatory markers STAT3 and haptaglobin, but suppressed phosphorylation of NF-kB and its downstream target MMP – 2. Protein synthesis was further suppressed in severely cachectic mice, independent of mTOR phosphorylation.

2.5 DISCUSSION

Our study has attempted to tease out the differential role of liver function in a cancerous state and in a cancerous state combined with cachexia. We report that liver inflammation increases with cachexia progression as seen by upregulation of haptaglobin transcription in the liver. Severely cachectic mice deplete liver glycogen stores along with upregulation of glycolytic enzyme PFK and gluconeogenic enzyme PEPCK. Liver protein synthesis is severely inhibited as seen by suppression of Akt and p-S6, independent of an inhibition in mTOR phosphorylation. Interestingly liver fibrosis and angiogenic marker MMP-2 is suppressed along with p – NF-κB and MAPK expression in the liver, but there

`

is a corresponding increase in the ER stress induced apoptotic marker CHOP. Thus cachexia progression is marked by an increase in liver acute phase response, severely depleted glycogen stores and inhibition of liver protein synthesis.

Non – cachectic $Apc^{Min/+}$ mice have a similar number of tumors as severely cachectic $Apc^{Min/+}$, but these tumors are smaller in diameter [59]. And though these tumors show do not affect any functional outcomes and body mass; their ability to induce systemic stress via Warburg effect and localized intestinal inflammation in the non – cachectic $Apc^{Min/+}$ mouse is highly probable. Correspondingly, we report and increase in ER stress markers in the non – cachectic $Apc^{Min/+}$ mouse, indicating problems hepatic protein folding. This increase in the unfolded protein response in the liver could be due to elevated levels of plasma MCP-1 which is via activation of the zinc finger protein MCPIP (MCP- 1 inducible protein) can lead to induction of ER stress[18,80]. Non – cachectic mice have negligible levels of serum IL – 6 [73] and no change is seen in the levels of the downstream IL-6 receptor, gp130 protein expression. However, we report that cancer exerts secondary effects on liver function in the $Apc^{Min/+}$. There is an IL- 6 independent increase in liver STAT-3 phosphorylation and SOCS-3 mRNA expression. Liver acute phase response is not induced with cancer alone, as liver haptaglobin levels are comparable to the healthy C57BL/6 mice. IL – 10 and other IL – 6 family cytokines like LIF, OSM, IL -11 are known to be elevated in the plasma of injectable cachexia models[14, 81] and though the presence of these cytokines has not been established in the $Apc^{Min/+}$ mouse, there is a possibility that these could play a role in STAT-3 activation in the non – cachectic mice. Increased SOCS3 at this stage could be a downstream response to upregulated STAT3. Interestingly blocking of the IL – 6 pathway is known to induce liver fibrosis by induction of MMP-2 [82]. The

`

slight induction of MMP – 2 expression by cancer could possibly be the result of SOCS3 mediated IL – 6 pathway inhibition. Since IL – 6 serum levels are negligible at this stage; we explored the possibility of endogenous IL-6 production in the liver by measuring mRNA levels of IL -6 and its upstream modulator TLR-4. However, liver TLR-4 and IL – 6 mRNA expression was highly variable, and we speculate that this could be due individual variation during the transition to the cancer-induced chronic inflammatory state.

Tumor burden and IL – 6 levels increase as body weight drastically decreases in the *Apc*$^{Min/+}$ mouse [59]. While decreased body mass can be attributed to loss of fat and muscle, total loss is masked by hypertrophy of the spleen and liver in the severely cachectic mice. Liver hypertrophy combined with suppressed gluconeogenic signaling due to cancer could indicate a metabolic disruption related to glycogen utilization. Interestingly, liver glycogen levels were depleted in cachectic mice, but not in weight stable mice with cancer. The loss of liver glycogen was accompanied by increased PFK and PEPCK gene expression and could indicate upregulated glucose flux related to the hypermetabolic state in the cachectic mice. Studies have shown that even an acute inflammatory response is enough to inhibit proteins synthesis and deplete liver glycogen as seen during pathogen induced inflammation and starvation experiments [63, 64]. Irrespective of upregulated STAT-3 phosphorylation, cancer alone did not alter liver protein synthesis regulation through – Akt-mTOR-S6. But presence of tumors could possibly induce a Warburg effect increasing lactic acid concentrations in the cytosol[83], which could be converted to glucose via Cori's cycle in the liver [84]. Increased glycolysis rate and consequent glucose production in the liver could be instrumental in hepatic PEPCK mRNA suppression, since upregulation of glucose – insulin signaling acts as a negative feedback for gluconeogenesis inhibition [85-88].

`

Cachexia was accompanied systemic and liver inflammation. Severely cachectic have increased liver haptaglobin mRNA expression, an acute phase protein regulated by IL-6/STAT3 signaling. Liver STAT-3 levels are also upregulated as compared to the non – cachectic $Apc^{Min/+}$, but no further increase in SOCS-3 level is observed. Increased inflammatory and hypertrophy response is counterintuitively, accompanied by a suppression of the protein synthesis signaling intermediates Akt and S6. But interestingly, liver phosphorylated mTOR levels are upregulated in the severely cachectic mice, inspite of Akt inhibition and s6 suppression. The expression of fibrotic and angiogenic marker MMP-2 is also progressively inhibited with cachexia progression in the $Apc^{Min/+}$ and can be attributed to p-65 inhibition in the $Apc^{Min/+}$. IL – 6 is known to be protective against liver fibrosis, with IL – 6 knockout mice showing increased liver fibrosis and insulin resistance upon CCl4 administration [89]. But since phosphorylation of NF- κB is inhibited in the cachectic $Apc^{Min/+}$ along with a suppression of Akt, could point toward an apoptotic phenotype in the liver. NF-κB liver knockouts under apoptosis in the face of an immune and concavalin-A challenge [90, 91]. Endotoxin levels are known to be elevated in the cachectic $Apc^{Min/+}$ sera, along with highly upregulated IL – 6 levels. Thus increased inflammatory response coupled with inhibition of the p-65 expression could trigger hepatocyte apoptosis in the $Apc^{Min/+}$ mice. And tough, upregulation of the IL – 6/STAT3 pathway is known to be pro – survival, with activated STAT3 blocking the effects of FAS activation[92], these beneficial effects are only observed with an acute bout of IL -6[93]. Chronic exposures to IL – 6 can in fact induce apoptosis and lead to liver failure [93].

Thus the downregulation of survival signals combined with suppression of protein synthesis, could point towards an endoplasmic reticulum (ER) stress induced apoptosis.

`

Severely cachectic *Apc*$^{Min/+}$ mice upregulate the late ER stress marker CHOP that is known to induced apoptosis in cells possibly by suppression of anti – apoptotic protein Bcl -2 and Bcl-xL and induction of genes that enhance production of reactive oxygen species[94-96].

In conclusion, liver function severely deteriorates with cachexia progression. As compared to non – cachectic cancer mice, the liver in severely cachectic mice is under metabolic stress with depleted glycogen and highly upregulated glucose flux. Severely cachectic mice display a robust acute phase protein response to the elevated levels of IL6/STAT3 signaling. Liver protein synthesis is also inhibited as seen by inhibition of Akt and S6, regardless of an upregulation of p-mTOR. An inhibition of both Akt and NF-kB in the cachectic liver, points towards a transition of the liver toward an apoptotic phenotype with cachexia progression and can be pursued as a future line of enquiry.

2.6 ACKNOWLEDGEMENTS

The authors thank Ms. Tia Davis for technical assistance with the animal breeding. The research described in this report was supported by research grant R01 CA121249 to JAC from the National Cancer Institute.

`

2.7: FIGURE LEGEND

Figure 1: Effect of cachexia progression on liver morphology and MAPK signaling A) Hematoxlyin and Eosin Staining of liver section for C57BL/6, Non – cachectic and severely cachectic $Apc^{Min/+}$ mice. B) Expression of levels of phosphorylated ERK and JNK in the liver

Figure 2: Effect of cancer on ER stress markers. Bip1, IRE-1 and ATF-6 p50 expression in the liver of non – cachectic $Apc^{Min/+}$

Figure 3: Effect of cancer liver glycogen stores. A) Glycogen stores as determined by PAS staining. B) Morphometry for the PAS stain to estimate glycogen stores in the WT and non – cachectic liver

Figure 4: Effect of cancer on liver metabolic, and anabolic signaling in non – cachectic mice. A) Liver mRNA expression of metabolic genes PFK and PEPCK B) Protein expression liver anabolic and apoptotic signaling in the non-cachectic mice. Values are expressed as SEM ± SE. * denotes significantly different from C57BL/6 Values are normalized either to the respective total protein for phosphoproteins and to GAPDH for non – phosphorylated proteins. (n = 5- 6 per group, $p < 0.05$) Dotted line indicates levels of C57BL/6. Abbreviations: Non = Non – Cachectic $Apc^{Min/+}$;

Figure 5: Effect of cancer on liver inflammatory signaling in non – cachectic mice. A) Liver mRNA expression inflammatory markers B) Protein expression liver inflammatory signaling in the non-cachectic mice. Values are expressed as SEM ± SE. *

`

denotes significantly different from C57BL/6 Values are normalized either to the respective total protein for phosphoproteins and to GAPDH for non – phosphorylated proteins. (n = 5- 6 per group, $p < 0.05$) Dotted line indicates levels of C57BL/6. Abbreviations: Non = Non – Cachectic $Apc^{Min/+}$;

Figure 6: Changes in liver morphology with cachexia progression. Histological evaluation for liver glycogen. Glycogen content severely depleted in the 20 week severely cachectic mice and morphometry of PAS staining using ImageJ Values are expressed as SEM ± SE. (n = 6- 8 per group, $p < 0.05$

Figure 7: Changes in liver metabolic and anabolic markers with cachexia progression. A) Liver mRNA expression of metabolic genes PFK and PEPCK B) Protein expression liver anabolic and apoptotic signaling with cachexia progression. Values are expressed as SEM ± SE. * denotes significantly different from C57BL/6 Values are normalized either to the respective total protein for phosphoproteins and to GAPDH for non – phosphorylated proteins. (n = 5- 6 per group, $p < 0.05$) Dotted line indicates levels of C57BL/6. Non = Non – Cachectic $Apc^{Min/+\ Sev}$ = severely cachectic $Apc^{Min/+}$;

Figure 8: Liver inflammatory signaling with cachexia progression. A) Liver mRNA expression inflammatory markers B) Protein expression liver inflammatory signaling with cachexia progression. Values are expressed as SEM ± SE. * denotes significantly different from C57BL/6 Values are normalized either to the respective total protein for phosphoproteins and to GAPDH for non – phosphorylated proteins. (n = 5- 6 per group, $p < 0.05$) Dotted line indicates levels of C57BL/6. Abbreviations: Non = Non – Cachectic $Apc^{Min/+}$ Sev = severely cachectic $Apc^{Min/+}$

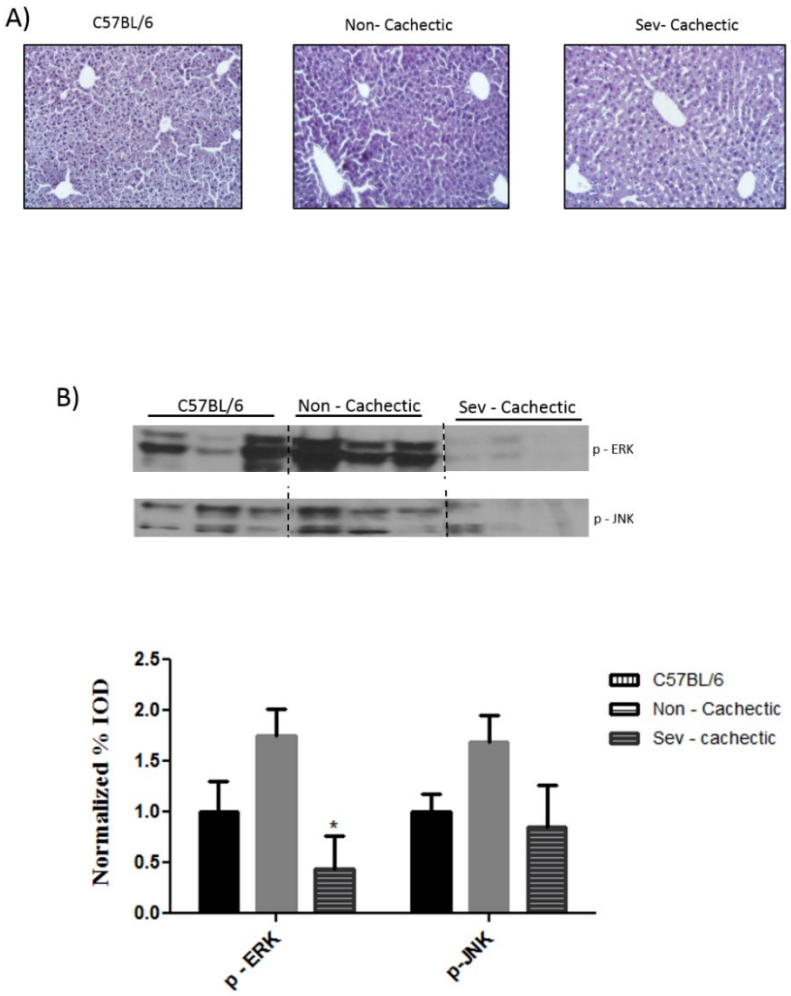

Figure 2.1: Effect of cachexia progression on liver morphology and MAPK signaling A) Hematoxlyin and Eosin Staining of liver section for C57BL/6, Non – cachectic and severely cachectic $Apc^{Min/+}$ mice. B) Expression of levels of phosphorylated ERK and JNK in the liver

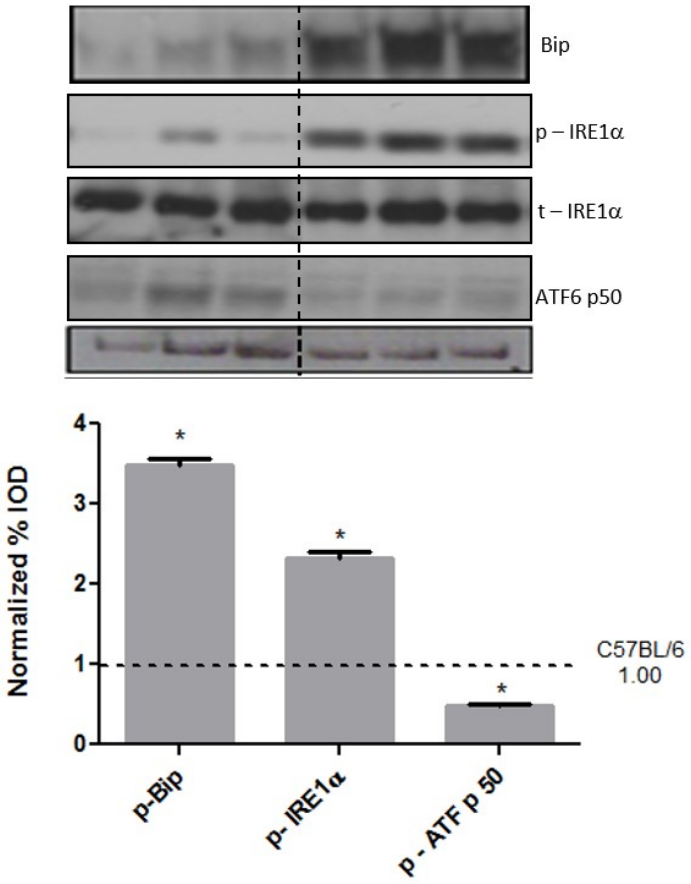

Figure 2.2: Effect of cancer on ER stress markers. Bip1, IRE-1 and ATF-6 p50 expression in the liver of non – cachectic *Apc*$^{Min/+}$

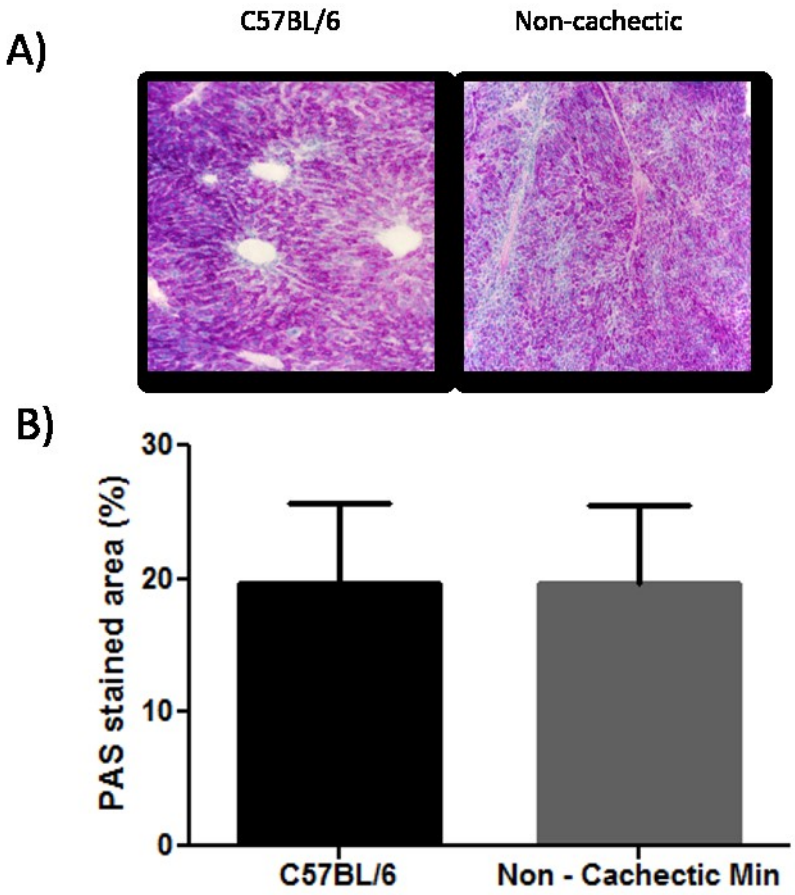

Figure 2.3: Effect of cancer liver glycogen stores. A) Glycogen stores as determined by PAS staining. B) Morphometry for the PAS stain to estimate glycogen stores in the WT and non – cachectic liver

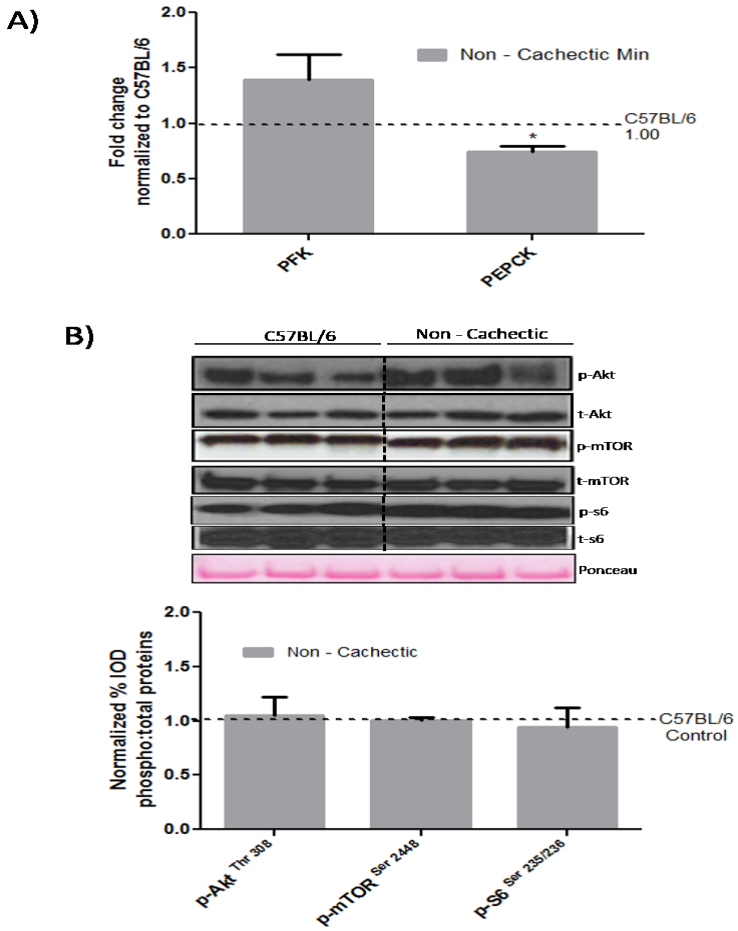

Figure 2.4**: Effect of cancer on liver metabolic, and anabolic signaling in non – cachectic mice.** A) Liver mRNA expression of metabolic genes PFK and PEPCK B) Protein expression liver anabolic and apoptotic signaling in the non-cachectic mice. Values are expressed as SEM ± SE. * denotes significantly different from C57BL/6 Values are normalized either to the respective total protein for phosphoproteins and to GAPDH for non – phosphorylated proteins. (n = 5- 6 per group, $p < 0.05$) Dotted line indicates levels of C57BL/6. Abbreviations: Non = Non – Cachectic $Apc^{Min/+}$;

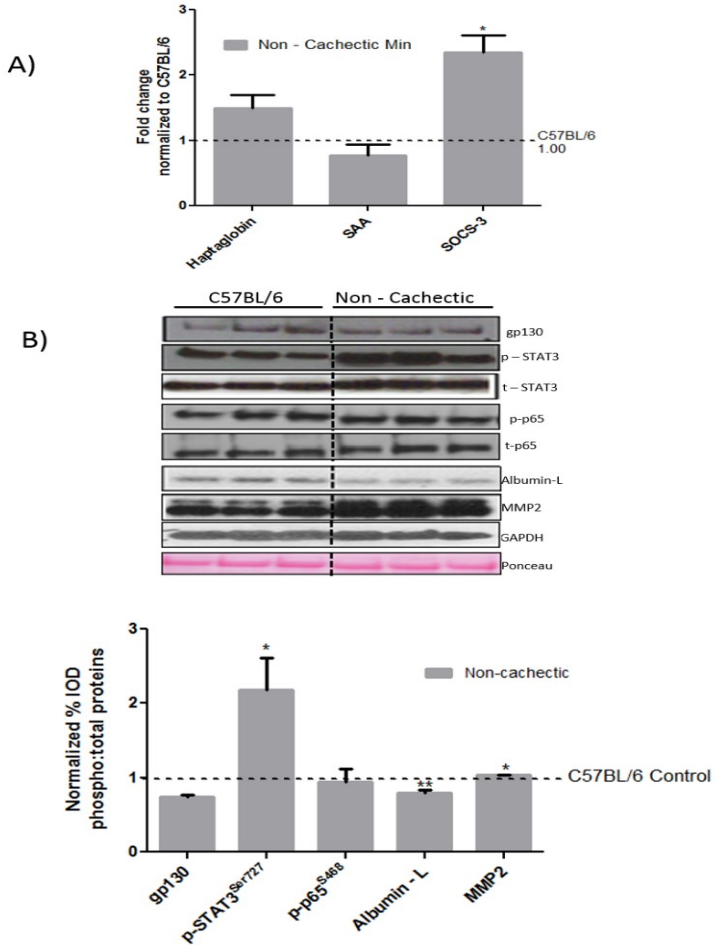

Fig 2.5**: Effect of cancer on liver inflammatory signaling in non – cachectic mice.** A) Liver mRNA expression inflammatory markers B) Protein expression liver inflammatory signaling in the non-cachectic mice. Values are expressed as SEM ± SE. * denotes significantly different from C57BL/6 Values are normalized either to the respective total protein for phosphoproteins and to GAPDH for non – phosphorylated proteins. (n = 5- 6 per group, $p < 0.05$) Dotted line indicates levels of C57BL/6. Abbreviations: Non = Non – Cachectic *Apc*$^{Min/+}$

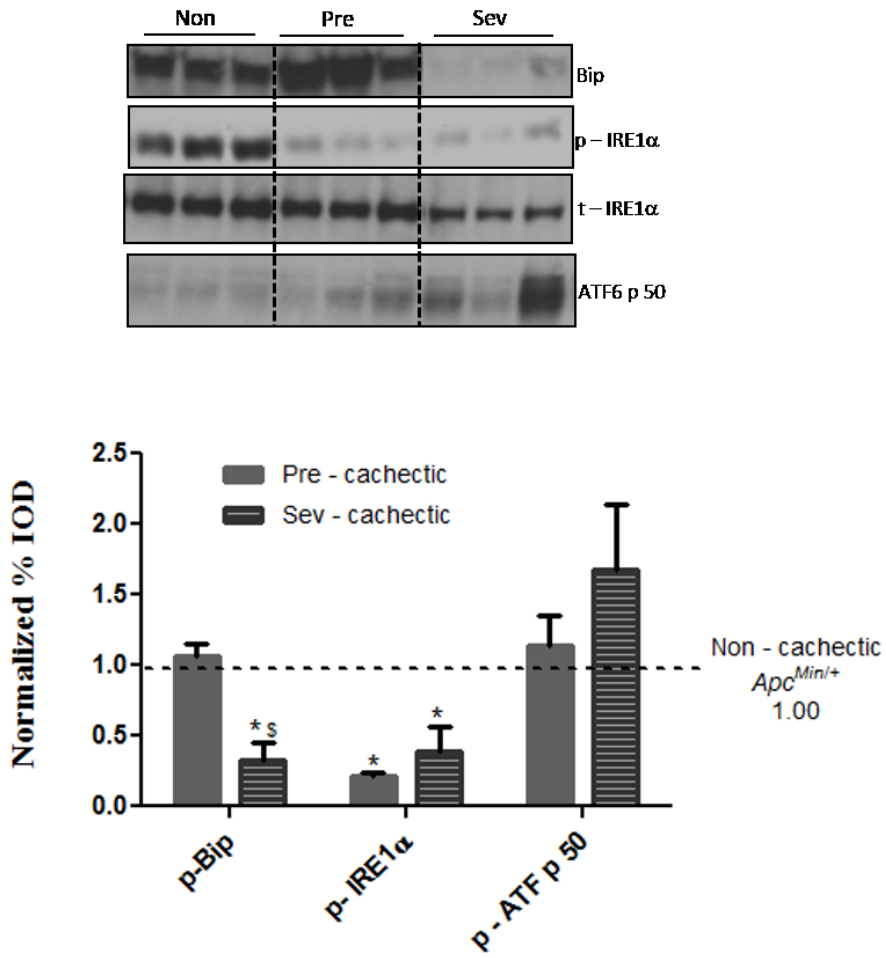

Figure 2.6: Hepatic ER stress markers with cachexia progression. ER stress markers Bip, IRE1α and ATF p50 were examined in the liver of non, pre and severely cachectic mice. Values are expressed as SEM ± SE. (n = 6- 8 per group, $p < 0.05$) Dotted line indicates levels of Non – cachectic mice. Non = Non – Cachectic $Apc^{Min/+}$ Sev = severely cachectic $Apc^{Min/+}$;

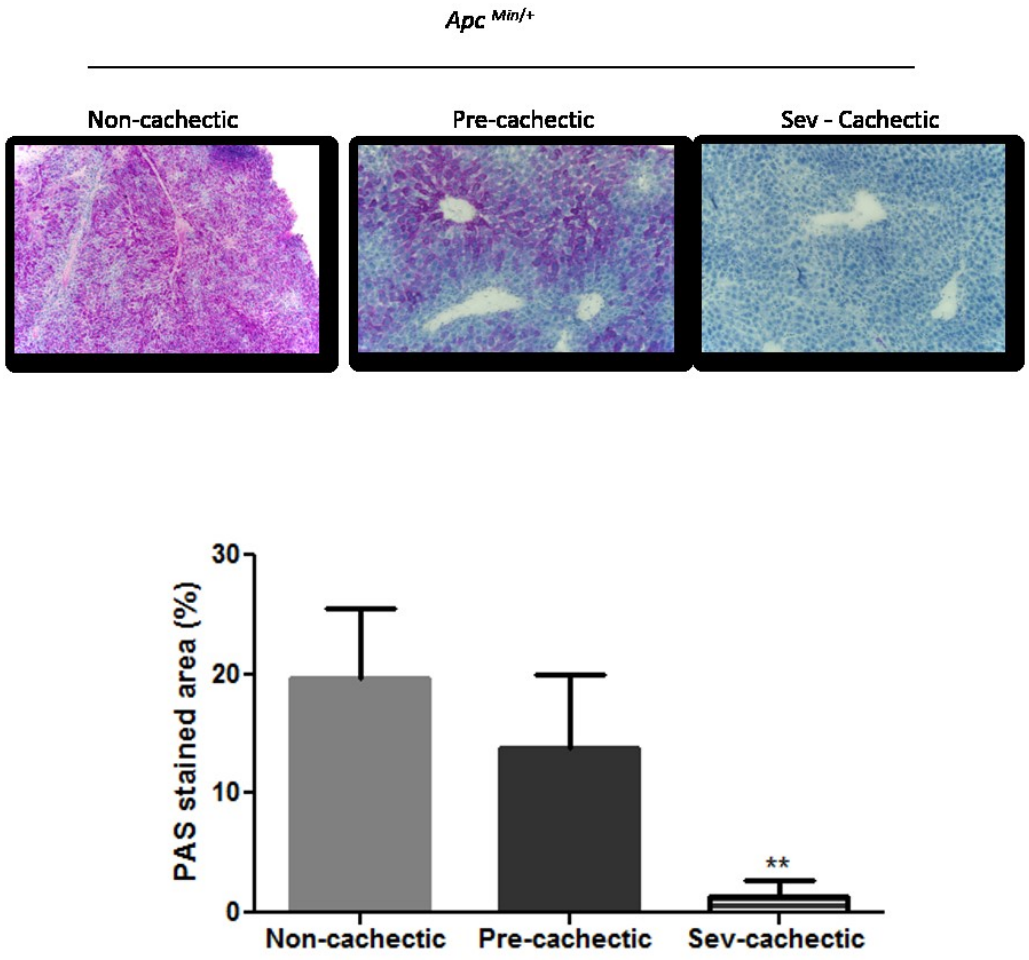

Figure 2.7: Changes in liver morphology with cachexia progression. Histological evaluation for liver glycogen. Glycogen content severely depleted in the 20 week severely cachectic mice and morphometry of PAS staining using ImageJ Values are expressed as SEM ± SE. (n = 6- 8 per group, $p < 0.05$) Dotted line indicates levels of Non – cachectic mice. Non = Non – Cachectic $Apc^{Min/+}$ Sev = severely cachectic $Apc^{Min/+}$;

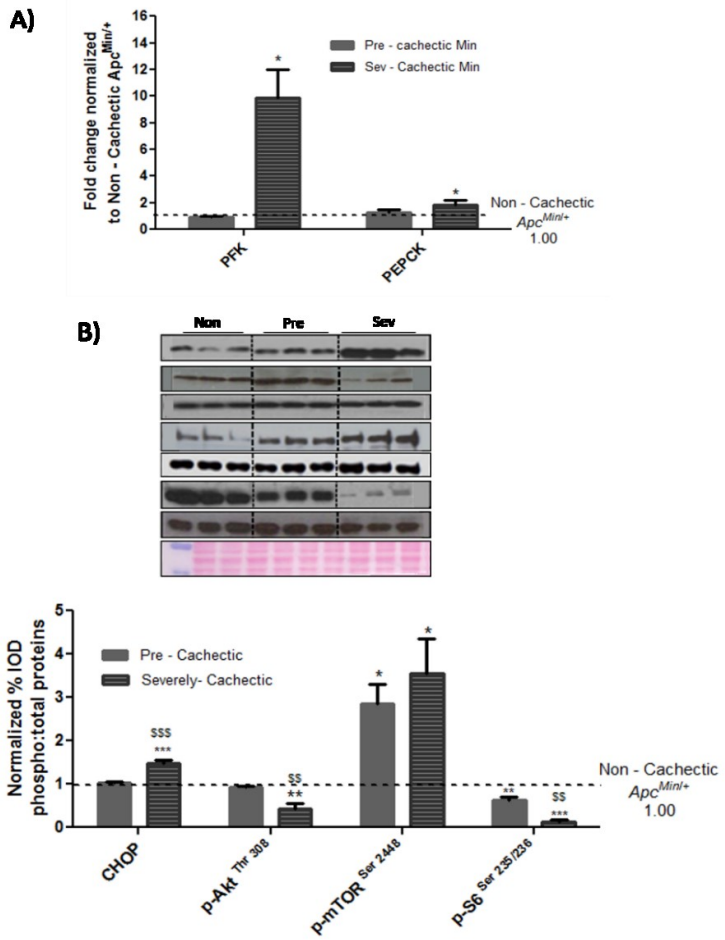

Figure 2.8: Changes in liver metabolic and anabolic markers with cachexia progression. A) Liver mRNA expression of metabolic genes PFK and PEPCK B) Protein expression liver anabolic and apoptotic signaling with cachexia progression. Values are expressed as SEM ± SE. * denotes significantly different from C57BL/6 Values are normalized either to the respective total protein for phosphoproteins and to GAPDH for non – phosphorylated proteins. (n = 5- 6 per group, $p < 0.05$) Dotted line indicates levels of Non – cachectic mice. Non = Non – Cachectic *Apc*$^{Min/+}$ Sev = severely cachectic *Apc*$^{Min/+}$;

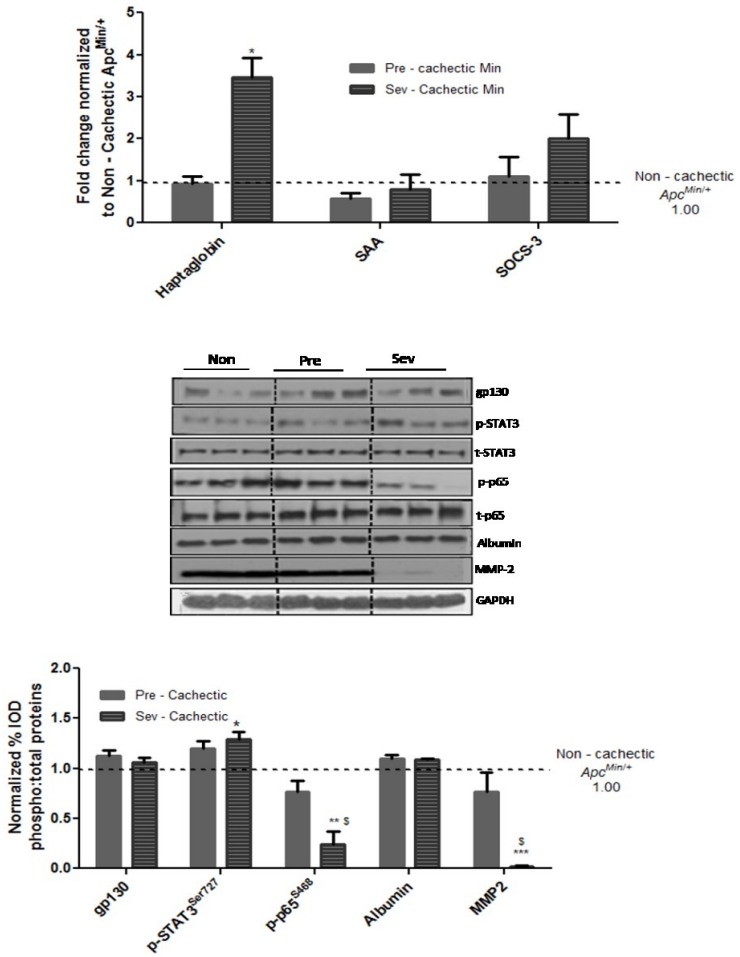

Fig 2.9: Liver inflammatory signaling with cachexia progression. A) Liver mRNA expression inflammatory markers B) Protein expression liver inflammatory signaling with cachexia progression. Values are expressed as SEM ± SE. * denotes significantly different from C57BL/6 Values are normalized either to the respective total protein for phosphoproteins and to GAPDH for non – phosphorylated proteins. (n = 5- 6 per group, $p < 0.05$) Dotted line indicates levels of Non – cachectic Min. Abbreviations: Non = Non – Cachectic $Apc^{Min/+}$ Sev = severely cachectic $Apc^{Min/+}$;

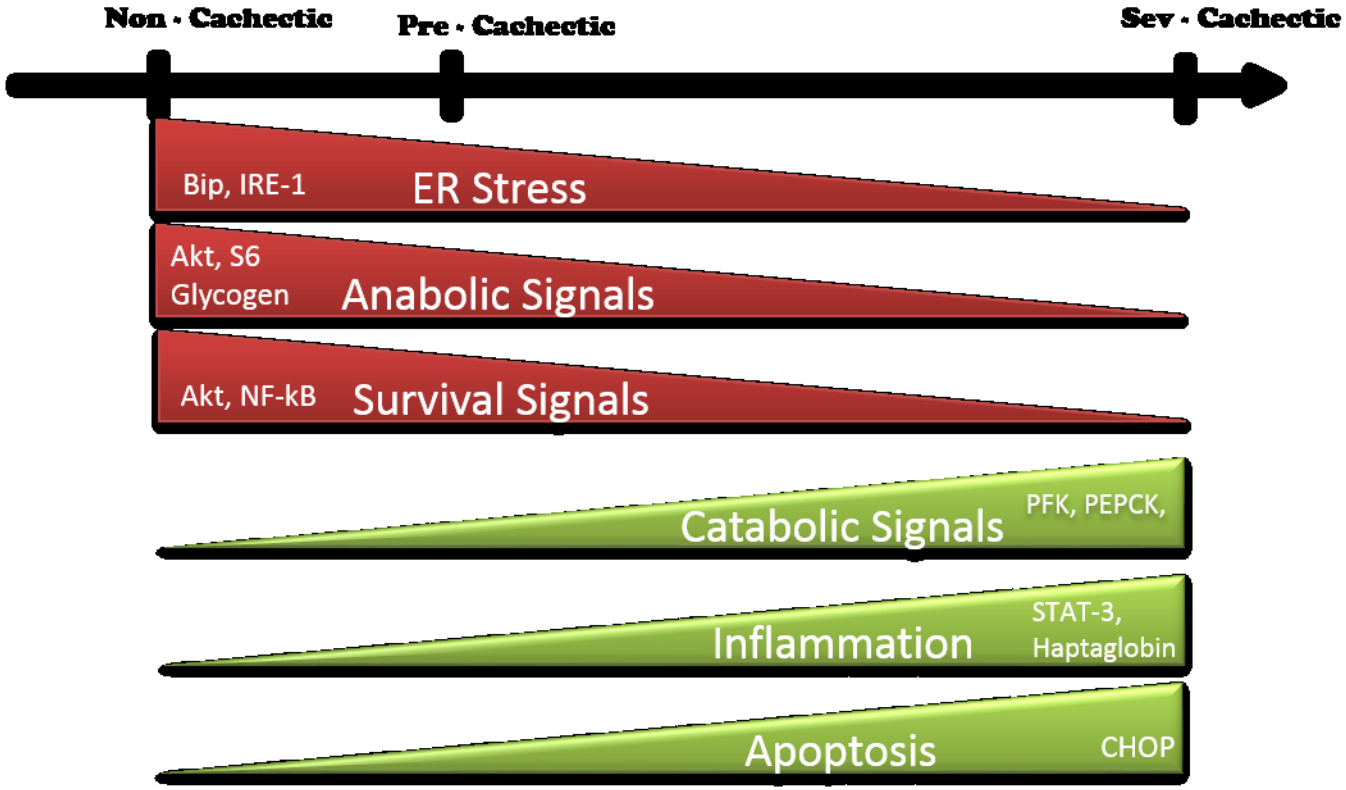

Figure 2.10: Schematic diagram describing the molecular signaling associated with cachexia progression in the liver

CHAPTER 3

ROLE OF CHRONIC INFLAMMATION ON LIVER FUNCTION IN CACHECTIC *APC*$^{MIN/+}$ MICE[2]

[2] Narsale, A., et. al. 2014 The Role of Chronic Inflammation on Liver Function in Cachectic *Apc*$^{Min/+}$ mice To be submitted to Biochemica et Biophysica Acta

3.1 ABSTRACT:

Cancer Cachexia is a multifactorial syndrome characterized by loss of muscle and fat mass. Although cachexia has many signature hallmarks related to the underlying disease, chronic inflammation is a unifying characteristic of cachexia progression. The $Apc^{Min/+}$ mouse is an established model of cancer cachexia where the chronic inflammatory state is sustained by high plasma IL – 6 levels. The liver's acute phase inflammatory response is maintained in despite depleted glycogen stores, altered AKT/mTOR signaling, and the induction of ER stress. The inhibition of chronic inflammation has the potential to alter cachexia progression. The purpose of this study was to examine if inhibition of chronic inflammation can alter cachexia-induced liver dysfunction $Apc^{Min/+}$ mice. To inhibit chronic inflammation $Apc^{Min/+}$ mice were administered pyrrolidine dithiocarbamate (PDTC), a global STAT3 and NF-kB inhibitor, or a trans IL – 6 signaling inhibitor, a soluble gp130 fusion protein (sFcgp130), for a period of two weeks after the initiation of cachexia. Mice were analyzed for liver function related to inflammation, and metabolic signaling. PDTC attenuated body weight loss and fat mass loss. PDTC also increased liver glycogen content, liver lipid content, liver weight, and PFK mRNA expression, while suppressing PEPCK expression. Liver inflammation and AKT/mTOR signaling were not altered by PDTC. Administration of sFcgp130 attenuated body weight loss and mesenteric fat loss without significantly rescuing total muscle mass loss. It also increased liver PEPCK mRNA expression without affecting PFK mRNA expression. sFcgp130 administration did not affect haptaglobin mRNA levels or inhibition of the protein synthesis markers. Together these results indicate that chronic inflammation directly

influences indices of liver glycolysis and gluconeogenesis, but is not the primary source for inflammatory and protein synthesis disruption in the cachectic liver.

Keywords: PDTC, sFcgp130, IL – 6, trans – signaling, acute phase response

3.2 INTRODUCTION

Cachexia is a wasting syndrome seen with the later stages of chronic diseases like Rheumatoid Arthritis, COPD, AIDS and cancer. Once developed cachectic symptoms persists independent of the chronic disease and hence current treatments of many chronic diseases tough effectively improve lifespan, do little to improve quality of life in patients. Treatment and therapies for cachexia are thus important, to allow complete and effective recovery in patients. But no therapies are currently approved for cachexia due its multifactorial nature[34] with cachexia symptoms varying between patients and the underlying chronic disease. However, all the signature hallmarks of cachexia are underlined by a chronic inflammatory state leading to loss of muscle and fat mass. Thus resolving this chronic inflammatory state might be the key to restrict and reverse this wasting syndrome.

Chronic inflammation is an energy expensive process resulting from the constitutive activation of the immune system. In hypermetabolic diseases like cancer, sustained activation of the immune responses compete with proliferating tumors for the inadequate energy reserves, accelerating catabolic processes degrading skeletal muscle to amino acids. Liver can take up these free amino acids to trigger the energy expensive acute phase response (APR), by the secreting acute phase proteins which can help fight the tumor but can also further degrade skeletal muscle[14]. Thus liver induced inflammatory response

could be central to both chronic inflammation and sustained hypermetabolic state and suppression of liver based inflammation may attenuate cachexia progression

Our previous studies with the *Apc*$^{Min/+}$ mouse have established it as an IL – 6 dependent model of cancer cachexia, that gradually loses muscle and fat mass. The cachectic *Apc*$^{Min/+}$ mouse also exhibits splenomegaly, anemia, increased gut permeability, elevated plasma endotoxin and a liver mediated APR. Previous studies have also shown that inhibition of IL – 6 in the *Apc*$^{Min/+}$ mouse by administration of the IL – 6 receptor antibody attenuates cachexia progression by suppression degradation pathways in skeletal muscle [19], possibly due the presence of the soluble IL – 6 receptor (sIL-6R) pathway, blunting the efficacy of the inhibitor and antibodies. Moreover, STAT-3 phosphorylation in the liver was observed independent of IL – 6 in the cancerous *Apc*$^{Min/+}$ mouse, reiterating that yet unknown IL – 6 independent factors can trigger inflammatory intermediates in the *Apc*$^{Min/+}$ (unpublished data). In this study we test the efficacy of two new compounds – pyrrolidine dithiocarbamate (PDTC) and gp130 fusion protein (sFcgp130) - as possible therapeutic agents to inhibit cachexia progression. PDTC is an anti – oxidant and a metal chelator that works via inhibition of the inflammatory intermediates STAT-3 and NF-kB. Administration of PDTC in the *Apc*$^{Min/+}$ mouse would allow us to inhibit both STAT-3 and NF-kB induced inflammation during cachexia progression. But since PDTC is a global non – specific inhibitor of inflammatory signaling intermediates, it could possibly have adverse effects on essential function of immune cells during disease. Hence we also propose to use the recently developed sFcgp130 which can bind to the sIL-6 – IL6R complex in plasma to inhibit the pro – inflammatory arm of IL – 6 signaling, while maintaining the classical signaling essential for tissue growth and regeneration intact.

Taken together, cachexia in the *Apc*$^{Min/+}$mouse is related to the underlying chronic inflammatory state. It is not certain if the liver's IL – 6 induced APR during cachexia leads to muscle degradation [14]. We have already established that cachexia progression disrupts liver metabolic, and inflammatory signaling (Narsale, A, et.al). These results suggest that during severe cachexia mice demonstrate elevated glucose flux, APR, and altered protein turnover regulation. It remains unclear if altered liver function is causal to the progression of cachexia. The purpose of this study was to examine if inhibition of chronic inflammation can alter cachexia-induced liver dysfunction *Apc*$^{Min/+}$ mice. We hypothesized that systemic inhibition of chronic inflammation in the *Apc*$^{Min/+}$ mouse would improve liver function by suppressing liver APR and restoring metabolic signaling. *S*everely cachectic *Apc*$^{Min/+}$ mice were treated with PDTC or sFcgp130 for a period of two weeks to treat cachexia symptoms. Liver function was measured in terms of inflammatory, metabolic, apoptotic and protein synthesis markers and correlated to cachexia progression in the treated mice to determine the role of chronic inflammation inhibition on liver function and cachexia progression.

3.3 METHODS:

3.3. I ANIMALS

All animal procedures were approved by the University of South Carolina's Institutional Animal Care and Use Committee. All mice were housed in standard cages and kept on a 12hr: 12hr light: dark cycle with the light period starting 0700 hrs. The mice were had an ad libitum access to water and food (standard rodent chow, cat. no. 8604 Rodent Diet; Harlan Teklad, Madison, WI). 8 week old C57BL/6 and *Apc*$^{Min/+}$ mice were introduced into the study and monitored for Body weight loss, Food intake and body temperature, throughout the course of the study. Following an overnight fast, mice were

sacrificed at 12 weeks (non – cachectic, N = 6), 14 weeks (pre – cachectic N = 6) and 18 – 20 weeks (severely cachectic, N=6), to delineate the systemic changes related to cancer from cachexia.

3.3. II PYRROLIDINE DITHIOCARBAMATE (PDTC) ADMINISTRATION

A subset of mice (N = 6) were treated with a STAT-3 and NF – KB inhibitor – Pyrrolidine dithiocarbamate (10mg/kg/mouse for 2 weeks, i.p.). PDTC treatment was initiated in mice displaying 8 – 10% weight loss at 16 – 18 weeks of age. C57BL/6 mice were used as WT controls

3.3. III GP130 FUSION PROTEIN (SFCGP130) ADMINISTRATION

A subset of moderately cachectic *Apc*$^{Min/+}$ mice, (8 – 10%) body weight loss were injected with 300ug/week of gp130 fusion protein (gift from Dr. Stephan Rose – John[97], intraperitoneally for 2 weeks. C57BL/6 mice were used as WT controls. Animals were monitored for body weight, body composition and food intake through the course of the study.

3.3 IV TISSUE COLLECTION

Mice were anesthetized using the ketamine cocktail. Plasma was collected prior to tissue collection via blood draws through the retro-orbital sinus. Muscle and liver were collected during the sacrifice and were either snap frozen in liquid nitrogen and stored at -80^{0}C. Intestine segments were isolated, cleaned and cut into 4 equal segments of the small intestine and a segment for the colon. These were used to account for tumor burden in the cachectic *Apc* $^{Min/+}$ mice.

3.3. V IL – 6 PLASMA LEVELS

IL – 6 levels in the plasma were quantified using the BD BioSciences, Mouse – IL – 6 ELISA kit. Briefly, 25 – 50ul of plasma was diluted down to 100ul and the ELISA was performed according to manufacturer's instructions.

3.3. VI RNA EXTRACTION, cDNA PREPARATION AND REAL – TIME PCR

PCR was performed as described previously [76]. Briefly, RNA was isolated by homogenizing the liver tissue in Trizol (Invitrogen, Cat # 15596), followed by a chloroform/isopropyl alcohol extraction. cDNA and RT-PCR assays were performed using reagents purchased from (ABI, Foster City, USA). Primers for SOCS-3[14], Haptaglobin[14], PFK[77] and PEPCK[77] primers purchased from IDT (Coralville, IA, USA). Data was analyzed using the comparative cycle threshold [Ct] method calculated by the ABI software.

3.3.VII WESTERN BLOT

Western blots were performed as described previously [78]. Briefly, a piece of the liver was cut, weighed and placed in 10 times the volume of Muller Buffer. The tissue was homogenized in the buffer using a glass or glass homogenizer. The resultant homogenate was quantified for protein concentration using the Bradford assay. All protein samples were diluted to 3ug/µl concentration to aid equal loading on the gel. Homogenates were fractionated on SDS – PAGE acrylamide gels (6% - 15%) and transferred overnight onto a PVDF membrane. The membrane was Ponceaued following the transfer to ensure equal loading. The PVDF membrane was then probed for STAT-3, mTOR, S6, Akt, MMP-2, p-p65, GAPDH (Cell Signaling Technology, Danvers, MA, USA) gp130 and Albumin (Santa Cruz Biotechnology). A corresponding secondary antibody was used along with the

chemiluminescent agent Quantum ECL (BioExpress, Kaysville, UT, USA) to visualize the protein bands. ImageJ (NIH, Bethesda, MD, USA) software was used for quantification of the integrated optical density (IOD) for Western blot bands.

3.3. VIII PERIODIC ACID SCHIFF'S STAINING

A small piece of liver tissue was mounted on an OCT block and sectioned at -16^{0}C. The slides were fixed in Carnoy's fixative for 10 minutes followed by 30 minute incubation in the Periodic Acid. Slides were then washed with water and exposed to Schiff's reagent for 30 minutes. The slides were counter stained with Hematoxylin, dehydrated through alcohol grades and mounted using Permount. The slides were imaged the next day using the DP70 Olympus microscope.

3.3.IX HEMATOXYLIN AND EOSIN STAINING

A subset of severely cachectic *Apc* $^{Min/+}$ mice were perfused with 4% PFA in PBS. Liver was stored in 4% PFA overnight and transferred to a 30% sucrose solution. The perfused liver was mounted in a wax block and cut using a microtome. The sections were deprafinized and stained with Hematoxylin and Eosin stained, dehydrated using alcohol grades. Slides were mounted in the Permount media and imaged using the DP-70 (Olympus Imaging, Centre Valley, PA, USA) camera.

3.3. X LIPID EXTRACTION

Approximately 100 mg of frozen liver tissue was weighed and added to a tube containing 4ml of Chloroform: methanol mixture (2:1). The livers were homogenized in the organic solvents and the resulting mixture was gently mixed for the next 20 minutes. The homogenate was centrifuged to separate the organic and aqueous phases. The bottom

layer was pippeted out carefully in a new pre - weighed 5ml glass tube and evaporated using the nitrogen vacuum system. Once dried the tube was weighed again for a post weight. Lipid content was calculated by subtracting the post weight of the tube from the pre weight of the tube.

3.3. XI STATISTICAL ANALYSIS

All statistical analysis was performed using the GraphPad Prism software. Two – Way ANOVA was used to test the effect of body weight, muscle mass, fat mass and organ mass with PDTC and sFcgp130 treatment. Student Newman – Keul post hoc analysis was used to analyze the difference between groups. Pre – planned t – test was used to study the effect of treatment on the $Apc^{Min/+}$. Values were expressed as Mean ± SE. Significance was set at $p<0.05$.

3.4 RESULTS:

3.4. I EFFECT OF PDTC TREATMENT ON TUMOR BURDEN

We have previously established that tumor burden in the $Apc^{Min/+}$ mice correlates with cachexia progression. However, this correlation exists between tumor size rather than tumor number, which plateaus in the $Apc^{Min/+}$ mice at 12 weeks of age prior to cachexia initiation[59]. Two weeks of PDTC treatment did not affect tumor number as compared to untreated $Apc^{Min/+}$ (Fig 1A), however it did reduce tumor burden by decreasing the percentage of large (>2 mm) tumors. Total tumor was held steady by increasing the percentage of both small (<1mm) and mid-size (1 – 2mm) tumors (Fig 1B). The wild type mice treated with PDTC showed no obvious change in intestinal morphology as compared to the untreated wild type mice (data not shown).

3.4. II EFFECT OF PDTC TREATMENT ON BODY MASS

C57BL/6 and *Apc*$^{Min/+}$ mice were initiated into the study at 8 weeks of age and body weight was monitored on a daily basis. At 12 weeks of age the mice were divided into either a PBS injectable or a PDTC injectable group based such that both groups had comparable peak body weights. PDTC (100mg/ml) or PBS administration was started at 16 – 18 weeks of age after the *Apc*$^{Min/+}$ mice had lost about 6 – 8% of their peak body weight till sacrifice (Fig2). A Two Way ANOVA was used to determine the effect and possible interaction between PDTC treated and untreated WT and *Apc*$^{Min/+}$ mice, whereas a pre – planned t –test was used to determine the effect of PDTC treatment in the *Apc*$^{Min/+}$ only ($p < 0.05$). PDTC administration attenuated body weight loss in the *Apc*$^{Min/+}$ mouse over the two week period (Fig2A). PDTC treatments resulted in attenuated total fat mass (Fig 2B) and epididymal fat loss (Fig 2C) in the *Apc*$^{Min/+}$ mouse. Body composition analysis using a DEXA scan also revealed an increase in total lean mass in the PDTC treated as compared to the untreated *Apc*$^{Min/+}$ mice (Fig 2B, 2D). [98] Total muscle mass was decreased with the *Apc*$^{Min/+}$ mouse, but there was main effect of PDTC treatment on muscle mass in both the WT and cachectic mice (Fig 2E). However, there was a significant increase liver mass in the *Apc*$^{Min/+}$ as compared to the WT and PDTC administration enhanced liver hypertrophy independent of genotype (Fig 2F).

3.4. III EFFECT OF PDTC TREATMENT ON LIVER GLYCOGEN AND LIPID CONTENT

Hepatomegaly observed in the cachectic *Apc*$^{Min/+}$ was independent of liver glycogen stores which were severely depleted in the untreated cachectic *Apc*$^{Min/+}$ mice. PDTC treatment significantly increased liver glycogen content in the *Apc*$^{Min/+}$ mice (Fig 3A and

3B) but there was no difference in the glycogen content in the livers of treated and untreated WT mice (Fig 3A). Loss of glycogen in the severely cachectic *Apc*$^{Min/+}$ mouse was accompanied by a loss of liver lipid content as compared to the WT mouse (p=0.04), and PDTC treatment attenuated this loss of fat with lipid content in the liver being significantly higher than in the untreated *Apc*$^{Min/+}$ mouse (Fig 3C).

3.4. IV Effect of PDTC treatment on Liver metabolic markers

Altered glycolytic flux could affect liver glycogen and lipid content, and quantification of liver metabolic enzymes regulating glycolysis and gluconeogenesis was thus performed. Gluconeogenic enzyme PEPCK mRNA was not elevated in the cachectic *Apc*$^{Min/+}$ mice as compared to control, but it was suppressed with PDTC treatment. Levels of PFK mRNA the enzyme regulating a key step in glycolysis were elevated in the severely cachectic *Apc*$^{Min/+}$ mice and PDTC treatment further increased PFK transcription in the *Apc*$^{Min/+}$ (Fig 4A). Glycogen and lipid storage in the liver are upregulated under anabolic conditions, but levels of phosphorylated Akt in the cachectic liver were suppressed and PDTC treatment was unable to release this inhibition. Interestingly, levels of phosphorylated mTOR were upregulated in the untreated *Apc*$^{Min/+}$ and this increase was not affected by PDTC treatment (Fig 4B).

3.4. V Effect of PDTC treatment on liver inflammation

Severely cachectic mice upregulate plasma IL – 6 levels and two weeks of PDTC treatment did not attenuate the increase levels of this inflammatory cytokine (Fig 4A). STAT-3 the downstream target of IL – 6 was upregulated with no effect of PDTC treatment (Fig 4B). Subsequently haptaglobin mRNA transcription is controlled by phosphorylated STAT-3 levels and PDTC treatment did not attenuate liver haptaglobin mRNA levels as

compared to the untreated *Apc*$^{Min/+}$ (Fig 4C). Other markers of liver inflammation like p – p65, albumin and MMP2 were also unaffected by PDTC treatment in the *Apc*$^{Min/+}$ (Fig 4D).

3.4. VI EFFECT OF SFCGP130 TREATMENT ON TUMOR BURDEN

Two week administration of sFcgp130 did not affect total tumor number in the treated as compared to the untreated *Apc*$^{Min/+}$ mice (Fig 6A). When analyzed for percent tumor distribution there was an increase in mid – size tumor (1 – 2mm) but fusion protein did not decrease the number of large tumors in the small intestine (Fig 6B).

3.4. VII EFFECT OF SFCGP130 TREATMENT ON BODY MASS

sFcgp130 treatment attenuated weight loss in the *Apc*$^{Min/+}$ mice (Fig 7A) which can be attributed to attenuation of fat loss as measured by DEXA (Fig 7B) and Mesenteric Fat mass (Fig 7C). Total lean mass, the sum of skeletal muscle mass and visceral organ mass, as measured by DEXA showed a small but significant decrease (Fig 7D). Total muscle weight as measured at sacrifice exhibited an approximate 33% atrophy in the cachectic *Apc*$^{Min/+}$ as compared to the WT control. Further, administration of fusion protein did not rescue skeletal muscle atrophy in these mice (Fig 7E). Hepatomegaly was observed in the cachectic *Apc*$^{Min/+}$ mice as compared to the control and this hypertrophy in liver mass was not attenuated upon sFcgp130 administration (Fig 7F).

3.4. VIII EFFECT OF SFCGP130 TREATMENT ON LIVER GLYCOGEN CONTENT

Hypertrophied *Apc*$^{Min/+}$ mice liver were compared with the WT mice, for glycogen content and total lipid content. Severely cachectic ApcMin/+ mice severely depleted both glycogen and lipid content in the liver (Fig 8). Administration of sFcgp130 fusion protein did not rescue liver glycogen or lipid content (Fig 8). There was no effect of the treatment on WT mice (data not shown).

3.4. IX EFFECT OF SFCGP130 TREATMENT ON LIVER METABOLIC AND PROTEIN SYNTHESIS MARKERS

We next looked enzymes and proteins regulating liver's anabolic and catabolic processes. PEPCK and PFK mRNA was analyzed to estimate the glycolytic and gluconeogenic flux. PEPCK mRNA was not affected by cachexia progression but was elevated after sFcgp130 treatment (Fig 9A). On the other hand, levels of the glycolytic enzyme were elevated with cachexia and sustained in the sFcgp130 administered cachectic mice (Fig 9A). Protein synthesis signaling was suppressed in the cachectic liver with a severe suppression of Akt and S6 phosphorylation seen in the cachectic liver as compared to the WT mice. Administration of sFcgp130 did not rescue this inhibition of Akt and S6 phosphorylation (Fig 9B). Interestingly, cachectic ApcMin/+ did not suppress p-mTOR levels which though unaffected by fusion protein treatment, were sustained in the face of suppressed Akt and S6 (Fig 9B).

3.4. X EFFECT OF SFCGP130 ON LIVER INFLAMMATORY MARKERS

IL-6 the driver of cachexia progression in the $Apc^{Min/+}$ mice was suppressed with two week of sFcgp130 administration (Fig 10A). However, this suppression of plasma IL – 6 did not affect hepatic STAT-3 phosphorylation (Fig 10B). Subsequently, levels of mRNA levels of the acute phase protein haptaglobin were sustained even after sFcgp130 treatment of the cachectic $Apc^{Min/+}$ mice (Fig 10C). NF-KB, the inflammatory intermediate was still suppressed in post sFcgp130 treatment, which was mimicked by its downstream target MMP-2 (Fig 10D).

3.5 DISCUSSION:

The *Apc*$^{Min/+}$ mouse model of cancer cachexia exhibits chronically elevated IL – 6 levels that have been associated with the progression of wasting [19, 59]. Additionally, there is a chronic induction of APR with cachexia that is associated with liver dysfunction[99]. The progression of cachexia increases liver STAT-3 phosphorylation, promotes production of acute phase proteins, suppresses protein synthesis and alters glucose flux [99]. Severely cachectic *Apc*$^{Min/+}$ mice also demonstrate depleted liver glycogen levels. Our current study examined if the disruption of IL-6 dependent signaling and/or associated inflammation could improve liver function and slow the progression of cachexia. Our study establishes that the attenuation of cachexia progression by the inhibition of chronic inflammation coincides with improvements in some aspects of cachexia-induced liver dysfunction. PDTC treatment led to an increase in liver glycogen levels, and coincided with suppression of the gluconeogeneic enzyme PEPCK mRNA expression. Both treatments affect percentage tumor size distribution but neither treatment affected cachexia-induced changes in liver APR or protein synthesis. Taken together our results demonstrate that chronic inflammation directly influences indices of liver glycolysis and gluconeogenesis, but is not the primary source for inflammatory and protein synthesis disruption in the cachectic liver.

Our current study demonstrates that PDTC administration can lead to a decrease in number of large intestinal tumors, but increasing the number of small and mid – size tumors. Though the current experimental set up does not allow us to tease out if the tumor burden redistribution was due to shrinkage of large tumors or due to the an arrest in tumor growth at 16 weeks, the reduced tumor burden attenuates cachexia progression in the face of elevated plasma IL – 6 levels. We report the novel finding that PDTC administration

can reverse bodyweight loss in $Apc^{Min/+}$ mice that have initiated cachexia. The body mass increase could be accounted for by increased fat mass and hypertrophy of internal organs, such as the liver. Hepatomegaly of the liver is in the cachectic untreated $Apc^{Min/+}$ mouse is interesting and occurs even as the liver depletes its lipid and glycogen stores. However, it can be possibly explained by the ability of chronic IL – 6 exposure to induce hyperplasia in rodent liver[98]. Interestingly, PDTC treatment also led to liver hypertrophy independent of the genotype. PDTC treatment possibly increased protein translation in the WT mice as observed via the upregulation of S6 levels in the WT mice. But protein synthesis is suppressed in the cachectic $Apc^{Min/+}$ liver and hepatomegaly in the PDTC treated $Apc^{Min/+}$ liver could possibly due to rescuing of liver glycogen and lipid content, possibly by altering the metabolic signaling in the face of a reduced tumor burden. Zhu et.al, 2011 demonstrated that PDTC administration to septic mice could suppress liver gluconeogenic enzymes and alter liver glucose flux. We extend these findings by showing that PDTC was able to suppress liver gluconeogenic enzyme PEPCK mRNA expression in cachectic $Apc^{Min/+}$ mice. Interestingly, the suppression of gluconeogenesis was associated with increased expression of glycolytic enzyme PFK mRNA, which suggests PDTC altered glucose flux in the cachectic liver. Our findings related to liver gluconeogenesis, glycogen stores and lipid content suggest that PDTC treatment can attenuate the liver hypermetabolic state that accompanies cancer cachexia.

Although, it needs to be noted that, this attenuation in metabolic signaling occurs independent of inflammatory signaling responses in the liver which remain unchanged upon PDTC administration in our model. PDTC administration in the $Apc^{Min/+}$ mouse did not suppress plasma IL – 6 levels and thus we did not see a suppression of STAT-3 or

haptaglobin activation in the *Apc*$^{Min/+}$liver. Since the inflammatory marker, NF-KB is already suppressed in the cachectic liver, we hypothesize that the potency of PDTC to suppress liver inflammation is diminished in the liver. Moreover, liver inflammation in the cachectic *Apc*$^{Min/+}$ model is independent of the traditional TNF/TLR/NF-kB signaling and is governed by a strong upregulation of the liver's APR response. Recent studies have shown that suppression of liver APR in models of sepsis and inflammation are more harmful than beneficial[100,101,102,103]. Transgenic mice with a suppressed APR in models of cancer had shorter life spans as compared to the wild type littermates indicating that liver induced APR is essential to suppress tumor growth during cancer [100],[23]. Taken together these results indicate that increased PDTC treatment attenuates liver metabolic functions by attenuation of the hypermetabolic response, independent of liver inflammation and plasma IL – 6.

On the other hand, administration of sFcgp130, reduced plasma IL – 6 levels but did not reduce tumor burden in the small intestine. The sFcgp130 is designed specifically to inhibit trans – IL-6 signaling in the cachectic *Apc*$^{Min/+}$ mouse. Activation of the trans-IL-6 signaling pathway is indicative of soluble IL-6 receptor mediated signaling and is considered pro – inflammatory as opposed to the classical IL – 6 pathway which is known to exhibit anti – inflammatory properties[24]. Administration of this protein for two weeks significantly reduced plasma IL – 6 levels, demonstrating the almost all of the circulating IL – 6 during cachexia progression signals via the soluble IL – 6 receptor. This suppression of plasma IL – 6, corresponded with a decrease in the body weight loss in the sFcgp130 treated cachectic mice as compared to the untreated controls. Rescuing of body mass loss could be attributed to sparing of fat mass, with no effect of the treatment on lean mass.

Total lean mass as calculated by DEXA scans decreased in the cachectic $Apc^{Min/+}$ mice revealing a severe loss of muscle mass loss which could not be compensated by the hypertrophy of visceral organs like spleen and liver on the DEXA. This loss of skeletal muscle mass could be ascribed to the still elevated levels of STAT 3 and its downstream target haptaglobin in the liver, which seem to be degrading muscle mass independent of plasma IL – 6 levels. We have recently reported that ER stress is initiated early in the $Apc^{Min/+}$ mice, prior to initiation of cachexia, and is propagated downstream towards apoptosis with cachexia progression[99], and intermediates of the ER stress pathway like ATF 6 can induce induction of acute phase response proteins independent of IL – 6[104]. With a sustained hypermetabolic state as seen in the severely cachectic mice, skeletal muscle is broken down to simple amino acids, which are being used as an energy source instead of the usual sugars and fats. Thus degradation of muscle mass loss in the cachectic $Apc^{Min/+}$ mouse seems to be function of hypermetabolism rather than elevated plasma IL – 6. SFcgp130 administration did not affect hepatomegaly seen in the cachectic $Apc^{Min/+}$ mice, nor did it affect the Akt/S6 signaling or glycogen content in liver in the treated vs untreated mice. The inability to affect the Akt/S6 signaling intermediates was not surprising as previous studies from our lab using the generic IL -6R antibody and skm-gp130KO study has shown that IL- 6 work on attenuation of body mass by inhibition of degradation pathway rather than rescuing the protein synthesis inhibition[19, 20]. sFcgp130 administration in $Apc^{Min/+}$ mouse led to an increase in expression of the gluconeogenic enzyme PEPCK while levels of the glycolytic enzyme PFK, which were elevated with cachexia progression were sustained. And tough this is the first study to report the role of glycolytic enzymes with trans – signaling inhibition, IL-6 signaling in general (both

classical and trans together) is known to induce gluconeogenesis[105]. Since chronic IL – 6 secretion is only seen with a diseased state increased gluconeogenesis provides the necessary fuel to sustain the elevated metabolic rate during disease. But we see an upregulated gluconeogenic response in the absence of plasma IL – 6 levels, suggesting that trans IL – 6 signaling might be inhibit gluconeogenesis during cachexia progression.

It is important to note that when compared to the PDTC treatment, WT mice treated with sFcgp130 did not increase S6 phosphorylation in the WT mice indicating a role for NF-kB in constitutively inhibiting baseline protein synthesis markers. As stated earlier the effect of PDTC on liver process could be minimized due suppression of NF- kB phosphorylation in the liver with cachexia progression but NF-kB is upregulated with cachexia progression in the skeletal muscle and PDTC administration rescues protein synthesis pathways in the cachectic skeletal muscle[21]. In conclusion, inhibition of IL – 6 related pathways attenuate cachexia progression by independent of the hepatic inflammation and anabolic state as measured by the Akt/mTOR pathway. However, loss of IL – 6 does alter liver metabolic functions possibly due to the indirect effect of IL – 6 on tumor development and growth.

3.6 ACKNOWLEDGEMENTS:

The authors thank Song Gao, Justin Hardee, Kimbell Hetzler and Dennis Fix for helping with all the animal sacrifice. The research described in this report was supported by research grant R01 CA121249 to JAC from the National Cancer Institute.

3.7 FIGURE LEGENDS:

Figure 1: Effect of PDTC treatment on tumor number and distribution in the cachectic *Apc*$^{Min/+}$ mouse A) Total tumor number in the intestine B) Tumor distribution according to tumor size in the intestine. Values are expressed as Mean ± SE. $P < 0.05$. A pre – planned t – test was performed between the PDTC treated and untreated groups.

Figure 2: Effect of PDTC treatment on the body mass in the wild type and cachectic *Apc*$^{Min/+}$ mouse. A) Percent change in body weight loss from Peak body weight to sacrifice weight B) Total fat mass C) Epididymal fat mass D) Total lean mass E) Total muscle weight F) Liver weight in the cachectic *Apc*$^{Min/+}$ mice. Values are expressed as Mean ± SE. $P < 0.05$. A Two – WAY ANOVA was used to analyze the data. Student – Newman Keul's post hoc test was used to analyze the main effects and interactions. A pre – planned t-test was used to determine the effect of PDTC treatment within the *Apc*$^{Min/+}$ $ - denotes different from all the other groups by ANOVA, * different from the *Apc*$^{Min/+}$ as compared by the pre – planned test

Figure 3: Effect of PDTC treatment on liver weight, glycogen and lipid content A) Histology images for PAS staining, counterstained with hematoxylin imaged at 10 X B) Morphometric analysis of the cachectic liver tissue represented as percentage of the stained/total area. C) Liver lipid content. Values are expressed as Mean ± SE. $P = 0.05$. * denotes significant difference from the PBS treated *Apc*$^{Min/+}$ mouse determined by a pre – planned t-test. Dotted line indicates the C57BL/6 control value

Figure 4: Effect of PDTC treatment on liver metabolic signaling A) mRNA expression of metabolic enzymes PEPCK and PFK. B) Protein expression for Akt/mTOR signaling. Values expressed as Mean ± SE $p = 0.05$ * denotes significant difference from the PBS

treated $Apc^{Min/+}$ mouse determined by a pre – planned t-test. Dotted line indicates the C57BL/6 control value

Figure 5: Effect of PDTC on systemic and liver inflammation. A) Plasma IL – 6 levels. B) Liver STAT-3 levels C) Haptaglobin mRNA levels D) Liver inflammatory markers. Mean ± SE. $P < 0.05$. A Two – WAY ANOVA was used to analyze the data. Student – Newman Keul's post hoc test was used to analyze the main effects and interactions. A pre – planned t-test was used to determine the effect of PDTC treatment within the $Apc^{Min/+}$ $ - denotes different from all the other groups by ANOVA, * different from the $Apc^{Min/+}$ as compared by the pre – planned test. An unpaired t – test was used to compare the effect of PDTC treatment between treatment and control groups in the $Apc^{Min/+}$

Figure 6: **Effect of sFcgp130 treatment on tumor number and distribution in the cachectic $Apc^{Min/+}$ mouse** A) Total tumor number in the intestine B) Tumor distribution according to tumor size in the intestine. Values are expressed as Mean ± SE. $P < 0.05$. A pre – planned t – test was performed between the sFcgp130 treated and untreated groups.

Figure 7: **Effect of sFcgp130 treatment on the body mass in the wild type and cachectic $Apc^{Min/+}$ mouse**. A) Percent change in body weight loss from Peak body weight to sacrifice weight B) Total fat mass C) Epidydimal fat mass D) Total lean mass E) Total muscle weight F) Liver weight in the cachectic $Apc^{Min/+}$ mice. Values are expressed as Mean ± SE. $P < 0.05$. A Two – WAY ANOVA was used to analyze the data. Student – Newman Keul's post hoc test was used to analyze the main effects and interactions. A pre – planned t-test was used to determine the effect of PDTC treatment within the $Apc^{Min/+}$ $

- denotes different from all the other groups by ANOVA, * different from the $Apc^{Min/+}$ as compared by the pre – planned test

Figure 8: **Effect of sFcgp130 treatment on liver weight, glycogen and lipid content** A) Histology images for PAS staining, counterstained with hematoxylin imaged at 10 X B) Morphometric analysis of the cachectic liver tissue represented as percentage of the stained/total area. C) Liver lipid content. Values are expressed as Mean ± SE. P = 0.05. * denotes significant difference from the PBS treated $Apc^{Min/+}$ mouse determined by a pre – planned t-test. Dotted line indicates the C57BL/6 control value

Figure 9: **Effect of sFcgp130 treatment on liver metabolic signaling** A) mRNA expression of metabolic enzymes PEPCK and PFK. B) Protein expression for Akt/mTOR signaling. Values expressed as Mean ± SE p = 0.05 * denotes significant difference from the PBS treated $Apc^{Min/+}$ mouse determined by a pre – planned t-test. Dotted line indicates the C57BL/6 control value

Figure 10: **Effect of sFcgp130 on systemic and liver inflammation**. A) Plasma IL – 6 levels. B) Liver STAT-3 levels C) Haptaglobin mRNA levels D) Liver inflammatory markers. Mean ± SE. P < 0.05. A Two – WAY ANOVA was used to analyze the data. Student – Newman Keul's post hoc test was used to analyze the main effects and interactions. A pre – planned t-test was used to determine the effect of sFcgp130 treatment within the $Apc^{Min/+}$ $ - denotes different from all the other groups by ANOVA, * different from the $Apc^{Min/+}$ as compared by the pre – planned test. An unpaired t – test was used to compare the effect of PDTC treatment between treatment and control groups in the $Apc^{Min/+}$

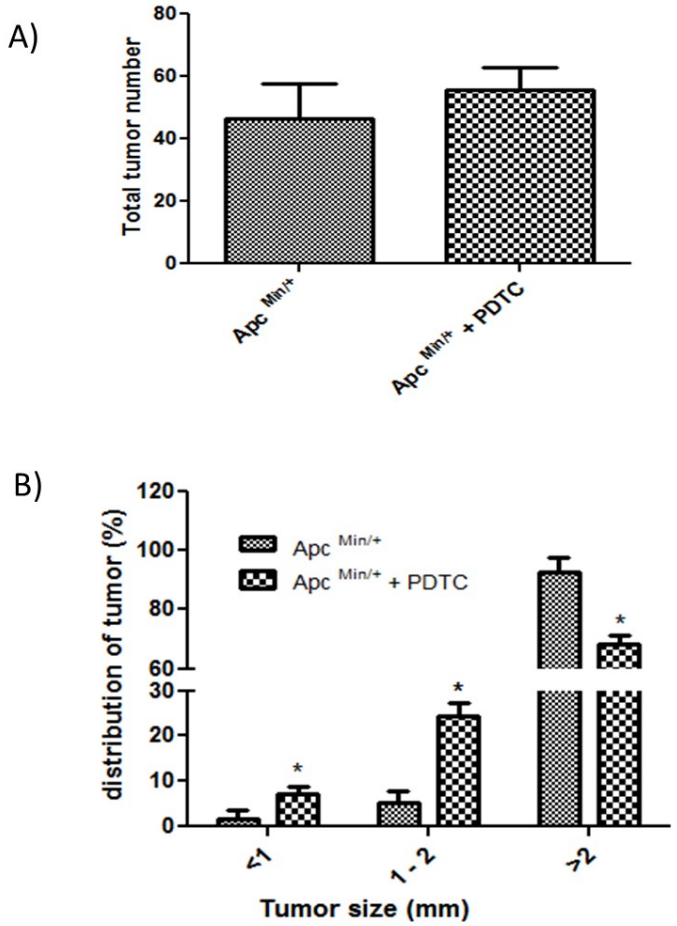

Figure 3.1: **Effect of PDTC treatment on tumor number and distribution in the cachectic *Apc*$^{Min/+}$ mouse** A) Total tumor number in the intestine B) Tumor distribution according to tumor size in the intestine. Values are expressed as Mean ± SE. $P < 0.05$. A pre – planned t – test was performed between the PDTC treated and untreated groups.

A)

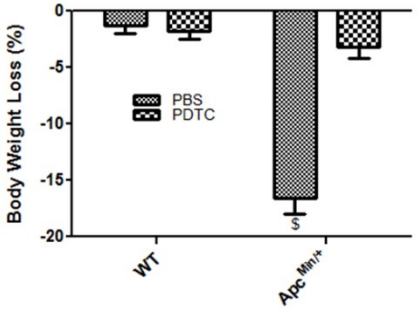

B)

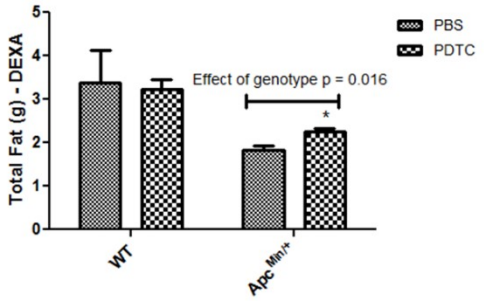

C)

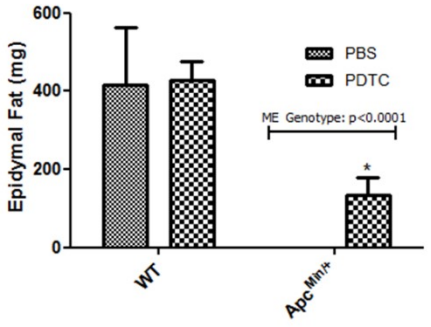

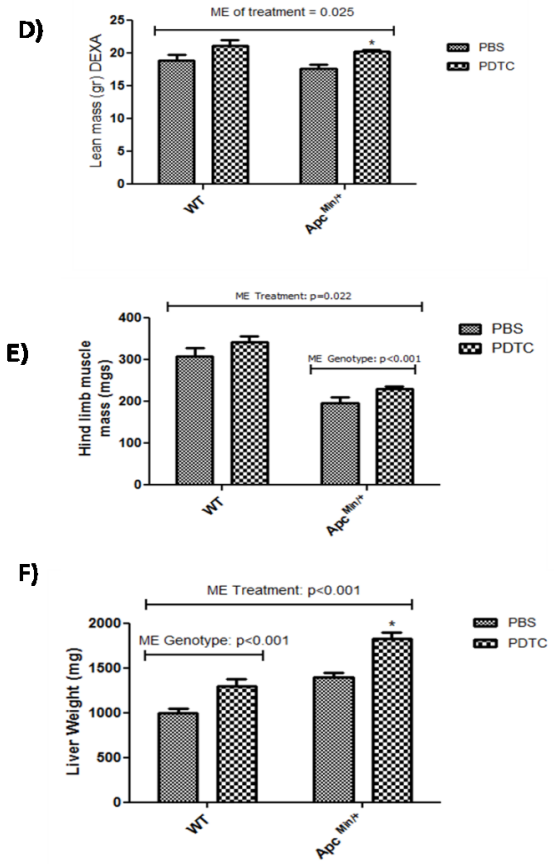

Figure 3.2: Effect of PDTC treatment on the body mass in the wild type and cachectic *Apc*$^{Min/+}$ mouse. A) Percent change in BW loss from Peak BW to sacrifice weight B) Total fat mass C) Epididymal fat mass D) Total lean mass E) Total muscle weight F) Liver weight in the cachectic *Apc*$^{Min/+}$ mice. Values are expressed as Mean ± SE. $P < 0.05$. A Two – WAY ANOVA with Student – Newman Keul's post hoc was used to analyze the data. A pre – planned t-test was used to determine the effect of PDTC treatment within the *Apc*$^{Min/+}$ $ - denotes different from all the other groups by ANOVA, * different from the *Apc*$^{Min/+}$ as compared by the pre – planned test

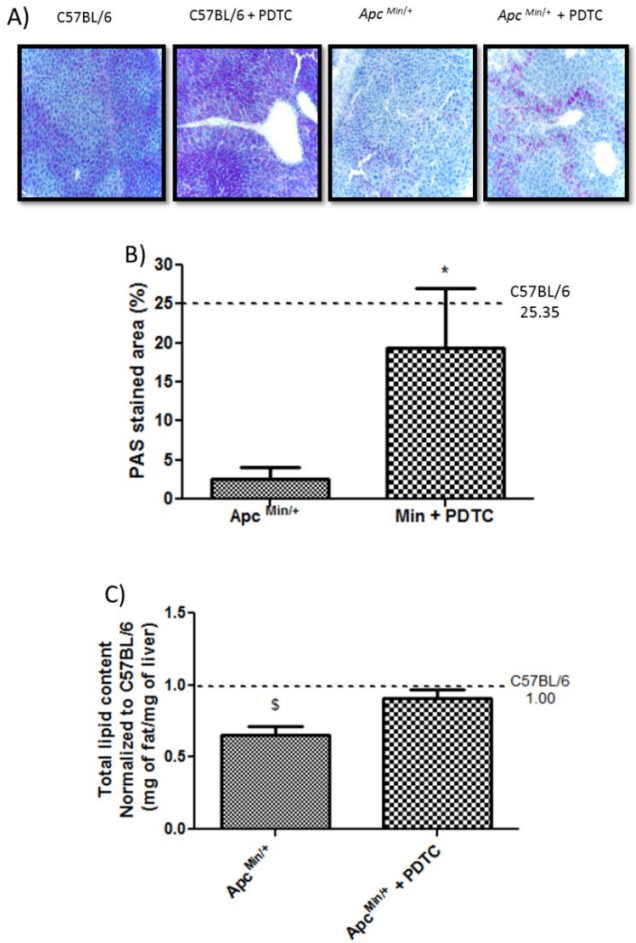

Figure 3.3: Effect of PDTC treatment on liver weight, glycogen and lipid content A) Histology images for PAS staining, counterstained with hematoxylin imaged at 10 X B) Morphometric analysis of the cachectic liver tissue represented as percentage of the stained/total area. C) Liver lipid content. Values are expressed as Mean ± SE. P = 0.05. * denotes significant difference from the PBS treated *Apc*$^{Min/+}$ mouse determined by a pre – planned t-test. Dotted line indicates B6 control value

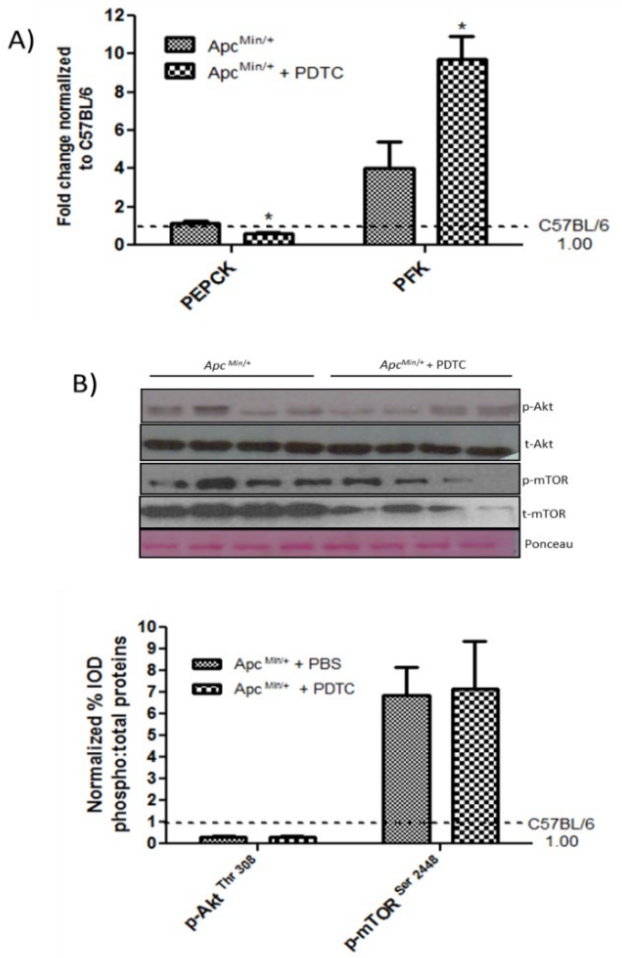

Figure 3.4: Effect of PDTC treatment on liver metabolic signaling A) mRNA expression of metabolic enzymes PEPCK and PFK. B) Protein expression for Akt/mTOR signaling. Values expressed as Mean ± SE p = 0.05 * denotes significant difference from the PBS treated *Apc*$^{Min/+}$ mouse determined by a pre – planned t-test. Dotted line indicates the C57BL/6 control value

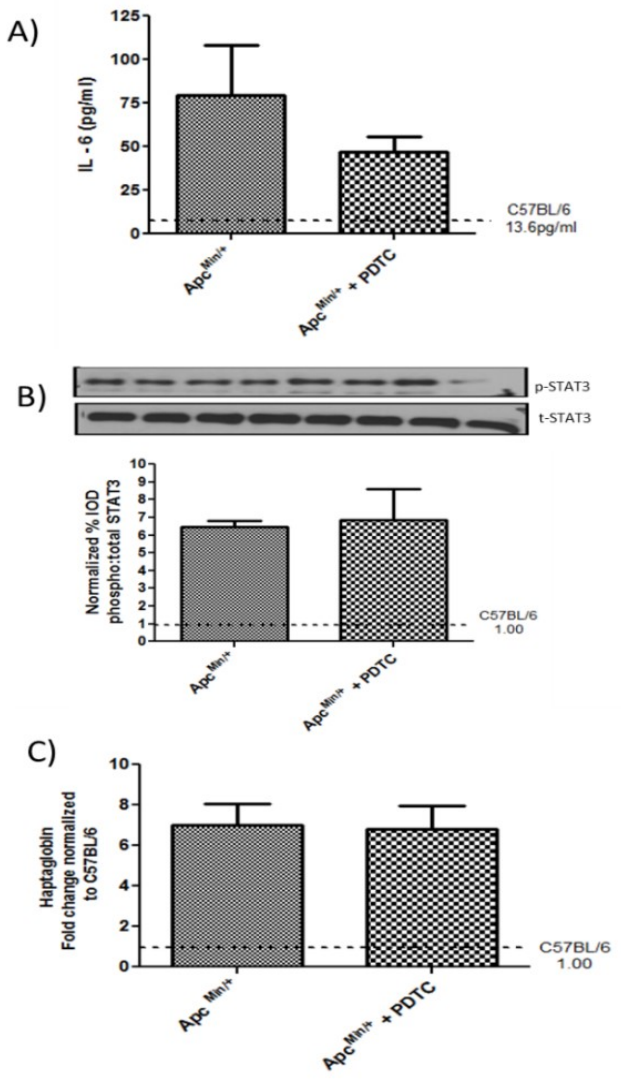

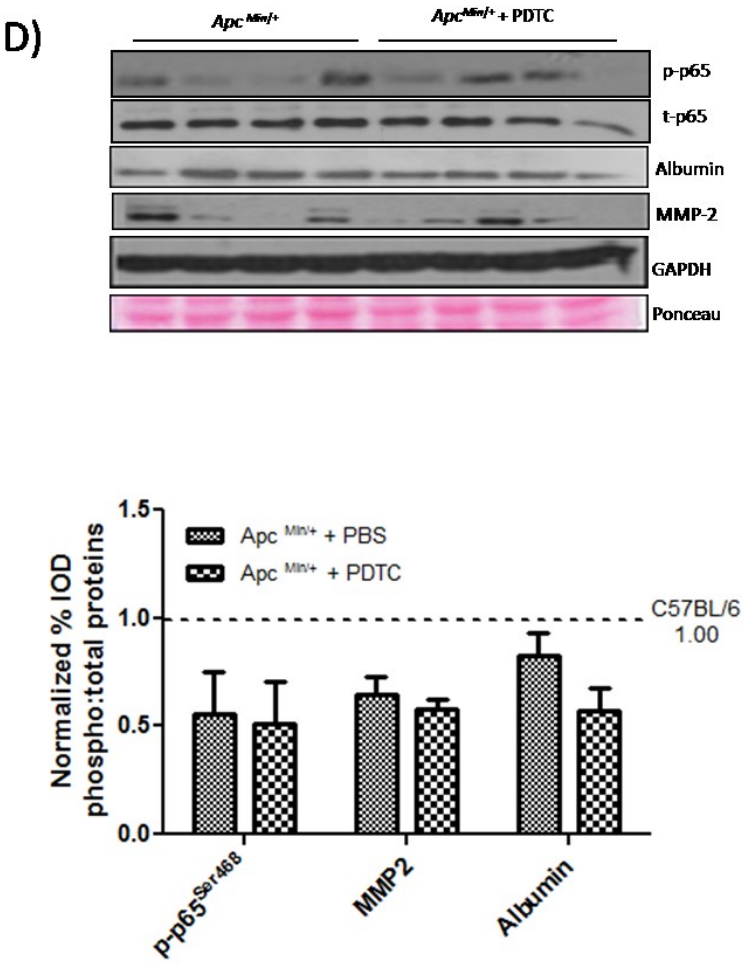

Figure 3.5: Effect of PDTC on systemic and liver inflammation. A) Plasma IL – 6 levels. B) Liver STAT-3 levels C) Haptaglobin mRNA levels D) Liver inflammatory markers. Mean ± SE. $P < 0.05$. A Two – WAY ANOVA was used to analyze the data. Student – Newman Keul's post hoc test was used to analyze the main effects and interactions. A pre – planned t-test was used to determine the effect of PDTC treatment within the *Apc*$^{Min/+}$

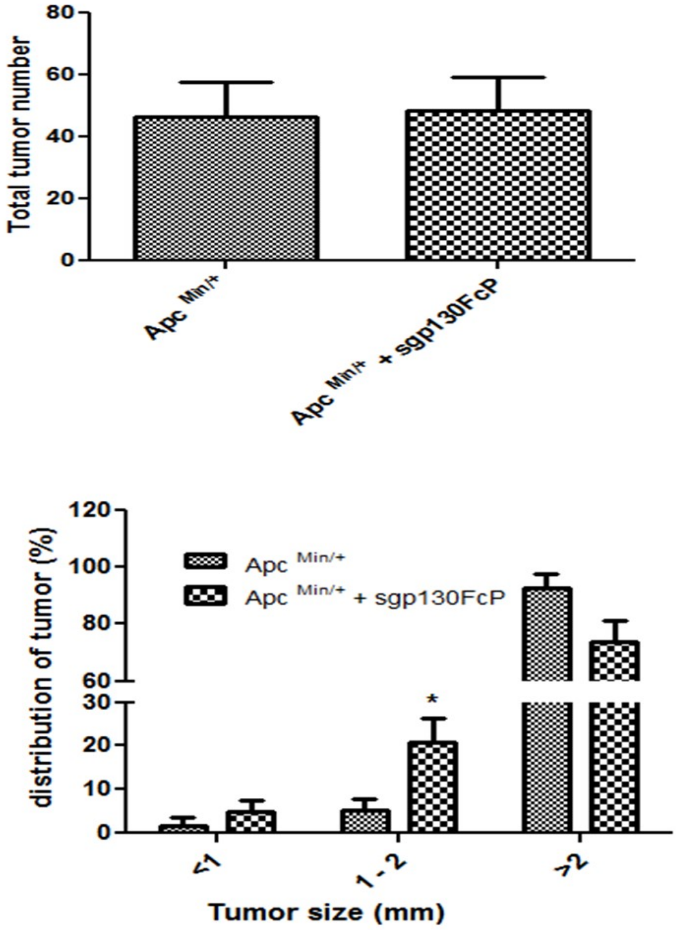

Figure 3.6: **Effect of sFcgp130 treatment on tumor number and distribution in the cachectic *Apc*$^{Min/+}$ mouse** A) Total tumor number in the intestine B) Tumor distribution according to tumor size in the intestine. Values are expressed as Mean ± SE. $P < 0.05$. A pre – planned t – test was performed between the sFcgp130 treated and untreated groups.

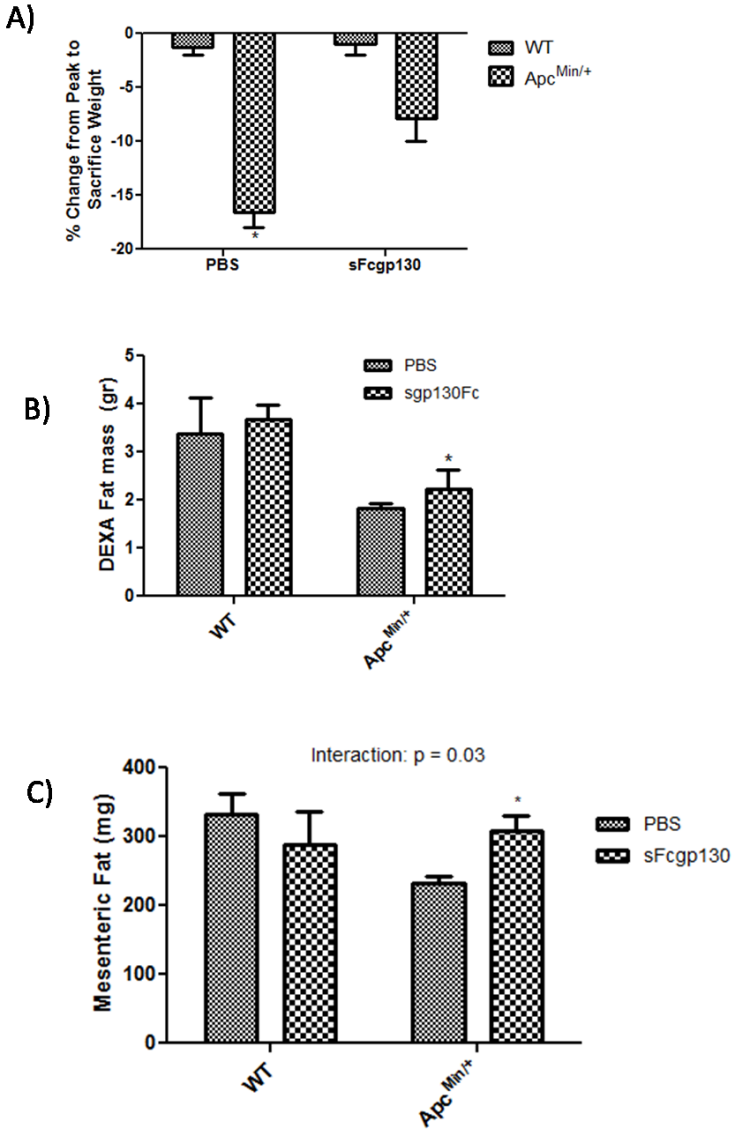

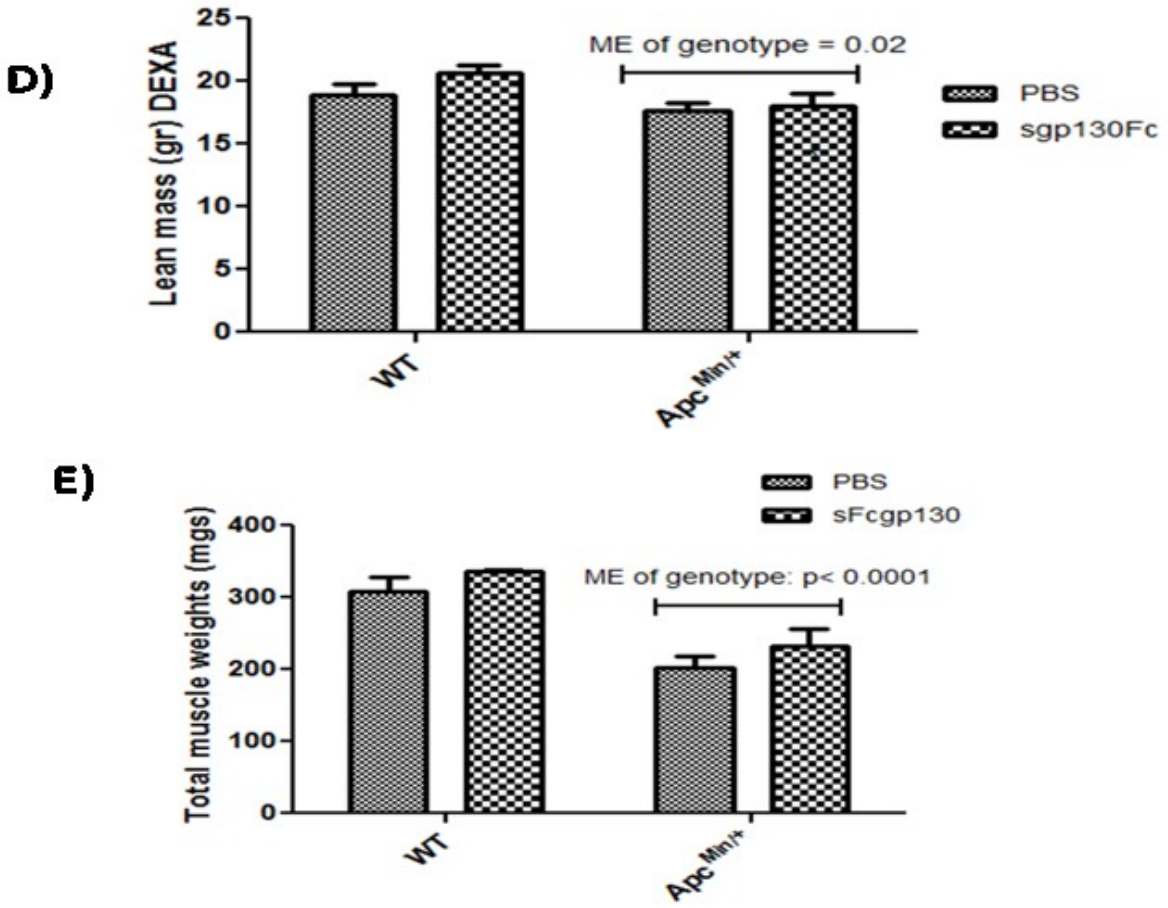

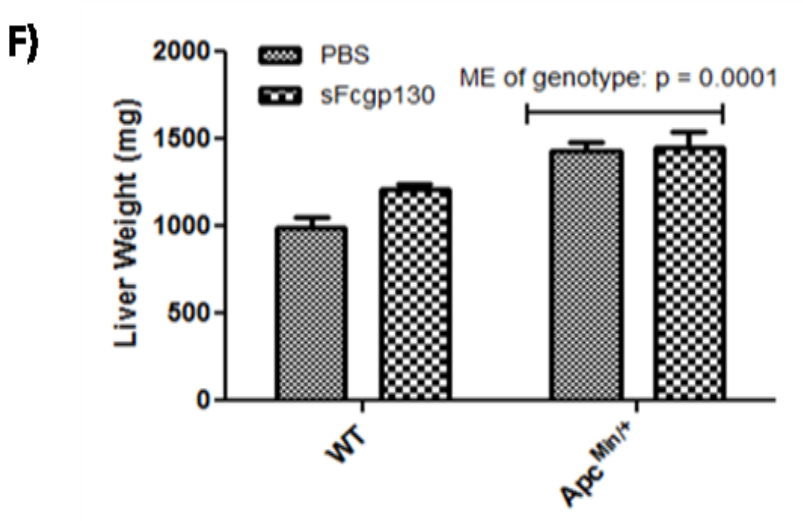

Figure 3.7: **Effect of sFcgp130 treatment on the body mass in the wild type and cachectic *Apc*$^{Min/+}$ mouse**. A) Percent change in body weight loss from Peak body weight to sacrifice weight B) Total fat mass C) Mesenteric fat mass D) Total lean mass E) Total muscle weight F) Liver weight in the cachectic *Apc*$^{Min/+}$ mice. Values are expressed as Mean ± SE. P < 0.05. A Two – WAY ANOVA was used to analyze the data. Student – Newman Keul's post hoc test was used to analyze the main effects and interactions. A pre – planned t-test was used to determine the effect of PDTC treatment within the *Apc*$^{Min/+}$ $ - denotes different from all the other groups by ANOVA, * different from the *Apc*$^{Min/+}$ as compared by the pre – planned test

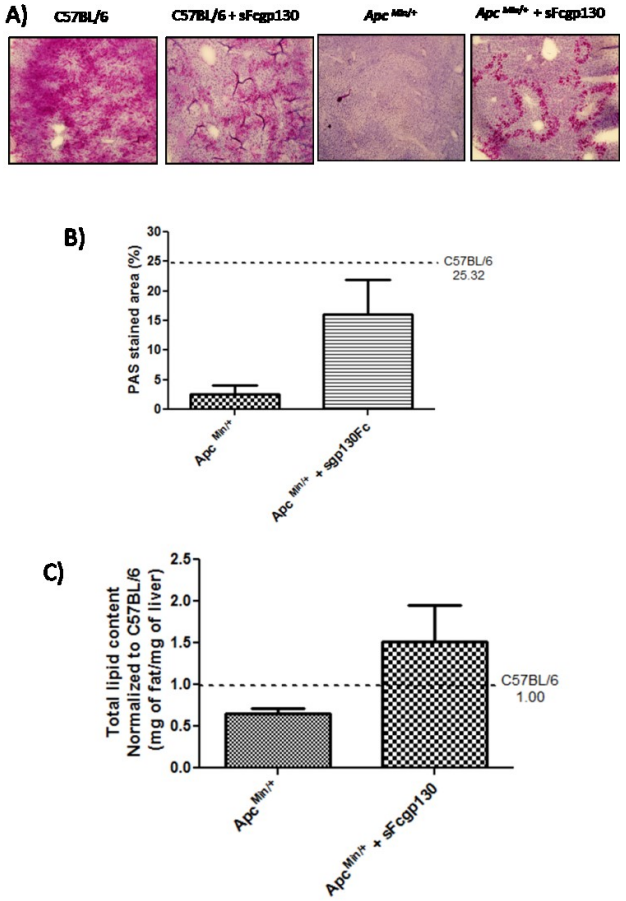

Figure 3.8: **Effect of sFcgp130 treatment on liver weight, glycogen and lipid content** A) Histology images for PAS staining, counterstained with hematoxylin imaged at 10 X B) Morphometric analysis of the cachectic liver tissue represented as percentage of the stained/total area. C) Liver lipid content. Values are expressed as Mean ± SE. P = 0.05. * denotes significant difference from the PBS treated $Apc^{Min/+}$ mouse determined by a pre – planned t-test. Dotted line indicates the C57BL/6 control value

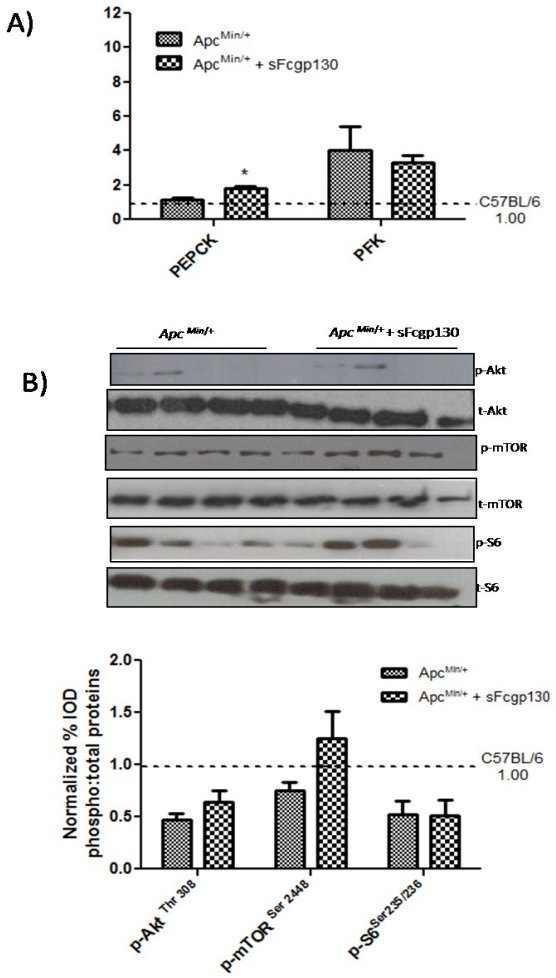

Figure 3.9: **Effect of sFcgp130 treatment on liver metabolic signaling** A) mRNA expression of metabolic enzymes PEPCK and PFK. B) Protein expression for Akt/mTOR signaling. Values expressed as Mean ± SE p = 0.05 * denotes significant difference from the PBS treated *Apc*$^{Min/+}$ mouse determined by a pre – planned t-test. Dotted line indicates the B6 control value

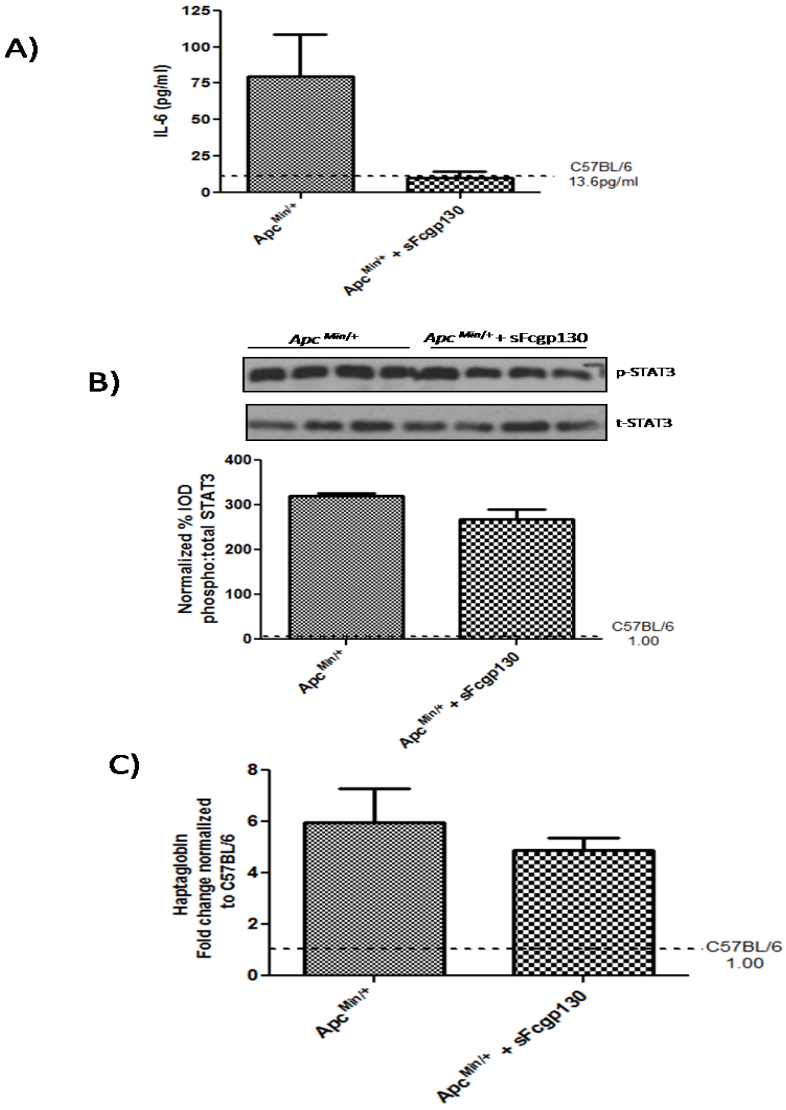

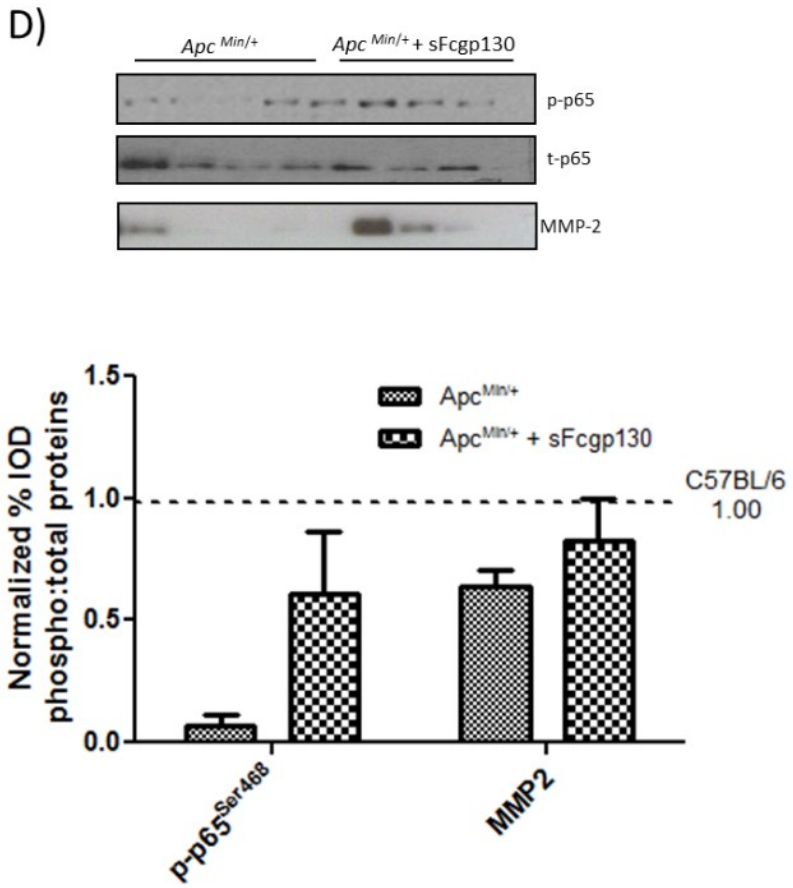

Figure 3.10: **Effect of sFcgp130 on systemic and liver inflammation**. A) Plasma IL – 6 levels. B) Liver STAT-3 levels C) Haptaglobin mRNA levels D) Liver inflammatory markers. Mean ± SE. $P < 0.05$. A pre – planned t-test was used to determine the effect of sFcgp130 treatment within the $Apc^{Min/+}$ * different from the $Apc^{Min/+}$ as compared by the pre – planned test.

CHAPTER 4

THE EFFECT OF AN ANTIBIOTIC TREATMENT ON LIVER FUNCTION IN CACHECTIC *APC*$^{MIN/+}$ MICE[3]

[3] Narsale, A., et. al, 2014 The Effect of an Antibiotic Treatment on Liver Function in an Cachectic ApcMin/+ mouse To be submitted to Biochemica et Biophysica et Acta

4.1 ABSTRACT:

Cachexia is a condition that occurs with many chronic diseases like cancer, AIDS and COPD. Patients suffering from cachexia display body weight loss that consists of both muscle and fat loss. The condition is also accompanied by metabolic disorders, lymphopenia, anemia and chronic inflammation. The $Apc^{Min/+}$ mouse model of cancer cachexia mimics many of these symptoms and is widely used for therapeutic testing. Wasting in the $Apc^{Min/+}$mouse is a downstream effect of the chronically activated inflammatory response primarily driven by pro-inflammatory cytokine IL – 6. However, cachectic mice also exhibit splenomegaly, hepatomegaly, swollen mesenteric lymph nodes, and elevated endotoxin levels which are associated with bacterial infection. Gut bacterial load through the portal vein can exacerbate liver inflammatory and metabolic status in severely cachectic $Apc^{Min/+}$ mouse. Therefore, we hypothesized that $Apc^{Min/+}$ mice treated with antibiotics targeting the gram – negative bacteria (Polymyxin) would attenuate cachexia progression and improve liver dysfunction. $Apc^{Min/+}$ mice were divided into to 3 groups (N = 10) consisting of the antibiotic treatment and a control group. The treatment was initiated at 13 weeks of age and mice were monitored till 20 weeks of age or when body temperature dropped below 34.5 ^{0}C. Livers from these mice were snap frozen and analyzed to study the inflammatory, anabolic and metabolic status of these mice. Antibiotic treatment reduced mesenteric lymph node swelling and spleen size as compared to untreated mice. Muscle wasting and fat pad loss was not alleviated by the antibiotic treatment. Also, circulating endotoxin levels were not affected by the administration of the antibiotic. Antibiotic treatment did not suppress liver STAT-3 phosphorylation nor liver haptaglobin mRNA expression. Antibiotic treatment failed to improve suppressed liver

glycogen stores or Akt signaling. We conclude that suppression of immune response does not rescue cachexia progression or liver function in the $Apc^{Min/+}$ mouse.

Keywords: Polymyxin, splenomegaly, STAT-3, IL -6, endotoxin

4.2 INTRODUCTION

Cancer Cachexia develops during the advanced stages of the disease and manifests as the progressive and massive loss of body weight in patients. This loss of body weight can be accounted for by a corresponding loss of muscle and fat loss in patient due to a chronic inflammatory state. High levels of plasma pro – inflammatory cytokines like IL – 6 and acute phase proteins (APP) have been shown to contribute to tissue loss in patients. Though chronic inflammation underlines all cachectic conditions, multiple factors contribute to this elevated immune response, complicating the treatment for cachexia.

The $Apc^{Min/+}$ mouse is model of colon cancer cachexia that mimics a gradual cachexia progression, as seen in humans. $Apc^{Min/+}$ mice initiate cachexia at approximately 14 weeks of age and are severely cachectic by 20 weeks of age. This loss of body mass in the $Apc^{Min/+}$ is dependent on the pro – inflammatory cytokine IL – 6, though levels of endotoxin are known to be upregulated in severely cachectic mice with a corresponding increase in gut permeability. Severely cachectic mice have negligible fat stores and depleted muscle mass, but are accompanied by a hypertrophy of the internal organs like spleen and the liver. Hepatomegaly is the $Apc^{Min/+}$ is interesting as it is accompanied by increased acute phase protein production but a depletion of liver glycogen, suppression of liver anabolic signaling by suppression of Akt – S6 activation and an increase in the glycolytic and gluconeogenic gene expression.

Suppression of systemic inflammation by inhibition of IL – 6 attenuates muscle and fat loss, but does not attenuate liver APR or STAT – 3 phosphorylation. But activation of STAT – 3 was seen even in non – cachectic mice, independent of IL – 6. Treatment of cachectic $Apc^{Min/+}$ mice with the STAT – 3/NF-kB inhibitor pyrrolidine dithiocarbamate (PDTC), did not attenuate liver APR or STAT – 3 phosphorylation. But it could be argued that inability of PDTC, to suppress plasma IL – 6 could be a factor in the upregulated liver APR in these mice. But liver STAT-3 and APR were not suppressed even in the gp130 fusion protein treated mice that did suppressed plasma IL – 6 levels. As chronic inflammation induced by a chronically activated immune cell proliferation and activation, leads to cachexia onset, it is possible a yet unknown signaling intermediate sustains liver APR independent of IL – 6. Interestingly, inhibition of the energy expensive APR is detrimental to survival in endotoxemic mice due the ability of acute phase proteins to activate the anti – inflammatory MDSCs in the septic tissue (20530204). Endotoxemia in the severely cachectic mouse could thus exacerbate hepatic inflammation (via the portal vein) aggravating systemic inflammation and hypermetabolism in the $Apc^{Min/+}$ mouse.

Cachectic $Apc^{Min/+}$ mice exhibit splenomegaly, hepatomegaly, swollen mesenteric lymph nodes, and elevated endotoxin levels which are associated with bacterial infection. Gut bacterial load through the portal vein has the potential to exacerbate liver inflammatory and metabolic status in severely cachectic $Apc^{Min/+}$ mouse. Gram – negative bacteria are known to be the major source of endotoxin due to their high LPS content and administration of antibiotics is the most common and effective method to suppress bacterial endotoxemia. Treatment of the $Apc^{Min/+}$ mouse with antibiotics could thus help reduce systemic bacterial load and endotoxemia. Thus the purpose of this study was to examine if antibiotic treatment

will attenuate cachexia progression and liver dysfunction in the cachectic $Apc^{Min/+}$ mouse. Mice were treated with the antibiotic – Polymyxin b at 13 weeks of age during the initiation of cachexia. Polymyxin at the dose of 1mg/ml was dissolved in drinking in water at fed to the mice starting 13 weeks of age to sacrifice. Polymyxin – b sulphate works by killing the gram – negative bacteria in the gut, and due to it prolonged administration was expected to suppress activation and proliferation of immune cells in the $Apc^{Min/+}$ mouse. Body weight, temperature were monitored throughout the course of the study. Mice were euthanized at 20 weeks of age and muscle and organs were harvested for further analysis.

4.3 METHODS AND MATERIALS:

4.3. I ANIMALS

All animal procedures were approved by the University of South Carolina's Institutional Animal Care and Use Committee. All mice were housed in standard cages and kept on a 12hr: 12hr light: dark cycle with the light period starting 0700 hrs. The mice were had an ad libitum access to water and food (standard rodent chow, cat. no. 8604 Rodent Diet; Harlan Teklad, Madison, WI). 12 week old C57BL/6 and $Apc^{Min/+}$ mice were single housed and monitored for Body weight loss, Food intake and body temperature, till sacrifice. Pre measurements for body weight and body temperature performed on the 12 week old mice and the $Apc^{Min/+}$ mice were randomized into either the control (untreated) group or Antibiotic treated group. C57BL/6 mice were used as absolute controls against the treated and untreated $Apc^{Min/+}$ adenoma model. A subset of the $Apc^{Min/+}$ mice were treated with antibiotic (1mg/ml), via drinking water, starting 13 weeks of age till sacrifice.

Body weight and body temperature (rectal probe TH-5 Thermalert Monitoring Thermometer (PhysiTemp, NJ, USA) was monitored on alternate days (Fig 1).

4.3. II ANTIBIOTIC TREATMENT ADMINISTRATION

Polymyxin b sulphate (Cat #, P4932, Sigma Aldrich, St. Louis, MO) was dissolved in drinking water (1mg/ml). Normal water bottle were replaced with medicated water bottles (15 ml capacity), in the treated cages. Medicated water was replenished everyday, to ensure that the mice had ad libitum access to the medicated water, throughout the course of the study.

4.3. III TISSUE COLLECTION

Mice were anesthetized by subcutaneous administration of a ketamine/xylazine/acepromazine (1.4mL/body weight) (Southern Anesthesia, Columbia, SC) cocktail as described earlier [106]. Plasma was collected prior to tissue collection via blood draws through the retro-orbital sinus. Muscle and liver were collected during the sacrifice and were either snap frozen in liquid nitrogen and stored at - 80^0C. Intestine segments were isolated, cleaned and cut into 4 equal segments of the small intestine and a segment for the colon. These were used to account for tumor burden in the cachectic *Apc* $^{Min/+}$ mice.

4.3. IV IL – 6 PLASMA LEVELS

IL – 6 levels in the plasma were quantified using the Mouse – IL – 6 ELISA kit (Life Technologies, NY, USA, Cat # KMC0062). Briefly, 25 – 50ul of plasma was diluted down to 100ul and the ELISA was performed according to manufacturer's instructions.

4.3. V RNA EXTRACTION, CDNA PREPARATION AND REAL – TIME PCR

Real time PCR was performed as described previously [76]. Briefly, RNA was isolated by homogenizing the liver tissue in Trizol (Invitrogen, NY, USA, Cat # 15596), followed by a chloroform/isopropyl alcohol extraction. cDNA and RT-PCR assays were performed using reagents purchased from (ABI, Foster City, USA). Primers for Haptaglobin[14], PFK[77] and PEPCK[77] primers purchased from IDT (Coralville, IA, USA). Data was analyzed using the comparative cycle threshold [Ct] method calculated by the ABI software.

4.3.VI WESTERN BLOT:

Western blots were performed as described previously [78]. Briefly, a piece of the liver was cut, weighed and placed in 10 times the volume of Muller Buffer. The tissue was homogenized in the buffer using a glass or glass homogenizer. The resultant homogenate was quantified for protein concentration using the Bradford assay. All protein samples were diluted to 3ug/ul concentration to aid equal loading on the gel. Homogenates were fractionated on SDS – PAGE acrylamide gels (6% - 15%) and transferred overnight onto a PVDF membrane. The membrane was Ponceaued following the transfer to ensure equal loading. The PVDF membrane was then probed for STAT-3, mTOR, S6, Akt, MMP-2, p-p65, GAPDH (Cell Signaling Technology, Danvers, MA, USA) gp130 and Albumin (Santa Cruz Biotechnology). A corresponding secondary antibody was used along with the chemiluminescent agent Quantum ECL (BioExpress, Kaysville, UT, USA) to visualize the protein bands. ImageJ (NIH, Bethesda, MD, USA) software was used for quantification of the integrated optical density (IOD) for Western blot bands.

4.3. VII PERIODIC ACID SCHIFF'S STAINING

A small piece of liver tissue was mounted on an OCT block and sectioned at -16^{0}C. The slides were fixed in Carnoy's fixative for 10 minutes followed by 30 minute incubation in the Periodic Acid. Slides were then washed with water and exposed to Schiff's reagent for 30 minutes. The slides were counter stained with Hematoxylin, dehydrated through alcohol grades and mounted using Permount. The slides were imaged the next day using the DP70 Olympus microscope.

4.3. VIII STATISTICAL ANALYSIS

All statistical analysis was performed using the GraphPad Prism software. One – Way ANOVA was used to test the effect of body weight, muscle mass, fat mass and organ mass with WT and the two (treated and untreated) *Apc*$^{Min/+}$ groups. Student Newman – Keul post hoc analysis was used to analyze the difference between groups. Pre – planned t – test was used to study the effect of treatment on the *Apc*$^{Min/+}$. Values were expressed as Mean ± SE. Significance was set at $p<0.05$.

4.4 RESULTS:

4.4.I EFFECT OF POLYMYXIN TREATMENT ON BODY MASS, TISSUE MASS, BODY TEMPERATURE AND PLASMA ENDOTOXIN LEVELS IN THE APC$^{MIN/+}$ MICE:

Severely cachectic *Apc*$^{Min/+}$ had a significant loss of body and muscle mass along with a loss of body temperature as measured by rectal temperature measures as compared to the healthy non – tumorous C57BL/6 mice. As shown previously and replicated in this study plasma endotoxin levels were also elevated in cachectic mice as cachectic mice as compared to the WT C57BL/6 mice. Splenomegaly, and hepatomegaly were some other

characteristics observed in the cachectic $Apc^{Min/+}$ mouse as compared to the WT animals (Fig 2A, 2C). Six weeks of antibiotic treatment with Polymyxin B did not attenuate any the cachectic characteristics with Polymyxin treated mice losing similar amounts of body mass, muscle mass, fat mass and body temperature. Levels of plasma endotoxin were also not different between the treated and untreated $Apc^{Min/+}$ mice (Table 1). However, antibiotic treatment did attenuate splenomegaly with the treated mice exhibiting a 22% decrease in spleen size ($p = 0.03$) in the polymyxin treated group (Fig 2A). Interestingly, Polymyxin treatment also significantly reduced size of mesenteric lymph nodes as compared to both the WT and the cachectic $Apc^{Min/+}$ mice (Fig2B), but did not attenuate hepatomegaly exhibited by the cachectic mice (Fig 2C).

4.4. II Effect of Polymyxin treatment on liver metabolic signaling

We have previously shown and replicated in this study that liver glycogen stores are severely depleted in the cachectic mice. Treatment with polymyxin attenuated glycogen stores as compared to the untreated $Apc^{Min/+}$ mouse (Fig 3A, 2B). Neither liver glycolytic enzyme PFK mRNA nor gluconeogenic enzyme PEPCK mRNA was significantly altered by Polymyxin administration to the cachectic mice (Fig 3C). Anabolic protein markers were not affected by antibiotic treatment in the cachectic mice (Fig 3D).

4.4. III Effect of Polymyxin treatment on liver inflammatory signaling

Administration of polymyxin did not reduce plasma IL – 6 levels in the treated cachectic mice (Fig 4A). Consequently, STAT-3 phosphorylation was sustained in the polymyxin treated ApcMin/+ liver. Hepatic haptaglobin (Fig 4C) the downstream target of STAT-3 too was sustained after Polymyxin treatment. Hepatic protein expression of NF-

kB, MMP-2 and albumin were unaffected by Polymyxin treatment in the *Apc*$^{Min/+}$ mouse (Fig 4D).

4.5 DISCUSSION:

Plasma endotoxin levels are increased with the progression of cachexia in the *Apc*$^{Min/+}$ mouse, which corresponds to an increase in gut barrier permeability[38]. Elevated levels of endotoxin have the potential to exacerbate the underlying chronic inflammatory response to cancer in the *Apc*$^{Min/+}$ mouse. The effect of an antibiotic treatment on *cachexia progression* from a non – cachectic to severely cachectic stage had not been examined. Thus, we determined if an antibiotic treatment consisting of administration of the gram – negative targeting antibiotic – Polymyxin could modulate an adjunct source of systemic inflammation and attenuate cachexia progression and liver dysfunction in the *Apc*$^{Min/+}$ mouse. We report that administration of Polymyxin inhibited splenomegaly and mesenteric lymph node swelling in the *Apc*$^{Min/+}$ mouse, indicating a possible suppression of immune cell proliferation in the treated mice. Moreover, attenuation of splenomegaly and mesenteric lymph node swelling did not attenuate cachexia progression in the antibiotic treated mice, possibly due to the inability of Polymyxin to attenuate plasma endotoxin and IL – 6 levels in the treated mice.

Administration of antibiotics in during infection is known to act independently of the immune response to eliminate the causative bacteria, thus speeding up the recovery process. Prolonged administration of antibiotics to the pre – cachectic *Apc*$^{Min/+}$ mice suppressed immune activation as evidenced by the shrinkage spleen and mesenteric lymph node weights. Thus is possible that bacterial toxins play a role in spleen and mesenteric lymph node enlargement in the cachectic mice. Surprisingly, antibiotic treatment did not

reduce plasma endotoxin levels in the treated mice. The lung and the liver are the major sites for endotoxin clearance in the body[107],[108] and liver dysfunction is seen in the severely cachectic *Apc*$^{Min/+}$ mice with a suppression of Akt/S6 signaling along with upregulation of CHOP a marker for liver apoptosis (Narsale et.al, 2014, Manuscript 1).As polymyxin treatment did exhibit systemic effects of immune suppression, the still elevated levels of endotoxin could be possibly due to the inability of the cachectic liver and lungs to clear systemic endotoxin levels brought in by the portal vein.

Hepatomegaly was not alleviated in the treated mice, possibly due to increased plasma IL – 6. Hepatic STAT-3 the downstream target of IL – 6, and haptaglobin a target of STAT-3 were elevated both in the treated and untreated *Apc*$^{Min/+}$ mice. Haptaglobin is a component of the acute phase protein response responsible for the degradation of skeletal muscle during cachexia[8], which can be activated by STAT-3 and ER stress[80, 104], but its suppression leads to decreased survival in the *Apc*$^{Min/+}$ mouse[23]. Thus increased haptaglobin levels tough detrimental to muscle mass are essential for survival. Consequently, we do not see an attenuation of muscle of fat loss in the treated *Apc*$^{Min/+}$ mice as compared to untreated controls. Our previous studies have established that liver STAT-3 phosphorylation is independent of plasma IL – 6 levels[109]. But administration of polymyxin did not attenuate liver STAT – 3, despite systemic suppression of immune proliferation. Activation of STAT- 3 along with IL – 6 can also be attributed to IL – 10, an anti – inflammatory cytokine often secreted by Kupffer cells in response to endotoxin as part of the local inflammatory response in the sinusoid[110]. It is known that nutrients and other toxins from the intestinal blood supply are first received by the liver via the portal vein. Kupffer cells in the liver are the first cells responsible of screening and clearance of

any toxins like endotoxin entering the system via the portal vein. It can be speculated that prolonged antibiotic treatment is unable to suppress hepatic APR due to a basal suppression of NF-kB along with sustained endotoxin and IL – 6 exposure.

Antibiotic treatment did not attenuate liver gluconeogenic and glycolytic markers PEPCK and PFKmRNA respectively, nor did it attenuate liver glycogen stores indicating that administration of antibiotic treatment did not affect systemic hypermetabolic state[99, 109]. Assuming that the antibiotic treatment did suppress systemic immune proliferation, this would suggest that the metabolic load from immune proliferation is redundant in the sustenance of a hypermetabolic state, making the hypermetabolic state a possible outcome of tumor burden and acute phase response proteins in the *Apc*$^{Min/+}$ mouse. In conclusion, antibiotic treatment attenuated splenomegaly and mesenteric lymph node swelling in the *Apc*$^{Min/+}$ mouse, independent of loss of body mass loss and elevated plasma endotoxin and inflammatory cytokines. But antibiotic treatment did not attenuate STAT-3, APR, metabolic markers or suppressed Akt/S6 signaling in the liver.

4.6 ACKNOWLEDGEMENTS:

The authors would like to acknowledge the technical expertise of Ms. Tia Davis and Ms. Pam Rudd for all their help with animal breeding and maintenance. The authors would also like to acknowledge the help of Dr. Jim White, Dr. Shuichi Sato, Dr. Kandy Velazquk and Song Gao for their help with the animal sacrifices and guidance and help with troubleshooting the laboratory techniques.

Table 4.1: Body weight, body temperature, endotoxin levels and muscle mass in the WT, treated and untreated *Apc*$^{Min/+}$ mice

Group	N	Peak Weight (g)	Sac Weight (g)	Body Weight Loss %	Rectal Temperature ^{o}C	Endotoxin levels EU/mL	Gasctrocnemius mass (mg)	Epididymal Fat (mg)
C57BL/6	5	27.6 ± 0.54	27.04 ± 0.52	- 2.0 % ± 1%	35.2 ± 0.13-	0.0 ± 0	112.0 ± 5.54	344 ± 28.01
Apc$^{Min/+}$	8	23.9 ± 036*	20 ± 0.58*	-13.0% ± 3%*	34.9 ± 0.26*	7.05 ± 1.44*	73.88 ± 4.72*	11.25 ± 9.53*
Apc$^{Min/+}$ + Polymyxin	6	22.9 ± 0.6*	20.98 ± 1.05*	-8.56% ± 3%*	34.22 ± 0.59*	7.07 ± 2.52*	75.6 ± 3.81*	0.00 ± 0.00*

WT type mice at 20 weeks were used as non – tumor bearing controls
Values expressed as Mean ± SE
* Signifies different from C57BL/6

Figure Legends:

Fig 4.1: Schematic Experimental Design: Mice were introduced into the study at 13 weeks of age and underwent pre measurements for body mass, activity and blood measurements. The mice were given 1mg/ml of antibiotic in drinking water starting 14 weeks of age till sacrifice. The control group received normal drinking water. Post measurements were performed the week before sacrifice at approximately 19 weeks of age. Mice were analyzed for body weight, rectal temperature, food intake and activity through the course of the study.

Fig 4.2: Effect of Polymyxin treatment on tissue mass in the *Apc*$^{Min/+}$ mice: A) Spleen Weight B) Mesenteric Fat Weight C) Liver weight. Values expressed as Mean ± SE. $p<0.05$. A One – Way ANOVA was used to test differences between WT, treated and untreated *Apc*$^{Min/+}$ groups. Student – Newman Keul's t-test was used to test for differences between any two groups. A pre – planned t –test was used to analyze the effect of polymyxin treatment in the *Apc*$^{Min/+}$ mouse. "a" represents significantly different from the untreated *Apc*$^{Min/+}$ mouse

Fig 4.3: Effect of Polymyxin treatment on liver metabolic signaling: A) Liver glycogen stores B) Morphometric analysis of liver glycogen stores C) Expression of metabolic mRNA levels PFK and PEPCK in the treated and untreated cachectic *Apc*$^{Min/+}$ mouse D) Protein synthesis signaling intermediates. Values expressed as Mean ± SE. $p<0.05$. A pre – planned t –test was used to analyze the effect of Polymyxin treatment within the *Apc*$^{Min/+}$. "a" represents significantly different from the untreated *Apc*$^{Min/+}$ mouse

Fig 4.4: Effect of Polymyxin treatment on hepatic inflammation: A) Plasma IL -6 levels B) Liver STAT-3 levels and C) Expression of metabolic mRNA levels for haptaglobin D) Liver Protein expression of inflammatory markers in the treated and untreated cachectic $Apc^{Min/+}$ mouse. Values expressed as Mean ± SE. $p<0.05$. A pre – planned t –test was used to analyze the effect of cachexia in the $Apc^{Min/+}$. "a" represents significantly different from the untreated $Apc^{Min/+}$ mouse

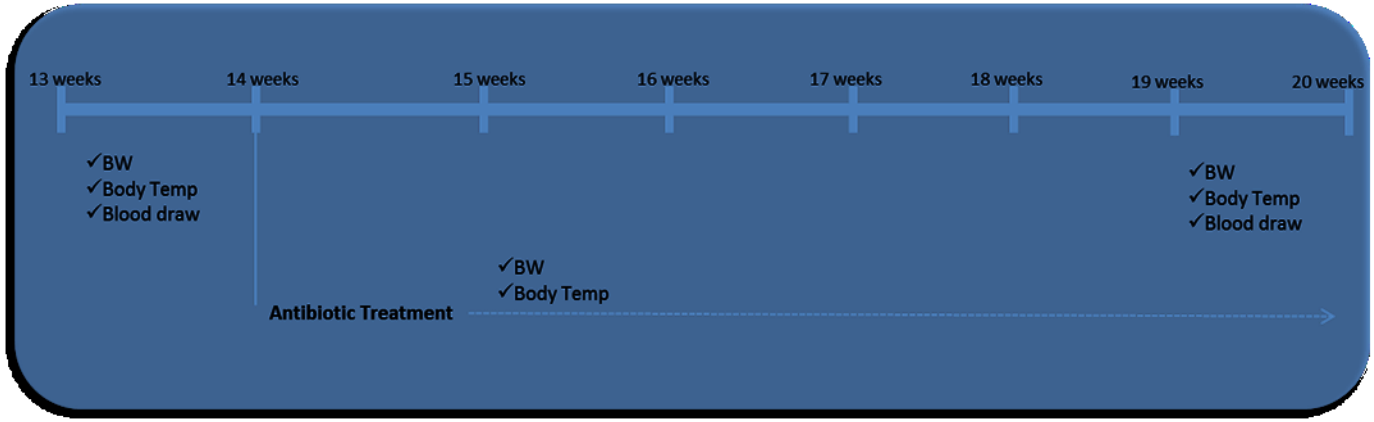

Figure 4.1: Schematic Experimental Design: Mice were introduced into the study at 13 weeks of age and underwent pre measurements for body mass, activity and blood measurements. The mice were given 1mg/ml of antibiotic in drinking water starting 14 weeks of age till sacrifice. The control group received normal drinking water. Post measurements were performed the week before sacrifice at approximately 19 weeks of age. Mice were analyzed for body weight, rectal temperature, food intake and activity through the course of the study.

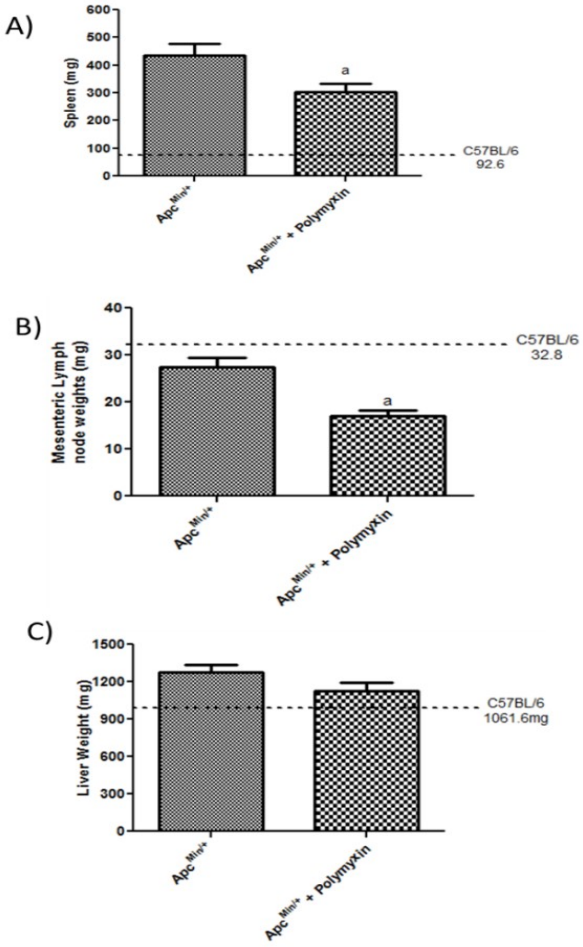

Figure 4.2: Effect of Polymyxin treatment on tissue mass in the *Apc*$^{Min/+}$ mice: A) Spleen Weight B) Mesenteric Fat Weight C) Liver weight. Values expressed as Mean ± SE. $p<0.05$. A One – Way ANOVA with Student – Newman Keul post hoc was used to test differences between WT, treated and untreated *Apc*$^{Min/+}$ groups. A pre – planned t –test was used to analyze the effect of polymyxin treatment in the *Apc*$^{Min/+}$ mouse. "a" represents significantly different from untreated *Apc*$^{Min/+}$

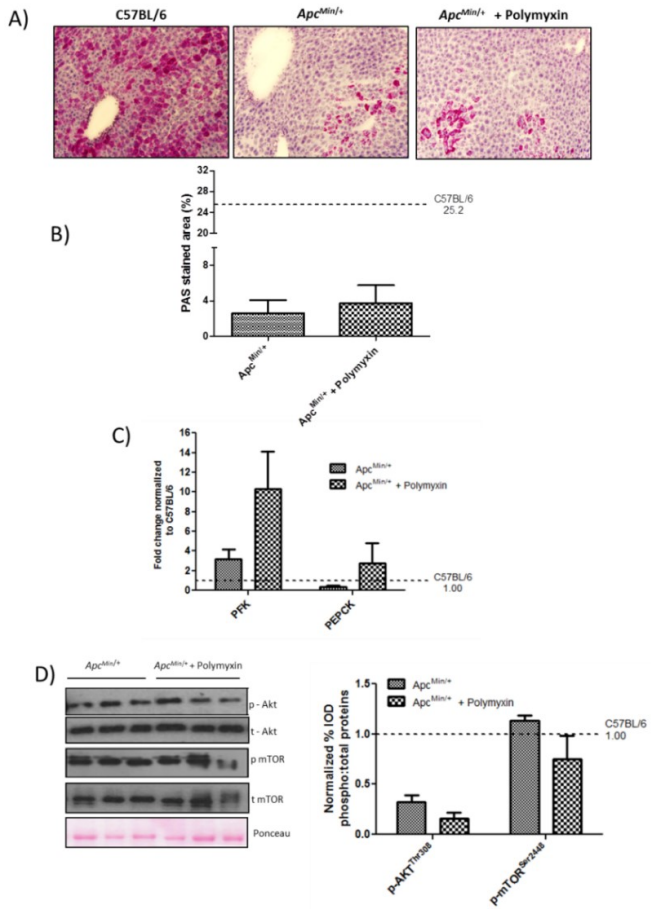

Figure 4.3: Effect of Polymyxin treatment on liver metabolic signaling: A) Liver glycogen stores B) Morphometric analysis of liver glycogen stores C) Expression of metabolic mRNA levels PFK and PEPCK in the treated and untreated cachectic *Apc*$^{Min/+}$ mouse D) Protein synthesis signaling intermediates. Values expressed as Mean ± SE. $p<0.05$. A pre – planned t –test was used to analyze the effect of Polymyxin treatment within the *Apc*$^{Min/+}$. "a" represents significantly different from the untreated *Apc*$^{Min/+}$

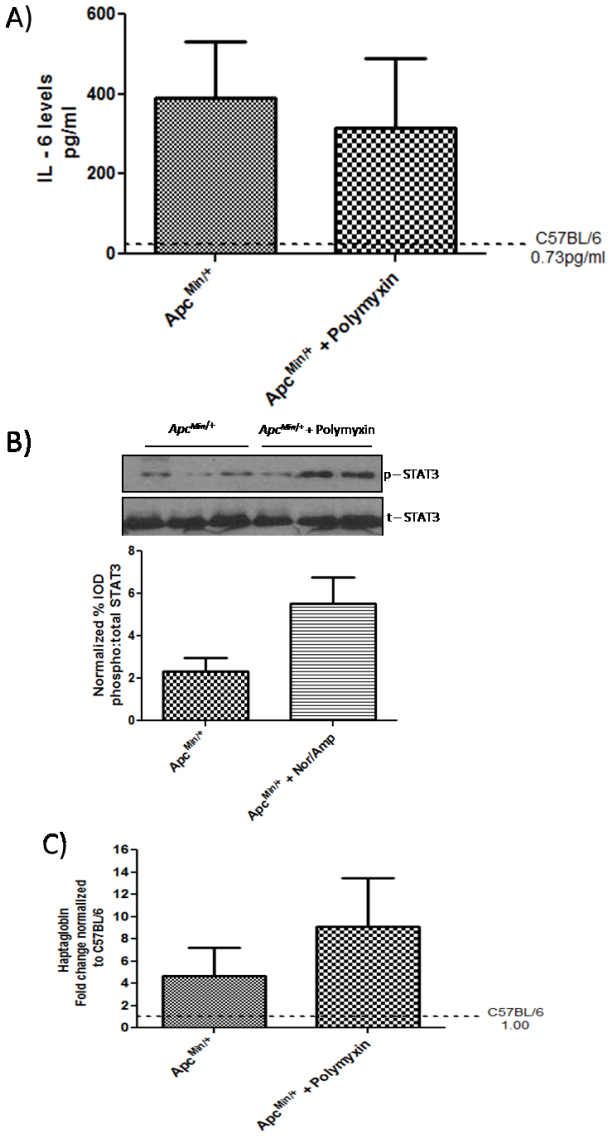

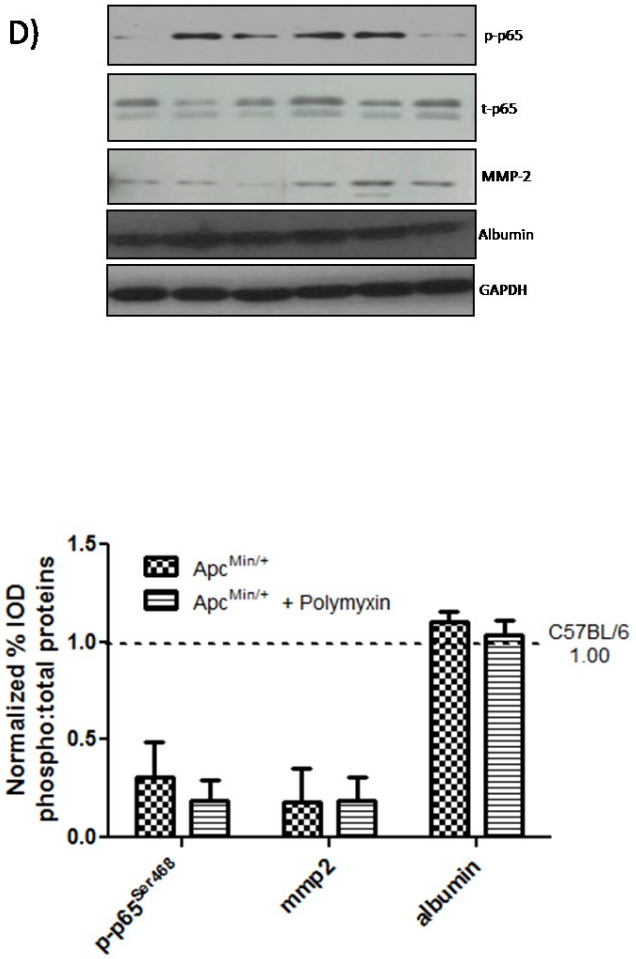

Figure 4.4: Effect of Polymyxin treatment on hepatic inflammation: A) Plasma IL -6 levels B) Liver STAT-3 levels and C) Expression of metabolic mRNA levels for haptaglobin D) Liver Protein expression of inflammatory markers in the treated and untreated cachectic *Apc*$^{Min/+}$ mouse. Values expressed as Mean ± SE. $p<0.05$. A pre – planned t –test was used to analyze the effect of cachexia in the *Apc*$^{Min/+}$. "a" represents significantly different from the untreated *Apc*$^{Min/+}$ mouse

CHAPTER 5

OVERALL DISCUSSION

Overall, the purpose of this study was to look at the role of liver function with cachexia progression using the *Apc*$^{Min/+}$ model of cancer cachexia. Liver function for the purpose of this study was defined as markers of liver inflammation, metabolic function and protein synthesis and cachexia progression was measured by tracking body weight and muscle and fat mass. We report the novel finding that ER stress pathways are activated in the liver of non – cachectic mice along with a suppression of liver glycogen stores and the gluconeogenic enzyme PEPCK and an IL – 6 independent activation of STAT-3. However cachexia progression leads to activation of the ER stress induced apoptotic marker CHOP, suppresses phosphorylation of Akt and S6 independent of mTOR and a STAT -3 dependent acute phase response. Interestingly, cachexia progression downregulates the inflammatory mediator NF –κB along with its downstream target MMP-2. Changes in liver function related to inflammation and protein synthesis are independent of IL – 6, tumor burden or activated immune responses as suppression of systemic IL – 6 and endotoxin levels failed to affect these pathways during cachexia progression. On the other hand, decrease in tumor burden independent did attenuate metabolic processes in the liver along with improving liver glycogen stores.

Cachexia Progression in the *Apc*$^{Min/+}$ can be characterized by a gradual IL – 6 dependent loss of muscle mass starting 14 weeks of age. We have previously established that during this period the mice also exhibit fat loss, gut barrier dysfunction, elevated plasma endotoxin levels, hypertrophy of the spleen, elevated liver triglycerides levels, anemia and insulin resistance[19, 38, 72, 106]. In this study we extend our finding in the *Apc*$^{Min/+}$ to the role of liver during cachexia progression. Analysis of liver pathology with establishes that severely cachectic mice display a regenerative phenotype along with signs of liver injury . However, mitotic marker ERK phosphorylation was inhibited in the cachectic liver suggesting an inhibition of growth. Since the mice used for pathology and the ones used for the rest of the analysis come from two different subsets, it is possible that they follow different trajectories of cachexia progression. However, both results indicate a disruption of liver function in severely cachectic mice. Interestingly, we see an upregulation of the ER stress markers in liver prior to the onset of cachexia. Since IL – 6 levels in plasma are elevated only during cachexia progression; induction of ER stress could be induced by elevated levels of plasma MCP -1[80]. MCP – 1 is a chemokine secreted by the tumor microenvironment to attract more macrophages to the site of the tumor [18]. However, MCP – 1 has been recently implicated in the induction of ER stress in the liver leading to the inhibition of NF – κB[80]. We see similar results in the liver as cachexia progression surprisingly suppresses liver NF-κB expression in the face of elevated plasma IL – 6 and endotoxin levels. MMP-2, a fibrosis and angiogenic marker and the downstream target of NF – κB is also suppressed actively with cachexia progression. This suppression possibly aids in protecting the liver from fibrosis, thus maximizing liver function[111]. On the other hand, cachexia progression steers liver signaling towards an ER stress induced inhibition

of protein synthesis pathways in the liver along with activation of the apoptotic marker CHOP in the severely cachectic mice. However it is interesting to note that inhibition of Akt/S6 phosphorylation is independent of mTOR phosphorylation. This dysregulation the Akt/mTOR/S6 pathway could be due to stimulation of mTOR by the amino acids broken down and shuttled to the liver to sustain the body's acute phase response and basal metabolic rate[8]. However, severely cachectic mice lack the ability to utilize this mTOR phosphorylation as expression of the downstream marker S6 remains suppressed. Also, the current study only measures the baseline activity of Akt/S6 phosphorylation, and it is possible that stimulation of hepatocytes by an anabolic stimulus like glucose could still be able to stimulate Akt and S6 phosphorylation in the $Apc^{Min/+}$. Despite the suppression of anabolic processes in the liver, the energy demand continues to be high as estimated from the upregulation of the glycolytic and gluconeogenic liver enzymes. However, it is possible that due to the ER stress induced inhibition of protein synthesis these do not get converted to functional proteins in the liver. Taken together, cachexia progression is detrimental to liver function and possibly survival with inhibition survival markers like Akt, ERK and NF-κB and upregulation of the apoptotic marker CHOP[104, 112, 113]. As cachexia progression in the $Apc^{Min/+}$ mice is a function of liver plasma IL – 6 levels and IL – 6 mediated STAT-3 activation can induce acute phase protein haptaglobin, we investigated the role of IL – 6 inhibition on liver function in the $Apc^{Min/+}$ mouse

Administration of PDTC, a global STAT-3 and NF-kB inhibitor attenuated body weight loss in the $Apc^{Min/+}$ mouse by sparing of both muscle and fat loss. PDTC further exacerbated hepatomegaly and did not suppress plasma IL – 6 levels seen in the $Apc^{Min/+}$ mouse indicating a partial effect of the drug on indices of cachexia progression. Analysis

of muscle tissue treated with PDTC exhibited an attenuation of STAT-3 and NF – κB levels, however the treatment had no effect on hepatic STAT-3 levels. Furthermore, contradictory to our hypothesis, NF – κB mediated liver inflammation was actively suppressed in the cachectic liver, minimizing the efficacy of PDTC in the liver. PDTC suppresses activation of STAT-3 and NF – κB by downregulating reactive oxygen species stimulated by chronic inflammation[21, 29, 114]. However its ineffectiveness in the liver, points towards a lack of oxidative damage. PDTC treatment affected tumor distribution by reducing the number of large tumors either by inhibiting of tumor growth or by shrinkage of large tumors. It is important to note that the shift in tumor distribution was seen during a sustained IL – 6 response. Reduction in tumor burden is associated with an attenuation of basal metabolic rate and PDTC treated mice did attenuate hepatic glycogen and lipid stores as compared to the untreated *Apc*$^{Min/+}$ mice[29]. Administration of PDTC also suppressed PEPCK mRNA, but surprisingly it further upregulated the glycolytic enzyme PFK. However a recent study with the endotoxemia model has shown that PDTC administration can suppress PEPCK mRNA possibly via suppression of systemic ROS, validating its efficacy in the liver[115]. It was speculated that sustained plasma IL – 6 response could be reason sustained STAT-3 and haptaglobin activation in the liver post PDTC treatment, but his hypothesis was rejected when STAT-3 and haptaglobin levels were sustained even in the sFcgp130 mice, which reduced plasma IL – 6 levels in the fusion protein treated *Apc*$^{Min/+}$ mice. This is the first study to report the effect of trans – IL -6 inhibition on liver function during cachexia progression in the *Apc*$^{Min/+}$ mouse. We report that inhibition of trans – IL6 signaling rescues fat loss, but does not rescue total lean mass. Further, sFcgp130 administration has no effect on hepatomegaly. Liver Akt/mTOR/S6 pathway and liver inflammatory pathways are also

not altered by fusion protein administration. Thus deterioration of liver function during cachexia progression seems to be independent of IL – 6 which contributes towards wasting of peripheral tissue to feed the metabolic demands of the liver. However, IL – 6 is not causal to liver dysfunction in the $Apc^{Min/+}$ mouse.

The severely cachectic $Apc^{Min/+}$ mouse shows elevated levels of plasma endotoxin. As endotoxin levels are only observed towards the later stages of cachexia due to increased gut permeability it is unclear if these levels of LPS further exacerbate cachexia progression in the $Apc^{Min/+}$ [16]. Antibiotic treatment was administered to the $Apc^{Min/+}$ mouse prior to cachexia initiation to eliminate gut bacteria in the $Apc^{Min/+}$[116]. Surprisingly administration of gut bacteria in the $Apc^{Min/+}$ mouse suppressed splenomegaly and mesenteric lymph node swelling. As both the spleen and the mesenteric lymph nodes are secondary lymphoid organs associated with activation of immune cells, it can be speculated that antibiotic administration suppressed cellular immune response in the $Apc^{Min/+}$. However, this also opens up the possibility that proliferation of immune cells in the $Apc^{Min/+}$ mouse is a function of systemic bacteria that leads to splenomegaly, independent of the plasma IL – 6 levels which were comparable to the untreated $Apc^{Min/+}$ mouse. Surprisingly, plasma endotoxin levels were also not affected by the antibiotic treatment opening up the possibility that elevated levels of plasma endotoxin in the $Apc^{Min/+}$ are due to the inability of the cachectic liver/lungs to filter plasma endotoxin levels[108]. However this suppression of immune responses did not attenuate liver dysfunction as characterized in the $Apc^{Min/+}$. Thus in conclusion, liver function is disrupted with cachexia progression in the $Apc^{Min/+}$ mouse, however this dysfunction is not related to the pro – inflammatory cytokine IL – 6, which is primarily responsible for muscle and fat wasting or factor responsible for inducing

hypertrophy of spleen and mesenteric lymph nodes. Liver dysfunction could be a response to chronic ER stress in the liver, possibly initiated by exposure to plasma MCP – 1 level.

REFERENCES

1. Tisdale, M.J. Mechanisms of cancer cachexia. *Physiological reviews* **89**, 381-410 (2009).
2. Fearon, K. Cancer cachexia: mediators, signaling, and metabolic pathways. *Cell Metab*, 153-166 (2012).
3. Fearon, K., Arends, J. & Baracos, V. Understanding the mechanisms and treatment options in cancer cachexia. *Nat Rev Clin Oncol* **10**, 90-99.
4. Groarke, J.D., Cheng, S., Jones, L.W. & Moslehi, J. Cancer cachexia: getting to the heart of the matter. *Eur Heart J*.
5. Tisdale, M.J. Cachexia in cancer patients. *Nat Rev Cancer* **2**, 862-871 (2002).
6. Lieffers, J.e.a. A viscerally driven cachexia syndrome in patients with advanced colorectal cancer: contributions of organ and tumor mass to whole-body energy demands. *The American Journal of Clinical Nutrition*, 1173 - 1179 (2009).
7. Lawson, D.H., Richmond, A., Nixon, D.W. & Rudman, D. Metabolic approaches to cancer cachexia. *Annu Rev Nutr* **2**, 277-301 (1982).
8. Bonetto, A., et. al STAT3 Activation in Skeletal Muscle Links Muscle Wasting and the Acute Phase Response in Cancer Cachexia. *Plos One*, e22538 (2011).
9. Nguyen, P. *et al.* Liver lipid metabolism. *J Anim Physiol Anim Nutr (Berl)* **92**, 272-283 (2008).
10. Yamaguchi, Y., Yamaguchi, K., Babb, J.L. & Gans, H. In vivo quantitation of the rat liver's ability to eliminate endotoxin from portal vein blood. *J Reticuloendothel Soc* **32**, 409-422 (1982).
11. Siegel, A.B. & Zhu, A.X. Metabolic syndrome and hepatocellular carcinoma: two growing epidemics with a potential link. *Cancer* **115**, 5651-5661 (2009).
12. Llovet, J.M., Bru, C. & Bruix, J. Prognosis of hepatocellular carcinoma: the BCLC staging classification. *Semin Liver Dis* **19**, 329-338 (1999).
13. Todd Gersten, M., Edn. 9/20/20132013).
14. Bonetto, A. *et al.* STAT3 activation in skeletal muscle links muscle wasting and the acute phase response in cancer cachexia. *PLoS One* **6**, e22538.
15. Jones, A., et.al, TSC22D4 is a molecular output of hepatic wasting metabolism. *EMBO molecular medicine*, 294 - 308 (2013).
16. Puppa, M. Gut barrier dysfunction in the Apc(Min/+) mouse model of colon cancer cachexia. *Biochim Biophys Acta* **1812**, 1601-1606 (2011).
17. White, J.P. *et al.* Muscle mTORC1 suppression by IL-6 during cancer cachexia: a role for AMPK. *Am J Physiol Endocrinol Metab* **304**, E1042-1052.

18. McClellan, J., et.al. Intestinal inflammatory cytokine response in relation to tumorigenesis in the Apc(Min/+) mouse. *Cytokine.*, 113-119 (2012).
19. White, J.P. *et al.* The regulation of skeletal muscle protein turnover during the progression of cancer cachexia in the Apc(Min/+) mouse. *PLoS One* **6**, e24650.
20. Puppa, M.J., Gao, S., Narsale, A.A. & Carson, J.A. Skeletal muscle glycoprotein 130's role in Lewis lung carcinoma-induced cachexia. *FASEB J.*
21. Puppa, M.J., Murphy, E.A., Fayad, R., Hand, G.A. & Carson, J.A. Cachectic Skeletal Muscle Response to a Novel Bout of Low Frequency Stimulation. *J Appl Physiol (1985)*.
22. Murphy, E.A., Davis, J.M., McClellan, J.L. & Carmichael, M.D. Quercetin's effects on intestinal polyp multiplicity and macrophage number in the Apc(Min/+) mouse. *Nutr Cancer* **63**, 421-426.
23. Barbour, K.W., Davis, T., White, A., Baumann, H. & Berger, F.G. Haptoglobin, inflammation, and tumorigenesis in the MIN mouse. *Redox Rep* **6**, 366-368 (2001).
24. Jones, S.A., Richards, P.J., Scheller, J. & Rose-John, S. IL-6 transsignaling: the in vivo consequences. *J Interferon Cytokine Res* **25**, 241-253 (2005).
25. Croker, B.A. *et al.* SOCS3 negatively regulates IL-6 signaling in vivo. *Nat Immunol* **4**, 540-545 (2003).
26. Fischer, C.P. Interleukin-6 in acute exercise and training: what is the biological relevance? *Exerc Immunol Rev* **12**, 6-33 (2006).
27. Rose-John, S. IL-6 trans-signaling via the soluble IL-6 receptor: importance for the pro-inflammatory activities of IL-6. *Int J Biol Sci* **8**, 1237-1247.
28. DP., K. Cachexia. **133** (2000).
29. Norton, J. Cancer cachexia. *Critical Reviews in Oncology/Hematology*, 289-327 (1987).
30. Inui, A. Cancer anorexia-cachexia syndrome: are neuropeptides the key? *Cancer Res.*, 4493-4501. (1999).
31. MJ., T. Mechanisms of Cancer Cachexia. *Physiological Reviews*, 381 - 410 (2009).
32. Sallie, R., et. al Drugs and the liver part 1: Testing liver function. *Biopharmaceutics & Drug Disposition*, 251 - 259 (1991).
33. al., H.C.e. Altered glucose metabolism in metastatic carcinoma. *Cancer Research*, 3710 - 3714 (1975).
34. Serrano, A. Interleukin-6 Is an Essential Regulator of Satellite Cell-Mediated Skeletal Muscle Hypertrophy. *Cell metabolism*, 33 - 44 (2008).
35. Haddad, F. IL-6-induced skeletal muscle atrophy. *Journal of Applied Physiology*, 911 - 917 (2005).
36. JA, C. Interleukin-6 as a Key Regulator of Muscle Mass during Cachexia. *Exerc Sport Sci Rev*, 168 - 176 (2010).

37. JOHN-ROSE, S. IL-6 TRANS-SIGNALING VIA THE SOLUBLE IL-6 RECEPTOR: IMPORTANCE FOR THE PRO-INFLAMMATORY ACTIVITIES OF IL-6. *INTERNATIONAL JOURNAL OF BIOLOGICAL SCIENCES*, 1237 - 1247 (2012).
38. PUPPA, M., ET. AL THE EFFECT OF EXERCISE ON IL-6-INDUCED CACHEXIA IN THE APCMIN/+ MOUSE. *J CACHEXIA SARCOPENIA MUSCLE*, 117 - 137 (2012).
39. HIRANO, T. SIGNALING MECHANISMS THROUGH GP130: A MODEL OF THE CYTOKINE SYSTEM. *CYTOKINE GROWTH FACTOR REV*, 241-252 (1997).
40. KISHIMOTO, T. CYTOKINE SIGNAL TRANSDUCTION. *CELL*, 253 - 262 (1994).
41. TAKAHASHI-TEZUKA M, E.A. GAB1 ACTS AS AN ADAPTER MOLECULE LINKING THE CYTOKINE RECEPTOR GP130 TO ERK MITOGEN-ACTIVATED PROTEIN KINASE. *MOL. CELL BIOL.*, 4109-4117. (1998).
42. KIM, T., ET.AL, IL - 6 INDUCTION OF TLR -4 GENE EXPRESSION VIA STAT3 HAS AN EFFECT ON INSULIN RESISTANCE IN HUMAN SKELETAL MUSCLE. *ACTA DIABETOL* (2011).
43. FRITSCHE, L. IL-6 DEFICIENCY IN MICE NEITHER IMPAIRS INDUCTION OF METABOLIC GENES IN THE LIVER NOR AFFECTS BLOOD GLUCOSE LEVELS DURING FASTING AND MODERATELY INTENSE EXERCISE. *DIABETOLOGIA.*, 1732-1742 (2010).
44. KIM, H. DIFFERENTIAL EFFECTS OF INTERLEUKIN - 6 AND INTERLEUKIN 10 ON SKELETAL MUSCLE AND LIVER INSULIN ACTION IN VIVO. *DIABETES.*, 1060 - 1067 (2004).
45. GUBBINS, P. EFFECT OF INTERLEUKIN 6 ON THE HEPATIC METABOLISM OF ITRACONAZOLE AND ITS METABOLITE HYDROXYITRACONAZOLE USING PRIMARY HUMAN HEPATOCYTES. *PHARMACOLOGY*, 195 - 201 (2003).
46. NAUGLER, W. GENDER DISPARITY IN LIVER CANCER DUE TO SEX DIFFERENCES IN MYD88-DEPENDENT IL-6 PRODUCTION. *SCIENCE.*, 121-124. (2007).
47. HAN, D.-W. INTESTINAL ENDOTOXEMIA AS A PATHOGENETIC MECHANISM IN LIVER FAILURE. *WORLD J GASTROENTEROL*, 961 - 965 (2002).
48. RIVERA, C., ET. AL. ROLE OF ENDOTOXIN IN THE HYPERMETABOLIC STATE AFTER ACUTE ETHANOL EXPOSURE. *AM J PHYSIOL*, G1252-1258. (1998).
49. MASUBUCHI, Y. ENDOTOXIN-MEDIATED DISTURBANCE OF HEPATIC CYTOCHROME P450 FUNCTION AND DEVELOPMENT OF ENDOTOXIN TOLERANCE IN THE RAT MODEL OF DEXTRAN SULFATE SODIUM-INDUCED EXPERIMENTAL COLITIS. *DRUG METABOLISM AND DISPOSITION*, 437–441 (2004).
50. BOELSTERLI U., E.A. EFFECTS OF ENDOTOXIN TOLERANCE ON HEPATIC EXCRETORY FUNCTION: IN VIVO STUDY. *TOXICOLOGY LETTERS*, 207 - 212 (1982).
51. J., G. TOLL-LIKE RECEPTOR 4 SIGNALING IN LIVER INJURY AND HEPATIC FIBROGENESIS. *FIBROSIS AND TISSUE REPAIR*, 21 (2010).
52. A., G. MODE OF ACTION OF POLYMYXIN B: PHYSIOLOGICAL STUDIES WITH BACILLUS SUBTILIS-RESISTANT MUTANT. *ANTIMICROB AGENTS CHEMOTHER*, 366-369 (1975).
53. DC, M. BINDING OF POLYMYXIN B TO THE LIPID A PORTION OF BACTERIAL LIPOPOLYSACCHARIDES. *IMMUNOCHEMISTRY.*, 813-818. (1976).
54. GOLDSTEIN, E.J.C. NORFLOXACIN, A FLUOROQUINOLONE ANTIBACTERIAL AGENT: CLASSIFICATION, MECHANISM OF ACTION, AND IN VITRO ACTIVITY. *THE AMERICAN JOURNAL OF MEDICINE*, 3 - 17 (1987).

55. ADACHI, Y. ANTIBIOTICS PREVENT LIVER INJURY IN RATS FOLLOWING LONG-TERM EXPOSURE TO ETHANOL *GASTROENTEROLOGY*, 218–224 (1995).
56. TAZI, E. & ERRIHANI, H. TREATMENT OF CACHEXIA IN ONCOLOGY. *INDIAN J PALLIAT CARE* **16**, 129-137.
57. LIEFFERS, J.R. *ET AL.* A VISCERALLY DRIVEN CACHEXIA SYNDROME IN PATIENTS WITH ADVANCED COLORECTAL CANCER: CONTRIBUTIONS OF ORGAN AND TUMOR MASS TO WHOLE-BODY ENERGY DEMANDS. *AM J CLIN NUTR* **89**, 1173-1179 (2009).
58. HOLROYDE, C.P., SKUTCHES, C.L., BODEN, G. & REICHARD, G.A. GLUCOSE METABOLISM IN CACHECTIC PATIENTS WITH COLORECTAL CANCER. *CANCER RESEARCH* **44**, 5910-5913 (1984).
59. PUPPA, M.J. *ET AL.* GUT BARRIER DYSFUNCTION IN THE APC(MIN/+) MOUSE MODEL OF COLON CANCER CACHEXIA. *BIOCHIM BIOPHYS ACTA* **1812**, 1601-1606.
60. LEITCH, E.F. *ET AL.* COMPARISON OF THE PROGNOSTIC VALUE OF SELECTED MARKERS OF THE SYSTEMIC INFLAMMATORY RESPONSE IN PATIENTS WITH COLORECTAL CANCER. *BR J CANCER* **97**, 1266-1270 (2007).
61. KOUKOURAKIS, M.I. *ET AL.* ENDOGENOUS MARKERS OF HYPOXIA/ANAEROBIC METABOLISM AND ANEMIA IN PRIMARY COLORECTAL CANCER. *CANCER SCI* **97**, 582-588 (2006).
62. SASSE, D. DYNAMICS OF LIVER GLYCOGEN: THE TOPOCHEMISTRY OF GLYCOGEN SYNTHESIS, GLYCOGEN CONTENT AND GLYCOGENOLYSIS UNDER THE EXPERIMENTAL CONDITIONS OF GLYCOGEN ACCUMULATION AND DEPLETION. *HISTOCHEMISTRY* **45**, 237-254 (1975).
63. MCCALLUM, R.E. & BERRY, L.J. EFFECTS OF ENDOTOXIN ON GLUCONEOGENESIS, GLYCOGEN SYNTHESIS, AND LIVER GLYCOGEN SYNTHASE IN MICE. *INFECT IMMUN* **7**, 642-654 (1973).
64. BRADLEY, S.G. CELLULAR AND MOLECULAR MECHANISMS OF ACTION OF BACTERIAL ENDOTOXINS. *ANNU REV MICROBIOL* **33**, 67-94 (1979).
65. FEARON, K.C., GLASS, D.J. & GUTTRIDGE, D.C. CANCER CACHEXIA: MEDIATORS, SIGNALING, AND METABOLIC PATHWAYS. *CELL METAB* **16**, 153-166.
66. PRESTON, T. *ET AL.* FIBRINOGEN SYNTHESIS IS ELEVATED IN FASTING CANCER PATIENTS WITH AN ACUTE PHASE RESPONSE. *J NUTR* **128**, 1355-1360 (1998).
67. AGUSTSSON, T. *ET AL.* MECHANISM OF INCREASED LIPOLYSIS IN CANCER CACHEXIA. *CANCER RES* **67**, 5531-5537 (2007).
68. MURPHY, K.T., CHEE, A., TRIEU, J., NAIM, T. & LYNCH, G.S. IMPORTANCE OF FUNCTIONAL AND METABOLIC IMPAIRMENTS IN THE CHARACTERIZATION OF THE C-26 MURINE MODEL OF CANCER CACHEXIA. *DIS MODEL MECH* **5**, 533-545.
69. JONES, A. *ET AL.* TSC22D4 IS A MOLECULAR OUTPUT OF HEPATIC WASTING METABOLISM. *EMBO MOL MED* **5**, 294-308.
70. FEARON, K.C., VOSS, A.C. & HUSTEAD, D.S. DEFINITION OF CANCER CACHEXIA: EFFECT OF WEIGHT LOSS, REDUCED FOOD INTAKE, AND SYSTEMIC INFLAMMATION ON FUNCTIONAL STATUS AND PROGNOSIS. *AM J CLIN NUTR* **83**, 1345-1350 (2006).
71. WHITE, J.P., PUPPA, M.J., NARSALE, A. & CARSON, J.A. CHARACTERIZATION OF THE MALE APCMIN/+ MOUSE AS A HYPOGONADISM MODEL RELATED TO CANCER CACHEXIA. *BIOL OPEN* **2**, 1346-1353.

72. Baltgalvis, K.A. *et al.* Interleukin-6 and cachexia in ApcMin/+ mice. *American journal of physiology. Regulatory, integrative and comparative physiology* **294**, R393-401 (2008).
73. White, J.P. *et al.* Muscle oxidative capacity during IL-6-dependent cancer cachexia. *Am J Physiol Regul Integr Comp Physiol* **300**, R201-211.
74. McClellan, J.L. *et al.* Intestinal inflammatory cytokine response in relation to tumorigenesis in the Apc(Min/+) mouse. *Cytokine* **57**, 113-119.
75. McMillan, D.C. *et al.* Longitudinal study of body cell mass depletion and the inflammatory response in cancer patients. *Nutr Cancer* **31**, 101-105 (1998).
76. White, J.P. *et al.* Overload-induced skeletal muscle extracellular matrix remodelling and myofibre growth in mice lacking IL-6. *Acta Physiol (Oxf)* **197**, 321-332 (2009).
77. Seth, R.K. *et al.* Environmental toxin-linked nonalcoholic steatohepatitis and hepatic metabolic reprogramming in obese mice. *Toxicol Sci* **134**, 291-303.
78. White, J.P., Baltgalvis, K.A., Sato, S., Wilson, L.B. & Carson, J.A. Effect of nandrolone decanoate administration on recovery from bupivacaine-induced muscle injury. *J Appl Physiol (1985)* **107**, 1420-1430 (2009).
79. Zhang, Y. *et al.* Activation of the nuclear receptor FXR improves hyperglycemia and hyperlipidemia in diabetic mice. *Proc Natl Acad Sci U S A* **103**, 1006-1011 (2006).
80. Kolattukudy, P.E. & Niu, J. Inflammation, endoplasmic reticulum stress, autophagy, and the monocyte chemoattractant protein-1/CCR2 pathway. *Circ Res* **110**, 174-189.
81. Barton, B.E. & Murphy, T.F. Cancer cachexia is mediated in part by the induction of IL-6-like cytokines from the spleen. *Cytokine* **16**, 251-257 (2001).
82. Bansal, M.B. *et al.* Interleukin-6 protects hepatocytes from CCl4-mediated necrosis and apoptosis in mice by reducing MMP-2 expression. *J Hepatol* **42**, 548-556 (2005).
83. Hsu, P.P. & Sabatini, D.M. Cancer cell metabolism: Warburg and beyond. *Cell* **134**, 703-707 (2008).
84. Vander Heiden, M.G., Cantley, L.C. & Thompson, C.B. Understanding the Warburg effect: the metabolic requirements of cell proliferation. *Science* **324**, 1029-1033 (2009).
85. Sutherland, C., O'Brien, R.M. & Granner, D.K. New connections in the regulation of PEPCK gene expression by insulin. *Philos Trans R Soc Lond B Biol Sci* **351**, 191-199 (1996).
86. Quinn, P.G. & Yeagley, D. Insulin regulation of PEPCK gene expression: a model for rapid and reversible modulation. *Curr Drug Targets Immune Endocr Metabol Disord* **5**, 423-437 (2005).
87. Kahn, C.R., Lauris, V., Koch, S., Crettaz, M. & Granner, D.K. Acute and chronic regulation of phosphoenolpyruvate carboxykinase mRNA by insulin and glucose. *Mol Endocrinol* **3**, 840-845 (1989).

88. Wang, B., Hsu, S.H., Frankel, W., Ghoshal, K. & Jacob, S.T. Stat3-mediated activation of microRNA-23a suppresses gluconeogenesis in hepatocellular carcinoma by down-regulating glucose-6-phosphatase and peroxisome proliferator-activated receptor gamma, coactivator 1 alpha. *Hepatology* **56**, 186-197.
89. Brauer, M. *et al.* Insulin protects against hepatic bioenergetic deterioration induced by cancer cachexia: an in vivo 31P magnetic resonance spectroscopy study. *Cancer Res* **54**, 6383-6386 (1994).
90. Elsharkawy, A.M. & Mann, D.A. Nuclear factor-kappaB and the hepatic inflammation-fibrosis-cancer axis. *Hepatology* **46**, 590-597 (2007).
91. Lavon, I. *et al.* High susceptibility to bacterial infection, but no liver dysfunction, in mice compromised for hepatocyte NF-kappaB activation. *Nat Med* **6**, 573-577 (2000).
92. Taub, R. Hepatoprotection via the IL-6/Stat3 pathway. *J Clin Invest* **112**, 978-980 (2003).
93. Jin, X. *et al.* Paradoxical effects of short- and long-term interleukin-6 exposure on liver injury and repair. *Hepatology* **43**, 474-484 (2006).
94. Ji, C. & Kaplowitz, N. ER stress: can the liver cope? *J Hepatol* **45**, 321-333 (2006).
95. Ma, Y., Brewer, J.W., Diehl, J.A. & Hendershot, L.M. Two distinct stress signaling pathways converge upon the CHOP promoter during the mammalian unfolded protein response. *J Mol Biol* **318**, 1351-1365 (2002).
96. Hetz, C., Chevet, E. & Harding, H.P. Targeting the unfolded protein response in disease. *Nat Rev Drug Discov* **12**, 703-719.
97. Garbers, C. *et al.* Inhibition of classic signaling is a novel function of soluble glycoprotein 130 (sgp130), which is controlled by the ratio of interleukin 6 and soluble interleukin 6 receptor. *J Biol Chem* **286**, 42959-42970.
98. Zimmers, T.A., McKillop, I.H., Pierce, R.H., Yoo, J.Y. & Koniaris, L.G. Massive liver growth in mice induced by systemic interleukin 6 administration. *Hepatology* **38**, 326-334 (2003).
99. Narsale, A.e.a. Role of Cachexia Progression on Liver Function in the *Apc*$^{Min/+}$ Mouse. *In preparation* (2014).
100. Streetz, K.L. *et al.* Lack of gp130 expression in hepatocytes promotes liver injury. *Gastroenterology* **125**, 532-543 (2003).
101. Lim, S.K. *et al.* Increased susceptibility in Hp knockout mice during acute hemolysis. *Blood* **92**, 1870-1877 (1998).
102. Hochepied, T., Ameloot, P., Brouckaert, P., Van Leuven, F. & Libert, C. Differential response of a(2)-macroglobulin-deficient mice in models of lethal TNF-induced inflammation. *Eur Cytokine Netw* **11**, 597-601 (2000).
103. Burgess-Beusse, B.L. & Darlington, G.J. C/EBPalpha is critical for the neonatal acute-phase response to inflammation. *Mol Cell Biol* **18**, 7269-7277 (1998).
104. Verfaillie, T., Garg, A.D. & Agostinis, P. Targeting ER stress induced apoptosis and inflammation in cancer. *Cancer Lett* **332**, 249-264.

105. Ritchie, D.G. Interleukin 6 stimulates hepatic glucose release from prelabeled glycogen pools. *Am J Physiol* **258**, E57-64 (1990).
106. Mehl, K.A. *et al.* Decreased intestinal polyp multiplicity is related to exercise mode and gender in ApcMin/+ mice. *J Appl Physiol (1985)* **98**, 2219-2225 (2005).
107. Nakatani, Y. *et al.* Endotoxin clearance and its relation to hepatic and renal disturbances in rats with liver cirrhosis. *Liver* **21**, 64-70 (2001).
108. Fox, E.S., Thomas, P. & Broitman, S.A. Clearance of gut-derived endotoxins by the liver. Release and modification of 3H, 14C-lipopolysaccharide by isolated rat Kupffer cells. *Gastroenterology* **96**, 456-461 (1989).
109. Narsale, A.A. Role of chronic inflammation on liver function during cachexia. (2014).
110. Knolle, P. *et al.* Human Kupffer cells secrete IL-10 in response to lipopolysaccharide (LPS) challenge. *J Hepatol* **22**, 226-229 (1995).
111. Sunami, Y. *et al.* Hepatic activation of IKK/NFkappaB signaling induces liver fibrosis via macrophage-mediated chronic inflammation. *Hepatology* **56**, 1117-1128.
112. Li, Z.W. *et al.* The IKKbeta subunit of IkappaB kinase (IKK) is essential for nuclear factor kappaB activation and prevention of apoptosis. *J Exp Med* **189**, 1839-1845 (1999).
113. Hacker, H. & Karin, M. Regulation and function of IKK and IKK-related kinases. *Sci STKE* **2006**, re13 (2006).
114. Daniel, K.G. *et al.* Clioquinol and pyrrolidine dithiocarbamate complex with copper to form proteasome inhibitors and apoptosis inducers in human breast cancer cells. *Breast Cancer Res* **7**, R897-908 (2005).
115. Zhu, T., Zhao, R., Zhang, L., Bernier, M. & Liu, J. Pyrrolidine dithiocarbamate enhances hepatic glycogen synthesis and reduces FoxO1-mediated gene transcription in type 2 diabetic rats. *Am J Physiol Endocrinol Metab* **302**, E409-416.
116. Goris, H., de Boer, F. & van der Waaij, D. Oral administration of antibiotics and intestinal flora associated endotoxin in mice. *Scand J Infect Dis* **18**, 55-63 (1986).
117. JP, W. The regulation of skeletal muscle protein turnover during the progression of cancer cachexia in the Apc(Min/+) mouse. *PLOS One* (2011).
118. Benrick, A. Interleukin-6 mediates exercise-induced increase in insulin sensitivity in mice. *Exp Physiol.*, 1224-1235 (2012).
119. Strassmann, G. Suramin interferes with interleukin-6 receptor binding in vitro and inhibits colon-26-mediated experimental cancer cachexia in vivo. *J Clin Invest*, 2152-2159. (1993).
120. Nishimoto, N. Mechanisms and pathologic significances in increase in serum interleukin-6 (IL-6) and soluble IL-6 receptor after administration of an anti-IL-6 receptor antibody, tocilizumab, in patients with rheumatoid arthritis and Castleman disease. *Blood*, 3959-3964 (2008).
121. A, S. The gut and intestinal bacteria in chronic heart failure. *Curr Drug Metab*, 22-28 (2009).

122. Liu, H. Early gut mucosal dysfunction in patients with acute pancreatitis. *Pancreas*, 192-196 (2008).
123. Hulsewé, K. Liver protein and glutamine metabolism during cachexia. *Proc Nutr Soc*, 801-806 (1997).
124. Stein, T.P. Cachexia, gluconeogenesis and progressive weight loss in cancer patients. *Journal of Theoretical Biology*, 51–59 (1978).
125. Barton, B., and Murphy, T., Cancer cachexia is mediated in part by the induction of IL - 6 like cytokines from the spleen. *Cytokine*, 251 - 257 (2001).
126. Zhai JX, e.a. PDTC attenuate LPS-induced kidney injury in systemic lupus erythematosus-prone MRL/lpr mice. *Mol Biol Rep*, 6763-6771. (2012).
127. Nakanishi, Y., et. al. COX-2 inhibition alters the phenotype of tumor-associated macrophages from M2 to M1 in ApcMin/+ mouse polyps. *Carcinogenesis* 1333-1339 (2011).
128. Baltgalvis, K.e.a. Effect of exercise on biological pathways in ApcMin/+ mouse intestinal polyps. *Journal of applied Physiology*, 1137-1143 (2008).
129. Baltgalvis, K., et. al Interleukin-6 and cachexia in ApcMin/+ mice. *Am J Physiol Regul Integr Comp Physiol*, R393-401 (2008).
130. Liaskou, E. Innate Immune Cells in Liver Inflammation. *Mediators Inflamm* (2012).
131. Mabley, J., et. al Suppression of intestinal polyposis in Apcmin/+ mice by targeting the nitric oxide or poly(ADP-ribose) pathways. *Fundamental and Molecular Mechanisms of Mutagenesis*, 107 - 116 (2004).
132. Su, L., et. al Multiple intestinal neoplasia caused by a mutation in the murine homolog of caused by the APC gene. *Science*, 668-670 (1992).
133. Mehl, K. Myofiber degeneration/regeneration is induced in the cachectic ApcMin/+ mouse. *Journal of Applied Physiology*, 2379 - 2387 (2005).
134. Gerritsen, J., et. al. Intestinal microbiota in human health and disease: the impact of probiotics. *Genes Nutr.* , 209 - 240 (2011)

APPENDIX A

SUPPLEMENTAL DATA

Table A.1: Body weight, temperature, endotoxin levels and muscle mass in the WT, treated and untreated *Apc*$^{Min/+}$ mice

	N	Peak Weight (g)	Sac Weight (g)	Body Weight Loss %	Rectal Temperature ^{o}C	Endotoxin levels EU/mL	Gasctrocnemius (mg)
C57BL/6	5	27.6 ± 0.54*	27.04 ± 0.52*	- 2% ± 1%*	35.2 ± 0.13*	0 ± 0*	112 ± 5.54*
Apc$^{Min/+}$	8	23.9 ± 036	20 ± 0.58	-13% ± 3%	34.9 ± 0.26	7.05 ± 1.44	73.88 ± 4.72
Apc$^{Min/+}$ + Nor/Amp	8	23.4 ± 0.62	21.71 ± 0.63	-7.04% ± 2%	33.3 ± 0.23	8.42 ± 0.75	75.63 ± 4.49

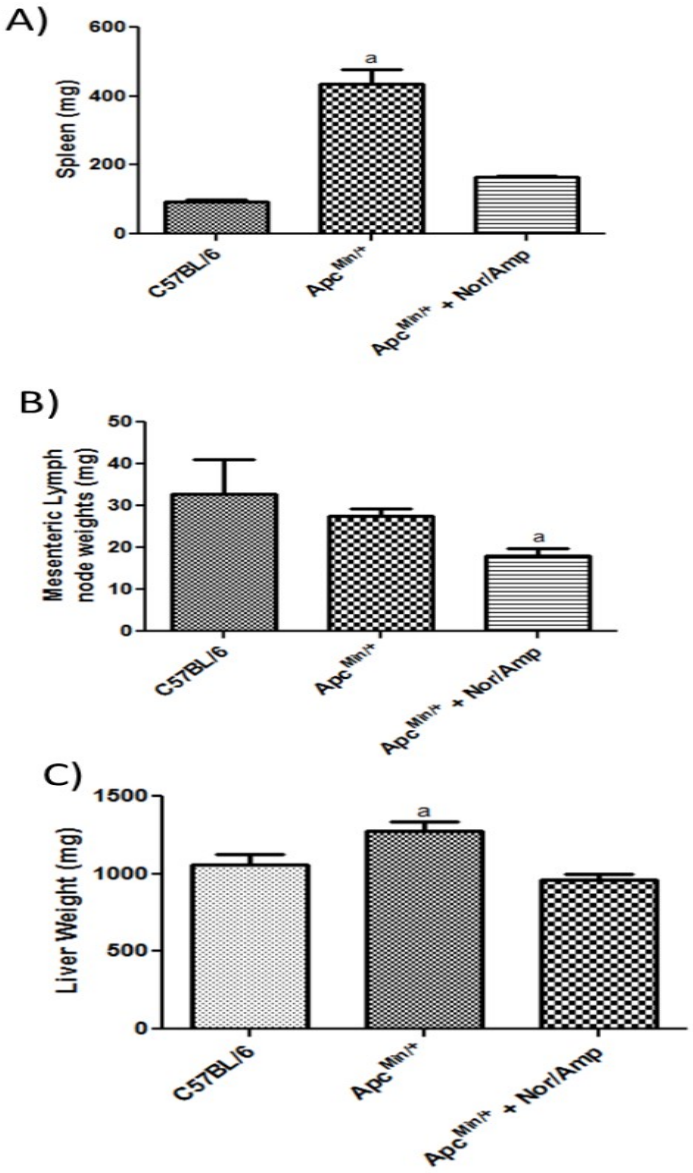

Figure A.1: Effect of Norfloxacin/Ampicillin treatment on tissue mass in the *Apc*$^{Min/+}$ mice: A) Spleen Weight B) Mesenteric Fat Weight C) Liver weight. Values expressed as Mean ± SE. $p<0.05$. A One – Way ANOVA was used to test differences between WT, treated and untreated *Apc*$^{Min/+}$ groups. Student – Newman Keul's t-test was used to test for differences between any two groups. A pre – planned t –test was used to analyze the effect of polymyxin treatment in the *Apc*$^{Min/+}$ mouse. "a" represents significantly different from the untreated *Apc*$^{Min/+}$ mouse

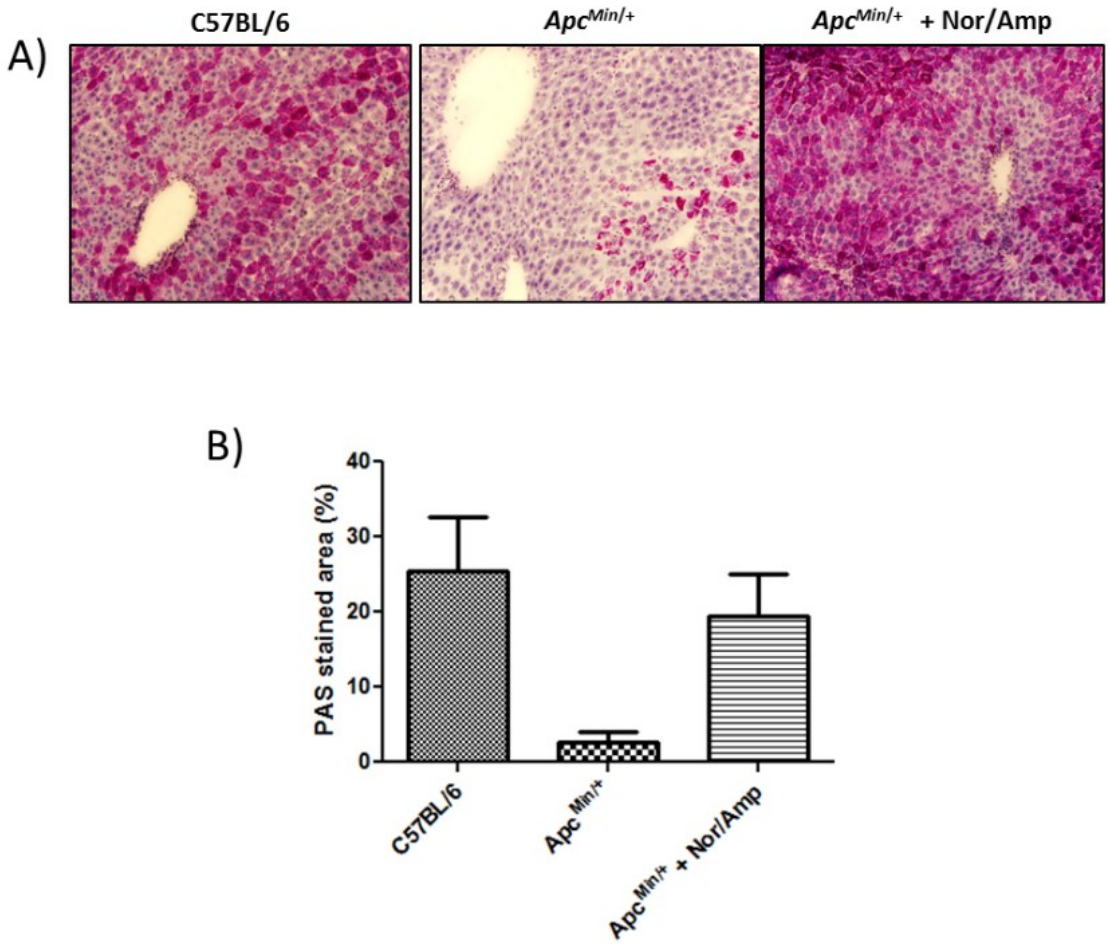

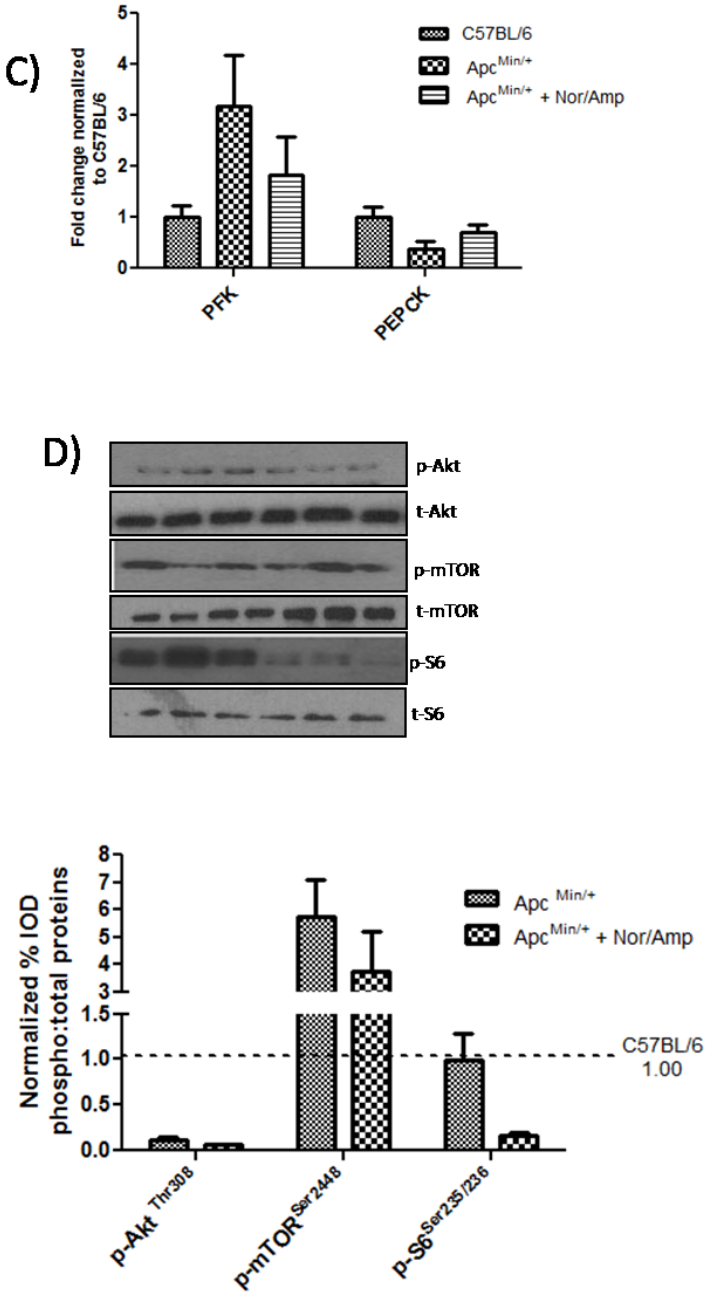

Figure A.2: Effect of Norfloxacin/Ampicillin treatment on liver metabolic signaling: A) Liver glycogen stores B) Morphometric analysis of liver glycogen stores C) Expression of metabolic mRNA levels PFK and PEPCK in the treated and untreated cachectic $Apc^{Min/+}$ mouse D) Protein synthesis signaling intermediates. Values expressed as Mean ± SE. $p<0.05$. A pre – planned t –test was used to analyze the effect of Polymyxin treatment within the $Apc^{Min/+}$. "a" represents significantly different from the untreated $Apc^{Min/+}$ mouse

A)

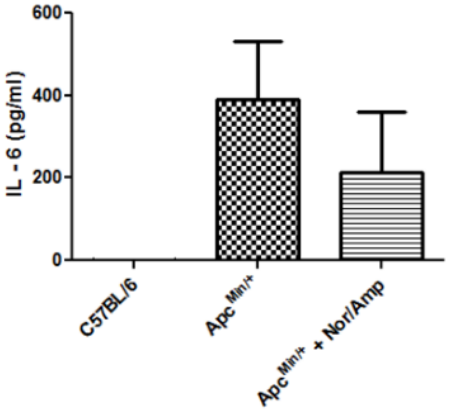

B)

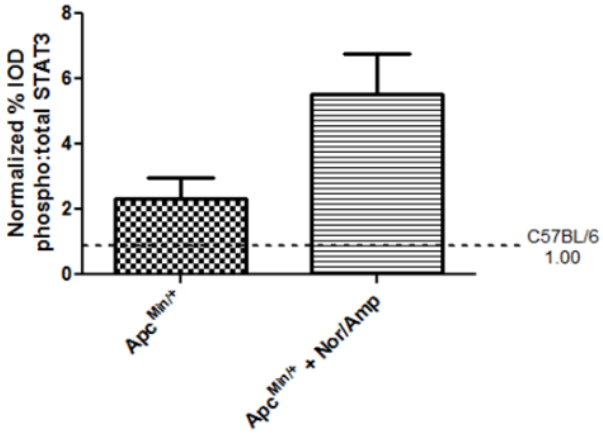

C)

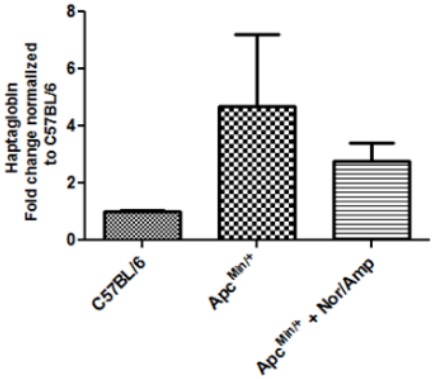

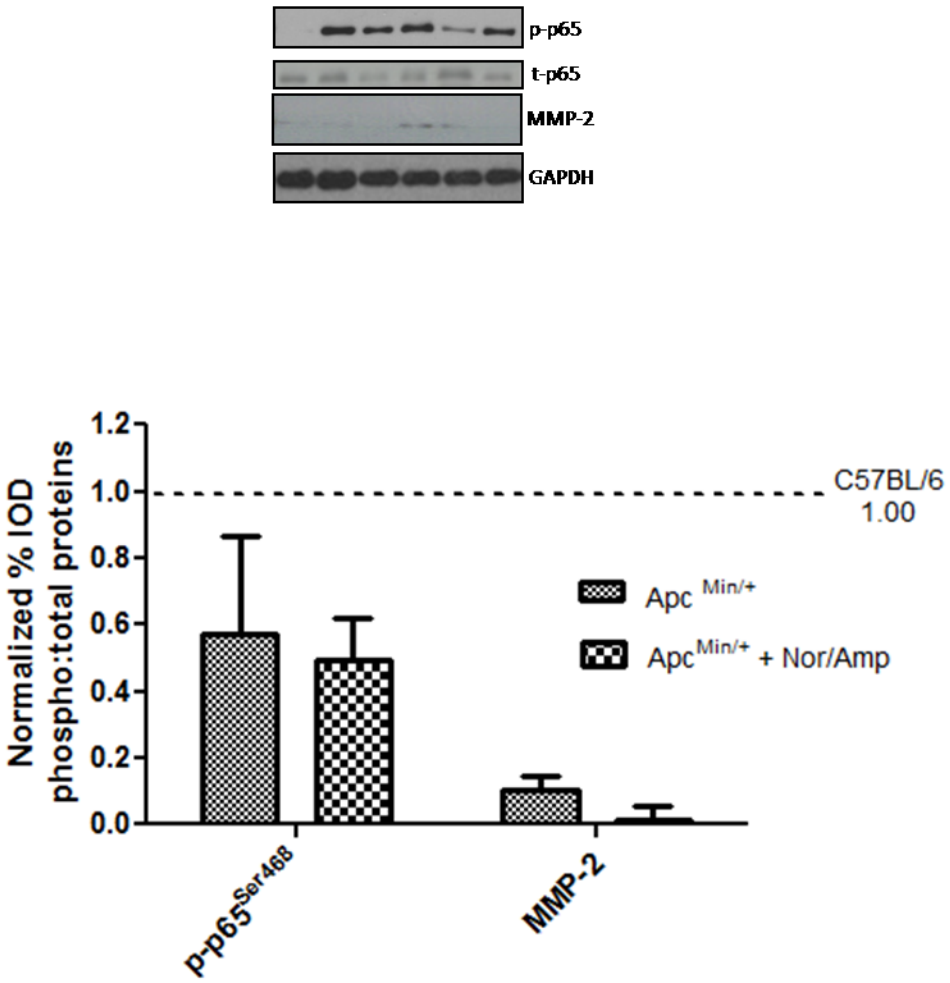

Figure A.3: Effect of Norfloxacin/Ampicillin treatment on hepatic inflammation: A) Plasma IL -6 levels B) Liver STAT-3 levels and C) Expression of metabolic mRNA levels for haptaglobin D) Liver Protein expression of inflammatory markers in the treated and untreated cachectic *Apc*$^{Min/+}$ mouse. Values expressed as Mean ± SE. $p<0.05$. A pre – planned t –test was used to analyze the effect of cachexia in the *Apc*$^{Min/+}$. "a" represents significantly different from the untreated *Apc*$^{Min/+}$ mouse

APPENDIX B

DETAILED PROTOCOLS

1.GENOTYPING

Genotyping sheet. cages, food, water, cage lids, cage cards/card holders, ear puncher, scissors, 1.5ml ependorf tubes, 15ml falcon tube, PCR tubes, Pipettes (p1000, p100, p20), pipette tips, primers, master mix, nuclease free water, thermocycler.

1. Turn on a water bath to approximately 55 ºC with 1-2 inch of water in the bottom

2. Wean pups- once mice are 4-5 weeks of age wean the pups by separating the male and the females into new cages (limit 5 mice/ cage).

3. On the genotyping sheet fill out the date of birth and the cross that the pups came from. Also write out animal numbers for the mice.

4. Punch the ear of the mouse and write down the ear and mouse number on both the genotyping sheet and the cage card.

5. Once the ear is punched, pinch the tip of the tail and snip just above your finger nails (do not take more than 2-4mm) and put into an eppendorf tube labeled with the animal number (not the ear punch).

6. Once this is complete for all of the animals make up the tail digest buffer. In a large (15ml) falcon tube add 200ul of tail buffer/ sample and 5ul of proteinase K/ sample. Mix by inversion.

7. Add 200ul of tail digest buffer to each eppendorf tube containing the tail and place in a blue tube rack.

8. Place tube rack in the water bath overnight (be sure the water covers the bottom of the tubes)

9. Turn Dri-bath to 95ºC

10. Label PCR tubes

11. Once bath is at 95 place ependorf tubes with tail digest into heat block for 10 minutes.

12. Set up PCR reaction

2. RNA ISOLATION

1. Label three sets of sterile 1.5mL tubes
2. Homogenize samples in 1mL of Trizol on ice. Be sure to clean the polytron with ethanol and water between samples.
3. Transfer homogenate to sterile 1.5mL tube and spin samples at 10,000 rpm for 15 minutes at 4ºC
4. Transfer supernatant to new 1.5mL tube
5. Add 200ul of chloroform to each sample and shake vigorously for 20 seconds (DO NOT VORTEX).
6. Spin samples at 10,000 rpm for 15 minutes at 4ºC
7. Be sure work space is clean.
8. Transfer clear supernatant to new 1.5mL ependorf tube being careful not to disturb the white protein interface.
9. Add 500ul of isopropanol and let sit at RT for 15-20 minutes or at 4ºC for longer
10. Centrifuge at 10,000 rpm for 15 min at 4ºC (should see white pellet after the spin)
11. Carefully dump off supernatant and add 1ml 75% EtOH (DEPC) to pellet and vortex
12. Centrifuge at 9,500 rpm for 5 minutes at 4ºC
13. Carefully dump off supernatant and add 1ml 75% EtOH (DEPC) to pellet and vortex

14. Centrifuge at 9,500 rpm for 5 minutes at 4ºC
15. Carefully dump off supernatant. Pipette any extra EtOH out of the tube being cautious not to disturb the pellet
16. Dry upside down on a tube rack for 5-15 minutes (bigger pellets take longer)
17. Resuspend pellet in DEPC H2O (15-40ul)
18. Heat in dry bath at 60ºC for 10 minutes
19. Pipette up and down to mix
20. Read on nanodrop or put 2ul of RNA in 800ul of dH_2O and read in quartz cuvette
21. Run on an agarose gel or denaturing gel to check quality of RNA
22. Proceed to make cDNA or store in -80ºC

3. cDNA Synthesis

Materials:

1. Sterile (RNAase/DNAase Free) Pipet tips
2. PCR tubes
3. DEPC H_2O
4. RT CDNA kit
5. Eppendorf tube
6. Cold block to hold PCR tubes

Methods:

1. Make cDNA cocktail from contents of RT cDNA kit (High Capacity cDNA kit from Applied BioSystems)
2. for each sample you will need:

DEPC water	4.2ul
10X RT buffer	2ul
dNTP mix	0.8ul
10X random primers	2ul
Reverse Transcriptase	1ul

3. Load 1ug of RNA into the appropriate tube and volume it to 10ul with DEPC H_2O.
4. Load 10ul of cDNA cocktail to each tube and pipet to mix
5. Centrifuge to get all contents to bottom of tube

6. Place tubes in thermocycler on program #25/ cDNA 407 on Dr. Fayad's thermal cycler.

4. REAL TIME PCR

1. Calculate the number of sample that need to be run. Do not forget to include in the blanks for each primer

2. Dilute cDNA to 1:10 or 1:100 dilution such that GAPDH CT is close to 18

3. 10ul of cDNA is needed per well. Samples will be run in duplicates atleast

4. Use the following table to calculate the volume of Sybr Green, Primers and dH2O needed for the entire reaction

TLR 4			
			1X
2X SYBR Green Master Mix			**12.5**
Forward	Occ		**1**
Reverse	Occ		**1**
dWater (sterile filtered)			**0.50**
			15.0
cDNA 1/100			**10**
			25

5. Set up the PCR plate (Applied Biosystems, 96 well PCR Plate). Make sure to draw out the plate plan with all the samples and the blank in advance in your notebook

6. Add the cDNA (10ul) followed by the Master mix (15ul) to each well in the plate

7. Cover the plate using the appropriate plate cover

8. Run plate in the Applied Biosystem 7300 machine in Dr. Davis's lab

9. Before starting the run

- Add the Sybr green tag for all the wells
- Add Dissociation stage
- Change volume to 25ul
- Save the SDS file

10. Hit Start and wait till you see the estimated time left (Approx. 2hr 40 mins)

11. Check on the PCR periodically, it is essential to switch the machine off as soon as the run is completed to enhance the life of the Bulb.

5. IL – 6 ELISA (BD BIOSCIENCES)

Day 1:

Prepare 10N NaOH solution

Prepare Coating Buffer - 100 mls

0.713g $NaHCO_3$,

0.159 Na_2CO3

pH to 9.5 with 10N NaOH

Make up volume to 100ml

Prepare 10X PBS (1 liter)

80g of NaCL

11.6g Na_2HPO_4

2.0 g KH_2PO_4,

2.0g KCL

pH to 7.0

Make up volume to 1L

Prepare 1X PBS - 1 L

100ml of PBS 10X

900ml of H_2O

Assay Diluent Buffer (to be used within 3 days)

1X PBS 50ml + 5mls of FBS

Store at 4℃

Wash Buffer 0.05% Tween

1X PBS - 900mls

Tween 20 - 450 µl

Store at 4 degrees

Reconstitute Standard (if using a new kit)

Refer to the Instruction/Analysis Certificate

It will give you the quantity of standard:

E.g. Quantity: 68ng/vial

Add 1ml of deionized water to this vial.

This will give you a standard stock of 68 **ng/ml**. Aliquot this in 50ul tubes and freeze immediately at -80℃

1. Calculate the standard curve + samples required wells

2. Prepare capture antibody solution in Coating buffer

- 1 in 250 dilution with 100 µl per well
- Thus for 96 wells we will need 9600ul
- 1- 250
- x - 9600
- = 9600/250 = *38.4ul of capture antibody + 9561.6 µl* of Coating buffer

3. Add 100 µl of the above diluted antibody in all the wells.

4. Seal the plate with the ELISA plate sealer and leave the plate at 4℃ for atleast 8 hours (I have used the coated plate 4 days later and works fine)

Day 2:

For the standard curve the highest point is 1000 **pg/ml**

Dilute the stock down with 14.7ul of stock (68ng/ml) in 985.29ul of diluent assay buffer.

Make serial dilutions of the stock from 1000 - 7.8pg/ml

Add 300µl of assay diluent to each tube expect for the 1000ng/ml tube

Add 300 µl of the 1000ng/ml to the 500ng/ml tube which already contains 300µl of assay diluent. Mix really well, vortex and add 300ul of the 500ng/ml to the 250ng/ml tube so on so forth till 15.6ng/ml.

The zero value is plain assay diluent buffer

Label tubes for the number of samples available. Dilute samples 1:1 (50ul of serum + 50ul of Assay diluent buffer). Mix well and set on ice.

1. Remove the plate coated with the coating antibody on Day 1 from 4 degrees
2. Aspirate out the coating antibody from all the wells
3. Wash wells with Wash buffer prepared on Day 1. Add around 300ul of Wash buffer to each well. To remove the wash buffer turn plate upside down and tap above a tray or waste container. **(3 washes)**
4. Add 100ul of Diluent buffer to each well and block the plate for 1 hour. (This buffer contains FBS and hence can be used for blocking)
5. After an hour tap the plate upside down to remove all the blocking solution and wash with 1X wash buffer 3 times
6. Make sure all the well are well emptied after the third wash with no bubble in any of the wells.
7. Add 100ul of the diluted standard or samples to each well
8. Incubate at RT for 2hrs
9. During the incubation calculate the amount of detection antibody and SAv-HRP required.
    1. For 96 wells we need 9600ul of the working detector. So we make 10,000ul of the working detector. To 10mls of diluent Assay buffer add 40ul of Detection antibody. To this add 40ul of SAv - Substrate. Mix well, vortex. Keep aside.
10. Aspirate all the standards and samples from the plate post 2hrs and wash with Wash Buffer 5 times.
11. Make sure all the bubbles and film are removed the end of the 5th wash.

12. Add 100ul of Working detector to the wells
13. Incubate for another hour.
14. Wash 7 times with wash buffer with a 30s to 1min incubation with the wash buffer for each wash
15. Before the last wash prepare the substrate TMB cocktail. For the 96 well plate mix 5mls of the Reagent with 5mls for reagent B. Mix well by vortexing. This mixture is light sensitive and turns blue on overexposure to light. Incubate in dark till ready to use.
16. Add 100ul of the substrate solution to each well and monitor the colour development over next 30 mins.
17. During this incubation prepare 2N sulfuric acid solution. (980ul of H2SO4 concentrated + 9020mls of water)
18. Over incubation of with the TMB substrate leads to color development in the blank. But too little incubation distorts the standard curve at the lower concentrations.
19. 30minutes usually is good enough incubation period. But stop the reaction earlier if colour starts developing in the negative. Stretch it beyond 30 mins if no gradation is seen between the lower 3 standards - 0, 7.8, 15.6
20. Add 50ul of the stop solution
21. Colour changes from blue to yellow.
22. Read the plate at 450nm and 570nm.

7. ENDOTOXIN ASSAY

Endotoxin Assay - Hycult Biotechnology

Limulus Ameboyte Lysate Chromogenic Endpoint Assay

Only use Endotoxin free water and tips for the assay

Reconstitute the standard vial by referring to the batchcontrol item sheet. Vortex the standard solution for atleast 5 minutes after reconstitution. Reconstituted standard has a concentration of ~ 50nEU/ml. Aliquot the standard in endotoxin free Eppendorf tubes, seal with parafilm and store @ -20℃ for further use.

Reconstitute the LAL assay vial with 4ml of endotoxin free water. Quickly make 1ml aliquots (solution turns yellow with time) and freeze them at -80℃. The LAL reagent is light sensitive, hence it's better to cover the Eppendorf's with foil.

Reconstitute the STOP solution- Use 1part of glacial acetic acid + 1.5 parts water to prepare dilutions depending on the final number of wells to be used.

The standards in duplicates take up 2 columns.

On the template sheet draw out the number of samples + the standards and calculate the total number of wells to be used.

Remove the plate from the kit. Do not remove the strips/plate from the bag unless the bag has reached room temperature. Otherwise there is a risk of condensation forming on the wells.

Count the equivalent number of endotoxin well strips on the plate. Remove the excess strips and place them in the re-sealable bag obtained with the plate. Make sure the desiccator pouch is in the bag while resealing the strips. Store the strips back at 4℃

Label eppendorf tubes for standards and samples.

For standards: From the reconstituted stock - Take 50ul of the ~50EU/ml standard and

add it to 35ul of endotoxin free water. This gives you a working standard of 30EU/ml.

make the following concentrations with the standards. Thus for every subsequent

standard, make serial dilution to a factor of 3. For this fill up all

the standard Eppendorf's with 100µl endotoxin free water (EFW). Add 50ul of 30EU/ml working standard to the tube labelled 10 EU/ml. Pipette vigorously to allow the standard to mix completely. Now transfer 50µl from the 10EU/ml concentration to the next Eppendorf with a concentration of 3.3EU/ml. 50ul of standard added to 100ul for EFW for every subsequent dilution will give the following standard dilutions.

10	10	S1	S1
3.3	3.3	S2	S2
1.1	1.1	S3	S3
0.37	0.37	S4	S4
0.123	0.123	S5	S5
0.041	0.041	S6	S6
0.014	0.014	S7	S7
0	0	S8	S8

Sample dilutions can be varied depending on the availability of the samples and if they fall within the standard curve. But the general standard for samples is 1:1 i.e. 25µl of sample + 25 µl of EFW for samples that do not require heating (50µl of sample in duplicate) and 5µl of sample + 45µl of EFW for samples that are heated in a water bath for 10minutes. (10ul of sample in duplicate).

Sample preparation - without heating

Take 25µl of sample and dilute it with equal amounts of EFW. Mix thoroughly with a pipette and transfer it to the appropriate well on the plate. (You would need 50ul of the sample if you are running the assay is duplicates).

After adding all the standards and the samples take a blank reading of the plate at 405nm. This is the background reading for the sample without the LAL reagent, to eliminate any colour contamination after the final reading. Note this reading down as the 'Pre" reading

Add 50ul of reconstituted LAL reagent to each well.

Read the plate again at 405nm and not this reading down as the 0min reading.

Read the plate every 10minutes after that to check on the absorbance of 10EU/ml standard. Once the absorbance for 10EU/ml standard reaches ~0.8. Take the plate out and add 50µl the diluted stop solution. Add the stop solution in the same order as the LAL reagent to reduce variability in reaction time and hence the final readings.

Read the plate again and mark this reading as STOP.

Sample preparation - with heating

Serum samples contain compound like albumin which can bind to endotoxin and inhibit its detection by the assay. For such samples:

Take 5ul of the sample and dilute it with 45ul of EFW. Mix thoroughly with a pipette in the Eppendorf tube. (Double the volume if you need to run the samples in duplicates).

Fill up a dry heat block wells with water and set it to reach 75 deg. Place the diluted samples in the water bath for 10 mins.

After the incubation, place the tubes in a centrifuge and give the tubes a quick spin to get all the diluted sample to the bottom of the tube. (Do not spin for too long as the endotoxin because of its weight would tend to accumulate to the bottom.

Mix the spun down sample and add 50ul of it to the plate.

After adding all the standards and the samples take a blank reading of the plate at 405nm. This is the background reading for the sample without the LAL reagent, to eliminate any colour contamination after the final reading. Note this reading down as the 'Pre" reading

Add 50ul of LAL reagent to each well.

Read the plate again at 405nm and not this reading down as the 0min reading.

Read the plate every 10minutes after that to check on the absorbance of 10EU/ml standard. Once the absorbance for 10EU/ml standard reaches ~0.8. Take the plate out and add 50ul the diluted stop solution. Add the stop solution in the same order as the LAL reagent to reduce variability in reaction time and hence the final readings.

Read the plate again and mark this reading as STOP.

Analysis of the data

From the STOP values subtract the Pre - LAL values to eliminate any internal colour variation (esp. with plasma samples which are hemolyzed).

After this subtract the zero reading at 0 minutes from STOP reading.

After subtracting the background and the 0 reading from the final readings plot the standard curve as a logarithmic plot in excel.

Use the slope of this logarithmic curve to identify the endotoxin content in each sample.

8. HISTOLOGY

Deparaffinazation of sections

1. Heat the incubator to 60 degree Celsius
2. Check solutions (100% EtOH, 50%EtOH/50% xylene, 100% Xylene)
3. Change solution which are old and are low
4. Place slides in the incubator at 60deg for 30 mins
5. Place in 100% xylene for 3 mins
6. Put in 2nd 100% xylene for 4 mins
7. Back in the first xylene for 4 mins
8. 100% EtOH for 2 mins
9. 100% EtOH of 2 mins
10. 95% EtOH for 1 min

Slides are deparrafinzed

Hematoxylin and Eosin Sectioning

Deparaffinize slides

1. Post deparaffinization dry slides for a few minutes (air dry)
2. Dip a few times in hematoxylin (5- 6X) then leave for 7mins
3. Dip in H2O - 6 times then let it sit in H2O for 5 mins
4. 6 dips in distilled water
5. 4 dips in distilled water
6. 6 dips in ammonia H2O
7. Place in H2O for 10 mins
8. Place in alcohol - eosin for 3 mins
9. Dehydrate with 6 dips of each of the following
    1. 35% EtOH
    2. 50% EtOH
    3. 75% EtOH
    4. 95% EtOH
    5. 95% EtOH
10. Clear in xylene
    1. One dip in 50% EtOH xylene
    2. 2 mins in 100% xylene
    3. 1 min in 2nd 100% xylene

Periodic Acid Schiff's Staining

Stains glycogen content in the tissue

Solutions required:

1. Carnoy's Fixative: Prepare in fume hood

    100% EtOH: 60ml

    Chloroform: 30ml

    Glacial Acetic Acid: 10ml

2. Periodic Acid Solution: (0.5% w/v) - Prepare fresh

    Periodic Acid: 50mg (Periodic Acid is always stored in the desiccator)

    dH2O: 10ml

3. Schiff's Reagent to be removed to Room Temperature 30 minutes before use

Protocol:

1. Thaw sections with cold Carnoy's fixative on petri dish. Leave it for a couple of minutes
2. Incubate slides with Carnoy's fixative at RT for 10mins
3. Dry slides for 10mins
4. Wash slides with dH2O 3 times
5. 0.5% Periodic acid solution for 30mins
6. Wash slides with dH2O for 25 minutes
7. Schiff's reagent for 25mins
8. Wash in running H2O for 10mins
9. Dehydrate slides with graduated alcohol
10. Clear in xylene
11. Mount with mount medium

9. Protein Estimation

Homogenization of tissue

Obtain 3 samples from instructor. Store the samples in liquid nitrogen until homogenization.

2. Prepare Mueller buffer. This can be stored at room temperature. You will need 1 mL/100mg tissue of Mueller Buffer. To make a 15 mL solution of Mueller buffer, add the following solutions obtained from the instructor and add to a centrifuge tube:

1.5 mL 50 mM Hepes (pH 7.4)

1.5 µL 0.1% TritonX-100

120 µL 4 mM EGTA

300 µL 10 mM EDTA

2.25 mL 15 mM Na4P2O7

750 µL 100 mM β-glycerolphosphate

9.14 mL deionized H2O

Immediately before adding the Mueller buffer to the samples, add the following protease inhibitors to the solution:

15 µL leupeptin (50 µg/uL)

150 µL (0.2 M) PMSF

3. Prepare diluent buffer. Add the following solutions:

3.0 mL 100% glycerol

1.5 mL 100 mM Na4P2O7

1.5 mL 500 mM EGTA

5 µL 1 mM β-mercaptoethanol

4. Put the Mueller buffer on ice. Have a 600 mL beaker with deionized H2O and another 600 mL beaker with weak acid (splash of glacial acetic acid). Also, have a test

tube rack with 3 eppendorf homogenization tubes (1.5 ml, write the names of tissue and your initials) and some Kim-wipes nearby. Have a 600 mL beaker with ice and a homogenization tube. Also have a beaker for waste.

5. Weigh the samples on a scale. Trim down samples with a blade if necessary (wt. < 50 mg). Put the samples in the labeled 1.5 ml eppendorf and back in liquid nitrogen.

6. Put the sample in the homogenization tube. If the sample sticks to the side of the eppendorf, flick it with your finger to dislodge it. Immediately add 1 mL/100mg tissue of Mueller buffer to the sample. Homogenize in an up-and-down motion for a few seconds at a time. This prevents heat from accumulating. Also, turn the homogenizer off and on every few seconds. When the sample is liquefied, use a transfer pipette and put back into original eppendorf. Rinse the transfer pipette with deionized H2O. Rinse the glass probe first with weak acid, dry with Kim-wipe, rinse with deionized H2O, and wipe with Kim-wipe. Rinse the homogenization tube 3 times with weak acid and 3 times with deionized H2O and pour into waste beaker. Make new tubes with labels.

7. Centrifuge the samples for 15 min at 4°C for at 10K rpm (Centrifuge is located in the cell culture room). Transfer the supernatant into a new eppendorf tube and add half of original amount of Mueller of diluent buffer. Put these tubes in the ice. We don't use all volume of each sample we homogenized here.

Bradford Assay:

Using a plate reader (Bio-Rad)

8. Get BSA from instructor and dilute from stock to 1ug/µL working solution. Prepare a 1:5 dilution with deionized H2O of Bio-rad Bradford reagent. You will need 25 mL of 1:5 dilution of Bio-rad Bradford reagent.

9. Obtain 96-well microplate and pipet 300 µl of 1:5 dilution of Bradford reagent to each well as necessary.

10. Pipet BSA (0, 2, 4, 6, 8, 10ul) and 2 µl of samples to wells.

11. Cover the plate with foil and wait 15 min.

12. Place the plate in the safire2 and read absorbance at 595nm. All absorbance readings need to be within 10% of CV in each duplicate

13. Make a standard regression curve with BSA and calculate the protein concentration of samples.

Things you need to report

1. Name of samples and their weights

2. Absorbance of each sample (BSA and your samples)

3. Calculate CV (%) of each sample. CV defined as the ratio of the standard deviation to the mean:

$$CV\ (\%) = (/)*100$$

4. Graph to determine your standard curve (protein concentration vs. absorbance)

5. Calculate the concentration of your samples based on the standard curve.

SDS PAGE & Western blotting

1. Make gel by taking into consideration the molecular weight of the protein to be probed for.

10% acrylamide gel (10 mL/gel)

3.9 mL H2O

3.4 mL 30% bis: acrylamide mix

2.5 mL 1.5 M Tris (pH 8.8)

100 µL 10% SDS

100 µL 10% ammonium persulfate

8 µL TEMED (gel will start to harden once this is added)

Pour into a mold (leave room for comb) and covered with a small amount of isopropanol to prevent evaporation. Wait until the gel is polymerized (about 20-30 min).

5% acrylamide stacking gel (5 mL/gel):

3.4 mL distilled H2O

830 µL 30 % acrylamide mix

630 µL Tris (1.0 M, pH 6.8)

50 µL 10% SDS

50 µL 10% ammonium persulfate

5 µL TEMED (gel will start to harden once this is added)

*Acrylamide is a potent cumulative neurotoxin: wear gloves at all times.

Wait 20-30 min for gel to solidify. Remove comb and rinse gels with distilled H2O. Remove from stand and aspirate the wells.

2. Preparation of samples:

Determine volume of protein extract based on the tester blot data. Pipette into Eppendorfs. Add the same volume of 2x SDS dye. Boil samples for 5 min. Briefly centrifuge to collect all liquid at bottom of tube and pipette into wells.

Running buffer: 1x SDS, 1 L per bucket. Dilute from 5x SDS stock.

3. Loading the gel:

Connect gels to holder and put in case. Add running buffer. Load each sample into each well. Add 10 µL of marker to one lane (not in the middle of the gel). Add remaining running buffer. Connect to power supply (Protein is negatively charged so it will run from negative to positive-black to red). Run gel at appropriate voltage (200 V for 1 h). Stop when all dye has leaked into the running buffer.

4. Transfer to membrane:

You will need:

Methanol

Membrane

2 pieces of blotting paper

2 sponges

1 waffle sandwich

Pyrex dish

Transfer buffer

Spacer

* Don't touch the membrane with your fingers; use tweezers instead. Oils and proteins on the fingers will block efficient transfer and create dirty blots.

* Make sure the paper and membrane are cut smaller than sponges and to the same or slightly larger than the gel.

Pre-soak membrane in methanol (few minutes) to enhance the transfer process. Disconnect power and remove gels. Remove one piece of glass and carefully cut away stacking gel and throw away in trash. Use deionized H2O and a spacer to help remove gel into dish with deionized H2O.

The sandwich consists of 1) Waffle (black side down)

2) Sponge

3) Blotting paper

4) Gel

5) Membrane

6) Blotting paper

7) Sponge

8) Waffle (white side)

Bubbles were smoothed out with gel in each layer with spacers. Get the transfer holder. Put the sandwich in (black to black). Add ice pack. Put stir bar at bottom of container. Add transfer buffer. Pack entire unit on ice on a stir plate. Circulate the running buffer. Transfer with ice pack for an hour at 370 mA.

5. Ponceau Staining

After the membrane transfer, the membrane was rinsed with distilled H2O and put in a plastic dish with enough Ponceau stain to cover the membrane. It was put on a shaker for 5 min and the stain was poured off. The membrane was rinsed with dH2O until the membrane was no longer pink. Put the membrane in the plastic sheet and scan in to the computer to check for success for transfer.

6. Western Blotting:

1. Put the membrane in a plastic container with protein side up, pour a blocking solution (5% TBST milk, 5 g of milk + 100 mL of TBST) and put the container on a rocker for 30 min.

2. Add primary Ab at appropriate dilution in 5% TBST milk.

a. Example. 1:1000 dilution = 10 µl Ab in 10 ml milk

3. Incubate overnight at 4 °C, 1 h at RT, or 30 min at 37 °C with gentle rocking.

4. Wash 3 x 5 min with TBST with shaking.

5. Wash 1 x 10 min with TBST with shaking.

6. Add secondary Ab at appropriate dilution in 5% TBST milk

a. Example. 1:2000 dilution = 5 µl Ab in 10 ml milk.

7. Incubate 1 hour at RT with gentle rocking.

8. Wash 3 x 5 min with TBST with shaking.

9. Wash 1 x 10 min with TBST with shaking.

10. Make ECL or ECL+ reagent.

ECL

a. Wrap 15 ml plastic tube with foil.

b. Add 4 ml of Solution A.

c. Add 4 ml of Solution B.

d. Vortex.

ECL Quantum Plus - BioExpress

a. Wrap 15 ml plastic tube with foil.

b. Add 1 ml of Solution A.

c. Add 1ml of Solution B.

d. Dilute with 1ml of TBST if needed. Vortex.

11. Remove excess TBST by draining edge of membrane with Kim-wipe.

12. Lay membrane in flat dish.

13. Add ECL (1 min) on top of membrane.

14. Remove excess ECL by draining edge of membrane with Kim-wipe.

15. Place membrane face down (protein side down) on piece of plastic wrap.

7. Imaging

Case A: Using an image scanner on the 5th floor.

16. Place your membrane on the scanner and scan it in.

Case B: Developing a film on the 3rd floor.

16. To use machine, turn switch from “Standby” to “Run” and the red “Feed film” light will turn on.

17. Turn off the light of the room. Fold up edges and tape membrane in film cassette face up (protein side up).

a. To have film in correct orientation, the notch should be in the upper left corner.

18. Put on a piece of film on membrane in the darkroom.

19. Expose film for 5 min to develop.

20. In dark, open the lid of the developer, turn the film upside-down and sideways, and feed into the machine until it catches. You can turn on the light or put in another piece of film when the “Feed Film” light comes on again.

21. Turn machine to “Standby”.

22. Mark on film the edges of the membrane and the protein marker with a sharpie.

APPENDIX C

Role of Chronic Inflammation on Liver Function during Cachexia Progression in the *Apc* $^{Min/+}$ mouse model

by

Aditi Narsale

Dissertation Proposal

Committee Members:

Dr. James Carson

Dr. Larry Durstine

Dr. Raja Fayad

Dr. Marj Pena

INTRODUCTION AND AIMS

Cachexia is a wasting syndrome observed during the later stages of chronic diseases like cancer, AIDS, COPD. With the advent of modern medicine which mostly deals with managing chronic diseases like cancer rather than curing it, quality of life in such patients becomes critical. Colorectal cancer (CRC) is a leading cause of cancer mediated deaths and is associated with onset of cachexia during the advanced stages of the disease. CRC associated cachexia is characterized by loss of fat and muscle, chronic systemic inflammation, increased gut permeability, anemia and anorexia in patients[28, 31]. The *Apc* $^{Min/+}$ model of cancer cachexia mimics most of these symptoms with the mice losing muscle mass at later stages of the disease which co – relates to increased IL -6 levels in the mouse. Chronic systemic inflammation exacerbates wasting in the mouse accelerating mortality rate in the given model[36, 117].

Interleukin 6 (IL -6) is a pleiotropic cytokine, which is essential for wound healing and tissue repair when secreted in moderate amounts[34], but chronic levels of IL – 6 lead to deleterious effects leading to the muscle and fat loss seen during cachexia in the *Apc*$^{Min/+}$ mouse[36]. Acute exposure to IL – 6 is known to be protective as it can regulate macrophage infiltration to the site of injury and manipulate the immune system proliferation to counter the antigen attack. IL – 6 secretion post exercise is essential for satellite cell mediated muscle hypertrophy and growth and tissue repair response[34]. IL – 6 is also essential for insulin mediated glucose uptake in skeletal muscle after a single bout of exercise[118]. But chronic elevation of IL – 6 is detrimental as seen during most chronic diseases. Cancerous polyps and tumors along with immune cells are a major source of systemic IL – 6, leading

to deleterious wasting symptoms seen during cachexia. Chronic activation of IL - 6 antagonizes acute IL -6 responses. Pretreatment with IL – 6 exposure leads to a reduction in insulin mediated glucose uptake in both liver and skeletal muscle. Chronic IL – 6 exposures can also lead to glycogen depletion in the liver, possibly due to inhibition of glycogen synthase[44]. Gluconeogenesis is also blunted with IL – 6 downregulating the activity of key glycolytic enzymes like phosphoenolpyruvate carboxylase in the hepatic tissue and skeletal muscle. Administration of IL – 6 inhibitor suramin attenuates cachexia in the C – 26 colon carcinoma model by interfering with IL – 6 binding to its receptor[119]. This systemic inhibitor of IL – 6 is known to reduce IL – 6 activity in the liver, though its effect on liver function has not been studied. IL – 6 receptor antibody administration has also been shown to attenuate cancer cachexia both in the C – 26 and *Apc* $^{Min/+}$ model of cachexia but the role of liver in this process has not been teased out[117, 120]. IL – 6KO mice are protected from cachexia, even in the presence of colon tumors, on the other hand muscle specific KO of IL – 6 signaling is also known to attenuate gastrocnemius loss in the LLC model of cachexia (unpublished data). Thus complete systemic KO of IL – 6 signaling is protective against cachexia but targeted therapies with the suramin, IL – 6RA or skeletal muscle gp130 KO only attenuates muscle loss[119]. This indicates that the systemic action of IL – 6 contributes cachexia, rather than direct action of IL – 6 on muscle leading to muscle mass loss.

Chronic IL – 6 exposures can upregulate expression of TLR-4 receptor on skeletal muscle sensitizing the body to other inflammatory mediators like endotoxin[42]. Systemic Endotoxin or LPS levels are also known to be elevated in certain models of cachexia like cardiac cachexia, colorectal/pancreatic cancer cachexia[38, 121, 122]. Increase in plasma LPS

levels is attributed to a change in gut permeability with chronic inflammation and change in blood flow rates to the gut. Increased gut permeability allows transport of bacteria and bacterial byproducts like endotoxin to the blood[16]. Increased endotoxin in the blood can be sensed by specialized innate immune receptor – Toll – like receptor 4 (TLR4), which can activate NF – κB, the classical pro – inflammatory pathway downstream. Other members of the TLR family like TLR5, TLR 2 can recognize bacterial remnants like flagellin and can also phosphorylate NF – κB downstream[51].

Plasma concentration of serum cytokine MCP-1 is also shown to be elevated in the *Apc* $^{Min/+}$ model of cancer cachexia[18]. Thus chronic inflammation during CRC induced cachexia can be sustained by multiple sources in the *Apc* $^{Min/+}$ mice. Elevated serum levels affect both peripheral and visceral organs of the body. During cachexia, peripheral organs/tissues like skeletal muscle and adipose tissue experience atrophy, while the visceral organs are preserved or even undergo hypertrophy. Liver tissue is often known to hypertrophy during sepsis and trauma, with increased uptake of amino acids from the degrading muscle[123]. This increased rate of protein synthesis is often maintained to sustain the elevated energy demands of an activated immune response and proliferating tumor cells. Degradation of skeletal muscle leads to increased concentration of free amino acids in the blood, but no known feedback loop exist to inhibit muscle degradation, with elevated levels of free amino acids in the blood. On the other hand, carbon skeletons taken up by the liver are degraded and the unused amino acids are excreted as urea, leading to excess N excretion seen with chronic diseases[123, 124]. Thus the liver feeds the chronic inflammatory response by breaking down skeletal muscle, which further secretes pro – inflammatory cytokines like IL -6 ensuing a vicious cycle. Prolonged exposure to IL – 6 leads to

expression of acute phase proteins in the liver like increased alpha 2 macroglobulin, CRP, fibrinogen and reduces other molecules associated with the CYP system, albumin etc[8, 31, 45].

Chronic systemic inflammation thus seems to affect liver function by suppressing insulin mediated glucose production and upregulating utilization of amino acids to increase protein synthesis. It also elicits a varied acute phase protein response, leading to downregulation of key plasma proteins like albumin and CYP and increased expression of inflammatory markers like haptaglobin, fibrinogen, α2 – macroglobin[8, 45]. Liver function thus seems to be altered with chronic inflammation seen during cachexia, but its role in the development of cachexia has not been studied. It remains to be determined if liver function is altered early during cachexia initiation or if failure to sustain protein synthesis by the liver contributes to cachexia progression/ initiation during the later stages of the disease. Sepsis induced trauma is known to increase protein synthesis initially, but high levels of endotoxin suppresses liver function[16]. Plasma MCP -1 levels are also unknown to be upregulated early during cachexia[18]. Endotoxin is known promote both MCP – 1 and IL – 6 secretions. Antibiotic treatment is known to suppress endotoxin mediated immune response leading to a suppression of systemic inflammation, including repression of immune cell proliferation in the spleen (preliminary data). Antibiotic treatment has been effective in attenuating plasma endotoxin levels in liver injury models with alcohol and sepsis[55]. Thus it would be interesting to see if antibiotic treatment would attenuate liver function by suppression of chronic immune response in the *Apc* $^{Min/+}$ mouse

The overall purpose of the study was to determine if chronic inflammation affects liver functions contributing to cachexia progression.

Aim1: To determine if liver function contributes to cachexia progression in the *Apc* $^{Min/+}$ model of cancer cachexia

Rationale: Chronic inflammation leads to loss of peripheral tissues like adipose and skeletal muscle. This loss is dependent on the pro – inflammatory cytokine IL -6 in the *Apc* $^{Min/+}$ model of cachexia. The IL – 6 levels rise with the increase in tumor size in the *Apc* $^{Min/+}$ mice from ~14 – 20 weeks of age. Endotoxin is up only at the later stages, ~ 20weeks of age with cachexia[16]. Cachexia, in the C – 26 model is known to suppress VLDL production in the liver, possibly leading to altered cholesterol and fat distribution via serum[15]. But the effect of this chronic inflammation on the liver function has not been studied. Chronic exposure to IL – 6 has been shown to reduce insulin stimulated glucose uptake in the liver, with increased inflammatory response and alteration of acute phase response. But if these alterations are observed early with the onset of cachexia or occur during the later stages of cachexia is not known.

Aim 1.1: Is liver function altered in severely cachectic *Apc* $^{Min/+}$ mice?

Aim 1.2: Is liver function altered with cachexia progression in the *Apc* $^{Min/+}$ mice?

Aim 2: To determine if inhibition of IL – 6 signaling is necessary or sufficient to alter liver metabolic and inflammatory process in the *Apc* $^{Min/+}$ model of cancer cachexia

Rationale: Chronic IL – 6 is known to suppress insulin mediated glucose uptake in hepatocytes and skeletal muscle. IL – 6 is also known to lead to skeletal muscle degradation in the cachectic Min mouse. Previous studies in our lab have shown that administration of IL -6RA attenuates skeletal muscle loss in the Min. Acute phase response is fueled by the degradation of skeletal muscle, with free amino acids being utilized as energy source in the

liver. Thus it would be interesting to study if inhibition of IL – 6 in the *Apc*$^{Min/+}$ would lead to alteration/improvement of liver function.

Aim 2.1: To determine if administration of PDTC attenuates/ alters liver function in severely cachectic *Apc*$^{Min/+}$ mice

Aim 2.2: To determine if administration of sgp130Fc attenuates/ alters liver function in severely cachectic *Apc*$^{Min/+}$ mice

Aim 3: To determine if antibiotic mediated immune suppression affects liver function in the cachectic *Apc* $^{Min/+}$ mice model

Rationale: Although the *Apc*$^{Min/+}$ model exhibits an IL – 6 dependent atrophy, other cytokines like OSM, LIF, CNTF[125], MCP -1[18], TNF – alpha, IL – 1 have also been implicated in cachexia progression. Bacterial endotoxin is upregulated late in the cachectic mice[16]. This increase is also observed in pancreatic cancer patients. Gut barrier function is the most likely cause for elevation of endotoxin in the mice[16]. Chronic IL – 6 is known to upregulate TLR4 expression in skeletal muscle[42]. Also TLR 4 expression is upregulated on the cachectic livers as compared to the wild type controls (Prelim data). TLR-4 activation leads to NF – kB phosphorylation the classical pro – inflammatory pathway. Endotoxin is also known to activate TLR 4 and MCP -1, a chemokine known to attract and activate macrophages inducing further inflammation [18, 126]. But MCP – 1 levels are known to be up by 12 weeks on the *Apc* $^{Min/+}$ signaling a role for MCP-1 in the initiation of cachexia.[18]. Thus endotoxin upregulation during later stages of cachexia may be additive rather than being the primary source of MCP – 1 in the *Apc* $^{Min/+}$. Moreover, the macrophages attracted by MCP – 1 to the tumor have been shown to have an anti – inflammatory or M2 phenotype. Gene transcription of genes like IL – 4, IL – 10, IL – 13 is elevated in the macrophages residing in the intestinal tumor[127]. But there are no detectable levels of these cytokines in

the $Apc^{Min/+}$ plasma. Chronic inflammation during cachexia progression is thus comprised of factors independent of IL – 6. In Aim 3 for the study we propose to target IL – 6 independent mechanisms to suppress chronic inflammation. Antibiotic treatment is known to target bacteria by inhibiting the synthesis of bacterial cell wall. Elimination of bacterial component by antibiotics circumvents immune system activation leading to a suppressed immune response during infection. Hyperproliferation and activation of immune cells fuels the chronic pro – inflammatory response seen during cachexia. Splenomegaly seen with cancer cachexia is associated with secretion of IL – 6 family of cytokines from the spleen[125]. An aggravated or proliferating immune response is thus additive to chronic inflammation seen during cancer cachexia. The idea thus emerges that treatment with antibiotics would allow for inhibition of both immune cell proliferation and the subsequent secretion of proinflammatory cytokines by elimination of gut microbiota. Previous studies with antibiotic pretreatment for alcohol induced liver injury has proved to be protective from a chronic inflammatory response[55]. Considering the inflammatory cascade with cachexia is caught in a positive feedback loop, breaking this loop would logically serve to be beneficial to contain the inflammatory response.

Antibiotics could be either specific to gram negative bacteria or gram positive bacteria. Since endotoxin is the primary component of gram negative bacteria, it would be interesting to see if elimination of Gram negative bacteria alone was sufficient to attenuate the inflammatory response seen during cachexia, or both gram positive and gram negative bacterial suppression would be necessary to suppress inflammation and subsequent muscle mass loss.

Aim 3.1: To determine if antibiotic treatment with Polymyxin attenuates chronic inflammation to attenuate liver function during cancer cachexia

Aim 3.2: To determine if Norflaxacin/Ampicillin treatment attenuates chronic inflammation to attenuate liver function during cancer cachexia

Limitations and Pitfalls:

1) All mice are fasted prior to sacrifice to reduce variation in plasma glucose levels, protein synthesis rates in the mice. But starvation on its own can affect protein synthesis in the liver. Depending on the study the mice will be fasted either overnight or for 5 hours. This inherently can contribute to changes in p – mTOR and protein synthesis in the liver. The effect of starvation is striking when compared between the C57BL/6 and *Apc* $^{Min/+}$ mice. The 5 hour fast upregulates the levels of protein synthesis marker p – mTOR as compared to the C57BL/6 mice but p – mTOR is downregulated in severely cachectic *Apc* $^{Min/+}$ with overnight fasting. To keep eliminate the effect of fasting on the results of protein synthesis, control B6 mice fasted for the exact same amount of time are used. Also we believe that effect of overnight fasting will be uniform between the *Apc* $^{Min/+}$ groups (12 – 14 – 20 weeks of age). Thus the primary comparison to detect mTOR upregulation would be amongst Min mice in different stages of cachexia.
2) PDTC is a global inhibitor of systemic inflammation, has been shown to inhibit NF – κB along with STAT-3. But since IL – 6 can through secondary mechanisms lead to NF – κB activation, this could be considered as a secondary target for IL – 6.
3) Antibiotic treatment to eliminate gut microbiota does suppress an immune response, but gut microbiota play an important role in breakdown of digested food

in the gut, where most of the nutrient absorption takes place. Thus elimination of microbiota might have side effects in terms of decreased or impaired nutrient absorption in the gut, which would be detrimental to the hypermetabolic state.

4) Immune response during cachexia is known elicited against the tumor. The absence of an acute phase protein response during cancer increases mortality rate with tumor proliferation. Thus complete shutdown of the immune response might actually prove detrimental by allowing uninhibited tumor growth.

Working Model:

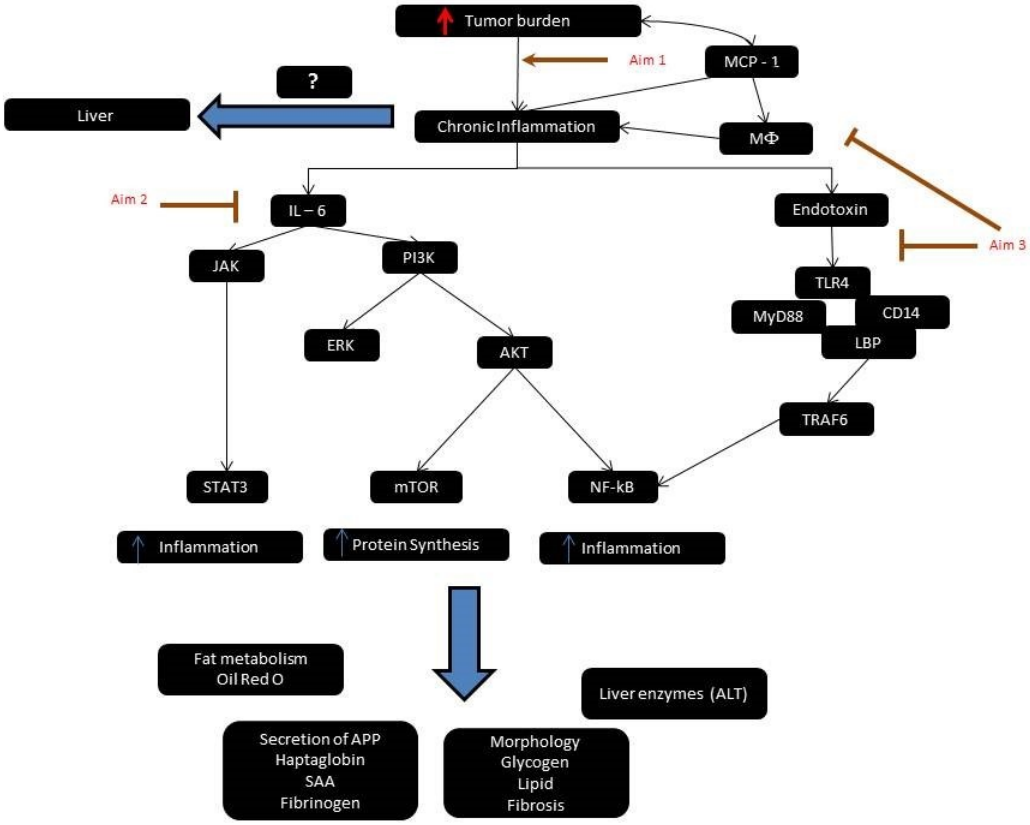

The *Apc* $^{Min/+}$ model of cancer cachexia is characterized by intestinal polyps in the colon and the small intestine. Macrophages are recruited to the tumor micro environment to fight the tumor antigen often by secretion of chemokines like MCP -1[18, 128]. But recruitment of these macrophages to the tumor is associated with tumor growth and cytokine secretion. As the tumor cells proliferate by evading apoptosis and cell cycle checkpoints, the inflammation cascades exhibiting a systemic pro – inflammatory response. The *Apc* $^{Min/+}$ mice start developing polyps at around 10 weeks of age and cachexia is initiated 4 weeks later at around 14 weeks of age. By 18 – 20 weeks of age

these mice are severely cachectic with a greater than 10% loss of Body mass in terms of skeletal muscle and adipose tissue. Chronic inflammation defined by high plasma IL – 6 levels, Splenomegaly, increased gut permeability, plasma endotoxin levels, increased plasma triglyceride levels is the underlying cause of the wasting and metabolic disorder observed in the cachectic mice[16, 129]. Aim 1 of this study will examine the role of chronic inflammation triggered by tumor burden on liver function. The liver is responsible for numerous body functions like maintaining blood glucose, secretion of albumin, beta – oxidation of fats and filtering of blood in the body[15, 31]. Aim 1 will establish the markers of liver function and chronic inflammation that are altered during cancer cachexia. Since *Apc* $^{Min/+}$ is IL – 6 driven model of muscle wasting, Aim 2 of the study will examine the role of IL – 6 in altering liver function during cachexia. IL – 6 overexpression is known for induction of acute phase proteins and insulin resistance in the hepatic tissue and altering IL - 6 expression would tease out the specific role of IL - 6 on liver function with cachexia. Factors other than IL – 6 are also associated with chronic inflammation associated with the Min. e.g. IL – 6 RA antibody administration, does attenuate muscle wasting but does not attenuate spleen size. Also protein synthesis is not rescued with the IL – 6 receptor antibody treatment indicating the continued presence of a hypermetabolic state[117]. Increased gut permeability is associated increased endotoxin levels in severely cachectic mice[16]. Also tumor associated macrophages are known to secrete a host of cytokines and chemokines[128]. The tumors themselves can secrete chemokine like MCP – 1 creating a cytokine milieu[18]. Induction of IL -6 family of cytokine like LIF, OSM are known to be upregulated in the Lewis lung Carcinoma (LLC) model and the C – 26 model of cancer cachexia[8, 125]. Though not measured in *Apc* $^{Min/+}$ model, their secretion in plasma cannot be ruled out. LLC model

of cancer cachexia induces the secretion of IL – 6 family cytokines due to immune cell proliferation in the spleen. Aim 3 of this study will suppress chronic inflammation by treatment with antibiotics. Antibiotics would allow for elimination of gut and systemic microbes. Antibiotic treatment also suppressed immune proliferation as exhibited by attenuation of splenomegaly and lymph node proliferation. Suppression of immune response could possibly also interfere with homing of macrophages to the tumor site in the antibiotic treated mice. Hepatic tissue is sensitive to both increased cytokines levels in the blood and immune proliferation of Kupffer cells lining the liver sinusoids. Aim 3 will therefore study the inhibition of systemic immune response on hepatic function in cachectic *Apc* $^{Min/+}$ mice.

Preliminary Data:

The liver is one of the most metabolically active and hence one of the most important organs to maintain homeostasis. The liver is known to perform over 500 function in the body including production of serum proteins like albumin, maintenance of blood sugar levels, filtering of blood toxins, maintaining blood iron levels etc. The liver has a dual blood supply with oxygenated blood entering the blood via the hepatic artery and nutrient rich blood and endotoxin laced blood entering via the portal vein[130]. The liver is equipped to with appropriate cellular architecture to detect foreign pathogens in the system. In the event of an infection the liver is known to alter production of acute phase proteins like albumin (decreased), fibrinogen, serum amyloid A (increased). The production of acute phase proteins requires a huge amount of energy increasing the body's metabolic demands. During cancer, the tumor is known to utilize glucose to produce lactic acid. The excess lactic acid is in the blood is converted back to glucose via the Cori's cycle, further

increasing liver metabolism. Liver mass increases during periods of prolonged infection and inflammation, but small increases in liver mass exponentially increase the energy demands in an accelerating the hypermetabolic state.

Cancer cachexia is primarily diagnosed as the loss of fat mass and skeletal mass in the absence of starvation. It is also characterized by a hypermetabolic rate and chronic inflammation. Proinflammatory cytokines like IL – 6[117], MCP – 1[18], endotoxin [16] have all been implicated in cachexia onset. The hypermetabolic state during cachexia is directly correlated to loss of skeletal muscle mass and adipose tissue, with cachectic patients exhibiting a higher body weight loss. Our lab has extensively studied the role of IL – 6 dependent cachexia in the Apc $^{Min/+}$ model of cancer cachexia. Skeletal muscle mass loss has been correlated to increasing levels of IL – 6, with administration of IL – 6 receptor antibody attenuating but not completely inhibiting muscle loss[117]. Interestingly whole body IL-6 knockout in the *Apc* $^{Min/+}$ mouse rescues the skeletal muscle loss[129], but this effect is not mimicked in the skeletal muscle specific knockout of the gp130 receptor – skmgp130KO (Table 1). Since IL – 6 has been shown to be the major driver for muscle loss in the *Apc* $^{Min/+}$ mouse it can be implied that effects on organs other than skeletal muscle may also contribute to cachexia progression.

Table C. 1: Comparison of lean and fat tissue between skeletal muscle gp130 knock out (skmgp130KO) female mice, with and without the Apc gene mutation.

	skmgp130 KO		skmgp130 KO Apc $^{Min/+}$	
	Homozygote	**Heterozygote**	**Homozygote**	**Heterozygote**
N	5	9	1	4
% Fat	18.4	15.09	8.1	9.84
Mes Fat	332.7	349.4	235	235
Lean Tissue	16.28± 0.42	17.08 ± 0.41	13.6	14.94 ± 0.62
Gastrocnemius	106.6 ± 2.26	106.65 ± 2.33	60.5	59.5 ± 8.32
Liver	900.8 ± 34.6	1038.15 ± 25.9	1148	1148.7 ± 93.8

In a recent study using the C26 mouse model of cachexia it was shown that liver metabolic dysfunction occurs during cancer cachexia. The livers of the cachectic mice had diminished capacity to secrete very – low – density – lipoprotein (VLDL). This was shown to be responsible for the lower levels of serum triglycerides in the mice blood[15]. Interestingly the *Apc*$^{Min/+}$ model of cancer cachexia exhibits high levels of plasma triglyceride in cachectic mice. Since both the Apc $^{Min/+}$ and C26 are IL – 6 dependent models of cancer cachexia, this points to secondary factors other than IL – 6 influencing metabolic processes during cancer cachexia.

Liver in the Apc $^{Min/+}$ model of cancer cachexia shows an increased phosphorylation of STAT 3 the downstream target of IL – 6, in severely cachectic mice (Figure 1).

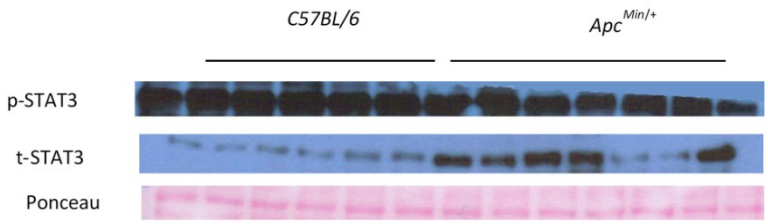

Figure C.1: p – STAT3 levels in the liver increase in the severely cachectic *Apc*$^{Min/+}$. Hepatic protein sample was probed for phosphorylated STAT3. Increased phosphorylation of STAT 3 levels in the 20 week old Apc Min/+ mice indicate local liver inflammation.

Upregulation of phosphorylated STAT 3 levels corresponded to cachexia progression in the Apc $^{Min/+}$ mice. Liver homogenates from 12 week (non – cachectic), 14 week (pre – cachectic) and 18 – 20 week (severely cachectic) Min mice were probed for activation of p – STAT3. Hepatic protein samples show a graded increase in p – STAT3 levels in the 12 – 4 – 20 week mice respectively.

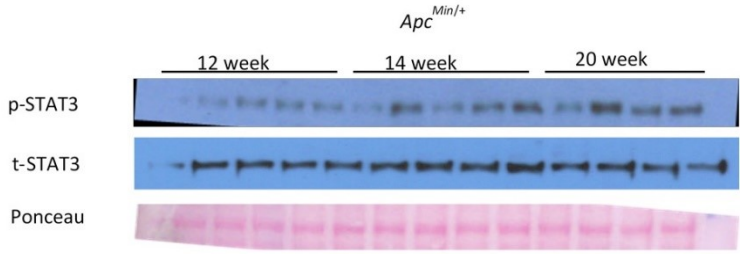

Figure C.2: p – STAT3 levels with cachexia progression. Phosphorylated STAT 3 levels increased with progression of cachexia in the Apc$^{Min/+}$ mouse.

This increase in hepatic inflammatory markers was mimicked by the protein synthesis marker p – mTOR (Figure 3). Phosphorylation of mTOR went up significantly in the hepatic protein from 12 week Min mice to 20 week Min mice.

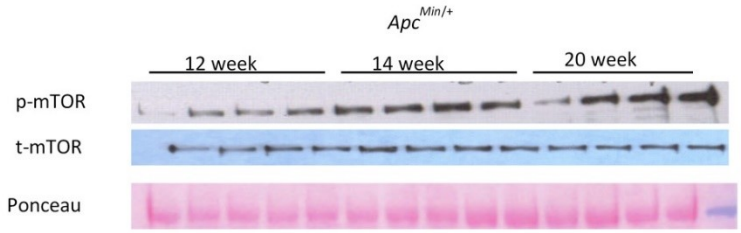

Figure C.3: p – mTOR levels with cachexia progression, Levels of phosphorylated mTOR increased with cachexia progression for 12 – 20 weeks.

Severely cachectic mice also exhibited an increase in liver glycogen levels in the severely cachectic Apc $^{Min/+}$ mice compared to the C57BL/6 mice (Figure 4).

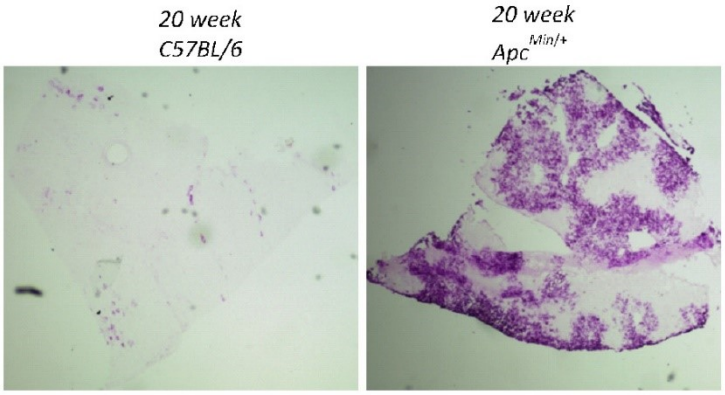

Figure C.4: Hepatic Glycogen content. Hepatic Glycogen content was increased in severely cachectic Apc $^{Min/+}$ mice as compared to age matched C57BL/6 mice at 20 weeks of age.

Albumin is a 65 kDa plasma protein synthesized in the liver. Albumin is known to be downregulated with cachexia[31]. Albumin is an abundant protein in the plasma and its

downregulation can thus be visualized by Ponceau staining. A 65kDa plasma protein in the blood is severely downregulated in the cachectic Apc $^{Min/+}$ mouse. This protein could be albumin signifying alteration in liver function with cachexia.

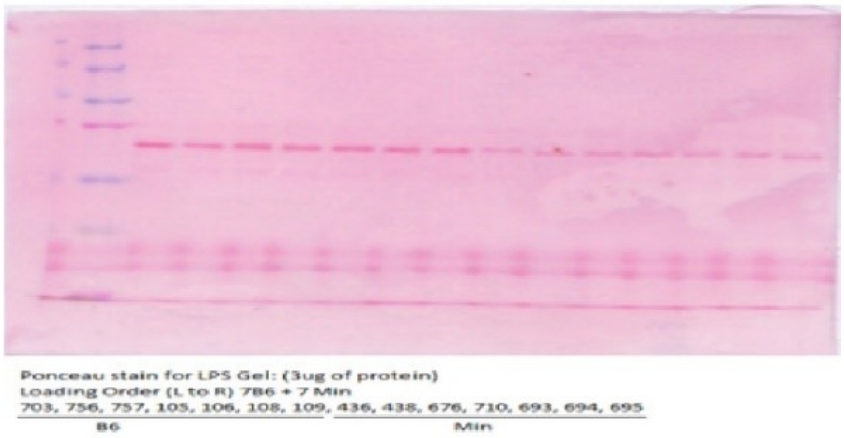

Figure C.5 Serum Albumin levels in cachectic *Apc*$^{Min/+}$ mice

Prior work from our lab has shown that administration of IL – 6 receptor antibody helps attenuate muscle loss by inhibition of protein degradation pathways in the skeletal muscle. Spleen size, the marker for immune activation and proliferation is not attenuated post IL – 6 receptor antibody administration in the Apc $^{Min/+117}$. But suppression of IL – 6 mediated inflammation upregulated endotoxin levels in the Apc $^{Min/+}$ mouse (Figure 6). This points towards room for redundancy in the IL – 6 dependent chronic inflammatory response in the Min. It would thus be interesting to see if manipulating IL – 6 levels in the Apc $^{Min/+}$ mouse rescues liver function with cachexia.

As suppression of IL – 6 elevates endotoxin levels in the Min, endotoxin mediated inflammation could play a secondary role in the chronic inflammatory processes of the Min and studies confirm that endotoxin and MCP – 1 levels are up regulated in the severely cachectic Apc $^{Min/+}$ mice[16, 18]. Endotoxin functions via the TLR 4 receptor and

the liver expresses low levels of TLR 4 in the normal healthy mouse. But TLR – 4 expression is upregulated in the cachectic livers (Figure 7).

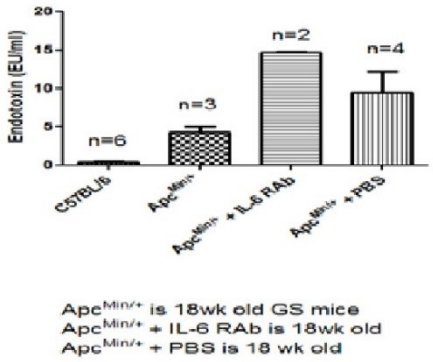

Figure C.6: Effect of IL 6 receptor antibody administration on plasma endotoxin levels.

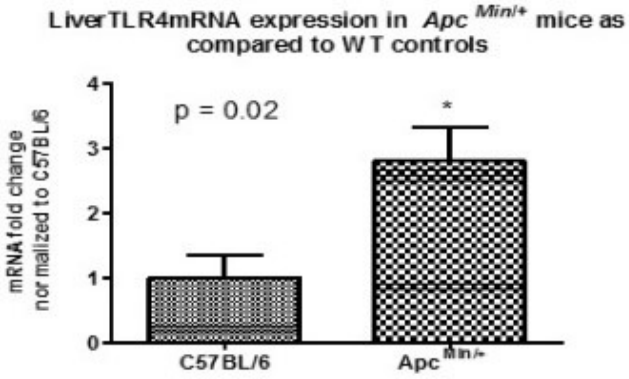

Figure C.7: *Apc*$^{Min/+}$ mice upregulate TLR 4 expression

Endotoxin secretion can lead to MCP – 1, IL – 6 and TNF – alpha production. Very high levels of endotoxin in the blood are seen during septic conditions. Antibiotic have been used treat LPS related ailments seen with sepsis and alcohol induced liver injury. Interestingly pretreatment with antibiotics can attenuate LPS mediated liver injury induced by alcohol consumption[55]. Administration of antibiotics to suppress systemic inflammation in the Apc Min/+ mouse leads to a suppression of splenomegaly and lymph node enlargement.

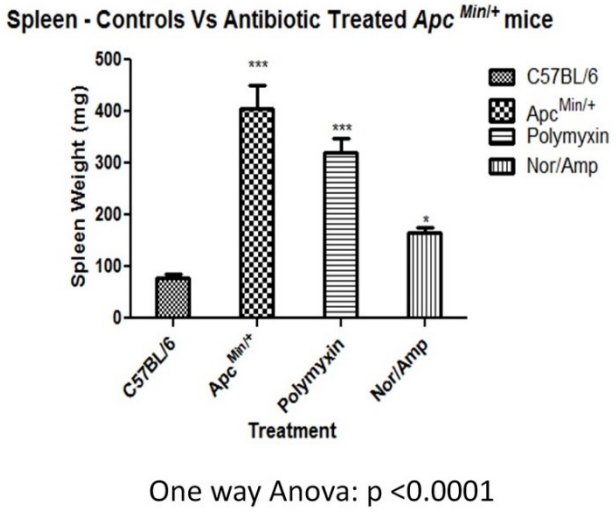

Figure C.8: Administration of antibiotics Polymyxin and Norflaxacin/Ampicillin led to attenuation of splenomegaly in the *Apc*$^{Min/+}$ mouse.

Research Design and Methods:

Overall Research Design: The overall purpose of the study is to monitor the role of liver function during the progression of cachexia. Chronic inflammation and energy deficit contribute heavily to the onset of cancer cachexia, but if liver dysfunction plays a role in cachexia development is yet to be determined.

The title of the project defines a study that would study the role of "chronic inflammation" on "liver function". Both chronic inflammation and liver function are a vague set of characteristics that need to be defined more clearly for the purpose of an experimental design setup. Chronic inflammation can be broadly classified into two components, the secreted inflammatory component (cytokines) and the cellular component (proliferation of immune cells). Both these compartments are engaged in a positive feedback loop allowing the inflammatory cascade to proceed. *For the purpose of this project we would the secretory component of the cascade will examine IL -6, MCP -1 and endotoxin. Spleen size and lymph node size will be a measurement marker for the cellular compartment proliferation*. The liver as we know performs numerous functions in the human body, but for the purpose of this study we would define *liver function in terms of protein synthesis, inflammatory response, ability for glycogen storage, fat deposition, fibrosis and measurement of ALT activity*.

Aim1: To determine if liver function contributes to cachexia progression in the *Apc* $^{Min/+}$ model of cancer cachexia

Rationale: A recent study by Jones et. al. showed that liver production of very low density lipoproteins is suppressed with cachexia in the C26 model. Effect of liver function in the *Apc* $^{Min/+}$ mouse leading to cachexia has not yet been studied. The liver shows signs of dysfunction with cachexia with loss of albumin and increased production of acute phase proteins in the serum but a detailed study to see how liver function contributes to cachexia and cachexia progression has not been studied. IL – 6 levels are known to increase progressively with cachexia onset from 14 week of age onwards. MCP – 1 levels are increased earlier around 12 weeks in the Min mice, whereas endotoxin levels are increased

only in severely cachectic Apc $^{Min/+}$ mice. It is would thus be interesting to see if liver function changes only in the severely cachectic mice or is altered progressively with correlating to skeletal muscle loss from 12 – 14 weeks of age. Aim of this study would thus first establish if liver function is altered in severely cachectic mice and if this alteration is progressive from 12 – 14 weeks of age.

Aim 1.1: Is liver function altered in severely cachectic *Apc* $^{Min/+}$ mice?

Aim 1.2: Is liver function altered with cachexia progression in the *Apc* $^{Min/+}$ mice?

Experimental design for specific aim #1: Experiment 1 will establish if markers of liver function change with cachexia. *Apc* $^{Min/+}$ mice will be randomized into 3 groups at approximately 5 weeks of age. Age matched wild type (WT) controls C57BL/6 mice would be used as controls. The mice will be divided into 3 groups: Mice will be sacrificed at 3 different ages: 12 weeks of age (non – cachectic stage), 14 weeks of age (pre – cachectic stage)[38] and 18 – 20 weeks of age (severely cachectic stage)[117]. The Apc $^{Min/+}$ mice start developing tumors very early at around 10 weeks of age[131], [132], cachexia develops only around week 16. The mice will be monitored for body weights from the time of weaning to the time of sacrifice. Skeletal muscle, blood plasma, liver and spleen will be collected from these mice and stored at - 80°C till further storage. Total body weight loss at sacrifice will be calculated and mice falling within the non – cachectic, pre- cachectic and severely cachectic mice would be include to determine liver function. Excised livers from these mice will be used to determine liver function in terms of protein synthesis, glycogen content, fat content, fibrosis and inflammatory response. Western blot technique, RNA extraction and PCR techniques, Histology techniques – Hematoxylin and Eosin staining, PAS staining, Oil Red O staining, Trichrome staining, ELISAs and glycogen content assay

would be performed to track attenuation of liver progression. Two comparisons will be analyzed for the two aims proposed. Aim1.1 will compare animals from the 20 week group to the 20 week C57BL/6 mice. Aim 1.2 will compare 12 week – 14 week and 20 week old Apc $^{Min/+}$ mice. Unpaired t – test and One Way ANOVA will be used for statistical analysis. P = 0.05

Experiment #1: This experiment will identify the markers and timeline for liver function alteration with cachexia, establishing the role of liver function in cachexia progression.

Apc $^{Min/+}$ male mice were will be bred with C57BL/6 female mice and genotype of the new borns will be identified by genotyping for the presence of APC gene mutation. The mice will be randomized into 3 different groups at 5 weeks of age. Group 1 will be the non – cachectic group to be sacrificed at 12 weeks of age, Group 2 will be the pre –cachectic group to be sacrificed at 14 weeks of age and group 3 will be the severely cachectic group and will be sacrificed at 20 weeks of age. The mice will be monitored throughout the length of the study for body weights and rectal temperatures. The animals will be fasted overnight prior to sacrifice and anesthetized with the ketamine/xylazine/acepromazine cocktail. Blood will be collected from these mice via retro – orbital puncture. Skeletal muscle, Liver and spleen will be excised from the mice at sacrifice, snap frozen in liquid nitrogen and stored at -80°C till further use. Based on the previous *Apc* $^{Min/+}$ work done in the laboratory on female and male *Apc* $^{Min/+}$ mice each of the *Apc* $^{Min/+}$ groups will have 8 mice at the start of the experiment [129, 133].

Table C. 2: Number of animals to be used for each of the groups for Aim 1:

Groups

	Non – Cachectic (12 weeks)	Pre – cachectic (14 weeks)	Severely cachectic (20 weeks)
C57BL/6 (WT)	N = 6	N = 6	N = 6
Apc $^{Min/+}$	N = 8	N = 8	N = 8

Primary Outcomes:

Inflammatory markers: Since IL – 6 is the primary driver of the inflammatory phenotype seen in the Apc Min/+ mice, activation of the IL – 6 signalling cascade will be confirmed. Activation of STAT – 3 via phosphorylation, activation of SOCS 3 would be measured via Western blot. If protein analysis proves to be inconclusive in mRNA levels for STAT-3, SOCS – 3 and the IL – 6 receptor gp130 would be measured. The liver responds to an inflammatory stimuli by triggering the acute phase protein (APP) secretion. The levels of APPs like haptaglobin, fibrinogen and SAA would be measured at the mRNA and protein level in the liver homogenates of the $Apc^{Min/+}$ mice and compared with age matched WT controls. For the IL – 6 independent mechanisms, spleen size between the different groups will be compared as a measure of immune cell proliferation. TLR 4 downstream cascade activating NF – κB will be estimated in terms of both protein and mRNA quantification in liver homogenates.

Protein Synthesis/Degradation markers: Infection or tumors are known to upregulate protein synthesis in the liver partially for the synthesis of APP, gluconeogenesis via the Cori's cycle and due to the systemic hypermetabolic state. But proinflammatory cytokine secretion is also known to increase MMP levels in the liver. The mTOR cascade will be probed for to estimate rate of protein synthesis, with p – mTOR and its downstream targets 4EBP-1 and ribosomal S6 kinase being measured using Western blot and quantitative PCR.

Protein degradation rate in the liver will be measured using matrix metalloproteinase 2 (MMP – 2).

Liver morphology analysis: Liver morphology will be observed by hematoxylin and Eosin (H&E) staining. The C57BL/6 sections will be compared to severely cachectic Apc Min/+ mice tissue. Min liver morphology will be compared for the non – cachectic, pre – cachectic and severely cachectic mice. The stained sections will be compared for morphological changes in liver anatomy with cachexia progression. Liver sections of C57BL/6 mice would be used as controls.

Liver glycogen content: Liver glycogen content allows us to study if any energy reserves are preserved in the cachectic liver or do glycogen stores deplete with cachexia progression. Glycogen levels in the liver will be studied in by staining the cryostat sections with Periodic Acid Schiff's (PAS) stain. A quantitative assay on liver glycogen content will be done using a colorimetric assay for glycogen measurement.

Liver lipid content: Liver lipid content will be measured using Oil Red O staining. Increased levels of pro inflammatory cytokines are known to increase lipolysis. The excessive fat can be broken down in the liver for energy. The Min model is hypermetabolic and comparing fat deposition in the liver from the non – cachectic to severely cachectic state will allow us to examine liver function with respect to fatty acid metabolism.

Liver injury makers: 1) Presence of fibrotic tissue in the liver will be measured using trichrome staining. Liver injury is commonly observed under chronic inflammatory conditions, but if fibrosis occurs in the liver with cachexia is not known.

Liver injury makers: 2) *Alanine aminoacyltranferase (ALT) measurement:* Plasma ALT levels are a marker for liver injury. The enzyme is usually located in liver parenchymal cells and allows the body to metabolize protein or more specifically alanine to glucose. Its presence in blood signifies liver injury. In a healthy mouse ALT levels usually range from 17 – 77 U/I.

Albumin content in liver and plasma: Liver synthesizes the protein albumin under normal healthy condition. During prolonged infections and cancer the production of albumin via the liver decreases. Albumin production is thus a marker for liver function and will be measured using Western blot and quantitative PCR. Since albumin is synthesized in the liver but is secreted in the blood, albumin protein levels will be analyzed by western blotting in plasma samples.

Specific Methodology Aim #1:

Genotyping: Litters born in a breeding cage will be weaned at 3 – 4 weeks of age and separated depending based on sex. The mice will be ear punched, given an identification number and a small piece of their tail will be sniped off. The tail snip will be digested in a cocktail of 200ul of tailing buffer and 5 µl of proteinase K. The sample will be vortexed and placed in a 37°C water bath overnight. The next day the tubes will be removed from the water bath and placed in a dry heat bath heated upto 95°C for 10 minutes. This will kill the proteinaseK activity. 2 µl of the tail digest will be used to run the PCR using the mutated APC gene primer. Apc gene primers - forward 5' TGAGAAAGACAGAAGTTA 3", reverse 5' TTCCACTTTGGCATAAGGC 3' will be used to amplify the template. The GoTaq based PCR will be run and the amplification product will be visualized under UV

light on a 1% agarose gel. The well that show an amplified product band will be marked as the Apc Min/+ mice. The samples that do not show a band in the genotyping PCR will be marked as wild type C57BL/6 mice.

Plasma collection: The mice will be anesthetized using either isoflurane of ketamine cocktail. Using a chelated glass capillary tube, blood will be collected via retro – orbital puncture. The collected blood will be stored in an eppendorf on ice. The blood will then be spun at 4°C for 10 minutes at 10,000 rpm. The supernatant plasma is transferred to a fresh eppendorf tube and stored at - 80°C till further use.

Tissue collection: Mice will be given a subcutaneous injection of ketamine (90mg/kg BW) – xylazine (7 mg/kg BW) – acepromazine (1mg/kg BW). Muscle collection will be started as soon as the mouse stops responding to toe/tail pinch. Skeletal muscle tissue like Gastrocnemius, Soleus, Plantaris, Tibialis Anterior (TA) and Quadricep will be excised washed with PBS, dried on a gauze pad and weighed. The weighed tissue is wrapped in foil and snap frozen in liquid nitrogen. Visceral organs like the liver, spleen, heart and fat will be collected after the muscle, cleaned with sterile PBS, dried, weighed and snap frozen in liquid nitrogen. Tibia length is measured with calipers to estimate body size.

Plasma IL – 6 levels: Plasma IL – 6 levels will be measured using the BD biosciences IL – 6 ELISA kit for mice. The plate is coated overnight with IL -6 antibody at 4°C. Samples are diluted 1:1 (50ul of plasma + 50 µl of diluent buffer), while serial dilutions of the standards are prepared ranging from 1000pg/ml to 15.6pg/ml. The samples will incubated in the coated plate for 2 hours and washed off with 5 washes. A second anti – IL 6 antibody will then be added to the plate and the plate will be incubated for 1 hour. The plate will

then be washed 7 times before the TMB substrate can be added to the plate for colour development. The colour development reaction is stopped after 30 minutes using 1% acetic acid as the stop solution. The plate is measured at 450nm wavelength. The standard curve is plotted after subtracting the blank and samples that fall off the curve are eliminated from the analysis. The samples falling on the curve are used to quantify plasma IL – 6 levels.

Plasma Endotoxin levels: Plasma endotoxin levels will be determined using the Hycult Limulus Ambeocyte lysate (LAL) assay kit. 5ul of the serum will be diluted with 45ul of endotoxin free water and heated in upto 75°C for 10 minutes. Standard curve will be prepared via serial dilutions in endotoxin free water. Standards too will be heated at 75°C for 10 minutes. The plate will be read for background at 450nm wavelength. The LAL reagent shall be reconstituted and 50ul of the reagent will be added to each well, except for the controls. LAL reacts with LPS and turn yellow. Color development will be allowed for 35 – 40 minutes after which the reaction will be stopped using 50ul acetic acid solution. The plate will be read at 450nm. The standard curve will be plotted as a sigmoidal curve after subtraction of the zero minute reading from the final reading. Concentrations of the samples will be calculated using the Michealis Menten enzyme kinetic reaction.

RNA isolation: A small piece of liver will be cut and weighed. The tissue should be approximately 15mgs or smaller in weight. The cut tissue will be resuspended in 1ml of trizol and homogenized using a polytron homogenizer. The homogenate will be transferred to an eppendorf tube and set on ice. 200ul of chloroform will be added to the trizol homogenate and the tube will be shaken well for 15 – 30 seconds. The tube will be allowed to incubate at room temperature for 10 minutes and the spun at maximum rpm for 15 minutes at 4°C. The supernatant will be removed and transferred to a fresh tube. More than

twice the amount of 100% EtOH will be added to the supernatant, to allow for RNA precipitation. The tubes will be incubated at RT for 10 minutes and spun at max rpm for 15 minutes. The resulting pellet will be washed with 70% ethanol in DEPC water centrifuged at 9500rpm for 5 minutes and air dried at 60°C. The dried pellet is dissolved in approximately 40ul of DEPC water. The quality and integrity of RNA is checked using the spectrophotometric analysis and by running the RNA on a 1% agarose gel. A spectrophotometric ratio (A260/A280) of > 1.8 implies good quality RNA without and protein contamination. Agarose gel with 3 distinct RNA bands implies high quality non – degraded RNA. Once checked for quality and integrity the RNA sample is stored -80°C till further use.

cDNA preparation: Isolated RNA will be converted to cDNA using the TaqMan cDNA synthesis kit. 1ug of RNA will be used to make the cDNA cocktail. Once synthesized the cDNA can be stored at -20°C till further use. The cDNA thus prepared is run with GAPDH primers on a normal PCR thermal cycler with GoTaq for 18 -20 cycles. The resulting product is run on a 1% agarose gel to check for cDNA quality.

Real time PCR: Once the quality of cDNA is determined to be good, the cDNA is amplified using the primers of interest and SyBr Green. The GAPDH gene is used an internal control/ housekeeping gene and the gene of interest is compared against it. The Δct method is used to calculate differences in gene expression between groups with respect to GAPDH.

Table C.3: Primer sequences that will be used for real time PCR amplification of target genes

Gene	Forward Primer	Reverse Primer	Size (bps)
mTOR	5′-CTTCGTGCCTGTCTGATTCT-3′	5′-CAAGGCTCCGTGGATTCGAT-3′	158
STAT3	5′-GAAGGTGGTGGAGAACCTC-3′	5′-GCTGCTGCATCTTCTGTCTG-3′	123
SOSC 3	5′-TGCAGGAGAGCGGATTCTAC-3	5′-TGACGCTCAACGTGAAGAAG-3′	132
SAA	5′-GCGAGCCTACACTGACATGA-3′	: 5′-TTTTCTCAGCAGCCCAGACT-3′	119
Fibrinogen	5′-GTACGTGGCCCAAGAGGTTGT-3′	5′-TAAAATCCTGGTTGGCTTCG-3′	145
Haptaglobin	: 5′-GTATGTCATGCTGCCTGTGG-3′	5′-CAGAAGGTGTGCTCGTTCAA-3′	129

Protein Extraction: Liver tissue is cut and weighed. The tissue is suspended in 10 times the volume of Muller buffer. (E.g. 30mg tissues is suspended in 300ul of Muller buffer on ice). The tissue is then quickly homogenized using a glass on glass homogenizer. The Muller buffer homogenate is transferred from the glass tube to an eppendorf tube and stored on ice. The glass homogenizer and glass tube is cleaned out with dilute acid followed by 3 deionized water washes, before homogenizing the next sample. Once all the samples are homogenized, they are spun at 10,000 rpm for 15 minutes at 4°C. The supernatant is transferred to afresh eppendorf tube and diluent buffer is added to the homogenate. The homogenate is half the amount of Muller buffer added 150ul). The homogenate will now be vortexed and 2 µl of the homogenate will be used to determine the protein concentration using a Bradford assay. Once the protein concentration of the homogenate is estimated, a 3ug/µl aliquot is prepared for the homogenate using 2:1 Muller buffer: Diluent buffer cocktail. The 3ug/µl aliquot is the working stock used to run Western blot analysis.

Western Blot: Protein extract are run on SDS – PAGE gel and transferred on to PVDF membrane overnight. Once transferred the Ponceau staining will be done to determine the uniform transfer onto the membrane. The membrane will then be probed with primary antibody, washed with TBST 3 times and incubated with an HRP tagged secondary antibody. Chemiluminescent agent will be used to estimate the HRP bound to the membrane. The chemiluminiscence is quantified by autoradiography techniques. The developed blot is scanned onto a computer and integrated optical density (IOD) is determined using the Image J software.

Cryostat Sectioning: Frozen liver sections will be cut and mounted on a chuck using Optimum Cutting Temperature (OCT) media. The sections will be allowed to thaw in the cryostat to -18°C and then cut. The section will be 8 – 10 microns thick. The unstained sections will be collected on to a charged slide and stored at - 80° C till further analysis. The sectioned slides will be used to perform all the histology techniques.

Staining of Cryostat Sections:

Hematoxylin and Eosin Staining: The frozen section will be cut 8 – 10um thick using a cryostat. The frozen sections will be thawed and air dried and stained with progressive hematoxylin for 5 – 7 minutes. The slides will then be washed with dH_2O six times followed by six dips in acid alcohol solution. The slides will then be dipped in Ammonia – H_2O solution six times and washed in dH_2O for 10 minutes. The slides are counterstained with eosin to stain for the cytoplasm. Following the eosin staining the slides will be progressively dehydrated in alcohol grades and cleared in xylene. The slide will be allowed

to dry and mounted using the Permount media. The slides will be observed under a light microscope using the appropriate magnification

Periodic Acid Schiff's (PAS) Staining: The frozen sections will be air dried and dehydrated using Carnoy's fixative. The fixed sections will be stained with PAS stain for 2hrs. The slides will be washed under running tap water and observed under the microscope at appropriate magnification. The slides randomized and scored blind on a scale of 1 – 5, with one being the lightest stain and 5 being the darkest stain. The histological score will be used to estimate glycogen content in the liver.

Oil Red O Staining: Frozen cryostat sections will be placed in propylene glycol for 2 minutes for fixation. The slides will then be stained with Oil Red O stain for 16 hrs. The slides will then differentiated in 85% propylene glycol for 1 minute and rinsed with distilled water. The slides will then be stained with hematoxylin for 5 minutes and rinsed thoroughly with distilled water. The slides will then be mounted in permount and allowed to dry. The slides will be observed under a light microscope under appropriate magnification.

Trichrome Staining: Sections will be fixed using Bouins fixative for 1 hr. at 56°C. The section will be rinsed under running tap water for 10 minutes till the yellow colour is removed. The tissue will then be stained with hematoxylin for 10 minutes and rinsed with warm tap water for 10 minutes. The slides will then be washed with distilled water and stained with Biebrich Scarlet – acid fuchsin solution for 10 – 15 minutes. The sections will then be washed with distilled water and differentiated with phosphomolybdic – phosphotungstunic acid solution for 10 – 15 minutes till the collagen stains red. The

sections will then be transferred to aniline blue stain for 10 minutes, rinsed with distilled water and differentiated in 1% acetic acid solution for 2 – 5 minutes. The slides will then be rinsed in distilled water and dehydrated through alcohol grades. Finally the slides will be mounted in permount media and allowed to dry. The sections will be observed under an appropriate magnification

Plasma ALT levels in the different group will be measured using ALT liver enzyme kit (Pointe Scientific). 5ul of plasma will be diluted to a 1:50 dilution. The ALT enzyme from the kit is added to the sample and absorbance is measured at 340nm over 1 minute interval for 3 minutes. The rate of NADPH degradation is plotted and the levels of ALT are determined from the slope of the degradation rate.

Glycogen content assay: Glycogen content will also be measured by extraction of glycogen from the liver homogenate. Liver tissue will be cut, weighed and stored in 10 ml tubes. 1 ml of 30% KOH/ Na2SO4 solution will be added to the tissue the tubes will be boiled for 30 minutes, covered with foil. The tubes will be cooled on ice. 2 ml of 95% EtOH will be added to the tubes to precipitated the glycogen out. The sample will be vortexed and stored on ice for 30 minutes. The tubes will then be centrifuged at 550g for 30 minutes. The supernatant will be discarded and the pellet will be air dried. The dried glycogen pellet will then be dissolved in 1 ml of ddH_2O till the glycogen is in solution. Glycogen standards will be prepared from known concentration of glycogen (0, 25, 50, 75 and 100ug/ml). Add 1 ml of 5% phenol to each of the samples. Dilute the liver samples to 50ul (25ul) of sample + 950 (975ul) of ddH_2O. Quickly add 1ml of 96 – 98 % H2SO4 to the sample/standard tubes. Incubate on ice bath for 30 minutes. Blank the spectrophotometer at 490nm using

1ml of ddH_2O, followed by reading of the standards and the samples. Glycogen content can be back calculated by taking into the total liver weight into account.

Aim 2: To determine if IL – 6 signaling is necessary or sufficient to alter liver metabolic and inflammatory process in the *Apc* $^{Min/+}$ model of cancer cachexia

Rationale: IL – 6 signaling is the major driver for skeletal muscle loss in the Apc Min/+ and C 26 model of cancer cachexia[15, 117]. Liver function has been shown to be disrupted in the C26 cachexia model by Jones et. al. IL -6 overexpression in different model of infection and cancer have been shown to have detrimental effects on liver function leading to increased inflammatory responses – NF – kB and APPs – in the liver. IL – 6 overexpression is also associated with a STAT3 dependent increase in the levels of TLR 4 and TLR 2 expression on the skeletal muscle. This increase in TLR 2 and TLR 4 levels is associated is skeletal muscle insulin resistance[42]. IL – 6 is also known to interfere with glucose utilization and lipid metabolism in the liver. IL – 6 thus seem to affect liver function in numerous ways, but its role in altering liver function with cachexia progression in the Apc Min/+ mice is unexplored. In this Aim we propose to elucidate the role of IL – 6 in altering liver function in cachectic Apc Min/+ mice. Inhibition and overexpression studies with IL – 6 in the Min mouse will help decipher mechanisms altered by IL – 6 in the liver.

Experiment 2.1 will use administration of two different IL – 6 inhibitors on liver function in cachectic *Apc*$^{Min/+}$ mice. IL – 6 inhibition in this aim will be brought about by administration of an anti – body against the trans IL – 6 signaling. Soluble IL – 6 receptor in the blood can buffer IL – 6 signaling, by binding to free IL – 6 molecules in the blood. Binding of the soluble receptor to the soluble receptor antibody often triggers immune cells in the blood eliciting and inflammatory response, but activation of the classical response

leads to leads to more anti – inflammatory responses like secretion of acute phase proteins from the liver[37]. It would thus be interesting to examine if inhibition of trans IL – 6 signaling alters liver function.

Since inhibition of IL – 6 by its antibody is only partial, the second part of this sub – Aim will study the effect of Pyrrolidine dithiocarbamate (PDTC) and systemic STAT3 and NF – kB inhibitor on liver function in cachectic Apc Min/+ mice.

Experimental Design for specific Aim 2:

Aim 2.1: This study will administer the IL – 6 trans signaling inhibitor (gp130fusion protein) and PDTC to severely cachectic Apc Min/+ mice. Chronic IL – 6 signalling levels will define chronic inflammation in this Aim, whereas Liver function parameters would remain the same as Aim 1.

Animals: All the animals required for this experiment will be housed in Animal Resource Facility, at the University of South Carolina. The animals will be divided into two different groups C57BL/6 and Apc Min/+ mice. The mice will be allowed to age to 16 – 18 weeks till they are severely cachectic and start losing body weight. The mice will be housed in standard caging and would be allowed an ad libitum access to food and water. The animals were maintained at a 12:12 light and dark cycle. The mice will be monitored for body weight from 12 weeks of age onwards. At the initiation of body weight loss, IL – 6 inhibitor – gp130fusion protein and PDTC – will be administered to the appropriate groups The gp130 fusion protein will inhibit the IL – 6 trans signaling and will be administered intraperitonially at a dose of 150ug/mouse once every week for two weeks. The PDTC on the other had has a shorter half-life and will be administered i.p. at a dose of

100ug/ml/ gram of body weight daily for two weeks. The control Min and WT group will be administered sterile PBS as a placebo in place of the drug. Based on the IL – 6 receptor antibody study, 6 mice group would suffice to show statistical significance ($p = 0.05$) with administration of PDTC and gp130 fusion protein administration

Table C.4: Animal treatment groups of the gp130 fusion protein experiment

Genotype	Treatment	Age	N
C57BL/6	PBS	16 – 18 weeks	6
C57BL/6	Gp130 fusion protein	16 – 18 weeks	6
Apc Min/+	PBS	16 – 18 weeks	6
Apc Min/+	Gp130 fusion protein	16 – 18 weeks	6

Table C.5: Animal treatment groups of the PDTC experiment

Genotype	Treatment	Age	N
C57BL/6	PBS	16 – 18 weeks	6
C57BL/6	PDTC	16 – 18 weeks	6
Apc Min/+	PBS	16 – 18 weeks	6
Apc Min/+	PDTC	16 – 18 weeks	6

Since both the studies utilize 16 – 18 week control mice treated with PBS the same control group will be used for both the studies.

Primary Outcomes:

Inflammatory markers: Since IL – 6 is the primary driver of the inflammatory phenotype seen in the *Apc* $^{Min/+}$ mice, activation of the IL – 6 signaling cascade will be confirmed. Activation of STAT – 3 via phosphorylation, activation of SOCS 3 would be measured via Western blot. If protein analysis proves to be inconclusive in mRNA levels for STAT-3, SOCS – 3 and the IL – 6 receptor gp130 would be measured. The liver responds to an inflammatory stimulus by triggering the acute phase protein (APP) secretion. The levels of APPs like haptaglobin, fibrinogen and SAA would be measured at the mRNA and protein level in the liver homogenates of the Apc Min/+ mice and compared with age matched WT controls. For the IL – 6 independent mechanisms, spleen size between the different groups will be compared as a measure of immune cell proliferation. TLR 4 downstream cascade activating NF – κB will be estimated in terms of both protein and mRNA quantification in liver homogenates.

Protein Synthesis/Degradation markers: Infection or tumors are known to upregulate protein synthesis in the liver partially for the synthesis of APP, gluconeogenesis via the Cori's cycle and due to the systemic hypermetabolic state. But proinflammatory cytokine secretion is also known to increase MMP levels in the liver. The mTOR cascade will be probed for to estimate rate of protein synthesis, with p – mTOR and its downstream targets 4EBP-1 and ribosomal S6 kinase being measured using Western blot and quantitative PCR. Protein degradation rate in the liver will be measured using matrix metalloproteinase 2 (MMP – 2).

Liver morphology analysis: Liver morphology will be observed by hematoxylin and Eosin (H&E) staining. The C57BL/6 sections will be compared to severely cachectic Apc Min/+

mice tissue. Min liver morphology will be compared for the non – cachectic, pre – cachectic and severely cachectic mice. The stained sections will be compared for morphological changes in liver anatomy with cachexia progression. Liver sections of C57BL/6 mice would be used as controls.

Liver glycogen content: Liver glycogen content allows us to study if any energy reserves are preserved in the cachectic liver or do glycogen stores deplete with cachexia progression. Glycogen levels in the liver will be studied in by staining the cryostat sections with Periodic Acid Schiff's (PAS) stain. A quantitative assay on liver glycogen content will be done using a colorimetric assay for glycogen measurement.

Liver lipid content: Liver lipid content will be measured using Oil Red O staining. Increased levels of pro inflammatory cytokines are known to increase lipolysis. The excessive fat can be broken down in the liver for energy. The Min model is hypermetabolic and comparing fat deposition in the liver from the non – cachectic to severely cachectic state will allow us to examine liver function with respect to fatty acid metabolism.

Liver injury makers: 1) Presence of fibrotic tissue in the liver will be measured using trichrome staining. Liver injury is commonly observed under chronic inflammatory conditions, but if fibrosis occurs in the liver with cachexia is not known.

Liver injury makers: 2) *Alanine aminoacyltranferase (ALT) measurement:* Plasma ALT levels are a marker for liver injury. The enzyme is usually located in liver parenchymal cells and allows the body to metabolize protein or more specifically alanine to glucose. Its presence in blood signifies liver injury.

Albumin content in liver and plasma: Liver synthesizes the protein albumin under normal healthy condition. During prolonged infections and cancer the production of albumin via the liver decreases. Albumin production is thus a marker for liver function and will be measured using Western blot and quantitative PCR. Since albumin is synthesized in the liver but is secreted in the blood, albumin protein levels will be analyzed by western blotting in plasma samples.

Specific Methodology Aim #2:

Genotyping: Litters born in a breeding cage will be weaned at 3 – 4 weeks of age and separated depending based on sex. Refer to Aim 1 – Genotyping for detailed protocol.

Administration of the gp130 fusion protein: Mice will be aged to 16 – 18 week of age. Body for these mice will be monitored every week. Administration of the fusion protein would be initiated after the mice show an initial body weight loss. 150ug/ mouse of the fusion protein will be administered once a week for two weeks.

Administration of PDTC: Mice will be aged to 16 – 18 week of age. Body for these mice will be monitored every week. Administration of PDTC would be initiated after the mice show an initial body weight loss. 100 µg/ml of PDTC will be administered once an everyday for a period of two weeks.

Plasma collection: The mice will be anesthetized using either isoflurane or ketamine cocktail. Using a chelated glass capillary tube, blood will be collected via retro – orbital puncture. The collected blood will be stored in an eppendorf on ice. The blood will then be spun at 4°C for 10 minutes at 10,000 rpm. The supernatant plasma is transferred to a fresh eppendorf tube and stored at - 80°C till further use.

Tissue collection: Mice will be given a subcutaneous injection of ketamine (90mg/kg BW) – xylazine (7 mg/kg BW) – acepromazine (1mg/kg BW). Muscle collection will be started as soon as the mouse stops responding to toe/tail pinch. Skeletal muscle visceral organs like the liver will be collected cleaned with sterile PBS, dried, weighed and snap frozen in liquid nitrogen. Tibia length is measured with calipers to estimate body size. Refer to Aim 1 for detailed protocol.

Plasma IL – 6 levels: Plasma IL – 6 levels will be measured using the BD biosciences IL – 6 ELISA kit for mice. Refer to Aim 1 for detailed protocol.

Plasma Endotoxin levels: Plasma endotoxin levels will be determined using the Hycult Limulus Ambeocyte lysate (LAL) assay kit. . Refer to Aim 1 for detailed protocol.

RNA isolation: RNA extraction will be done using Trizol, chloroform, ethanol method. Refer to Aim 1 for detailed protocol.

cDNA preparation: Isolated RNA will be converted to cDNA using the TaqMan cDNA synthesis kit. . Refer to Aim 1 for detailed protocol.

Real time PCR: Once the quality of cDNA is determined to be good, the cDNA is amplified using the primers of interest and SyBr Green. The GAPDH gene is used an internal control/ housekeeping gene and the gene of interest is compared against it. The Δct method is used to calculate differences in gene expression between groups with respect to GAPDH. . Refer to Aim 1 for detailed protocol.

Protein Extraction: Protein extraction is done by homogenization in Muller buffer and estimation of protein by Bradford Reagent. . Refer to Aim 1 for detailed protocol.

Western Blot: Protein extract are run on SDS – PAGE gel and transferred on to PVDF membrane overnight. Once transferred the Ponceau staining will be done to determine the uniform transfer onto the membrane. The membrane will then be probed with primary antibody, washed with TBST 3 times and incubated with an HRP tagged secondary antibody. Chemiluminescent agent will be used to estimate the HRP bound to the membrane. The chemiluminscence is quantified by autoradiography techniques. The developed blot is scanned onto a computer and integrated optical density (IOD) is determined using the Image J software.

Cryostat Sectioning: Frozen liver sections will be cut and mounted on a chuck using Optimum Cutting Temperature (OCT) media. The sections will be allowed to thaw in the cryostat to -18°C and then cut. The section will be 8 – 10 microns thick. The unstained sections will be collected on to a charged slide and stored at - 80° C till further analysis. The sectioned slides will be used to perform all the histology techniques. The slides were stained for H&E, PAS, Oil RedO and Trichrome stains. . Refer to Aim 1 for detailed protocol.

Plasma ALT levels in the different group will be measured using ALT liver enzyme kit (Pointe Scientific). 5ul of plasma will be diluted to a 1:50 dilution. The ALT enzyme from the kit is added to the sample and absorbance is measured at 340nm over 1 minute interval for 3 minutes. The rate of NADPH degradation is plotted and the levels of ALT are determined from the slope of the degradation rate.

Glycogen content assay: Glycogen content assay: Glycogen content will also be measured by extraction of glycogen from the liver homogenate. Glycogen will be extracted using

KOH/ Na2SO4 solution followed by EtOH precipitation. Extracted glycogen will be compared to the glycogen standard curve to estimate total glycogen content in the liver. Refer to Aim 1 for detailed protocol.

Aim 3: To determine if antibiotic mediated immune suppression affects liver function in the cachectic *Apc*$^{Min/+}$ mice model

Rationale: The *Apc*$^{Min/+}$ model of cancer cachexia characterized by loss of muscle mass, fat mass, splenomegaly, increased level of pro inflammatory cytokines like IL – 6, MCP - 1, increased gut permeability, increased levels of plasma endotoxin levels, swelling of mesenteric lymph nodes. Though IL – 6 is the primary driver for cachexia in the Apc Min/+ mice, factors other than IL – 6 are also involved in cachexia progression. Gut permeability is known to be affected in the ApcMin/+ mice[16]. Changes in gut permeability correspond to increased plasma endotoxin levels. Increased level of LPS in the blood can lead to the secretion of IL -6, MCP -1 and other pro – inflammatory cytokines. Pro – inflammatory conditions triggered by the tumor also allow of proliferation of the immune system leading to splenomegaly. Gut microbiota diversity and composition are known to change with colorectal cancer[134]. An altered gut flora can elicit an immune response further supplementing chronic inflammation. The liver receives the endotoxin contaminated blood via the portal vein. Thus the effect of altered gut microbiota or increased LPS could exacerbate localized inflammatory responses in the liver. Preliminary data shows that antibiotic treatment attenuated splenomegaly. In Aim 3 of this study we will study will employ antibiotics to suppress systemic endotoxin levels by elimination of systemic microbiota. Antibiotics will be administered to non – cachectic mice, suppressing immune response and systemic inflammation in the Apc Min/+ mice. The mice will be monitored

for the next seven weeks and sacrificed at 20 weeks of age. Since the liver filters blood from the portal vein and the hepatic artery, antibiotic treatment would protect the liver from endotoxin exposure protecting it from a chronic inflammatory response. We hypothesize that antibiotic suppression of systemic inflammation would attenuate liver function in $Apc^{Min/+}$ mice.

Experimental Design for Specific Aim 3:

Aim 3.1: To determine if polymyxin treatment attenuates chronic inflammation to attenuate liver function during cancer cachexia

Experiment 3.1 Animals will be treated with 1mg/ml dose of the antibiotic Polymyxin. Polymyxin B specifically binds to the lipid A component of bacteria leading to disruption of the cell wall of Gram negative bacteria. Polymyxin treatment does not affect the Gram positive population in the gut. Preliminary data shows an attenuation of spleen size with Polymyxin treatment, indicating a suppressed immune response. We hypothesize that Polymyxin treatment would suppress serum endotoxin levels and immune cell proliferation, attenuating liver function in severely cachectic ApcMin/+ mice.

Aim 3.2: To determine if Norflaxacin/Ampicillin treatment attenuates chronic inflammation to attenuate liver function during cancer cachexia

Experiment 3.2: Animals will be treated with 1mg/ml dose of Ampicillin – Norflaxacin (Nor/Amp) cocktail. The Nor/Amp cocktail targets both the gram positive and gram negative bacteria, allowing a greater suppression of systemic microbes. Norfloxacin act by inhibiting DNA gyrase necessary for bacterial replication, while Ampicillin inhibits bacterial cell wall synthesis. Inhibition via Nor/Amp would allow for complete elimination of both gram positive and gram negative microbes allowing for a greater suppression of

systemic inflammation. Preliminary data shows a greater attenuation of splenomegaly with Nor/Amp treatment as compared to Polymyxin treatment. Suppression of systemic immune response could attenuate inflammation induced liver dysfunction during cachexia in the $Apc^{Min/+}$ mice. We hypothesize that Nor/Amp treatment would suppress systemic endotoxin levels and immune cell proliferation, attenuating liver function in severely cachectic $Apc^{Min/+}$ mice.

Table C.6: Experimental animals used the antibiotic treatment

Genotype	Treatment	Age at initiation	Age at sacrifice	# of animals per group
C57BL/6	dH_2O	13 weeks	20 weeks	10
Apc Min/+	dH_2O	13 weeks	20 weeks	10
	Polymyxin	13 weeks	20 weeks	10
	Nor/Amp	13 weeks	20 weeks	10

Primary Outcomes:

Inflammatory markers: Since IL – 6 is the primary driver of the inflammatory phenotype seen in the Apc Min/+ mice, activation of the IL – 6 signalling cascade will be confirmed. Activation of STAT – 3 via phosphorylation, activation of SOCS 3 would be measured via Western blot. If protein analysis proves to be inconclusive in mRNA levels for STAT-3, SOCS – 3 and the IL – 6 receptor gp130 would be measured. The liver responds to inflammatory stimuli by triggering the acute phase protein (APP) secretion. The levels of APPs like haptaglobin, fibrinogen and SAA would be measured at the mRNA and protein

level in the liver homogenates of the Apc Min/+ mice and compared with age matched WT controls. For the IL – 6 independent mechanisms, spleen size between the different groups will be compared as a measure of immune cell proliferation. TLR 4 downstream cascade activating NF – κB will be estimated in terms of both protein and mRNA quantification in liver homogenates. Plasma endotoxin levels will be measured with antibiotic treatment.

Protein Synthesis/Degradation markers: Infection or tumors are known to upregulate protein synthesis in the liver partially for the synthesis of APP, gluconeogenesis via the Cori's cycle and due to the systemic hypermetabolic state. But proinflammatory cytokine secretion is also known to increase MMP levels in the liver. The mTOR cascade will be probed for to estimate rate of protein synthesis, with p – mTOR and its downstream targets 4EBP-1 and ribosomal S6 kinase being measured using Western blot and quantitative PCR. Protein degradation rate in the liver will be measured using matrix metalloproteinase 2 (MMP – 2).

Liver morphology analysis: Liver morphology will be observed by hematoxylin and Eosin (H&E) staining. The C57BL/6 sections will be compared to severely cachectic Apc Min/+ mice tissue. Min liver morphology will be compared for the non – cachectic, pre – cachectic and severely cachectic mice. The stained sections will be compared for morphological changes in liver anatomy with cachexia progression. Liver sections of C57BL/6 mice would be used as controls.

Liver glycogen content: Liver glycogen content allows us to study if any energy reserves are preserved in the cachectic liver or do glycogen stores deplete with cachexia progression. Glycogen levels in the liver will be studied in by staining the cryostat sections

with Periodic Acid Schiff's (PAS) stain. A quantitative assay on liver glycogen content will be done using a colorimetric assay for glycogen measurement.

Liver lipid content: Liver lipid content will be measured using Oil Red O staining. Increased levels of pro inflammatory cytokines are known to increase lipolysis. The excessive fat can be broken down in the liver for energy. The Min model is hypermetabolic and comparing fat deposition in the liver from the non – cachectic to severely cachectic state will allow us to examine liver function with respect to fatty acid metabolism.

Liver injury makers: 1) Presence of fibrotic tissue in the liver will be measured using trichrome staining. Liver injury is commonly observed under chronic inflammatory conditions, but if fibrosis occurs in the liver with cachexia is not known.

Liver injury makers: 2) *Alanine aminoacyltranferase (ALT) measurement:* Plasma ALT levels are a marker for liver injury. The enzyme is usually located in liver parenchymal cells and allows the body to metabolize protein or more specifically alanine to glucose. Its presence in blood signifies liver injury.

Albumin content in liver and plasma: Liver synthesizes the protein albumin under normal healthy condition. During prolonged infections and cancer the production of albumin via the liver decreases. Albumin production is thus a marker for liver function and will be measured using Western blot and quantitative PCR. Since albumin is synthesized in the liver but is secreted in the blood, albumin protein levels will be analyzed by western blotting in plasma samples.

Specific Methodology Aim #1:

Genotyping: Litters born in a breeding cage will be weaned at 3 – 4 weeks of age and separated depending based on sex. Refer to Aim 1 – Genotyping for detailed protocol.

Administration of antibiotics: Antibiotics were added to drinking water at a concentration of 1mg/ml. Polymyxin B, Norfloxacin and Ampicillin were purchased from Sigma, weighed and dissolved in 100mls of water each. The Nor/Amp cocktail was mixed in equal amounts. The treatment with antibiotics started at 13 weeks of age and was continued till sacrifice of the animal.

Plasma collection: The mice will be anesthetized using either isoflurane or ketamine cocktail. Using a chelated glass capillary tube, blood will be collected via retro – orbital puncture. The collected blood will be stored in an eppendorf on ice. The blood will then be spun at 4°C for 10 minutes at 10,000 rpm. The supernatant plasma is transferred to a fresh eppendorf tube and stored at - 80°C till further use.

Tissue collection: Mice will be given a subcutaneous injection of ketamine (90mg/kg BW) – xylazine (7 mg/kg BW) – acepromazine (1mg/kg BW). Muscle collection will be started as soon as the mouse stops responding to toe/tail pinch. Skeletal muscle Viseral organs like the liver will be collected cleaned with sterile PBS, dried, weighed and snap frozen in liquid nitrogen. Tibia length is measured with calipers to estimate body size. Refer to Aim 1 for detailed protocol.

Plasma IL – 6 levels: Plasma IL – 6 levels will be measured using the BD biosciences IL – 6 ELISA kit for mice. Refer to Aim 1 for detailed protocol.

Plasma Endotoxin levels: Plasma endotoxin levels will be determined using the Hycult Limulus Ambeocyte lysate (LAL) assay kit. . Refer to Aim 1 for detailed protocol.

RNA isolation. RNA extraction will be done using Trizol, chloroform, ethanol method. Refer to Aim 1 for detailed protocol.

cDNA preparation: Isolated RNA will be converted to cDNA using the TaqMan cDNA synthesis kit. . Refer to Aim 1 for detailed protocol.

Real time PCR: Once the quality of cDNA is determined to be good, the cDNA is amplified using the primers of interest and SyBr Green. The GAPDH gene is used an internal control/ housekeeping gene and the gene of interest is compared against it. The Δct method is used to calculate differences in gene expression between groups with respect to GAPDH. . Refer to Aim 1 for detailed protocol.

Protein Extraction: Protein extraction is done by homogenization in Muller buffer and estimation of protein by Bradford Reagent. . Refer to Aim 1 for detailed protocol.

Western Blot: Protein extract are run on SDS – PAGE gel and transferred on to PVDF membrane overnight. Once transferred the Ponceau staining will be done to determine the uniform transfer onto the membrane. The membrane will then be probed with primary antibody, washed with TBST 3 times and incubated with an HRP tagged secondary antibody. Chemiluminescent agent will be used to estimate the HRP bound to the membrane. The chemiluminscence is quantified by autoradiography techniques. The developed blot is scanned onto a computer and integrated optical density (IOD) is determined using the Image J software.

Cryostat Sectioning: Frozen liver sections will be cut and mounted on a chuck using Optimum Cutting Temperature (OCT) media. The sections will be allowed to thaw in the cryostat to -18°C and then cut. The section will be 8 – 10 microns thick. The unstained sections will be collected on to a charged slide and stored at - 80° C till further analysis. The sectioned slides will be used to perform all the histology techniques. The slides were stained for H&E, PAS, Oil RedO and Trichrome stains. . Refer to Aim 1 for detailed protocol.

Plasma ALT levels in the different group will be measured using ALT liver enzyme kit (Pointe Scientific). 5ul of plasma will be diluted to a 1:50 dilution. The ALT enzyme from the kit is added to the sample and absorbance is measured at 340nm over 1 minute interval for 3 minutes. The rate of NADPH degradation is plotted and the levels of ALT are determined from the slope of the degradation rate.

Glycogen content assay: Glycogen content will also be measured by extraction of glycogen from the liver homogenate. Glycogen will be extracted using KOH/ Na2SO4 solution followed by EtOH precipitation. Extracted glycogen will be compared to the glycogen standard curve to estimate total glycogen content in the liver. Refer to Aim 1 for detailed protocol.

APPENDIX D

RAW DATA

Table D.1: Spectrophotometer reading for the timecourse samples in Aim 1

Sample ID	User ID	Date	Time	ng/ul	A260	A280	260/280	260/230	Constant	Cursor Pos.	Cursor abs.	340 raw
586s	Default	9/17/2013	8:42 PM	502.99	12.575	6.920	1.82	2.37	40.00	230	5.308	0.355
732s	Default	9/17/2013	8:46 PM	191.66	4.791	2.816	1.70	2.47	40.00	230	1.936	-0.001
562s	Default	9/17/2013	8:48 PM	544.94	13.624	7.486	1.82	2.35	40.00	230	5.796	0.016
416s	Default	9/17/2013	8:50 PM	560.91	14.023	7.883	1.78	2.35	40.00	230	5.979	0.044
1177s	Default	9/17/2013	8:53 PM	467.36	11.684	6.484	1.80	2.35	40.00	230	4.970	0.058
803s	Default	9/17/2013	8:54 PM	483.13	12.078	7.230	1.67	2.34	40.00	230	5.165	0.013
1102s	Default	9/17/2013	8:57 PM	350.57	8.764	5.252	1.67	2.03	40.00	230	4.324	35.851
1155s	Default	9/17/2013	9:00 PM	486.89	12.172	6.876	1.77	2.16	40.00	230	5.638	15.027
537s	Default	9/17/2013	9:01 PM	468.51	11.713	6.869	1.71	2.29	40.00	230	5.107	0.044
608s	Default	9/17/2013	9:03 PM	171.81	4.295	3.515	1.22	0.96	40.00	230	4.465	30.555
682s	Default	9/17/2013	9:05 PM	252.63	6.316	3.953	1.60	2.06	40.00	230	3.066	39.689
439s	Default	9/17/2013	9:08 PM	494.57	12.364	6.854	1.80	2.34	40.00	230	5.291	0.058
463s	Default	9/17/2013	9:10 PM	433.80	10.845	6.288	1.72	2.16	40.00	230	5.012	0.020
487	Default	9/17/2013	9:12 PM	451.15	11.279	6.364	1.77	2.31	40.00	230	4.890	0.054
1080s	Default	9/17/2013	9:14 PM	569.70	14.242	7.724	1.84	2.13	40.00	230	6.690	0.241
633s	Default	9/17/2013	9:17 PM	453.06	11.326	6.459	1.75	2.34	40.00	230	4.835	0.692
752s	Default	9/17/2013	9:19 PM	805.26	20.132	11.090	1.82	2.38	40.00	230	8.466	0.053
775s	Default	9/17/2013	9:21 PM	641.93	16.048	8.777	1.83	2.36	40.00	230	6.798	0.039
1177b	Default	9/17/2013	9:23 PM	573.37	14.334	6.873	2.09	2.04	40.00	230	7.025	0.044
1177b1	Default	9/17/2013	9:24 PM	578.69	14.467	6.882	2.10	1.88	40.00	230	7.704	0.067
752b	Default	9/17/2013	9:26 PM	438.96	10.974	5.573	1.97	2.08	40.00	230	5.272	0.040
775b	Default	9/17/2013	9:27 PM	592.32	14.808	7.288	2.03	2.06	40.00	230	7.199	0.033
1155b	Default	9/17/2013	9:28 PM	494.37	12.359	5.972	2.07	1.97	40.00	230	6.290	0.230
732b	Default	9/17/2013	9:31 PM	448.53	11.213	5.649	1.98	2.07	40.00	230	5.413	0.088
487b	Default	9/17/2013	9:32 PM	475.23	11.881	6.005	1.98	1.34	40.00	230	8.883	0.108
608b	Default	9/17/2013	9:36 PM	473.39	11.835	5.989	1.98	1.85	40.00	230	6.391	0.455
416b	Default	9/17/2013	9:40 PM	485.45	12.136	6.109	1.99	1.96	40.00	230	6.179	0.129
1080b	Default	9/17/2013	9:43 PM	467.93	11.698	5.727	2.04	1.26	40.00	230	9.282	0.271
1203b	Default	9/17/2013	9:44 PM	542.49	13.562	6.521	2.08	2.09	40.00	230	6.489	0.027
439b	Default	9/17/2013	9:47 PM	492.64	12.316	5.939	2.07	1.93	40.00	230	6.375	0.068
775b	Default	9/17/2013	9:49 PM	257.04	6.426	3.529	1.82	2.41	40.00	230	2.669	0.006
1954	Default	9/17/2013	9:54 PM	1567.26	39.182	19.698	1.99	2.21	40.00	230	17.745	-0.042
1855	Default	9/17/2013	9:58 PM	2188.18	54.704	27.930	1.96	2.05	40.00	230	26.690	5.535
1998	Default	9/17/2013	10:00 PM	1880.46	47.011	23.414	2.01	1.78	40.00	230	26.432	0.058
1927	Default	9/17/2013	10:03 PM	1852.46	46.312	23.103	2.00	2.13	40.00	230	21.714	0.128
1976	Default	9/17/2013	10:04 PM	2648.19	66.205	33.123	2.00	2.07	40.00	230	31.936	0.057
2075	Default	9/17/2013	10:06 PM	1579.68	39.492	19.764	2.00	2.01	40.00	230	19.685	0.194
2051	Default	9/17/2013	10:07 PM	1412.51	35.313	17.729	1.99	1.98	40.00	230	17.822	0.255
2026	Default	9/17/2013	10:09 PM	2103.33	52.583	26.458	1.99	2.02	40.00	230	26.062	0.398
2099	Default	9/17/2013	10:10 PM	2335.47	58.387	29.401	1.99	2.08	40.00	230	28.103	0.270
2142	Default	9/17/2013	10:12 PM	1238.12	30.953	15.546	1.99	2.11	40.00	230	14.660	-0.010
2502	Default	9/17/2013	10:14 PM	2047.84	51.196	26.200	1.95	1.85	40.00	230	27.742	7.091
2477	Default	9/17/2013	10:15 PM	849.73	21.243	10.935	1.94	1.31	40.00	230	16.209	0.030
2535	Default	9/17/2013	10:17 PM	1500.66	37.516	18.750	2.00	2.08	40.00	230	18.053	0.178
2552	Default	9/17/2013	10:18 PM	793.14	19.828	10.166	1.95	2.00	40.00	230	9.907	0.151
2680	Default	9/17/2013	10:20 PM	1628.36	40.709	20.501	1.99	1.95	40.00	230	20.910	0.701
2833	Default	9/17/2013	10:21 PM	1909.28	47.732	23.876	2.00	2.07	40.00	230	23.038	0.024
2810	Default	9/17/2013	10:23 PM	2346.97	58.674	29.559	1.98	1.63	40.00	230	35.949	0.089
2859	Default	9/17/2013	10:25 PM	2258.75	56.469	28.422	1.99	2.03	40.00	230	27.780	0.285
2700	Default	9/17/2013	10:26 PM	1608.67	40.217	20.257	1.99	1.65	40.00	230	24.341	0.808
2651	Default	9/17/2013	10:28 PM	1858.45	46.461	23.462	1.98	1.91	40.00	230	24.334	0.558
2790	Default	9/17/2013	10:29 PM	1910.12	47.753	23.972	1.99	2.11	40.00	230	22.596	0.246
2524	Default	9/17/2013	10:31 PM	1833.49	45.837	22.947	2.00	2.03	40.00	230	22.552	0.522
2580	Default	9/17/2013	10:33 PM	1126.79	28.170	14.170	1.99	1.88	40.00	230	14.965	0.473
2725	Default	9/17/2013	10:34 PM	1296.40	32.410	16.261	1.99	1.73	40.00	230	18.770	0.730
2751	Default	9/17/2013	10:36 PM	1309.98	32.750	16.335	2.00	1.94	40.00	230	16.888	0.539

Table D.2: Spectrophotometer reading for 400ng dilution and cDNA synthesis dilutions for the time course samples in Aim 1

Sample ID	ng/ul	A260	A280	260/280	260/230	RNA dil to 400	water	Cal. Conc	Acutal spec conc	RNA	H2O	Geno	Age
2681	1628.3	40.709	20.501	1.99	1.95	12.283	37.717	400	426.39	2.35	7.65	B6	12
2700	1608.6	40.217	20.257	1.99	1.65	12.433	37.567	400	443.06	2.26	7.74	B6	12
2651	1858.4	46.461	23.462	1.98	1.91	10.762	39.238	400	431.12	2.32	7.68	B6	12
2725	1296.4	32.410	16.261	1.99	1.73	15.427	34.573	400	464.06	2.15	7.85	B6	12
2751	1309.9	32.750	16.335	2.00	1.94	15.268	34.732	400	443.89	2.25	7.75	B6	12
2502	2047.8	51.196	26.200	1.95	1.85	9.767	40.233	400	476.54	2.10	7.90	Min	12
2477	849.7	21.243	10.935	1.94	1.31	23.538	26.462	400	391.6	2.55	7.45	Min	12
2535	1500.6	37.516	18.750	2.00	2.08	13.328	36.672	400	428.64	2.33	7.67	Min	12
2552	793.1	19.828	10.166	1.95	2.00	25.218	24.782	400	424.79	2.35	7.65	Min	12
2833	1909.28	47.732	23.876	2.00	2.07	10.475	39.525	400	460.3	2.17	7.83	Min	12
2810	2346.9	58.674	29.559	1.98	1.63	8.522	41.478	400	469.22	2.13	7.87	Min	12
2859	2258.7	56.469	28.422	1.99	2.03	8.855	41.145	400	447.88	2.23	7.77	Min	12
2790	1910.1	47.753	23.972	1.99	2.11	10.471	39.529	400	474.25	2.11	7.89	Min	12
2524	1833.4	45.837	22.947	2.00	2.03	10.909	39.091	400	475.66	2.10	7.90	Min	12
2580	1126.7	28.170	14.170	1.99	1.88	17.751	32.249	400	470.65	2.12	7.88	Min	12
1855	2188.18	54.704	27.930	1.96	2.05	9.140	40.860	400	475.39	2.10	7.90	B6	14
2051	1412.5	35.313	17.729	1.99	1.98	14.159	35.841	400	437.73	2.28	7.72	B6	14
2026	2103.33	52.583	26.458	1.99	2.02	9.509	40.491	400	465.97	2.15	7.85	B6	14
1954	1567.26	39.182	19.698	1.99	2.21	12.761	37.239	400	432.14	2.31	7.69	Min	14
1998	1880.46	47.011	23.414	2.01	1.78	10.636	39.364	400	422.86	2.36	7.64	Min	14
1927	1852.46	46.312	23.103	2.00	2.13	10.796	39.204	400	463.81	2.16	7.84	Min	14
1976	2648.19	66.205	33.123	2.00	2.07	7.552	42.448	400	507.92	1.97	8.03	min	14
2075	1579.68	39.492	19.764	2.00	2.01	12.661	37.339	400	454.51	2.20	7.80	Min	14
2099	2335.40	58.387	29.401	1.99	2.08	8.564	41.436	400	486.71	2.05	7.95	Min	14
2142	1238.1	30.953	15.546	1.99	2.11	16.154	33.846	400	405.34	2.47	7.53	Min	14
Sample ID	ng/ul	A260	A280	260/280	260/230	RNA dil to 400	water	Cal. Conc	Acutal spec conc	RNA	H2O	Geno	Age
1102s	350.47	8.764	5.252	1.67	2.03	57.066	-7.066	400	350.47	2.85	7.15	B6	20
682s	252.63	6.316	3.953	1.60	2.06	79.167	-29.167	400	252.63	3.96	6.04	b6	20
463s	433.8	10.845	6.288	1.72	2.16	46.104	3.896	400	433.8	2.31	7.69	B6	20
1177b	573.37	14.334	6.873	2.09	2.04	34.881	15.119	400	573.37	1.74	8.26	B6	20
1155b	494.37	12.359	5.972	2.07	1.97	40.456	9.544	400	494.37	2.02	7.98	B6	20
608b	473.39	11.835	5.989	1.98	1.85	42.248	7.752	400	473.39	2.11	7.89	b6	20
416	485.45	12.136	6.109	1.99	1.96	41.199	8.801	400	485.45	2.06	7.94	b6	20
1080b	467.93	11.698	5.727	2.04	1.26	42.741	7.259	400	467.93	2.14	7.86	b6	20
1203b	542.49	13.562	6.521	2.08	2.09	36.867	13.133	400	542.49	1.84	8.16	b6	20
586s	502.99	12.575	6.920	1.82	2.37	39.762	10.238	400	502.99	1.99	8.01	Min	20
562s	544.94	13.624	7.486	1.82	2.35	36.701	13.299	400	544.94	1.84	8.16	Min	20
803	483.13	12.078	7.230	1.67	2.34	41.397	8.603	400	483.13	2.07	7.93	Min	20
537	468.51	11.713	6.869	1.71	2.29	42.689	7.311	400	468.51	2.13	7.87	Min	20
633	453.06	11.326	6.459	1.75	2.34	44.144	5.856	400	453.06	2.21	7.79	Min	20
752	438.96	10.974	5.573	1.97	2.08	45.562	4.438	400	438.96	2.28	7.72	Min	20
775	592.32	14.808	7.288	2.03	2.06	33.766	16.234	400	592.32	1.69	8.31	Min	20
732	448.53	11.213	5.649	1.98	2.07	44.590	5.410	400	448.53	2.23	7.77	min	20
487	475.23	11.881	6.005	1.98	1.34	42.085	7.915	400	475.23	2.10	7.90	min	20
439	492.64	12.316	5.939	2.07	1.93	40.598	9.402	400	492.64	2.03	7.97	min	20

cDNA mix		1x	46
Rnase free H2O		4.2	193.2
10xRT Bx		2	92
dNTP mix		0.8	36.8
10xRandom Primers		2	92
Rnase Inhibitor			0
Rev Transcriptase		1	46
	Total	10	460

Table D.3: Real time PCR data for the gene PEPCK in time course samples for Aim1

Treatment	PEPCK Ct	GAPDH Ct	Dct	DDct	fold change	Normalized
2580	19.21	23.285	-4.075	0.305	0.809	0.800
1927	18.995	23.34	-4.345	0.035	0.976	0.964
1998	18.27	23.445	-5.175	-0.795	1.735	1.714
1954	19.01	23.14	-4.13	0.250	0.841	0.831
1976	19.155	24.58	-5.425	-1.045	2.063	2.039
2075	18.07	22.71	-4.64	-0.260	1.197	1.183
803	19.06	23.8	-4.74	-0.360	1.283426	1.268
439	18.99	23.7	-4.71	-0.330	1.257013	1.242
487	19	23.335	-4.335	0.045	0.96929	0.958
752	18.125	24.165	-6.04	-1.660	3.160165	3.122
775	18.095	23.59	-5.495	-1.115	2.16595	2.140
732	18.74	24.48	-5.74	-1.360	2.566852	2.536
1855	18.06	22.22	-4.16	0.220	0.859	0.848
2477	19.315	23.805	-4.49	-0.110	1.079	1.066
2552	19.145	23.16	-4.015	0.365	0.776	0.767
2833	18.73	23.28	-4.55	-0.170	1.125	1.112
2810	18.375	23.05	-4.675	-0.295	1.226885	1.212
2859	19.45	23.84	-4.39	-0.010	1.006956	0.995

	Dct	*DDct*	*old change*	*Norm*	
Apc Min	-4.38	0.000	1.012	1.000	
(n=6)	0.248898	0.248898	0.168752	0.166797	
12 week	0.078708	0.078708	0.053364	0.052746	
Apc Min	-4.63167	-0.25167	1.270382	1.255078	
(n=6)	0.560068	0.560068	0.516458	0.510237	
14 week	0.228647	0.228647	0.210843	0.208303	0.271467
Apc Min	-5.17667	-0.79667	1.900449	1.877555	
(n=6)	0.675409	0.675409	0.867554	0.857103	
20 week	0.275734	0.275734	0.354178	0.349911	0.033575

Table D.4: Real time PCR data for the gene TLR4 in time course samples for Aim1

Treatment	TLR4 Ct	GAPDH Ct	Dct	DDct	fold change	Normalized
2502	30.44	18.875	11.565	1.178	0.442	0.308
2477	28.61	19.55	9.06	-1.327	2.508	1.746
2552	21.5	18.675	2.825	-7.562	188.925	131.539
2833	21.805	19.13	2.675	-7.712	209.625	145.952
2810	8.99	16.535	-7.545	-17.932	250017.000	174075.169
2859	28.26	19.275	8.985	-1.402	2.642	1.840
2580	29.795	18.835	10.96	0.573	0.672	0.468
1954	22.565	19.18	3.385	-7.002	128.148	89.223
1998	28.715	19.445	9.27	-1.117	2.168	1.510
1927	21.42	18.96	2.46	-7.927	243.313	169.407
1976	28.73	20.335	8.395	-1.992	3.977	2.769
2075	28.78	19.35	9.43	-0.957	1.941	1.351
803	28.12	19.59	8.53	-1.857	3.621699045	2.522
439	26.54	19.305	7.235	-3.152	8.886816301	6.187
487	29.155	19.545	9.61	-0.777	1.713168038	1.193
752	29.59	20.58	9.01	-1.377	2.596677176	1.808
775	28.915	20.195	8.72	-1.667	3.174802104	2.210
732	29.46	20.79	8.67	-1.717	3.286761258	2.288
2681	28.84	14.915	13.925	3.538	0.086	0.060
2700	28.25	18.56	9.69	-0.697	1.621	1.128
2651	28.33	19.025	9.305	-1.082	2.116	1.474
1203	28.775	19.225	9.55	-0.837	1.786	1.243
1177	28.63	19.32	9.31	-1.077	2.109157259	1.469
1155	30.175	19.635	10.54	0.153	0.899170536	0.626

	Dct	*DDct*	*Fold change*	*Norm*	
C57BL/6	10.38667	0.000	1.436	1.000	
(n=6)	1.792087	1.792087	0.90136907	0.555544	
	0.566708	0.566708	0.285037927	0.175679	
(n=6)	6.95684	6.95684	102036.0607	71042.95	
12 week	2.840118	2.840118	41656.04733	29003.16	0.340016
Apc Min	7.316667	-3.07	63.36979354	44.12143	
(n=6)	3.514643	3.514643	101.5413483	70.6985	
14 week	1.434847	1.434847	41.45408184	28.86254	0.166048
Apc Min	8.629167	-1.7575	3.879987321	2.701454	
(n=6)	0.783648	0.783648	2.542685327	1.770353	
20 week	0.319923	0.319923	1.038046938	0.722744	0.048494

Table D.5: Real time PCR raw data for the gene PEPCK in time course samples for Aim1

Treatment	PFK Ct	GAPDH Ct	Dct	DDct	fold change	Normalized
2502	28.97	22.76	6.21	0.306	0.809	0.798
2477	29.075	23.165	5.91	0.006	0.996	0.982
2552	27.9	22.545	5.355	-0.549	1.463	1.443
2833	28.75	23.065	5.685	-0.219	1.164	1.148
2810	28.275	23.19	5.085	-0.819	1.764	1.740
2859	28.38	23.68	4.7	-1.204	2.304	2.273
2580	29.295	23.18	6.115	0.211	0.864	0.852
1927	29.075	22.97	6.105	0.201	0.870	0.858
1998	28.885	23.77	5.115	-0.789	1.728	1.704
1954	28.49	22.935	5.555	-0.349	1.274	1.256
1976	29.38	24.07	5.31	-0.594	1.510	1.489
2075	28.715	23.265	5.45	-0.454	1.370	1.351
803	25.42	24.205	1.215	-4.689	25.79763	25.446
439	27.095	23.235	3.86	-2.044	4.12435	4.068
487	25.09	23.255	1.835	-4.069	16.78577	16.557
752	26.3	24.4	1.9	-4.004	16.04628	15.827
775	26.055	23.29	2.765	-3.139	8.810151	8.690
732	27.31	25.04	2.27	-3.634	12.41633	12.247
1855	29.805	24.33	5.475	-0.429	1.346	1.328
2700	28.4	22.35	6.05	0.146	0.904	0.892
2651	30.1	24.13	5.97	0.066	0.955	0.942
1203	29.87	23.625	6.245	0.341	0.790	0.779
1177	29.075	23.205	5.87	-0.034	1.023965	1.010
1155	29.915	24.1	5.815	-0.089	1.063756	1.049

	Dct	*DDct*	*fold change*	*Norm*	
C57BL/6	5.904167	0.000	1.014	1.000	
(n=6)	0.258871	0.258871	0.241891	0.186642	
	0.081862	0.081862	0.076493	0.059021	
Apc Min	5.490833	-0.41333	1.416778	1.397	
(n=6)	0.554828	0.554828	0.551471	0.543945	
12 week	0.226508	0.226508	0.225137	0.222065	0.121347
Apc Min	5.608333	-0.29583	1.269263	1.251942	
(n=6)	0.415616	0.415616	0.346992	0.342257	
14 week	0.169675	0.169675	0.141659	0.139726	0.144496
Apc Min	2.3075	-3.59667	13.99675	13.80574	
(n=6)	0.916934	0.916934	7.457919	7.356145	
20 week	0.374337	0.374337	3.044683	3.003134	0.001656

Table D.6: Raw Data for quantification of Akt western blots by Image J for the B6 VS Min Comparison

p-Akt Th308											2.118709		
		Area	Mean	Min	Max	pixels	Pixels - Bkg	Avg	statistics	Ratio	Normalized		
1	pAkt_th30	0.044	156.226	117	204	6.873944	1.756436	2.109609	0.247829	1.744171	0.823223	1.001654	0.827393
2	pAkt_th30	0.044	149.201	118	203	6.564844	1.447336	0.601695		1.534274	0.724155	0.336526	
3	pAkt_th30	0.044	154.96	121	212	6.81824	1.700732	0.245641		1.46933	0.693503	0.137386	
4	pAkt_th30	0.044	184.72	133	215	8.12768	3.010172			3.337945	1.575462		
5	pAkt_th30	0.044	176.032	130	216	7.745408	2.6279			2.507825	1.183657		
6	pAkt_th30	0.044	164.377	124	213	7.232588	2.11508			2.13973	1.009921		
7	pAkt_th30	0.044	195.95	137	216	8.6218	3.504292	3.079054		3.060431	1.444479	1.050397	
8	pAkt_th30	0.044	199.851	133	218	8.793444	3.675936	1.284394		3.078075	1.452807	0.384378	
9	pAkt_th30	0.044	175.246	132	212	7.710824	2.593316	0.524352		2.094241	0.988452	0.156922	
10	pAkt_th30	0.044	158.176	127	188	6.959744	1.842236			1.464612	0.691276		
11	pAkt_th30	0.044	155.876	114	207	6.858544	1.741036			1.430065	0.67497		
12	pAkt_th30	0.044	113.387	106	123	4.989028	5.117508						
13	pAkt_th30	0.044	114.697	110	120	5.046668							
14	pAkt_th30	0.044	117.608	109	126	5.174752							
15	pAkt_th30	0.044	119.536	111	140	5.259584							

t-Akt									
		Area	Mean	Min	Max	pixels	Pixels - Bkg	Avg	statistics
1	t-Akt_09-2	0.012	182.327	104	220	2.187924	1.007032	1.00767	0.001258
2	t-Akt_09-2	0.012	177.019	113	219	2.124228	0.943336	0.099166	
3	t-Akt_09-2	0.012	194.865	118	219	2.33838	1.157488	0.040484	
4	t-Akt_09-2	0.012	173.558	106	215	2.082696	0.901804		
5	t-Akt_09-2	0.012	185.731	110	216	2.228772	1.04788		
6	t-Akt_09-2	0.012	180.781	117	219	2.169372	0.98848		
7	t-Akt_09-2	0.012	193.827	123	215	2.325924	1.145032	1.210571	
8	t-Akt_09-2	0.012	197.927	135	215	2.375124	1.194232	0.043625	
9	t-Akt_09-2	0.012	201.6	138	218	2.4192	1.238308	0.01951	
10	t-Akt_09-2	0.012	203.227	148	220	2.438724	1.257832		
11	t-Akt_09-2	0.012	199.862	145	217	2.398344	1.217452		
12	t-Akt_09-2	0.012	99.031	91	114	1.188372	1.180892		
13	t-Akt_09-2	0.012	98.488	88	114	1.181856			
14	t-Akt_09-2	0.012	97.704	90	115	1.172448			

Table D.7: Raw data for quantification of Albumin western blots by Image J for the B6 VS Min Comparison

Albumin												
Sr. No.	Sample #	Genotype	Area	Mean	Min	Max	Pixel	Minus Bckgr	Stats	Normalized to B6	Stats	ttest
1	416	C57BL/6	84	1637.631	1039	2180	137561	98355.32	111537.3	0.881815279	1	0.001977
2	608	C57BL/6	84	1789.226	1123	2469	150295	111089.3	9068.687	0.995983156	0.081306	
3	1080	C57BL/6	84	1782.345	1001	2558	149717	110511.3	3702.276	0.990800999	0.033193	
4	1155	C57BL/6	84	1845.417	912	2936	155015	115809.3		1.038301222		
5	1177	C57BL/6	84	1964.179	681	3205	164991	125785.4		1.127742203		
6	1203	C57BL/6	84	1748.56	694	2784	146879	107673.4		0.96535714		
7	2810	Min	84	1684.69	678	2890	141514	102308.3	88997.97	0.917255934	0.797921	
8	2502	Min	84	1615.595	662	2527	135710	96504.3	9729.658	0.865219723	0.087232	
9	2552	Min	84	1581.56	758	2454	132851	93645.36	3972.116	0.839587586	0.035612	
10	2790	Min	84	1417.738	768	2043	119090	79884.31		0.716211419		
11	2833	Min	84	1418.607	503	2119	119163	79957.3		0.716865873		
12	2477	Min	84	1439.214	519	2176	120894	81688.29		0.732385233		
13		Blank	84	463.798	360	676	38959.03	39205.68		0.351502808		
14	Backgrou	blank	84	498.976	408	604	41913.98					
15	nd	Blank	84	437.429	352	532	36744.04					

Table D.8: Raw data for quantification of MMP-2 western blots by Image J for the B6 VS Min Comparison

MMP-2											
		Area	*Mean*	*Min*	*Max*	*Pixels*	*Pixel - Bckgrd*		*Normalize*	*Statistics*	*ttest*
1	FP_B6_12_wk_Min_7s	50	499.02	338	798	24951	8741.333	9437.667	0.926218	1.000	0.026534
2	FP_B6_12_wk_Min_7s	50	426.3	341	660	21315	5105.333	9844.000	0.540953	0.254	
3	FP_B6_12_wk_Min_7s	50	510.76	342	974	25538	9328.333	2459.884	0.988415	0.104	
4	FP_B6_12_wk_Min_7s	50	546.26	320	936	27313	11103.33	1004.243	1.176491		
5	FP_B6_12_wk_Min_7s	50	536.46	346	756	26823	10613.33		1.124572		
6	FP_B6_12_wk_Min_7s	50	558.88	355	838	27944	11734.33		1.243351		
7	FP_B6_12_wk_Min_7s	50	547.78	333	758	27389	11179.33		1.184544	1.301	
8	FP_B6_12_wk_Min_7s	50	588.66	342	1125	29433	13223.33	10581.000	1.401123	0.128	
9	FP_B6_12_wk_Min_7s	50	565.24	345	1079	28262	12052.33	4830.644	1.277046	0.052	
10	FP_B6_12_wk_Min_7s	50	602.98	375	967	30149	13939.33	1972.102	1.476989		
11	FP_B6_12_wk_Min_7s	50	574.86	363	796	28743	12533.33		1.328012		
12	FP_B6_12_wk_Min_7s	50	539.58	343	925	26979	10769.33		1.141101		
13	FP_B6_12_wk_Min_7s	50	343.56	305	435	17178	968.3333		0.098368		
14	FP_B6_12_wk_Min_7s	50	342.24	310	466	17112					
15	FP_B6_12_wk_Min_7s	50	317.7	293	346	15885	16209.67				
16	FP_B6_12_wk_Min_7s	50	312.64	290	346	15632					

Table D.9: Raw data for quantification of NF-κB western blots by Image J for the B6 VS Min Comparison

p-p65													
		Sample ID	*Area*	*Intensity*	*Min*	*Max*	*Area*	*Pixels*	*Pixels - bckgrd*	*normalized to t-nFkB*	*Stats*	*normalized to B6*	*Stats*
C57BL/6	1	Aditi_p-NFkB	2132	142.112	75	228	100	302982.8	146222.2	0.42847172	0.350242	1.223359	1
	2	Aditi_p-NFkB	2132	159.58	75	226	100	340224.6	183463.9	0.52186407	0.15932	1.49001	0.454887
	3	Aditi_p-NFkB	2132	162.524	75	238	100	346501.2	189740.5	0.47684173	0.065042	1.361463	0.185707
	4	Aditi_p-NFkB	2132	126.219	70	214	100	269098.9	112338.3	0.3484934		0.995007	
	5	Aditi_p-NFkB	2132	103.776	72	186	100	221250.4	64489.8	0.21343431		0.609391	
	6	Aditi_p-NFkB	2132	93.667	70	167	100	199698	42937.41	0.11234705		0.32077	
12 week Min	7	Aditi_p-NFkB	2132	121.044	71	210	100	258065.8	101305.2	0.29503247	0.443938	0.842367	1.267518
	8	Aditi_p-NFkB	2132	136.601	74	228	100	291233.3	134472.7	0.34434647	0.116051	0.983167	0.331345
	9	Aditi_p-NFkB	2132	160.682	79	227	100	342574	185813.4	0.54952621	0.047378	1.56899	0.135271
	10	Aditi_p-NFkB	2132	161.777	75	236	100	344908.6	188147.9	0.43714129		1.248112	
	11	Aditi_p-NFkB	2132	151.631	74	237	100	323277.3	166516.7	0.43864515		1.252406	
	12	Aditi_p-NFkB	2132	198.707	80	242	100	423643.3	266882.7	0.59893705		1.710066	

Table D.10: Raw data for quantification of STAT-3 western blots by Image J for the B6 VS Min Comparison

STAT-3									
	Area	mean	Min	Max	Pixels	Bkg	Mean - Bkg	Avg/Std	ttest
16	0.031	102.136	82	137	3.166216		0.450575	0.654627	
17	0.031	97.923	81	125	3.035613		0.319972	0.287816	
18	0.031	107.559	83	147	3.334329		0.618688		0.00745
19	0.031	104.923	85	154	3.252613		0.536972		
20	0.031	118.15	86	146	3.66265		0.947009		
21	0.031	121.619	92	157	3.770189		1.054548		
22	0.031	171.07	109	207	5.30317		2.587529	1.964331	
23	0.031	157.766	107	201	4.890746		2.175105	1.070287	
24	0.031	183.287	125	205	5.681897		2.966256		
25	0.031	178.101	119	203	5.521131		2.80549		
26	0.031	107.951	86	141	3.346481		0.63084		
27	0.031	107.626	83	171	3.336406		0.620765		
28	0.031	184.021	101	205	5.704651		2.98901		
29	0.031	85.416	81	92	2.647896	2.715641			
30	0.031	89.885	85	98	2.786435				
31	0.031	87.503	81	98	2.712593				

Table D.11: Raw data for quantification of MMP-2 western blots by Image J for the 12 vs 14 vs 20 week *Apc*$^{Min/+}$ Comparison for Aim 1

MMP-2		Area	Mean	Min	Max	Pixels	Pixel - Bckgrd			
1	12_14_20wk_	0.092	626.402	594	3127	57.62898	0.858682	3.090	0.006766	0.024
2	12_14_20wk_	0.092	667.321	605	866	61.39353	4.62323	2.231	0.036427	0.018
3	12_14_20wk_	0.092	633.604	604	1018	58.29157	1.521266	1.115	0.011986	0.009
4	12_14_20wk_	0.092	675.299	606	854	62.12751	5.357206		0.04221	
5	12_14_20wk_	0.092	649.714	607	813	59.77369	3.003386	97.415	0.023664	0.768
6	12_14_20wk_	0.092	1739.505	656	4131	160.0345	103.2642	54.814	0.813632	0.432
7	12_14_20wk_	0.092	1817.482	628	4366	167.2083	110.438	24.514	0.870156	0.193
8	12_14_20wk_	0.092	2139.597	638	4844	196.8429	140.0726		1.103651	
9	12_14_20wk_	0.092	2033.352	706	4244	187.0684	130.2981		1.026636	
10	12_14_20wk_	0.092	2241.776	750	4350	206.2434	149.4731	126.918	1.177718	1.000
11	12_14_20wk_	0.092	2065.58	750	4005	190.0334	133.2631	22.066	1.049997	0.174
12	12_14_20wk_	0.092	2162.705	737	4213	198.9689	142.1986	9.868	1.120401	0.078
13	12_14_20wk_	0.092	1862.174	777	3212	171.32	114.5497		0.902552	
14	12_14_20wk_	0.092	1650.799	657	3080	151.8735	95.10321		0.749331	
15	12_14_20wk_	0.092	618.088	596	665	56.8641	56.7703			
16	12_14_20wk_	0.092	616.049	594	740	56.67651				

Table D.12: Raw data for quantification of p-65 western blots by Image J for the 12 vs 14 vs 20 week *Apc*$^{Min/+}$ Comparison for Aim 1

p-p65														
		Sample ID	Area	Intensity	Min	Max	Area	Pixels	Pixels - bckgrd	normalized to gapdh	Stats	normalized to B6	Stats	
12 week Min	7	Aditi_p-NF	2132	121.044	71	210	100	258065.8	101305.2	44254.46	74859.73	0.591165	1	
	8	Aditi_p-NF	2132	136.601	74	228	100	291233.3	134472.7	60107.59	24057.95	0.802936	0.321374	
	9	Aditi_p-NF	2132	160.682	79	227	100	342574	185813.4	82905.03	9821.616	1.107472	0.1312	
	10	Aditi_p-NF	2132	161.777	75	236	100	344908.6	188147.9	78821.79		1.052927		
	11	Aditi_p-NF	2132	151.631	74	237	100	323277.3	166516.7	68049.87		0.909032		
	12	Aditi_p-NF	2132	198.707	80	242	100	423643.3	266882.7	115019.6		1.536469		
14 week Min	13	Aditi_p-NF	2132	165.302	76	236	100	352423.9	195663.2	85027.05	52881.41	1.135818	0.706407	
	14	Aditi_p-NF	2132	136.159	73	223	100	290291	133530.4	55861	20082.34	0.746209	0.268266	
	15	Aditi_p-NF	2132	141.051	72	224	100	300720.7	143960.1	61454.91	8198.58	0.820934	0.109519	
	16	Aditi_p-NF	2132	106.796	69	178	100	227689.1	70928.44	31099.15		0.415432		
	17	Aditi_p-NF	2132	108.861	71	190	100	232091.7	75331.02	32275.81		0.431151		
	18	Aditi_p-NF	2132	131.286	73	220	100	279901.8	123141.1	51570.52		0.688895		
20 week Min	19	Aditi_p-NF	2132	102.994	69	177	100	219583.2	62822.58	28444.45	19999.99	0.37997	0.267166	
	20	Aditi_p-NF	2132	94.39	67	153	100	201239.5	44478.85	31299.68	23119.65	0.418111	0.30884	
	21	Aditi_p-NF	2132	75.404	67	90	100	160761.3	4000.698	937.6949	9438.556	0.012526	0.126083	
	22	Aditi_p-NF	2132	76.579	67	94	100	163266.4	6505.798	3130.972		0.041825		
	23	Aditi_p-NF	2132	72.538	67	104	100	154651	-2109.61	-1015.27		-0.01356		
	24	Aditi_p-NF	2132	129.278	59	217	100	275620.7	118860.1	57202.44		0.764128		
backgroun	25	Aditi_p-NF	2132	72.981	44	84	100	155595.5	156760.6					
backgroun	26	Aditi_p-NF	2132	74.074	68	86	100	157925.8						

Table D.13: Raw data for quantification of STAT-3 western blots by Image J for the 12 vs 14 vs 20 week *Apc*$^{Min/+}$ Comparison in Aim 1

STAT-3									
	Area	***mean***	***Min***	***Max***	***Pixels***	***Bkg***	***Mean - Bk***	***Avg/Std***	***ttest***
1	0.033	125.417	88	161	4.138761		1.116902	1.151733	0.472245
2	0.033	121.443	89	163	4.007619		0.98576		0.035093
3	0.033	146.107	99	185	4.821531		1.799672		
4	0.033	112.923	93	142	3.726459		0.7046		
5	0.033	134.463	95	177	4.437279		1.41542	0.913787	0.128524
6	0.033	123.28	97	157	4.06824		1.046381		
7	0.033	108.597	90	135	3.583701		0.561842		
8	0.033	129.273	99	172	4.266009		1.24415		
9	0.033	100.697	87	128	3.323001		0.301142		
10	0.033	106.21	88	135	3.50493		0.483071	0.488458	
11	0.033	110.293	92	139	3.639669		0.61781		
12	0.033	109.077	88	138	3.599541		0.577682		
13	0.033	99.913	88	119	3.297129		0.27527		
14	0.033	90.913	82	98	3.000129	3.02186	-0.02173		
15	0.033	92.23	84	100	3.04359		0.021731		

Table D.14: Raw data for quantification of Albumin western blots by Image J for the 12 vs 14 vs 20 week *Apc*$^{Min/+}$ Comparison in Aim 1

Albumin								0.941623				
		Area	**Mean**	**Stdev**	**Min**	**Max**	**Pixels**	**Pixel - Bckg**	**Average**	**ttest**	**Normalized**	**Average**
20	1	0.014	168.566	25.775	99	207	2.360	0.977	0.942	0.025	1.04	1.00
20	2	0.014	160.44	29.488	97	206	2.246	0.863		0.132	0.92	0.07
20	3	0.014	171.606	26.899	97	220	2.402	1.019			1.08	0.04
20	4	0.014	163.684	30.207	98	213	2.292	0.908			0.96	
14	5	0.014	174.36	28.5	99	219	2.441	1.058	1.056	0.266	1.12	1.12
14	6	0.014	168.878	30.066	99	216	2.364	0.981			1.04	0.05
14	7	0.014	178.338	27.079	97	218	2.497	1.113			1.18	0.02
14	8	0.014	176.804	26.861	99	220	2.475	1.092			1.16	
14	9	0.014	172.893	28.884	101	216	2.421	1.037			1.10	
12	10	0.014	170.412	31.083	99	219	2.386	1.002	1.017		1.06	1.08
12	11	0.014	172.912	27.173	101	212	2.421	1.037			1.10	0.02
12	12	0.014	171.134	27.853	99	211	2.396	1.012			1.08	0.08
Bckgrd	13	0.014	97.372	1.609	93	112	1.363	1.383				
Bckgrd	14	0.014	98.138	1.572	93	112	1.374					
Bckgrd	15	0.014	99.307	3.284	93	117	1.390					
Bckgrd	16	0.014	100.444	4.174	95	120	1.406					

Table D.15: Raw data for quantification of p-S6 western blots by Image J for the 12 vs 14 vs 20 week *Apc*$^{Min/+}$ Comparison in Aim 1

p-S6											
		Area	Mean	Min	Max	Area*Inten	Minus bckg	normalized to t	Avg/stdev/SE	normalized	average
1	p-S6_09-24	0.04	199.811	96	223	7.99244	4.23308	4.87756E-05	3.68413E-05	1.323939	1
2	p-S6_09-24	0.04	194.537	111	229	7.78148	4.02212	4.28095E-05	9.00839E-06	1.162	0.244519
3	p-S6_09-24	0.04	177.522	97	222	7.10088	3.34152	3.58895E-05	4.02867E-06	0.974166	0.109352
4	p-S6_09-24	0.04	162.837	92	221	6.51348	2.75412	2.93617E-05		0.796978	
5	p-S6_09-24	0.04	159.31	91	220	6.3724	2.61304	2.737E-05		0.742916	
6	p-S6_09-24	0.04	157.497	92	219	6.29988	2.54052	2.62271E-05	2.35962E-05	0.711895	0.640482
7	p-S6_09-24	0.04	161.456	95	220	6.45824	2.69888	2.79734E-05	5.63728E-06	0.759297	0.153015
8	p-S6_09-24	0.04	158.203	95	223	6.32812	2.56876	2.66403E-05	2.52107E-06	0.72311	0.068431
9	p-S6_09-24	0.04	149.086	92	220	5.96344	2.20408	2.31111E-05		0.627315	
10	p-S6_09-24	0.04	127.328	88	212	5.09312	1.33376	1.4029E-05		0.380795	
11	p-S6_09-24	0.04	97.629	88	143	3.90516	0.1458	1.54621E-06	4.87005E-06	0.04197	0.13219
12	p-S6_09-24	0.04	103.116	86	162	4.12464	0.36528	3.95527E-06	2.88008E-06	0.10736	0.078175
13	p-S6_09-24	0.04	106.953	87	148	4.27812	0.51876	5.57215E-06	1.44004E-06	0.151247	0.039088
14	p-S6_09-24	0.04	111.534	88	206	4.46136	0.702	8.40656E-06		0.228183	
15	p-S6_09-24	0.04	93.176	87	99	3.72704	3.75936				
16	p-S6_09-24	0.04	94.937	89	122	3.79748					
17	p-S6_09-24	0.04	93.839	87	101	3.75356					
t-S6											
14	tS6_10-21-	468	185.442	159	209	86786.86	86786.86				
15	tS6_10-21-	468	200.756	161	219	93953.81	93953.81				
16	tS6_10-21-	468	198.944	165	215	93105.79	93105.79				
17	tS6_10-21-	468	200.427	163	218	93799.84	93799.84				
18	tS6_10-21-	468	203.998	168	218	95471.06	95471.06				
19	tS6_10-21-	468	206.979	178	221	96866.17	96866.17				
20	tS6_10-21-	468	206.154	173	219	96480.07	96480.07				
21	tS6_10-21-	468	206.034	173	220	96423.91	96423.91				
22	tS6_10-21-	468	203.78	170	220	95369.04	95369.04				
23	tS6_10-21-	468	203.145	167	220	95071.86	95071.86				
24	tS6_10-21-	468	201.485	168	219	94294.98	94294.98				
25	tS6_10-21-	468	197.335	167	220	92352.78	92352.78				
26	tS6_10-21-	468	198.929	166	219	93098.77	93098.77				
27	tS6_10-21-	468	178.432	156	212	83506.18	83506.18				
28	tS6_10-21-	468	164.605	156	177	77035.14	76839.36				
29	tS6_10-21-	468	165.141	155	173	77285.99					
30	tS6_10-21-	468	162.814	155	173	76196.95					

RAW DATA FOR AIM 2:

RNA EXTRACTION:

Table D.16: Spectrophotometer reading for 400ng dilution and cDNA synthesis dilutions for the timecourse samples in Aim 2

Sample ID	Date	260/280	ng/ul	RNA dil to 400	water	Cal. Conc	Acutal spec conc	RNA	H2O
105	11/5/2013	2.02	1770.5	11.30	38.70	400	442.5	2.259887	7.740113
684	11/5/2013	2.01	1592.94	12.56	37.44	400	446.79	2.238188	7.761812
3052	11/5/2013	2.00	1207.71	16.56	33.44	400	409.95	2.439322	7.560678
108	11/5/2013	1.98	3093.85	6.46	43.54	400	457.72	2.184742	7.815258
598	11/5/2013	1.98	852.42	23.46	26.54	400	493.32	2.027082	7.972918
658	11/5/2013	2.00	1127.55	17.74	32.26	400	448.71	2.228611	7.771389
3085	11/5/2013	2.01	1665.31	12.01	37.99	400	408.77	2.446363	7.553637
3048	11/5/2013	2.02	1149.866	17.39	32.61	400	436.44	2.291266	7.708734
660	11/5/2013	2.01	1607.03	12.45	37.55	400	408.02	2.45086	7.54914
2916	11/5/2013	2.00	2169.2	9.22	40.78	400	504.11	1.983694	8.016306
610	11/5/2013	2.00	1526.75	13.10	36.90	400	400.57	2.496443	7.503557
3112	11/5/2013	2.01	1330.05	15.04	34.96	400	440.46	2.270354	7.729646
3111	11/5/2013	1.98	3054.37	6.55	43.45	400	502.61	1.989614	8.010386
3113	11/5/2013	2.01	2036.57	9.82	40.18	400	471.16	2.122421	7.877579
3207	11/5/2013	2.01	1290.44	15.50	34.50	400	441.63	2.264339	7.735661
611	11/5/2013	2.00	1516.73	13.19	36.81	400	459.73	2.17519	7.82481
3221	11/5/2013	2.01	2103.43	9.51	40.49	400	489.43	2.043193	7.956807
3137	11/5/2013	2.02	1635.53	12.23	37.77	400	457.12	2.187609	7.812391
3218	11/5/2013	1.97	824.61	24.25	25.75	400	426.38	2.345326	7.654674
991	11/5/2013	2.00	925.14	21.62	28.38	400	447.83	2.23299	7.76701
988	11/5/2013	1.99	992.98	20.14	29.86	400	461.22	2.168163	7.831837
3086	11/5/2013	2.01	1569.38	12.74	37.26	400	443.5	2.254791	7.745209
990	11/5/2013	1.98	2702.37	7.40	42.60	400	470.08	2.127297	7.872703
3051	11/5/2013	2.01	1544.53	12.95	37.05	400	444.27	2.250883	7.749117
3209	11/5/2013	2.01	1661.13	12.04	37.96	400	451.73	2.213712	7.786288
106	11/5/2013	2.02	1869.22	10.70	39.30	400	461.24	2.168069	7.831931
992	11/5/2013	2.02	1532.46	13.05	36.95	400	474.44	2.107748	7.892252
989	11/5/2013	2.00	2166.41	9.23	40.77	400	479.49	2.085549	7.914451
3114	11/5/2013	2.00	1101.14	18.16	31.84	400	430.47	2.323042	7.676958

cDNA mix		1x	30
Rnase free H2O		4.2	126
10xRT Bx		2	60
dNTP mix		0.8	24
10xRandom Primers		2	60
Rnase Inhibitor			0
Rev Transcriptase		1	30
	Total	10	300

Table D.17: Real time PCR raw data for the gene Haptaglobin in PDTC and fusion protein treated samples for Aim2

		Haptaglobin	GAPDH				
	Treatment	Ct	Ct	Dct	DDct	fold change	Normalized
C57BL/6	105	17.305	21.83	-4.525	-0.050	1.035	0.976
	108	17.52	21.74	-4.22	0.255	0.838	0.790
	106	18.385	22.595	-4.21	0.265	0.832	0.785
	998	16.795	22.26	-5.465	-0.990	1.986	1.873
	990	18.57	22.785	-4.215	0.260	0.835	0.788
	991	17.995	22.21	-4.215	0.260	0.835	0.788
B6 + PDTC	3048	18.59	22.99	-4.4	0.075	0.949	0.895
	3051	17.775	22.31	-4.535	-0.060	1.042	0.983
	3052	18.41	23.24	-4.83	-0.355	1.279	1.206
	3085	17.695	22.465	-4.77	-0.295	1.227	1.157
	3086	17.955	22.475	-4.52	-0.045	1.032	0.973
Apc Min/+	660	15.34	21.955	-6.615	-2.140	4.40762	4.157
	684	14.77	22.135	-7.365	-2.890	7.412704	6.991
	2916	14.35	21.805	-7.455	-2.980	7.889862	7.441
	537	16.56	24.345	-7.785	-3.310	9.917662	9.354
	803	18.83	24.33	-5.5	-1.025	2.034959	1.919
$Apc^{Min/+}$ + PDTC	598	14.76	22.025	-7.265	-2.790	6.916	6.523
	610	15.18	22.075	-6.895	-2.420	5.352	5.047
	611	14.17	22.065	-7.895	-3.420	10.703	10.095
	658	15.08	22.11	-7.03	-2.555	5.877	5.542
$Apc^{Min/+}$ gp13 0 fusion protein	3111	15.965	22.825	-6.86	-2.385	5.223	4.926
	3112	16.25	22.765	-6.515	-2.040	4.112	3.879
	3113	15.18	22.35	-7.17	-2.695	6.476	6.107
	3114	15.82	22.59	-6.77	-2.295	4.908	4.628

	Dct	*DDct*	*Fold change*	*Norm*	
C57BL/6	-4.475	0.000	1.060301937	1	
(n=6)	0.50061	0.50061	0.460604805	0.434409	
	0.204373	0.204373	0.188041124	0.177347	
C57BL/6 + PDTC	-4.611	-0.136	1.105872324	1.043	
(n=5)	0.181535	0.181535	0.140212685	0.132238	
	0.081185	0.081185	0.062705019	0.059139	0.837203
Apc Min	-6.944	-2.469	6.333	5.972	
(n=4)	0.913649	0.913649	3.107234191	2.930518	
14 week	0.408596	0.408596	1.389597375	1.310568	0.000705
Apc Min + PDTC	-7.27125	-2.79625	7.21202576	6.80186	
(n=4)	0.443046	0.443046	2.416693927	2.279251	
20 week	0.221523	0.221523	1.208346963	1.139625	0.657457
Apc Min+gp130FP	-6.82875	-2.35375	5.179743024	4.885159	
(n=4)	0.270382	0.270382	0.982206849	0.926346	
20 week	0.135191	0.135191	0.491103425	0.463173	0.503188

Table D.18: Real time PCR raw data for the gene PEPCK in PDTC and fusion protein treated samples for Aim2

		PEPCK	GAPDH				
	Treatment	Ct	Ct	Dct	DDct	fold change	Normalized
C57BL/6	990	19.05	22.39	-3.34	0.625	0.648	0.610
	991	17.165	21.885	-4.72	-0.755	1.688	1.587
	988	18.16	22.16	-4	-0.035	1.025	0.964
	105	17.77	21.57	-3.8	0.165	0.892	0.839
B6 + PDTC	3048	17.78	22.955	-5.175	-1.210	2.313	2.176
	3051	17.615	22.4	-4.785	-0.820	1.765	1.661
	3052	18.3	23.085	-4.785	-0.820	1.765	1.661
	3085	17.335	22.315	-4.98	-1.015	2.021	1.901
Apc $^{Min/+}$	660	17.56	21.38	-3.82	0.145	0.904	0.851
	684	18.045	22.26	-4.215	-0.250	1.189	1.119
	2916	17.125	21.44	-4.315	-0.350	1.275	1.199
	537	19.67	24.29	-4.62	-0.655	1.575	1.481
Apc $^{Min/+}$ + PDTC	598	18.19	21.615	-3.425	0.540	0.688	0.647
	610	18.54	21.81	-3.27	0.695	0.618	0.581
	611	18.72	21.82	-3.1	0.865	0.549	0.516
	658	17.945	21.57	-3.625	0.340	0.790	0.743
B6 + gp130 fusion protein	3207	17.135	21.955	-4.82	-0.855	1.809	1.701
	3209	17.785	22.805	-5.02	-1.055	2.078	1.954
	3218	17.445	24.055	-6.61	-2.645	6.255	5.884
	3221	16.42	21.61	-5.19	-1.225	2.338	2.199
Apc $^{Min/+}$gp130 fusion protein	3111	17.25	22.18	-4.93	-0.965	1.952	1.836
	3112	17.515	22.385	-4.87	-0.905	1.873	1.761
	3113	17.4	22.505	-5.105	-1.140	2.204	2.073
	3114	18.03	22.69	-4.66	-0.695	1.619	1.523

	Dct	*DDct*	*Fold change*	*Norm*	
C57BL/6	-3.965	0.000	1.063134178	1.000	
(n=6)	0.574195	0.574195	0.444516458	0.418119	
	0.287098	0.287098	0.222258229	0.209059	
C57BL/6 + PDTC	-4.93125	-0.96625	1.966272811	1.850	
(n=5)	0.186698	0.186698	0.260870519	0.245379	
	0.093349	0.093349	0.130435259	0.122689	0.012756
Apc Min	-4.243	-0.277	1.236	1.162	
(n=4)	0.330164	0.330164	0.275867791	0.259485	
14 week	0.165082	0.165082	0.137933896	0.129743	8.71E-05
Apc Min + PDTC	-3.355	0.61	0.661141987	0.622	
(n=4)	0.223644	0.223644	0.102917364	0.096806	
20 week	0.111822	0.111822	0.051458682	0.048403	0.00796

Table D.19: Real time PCR raw data for the gene PEPCK in PDTC and fusion protein treated samples for Aim2

		PFK	GAPDH				
	Treatment	Ct	Ct	Dct	DDct	fold change	Normalized
C57BL/6	108	29.53	22.17	7.36	0.809	0.571	0.544
	991	28.4	22.09	6.31	-0.241	1.182	1.127
	988	27.985	21.845	6.14	-0.411	1.330	1.267
	105	28.49	22.095	6.395	-0.156	1.114	1.062
B6 + PDTC	3048	28.545	22.575	5.97	-0.581	1.496	1.426
	3051	28.315	22.48	5.835	-0.716	1.643	1.566
	3052	28.94	22.705	6.235	-0.316	1.245	1.187
	3085	29.145	23.185	5.96	-0.591	1.507	1.436
$Apc^{Min/+}$	660	25.885	21.31	4.575	-1.976	3.935	3.750
	684	25.84	22.065	3.775	-2.776	6.851	6.529
	2916	27.395	21.81	5.585	-0.966	1.954	1.862
	803	25.525	24.335	1.19	-5.361	41.105	39.175
$Apc^{Min/+}$ + PDTC	598	25.315	21.975	3.34	-3.211	9.262	8.827
	610	24.69	21.94	2.75	-3.801	13.941	13.286
	611	25.13	21.73	3.4	-3.151	8.884	8.467
	658	25.205	21.78	3.425	-3.126	8.732	8.322
B6 + gp130 fusion protein	3207	28.315	22.18	6.135	-0.416	1.334	1.272
	3209	29.365	23.065	6.3	-0.251	1.190	1.134
	3218	29.835	24.835	5	-1.551	2.931	2.793
	3221	28.14	22.195	5.945	-0.606	1.522	1.451
$Apc^{Min/+}$gp130 fusion protein	3111	26.555	21.815	4.74	-1.811	3.509	3.345
	3112	28.13	22.79	5.34	-1.211	2.315	2.207
	3113	27.905	23.175	4.73	-1.821	3.534	3.368
	3114	27.25	22.89	4.36	-2.191	4.567	4.353

	Dct	*DDct*	*Fold change*	*Norm*	
C57BL/6	6.55125	0.000	1.049279225	1.000	
(n=6)	0.54949	0.54949	0.331381193	0.315818	
	0.274745	0.274745	0.165690597	0.157909	
C57BL/6 + PDTC	6	-0.55125	1.472673138	1.404	
(n=5)	0.168276	0.168276	0.165803116	0.158016	
	0.084138	0.084138	0.082901558	0.079008	0.062349
Apc Min	3.781	-2.770	13.461	12.829	
(n=4)	1.879554	1.879554	18.53884899	2.347615	
14 week	0.939777	0.939777	9.269424495	1.173807	0.000434
Apc Min + PDTC	3.22875	-3.3225	10.20457079	9.725	
(n=4)	0.321154	0.321154	2.500811731	2.383362	
20 week	0.160577	0.160577	1.250405866	1.191681	0.025719

Table D.20: Raw data for quantification of MMP-2 western blots by Image J for the PDTC and fusion protein treated samples for Aim2

PDTC MMP2									
	Area	mean	Min	Max	Pixels	Bkg	Mean - Bk	Avg/Std	ttest
1	0.031	189.897	121	216	5.886807		2.958826	3.303649	0.447833
2	0.031	205.716	149	220	6.377196		3.449215		0.036655
3	0.031	207.448	158	221	6.430888		3.502907		
4	0.031	207.355	160	223	6.428005		3.500024		
5	0.031	203.129	143	222	6.296999		3.369018	3.453462	0.00247
6	0.031	207.075	158	223	6.419325		3.491344		
7	0.031	185.629	136	220	5.754499		2.826518	1.30834	0.637547
8	0.031	126.743	93	182	3.929033		1.001052		
9	0.031	94.924	86	106	2.942644		0.014663		
10	0.031	139.326	92	206	4.319106		1.391125		
11	0.031	98.141	87	128	3.042371		0.11439	0.938362	
12	0.031	116.125	90	171	3.599875		0.671894		
13	0.031	167.841	108	216	5.203071		2.27509		
14	0.031	116.776	86	181	3.620056		0.692075		
15	0.031	94.451	85	106	2.927981	2.927981	0		

Table D.21: Raw data for quantification of STAT-3 western blots by Image J for the PDTC and fusion protein treated samples for Aim2

Sr No	Title	Area	Intensity	Min	Max	Pixels	ixel - Bckgr	ospho: tot	Stats	5 Normalize	STATS
1	PDTC_pSTA	324	80.37	79	83	26039.88	273.56	0.01	0.09	0.11	1
2	PDTC_pSTA	324	81.571	79	86	26429.00	662.69	0.03	0.12	0.30	1.379306
3	PDTC_pSTA	324	97.358	81	127	31543.99	5777.68	0.23	0.07	2.59	0.796343
4	PDTC_pSTA	324	94.09	84	109	30485.16	4718.84	0.15	0.13	1.70	1.49265
5	PDTC_pSTA	324	88.957	82	100	28822.07	3055.75	0.10	0.03	1.10	0.338834
6	PDTC_pSTA	324	94.716	84	115	30687.98	4921.67	0.15	0.02	1.67	0.195626
7	PDTC_pSTA	324	156.679	85	210	50764.00	24997.68	0.66	0.58	7.34	6.44014
8	PDTC_pSTA	324	149.784	87	211	48530.02	22763.70	0.58	0.06	6.40	0.692824
9	PDTC_pSTA	324	150.287	88	206	48692.99	22926.67	0.57	0.03	6.36	0.346412
10	PDTC_pSTA	324	145.988	85	208	47300.11	21533.80	0.51		5.66	
11	PDTC_pSTA	324	166.201	90	208	53849.12	28082.81	0.72	0.62	7.99	6.833021
12	PDTC_pSTA	324	156.543	88	212	50719.93	24953.62	0.65	0.32	7.24	3.496476
13	PDTC_pSTA	324	173.997	89	212	56375.03	30608.71	0.92	0.16	10.17	1.748238
14	PDTC_pSTA	324	97.454	78	160	31575.10	5808.78	0.17		1.93	
15	PDTC_pSTA	324	79.929	78	83	25897.00	25766.32			0.00	
16	PDTC_pSTA	324	78.941	78	81	25576.88					
17	PDTC_pSTA	324	79.707	78	81	25825.07					

Sr No	Title	Area	Intensity	Min	Max	Pixels	ixel - Bckgr
18	t-STAT3	403	163.73	86	214	65983.2	28240.8
19	t-STAT3	403	153.494	85	212	61858.1	24115.7
20	t-STAT3	403	154.955	85	213	62446.9	24704.4
21	t-STAT3	403	169.834	90	213	68443.1	30700.7
22	t-STAT3	403	169.834	90	213	68443.1	30700.7
23	t-STAT3	403	174.357	90	213	70265.9	32523.4
24	t-STAT3	403	187.132	92	214	75414.2	37671.8
25	t-STAT3	403	191.303	97	214	77095.1	39352.7
26	t-STAT3	403	192.72	95	215	77666.2	39923.7
27	t-STAT3	403	198.203	106	215	79875.8	42133.4
28	t-STAT3	403	190.174	94	214	76640.1	38897.7
29	t-STAT3	403	188.278	93	214	75876.0	38133.6
30	t-STAT3	403	176.33	85	213	71061.0	33318.6
31	t-STAT3	403	176.33	85	213	71061.0	33318.6
32	t-STAT3	403	84.953	80	91	34236.1	37742.4
33	t-STAT3	403	110.953	81	255	44714.06	
34	t-STAT3	403	85.055	81	108	34277.17	

Table D.22: Raw data for quantification of gp130 western blots by Image J for the PDTC treated samples for Aim2

Sr No	Title	Area	Intensity	Min	Max	Pixels	ixel - Bckgr	GAPDH Normalized	Stats	B6 Normalized	STATS
1	PDTC_gp130	660	175.879	144	197	116080.1	22077.33	3347.460171	2493.73	1.342350129	**1.00**
2	PDTC_gp130	660	156.064	137	191	103002.2	8999.43	1289.872484	1072.55	0.517246033	0.43
3	PDTC_gp130	660	170.667	142	202	112640.2	18637.41	2843.860436	619.24	1.140403837	0.25
4	PDTC_gp130	660	143.8	138	153	94908	905.19	123.9634449	196.45	0.04971003	**0.08**
5	PDTC_gp130	660	147.27	139	163	97198.2	3195.39	503.0386438	277.54	0.201721291	0.11
6	PDTC_gp130	660	142.052	20	195	93754.32	-248.49	-37.65369691	160.24	-0.015099342	0.06
7	PDTC_gp130	660	183.303	80	213	120980	26977.17	4058.054926	4643.67	1.627302574	**1.86**
8	PDTC_gp130	660	193.276	152	210	127562.2	33559.35	5161.382453	551.67	2.069743044	0.22
9	PDTC_gp130	660	194.986	151	210	128690.8	34687.95	5064.744666	275.83	2.030990754	0.11
10	PDTC_gp130	660	186.467	146	206	123068.2	29065.41	4290.487519	137.92	1.720509336	
11	PDTC_gp130	660	188.088	150	207	124138.1	30135.27	4347.770949	4236.32	1.74348031	**1.70**
12	PDTC_gp130	660	176.524	146	206	116505.8	22503.03	3303.943937	745.70	1.324899878	0.30
13	PDTC_gp130	660	197.88	162	211	130600.8	36597.99	5120.863207	372.85	2.053494601	0.15
14	PDTC_gp130	660	188.218	153	211	124223.9	30221.07	4172.682462		1.673268853	
15	PDTC_gp130	660	141.83	137	152	93607.8	94002.81				
16	PDTC_gp130	660	143.027	134	158	94397.82					

Table D.23: Raw data for quantification of Albumin western blots by Image J for the PDTC treated samples for Aim2

Sr No	Title	Area	Intensity	Min	Max	Pixels	Pixel - Bckgrd	DH Normal	Stats	B6 Normalized	STATS
1	Albumin_PDTC	704	135.683	86	166	95520.83	51113.5	7750.042	7536.464	1.03	1
2	Albumin_PDTC	704	127.562	82	164	89803.65	45396.3	6506.567		0.86	0.12492
3	Albumin_PDTC	704	140.835	87	170	99147.84	54740.5	8352.782		1.11	0.072123
4	Albumin_PDTC	704	135.878	82	172	95658.11	51250.7	7018.656		0.93	1.013177
5	Albumin_PDTC	704	133.361	84	173	93886.14	49478.8	7789.262		1.03	0.073838
6	Albumin_PDTC	704	139.003	83	171	97858.11	53450.7	8099.391		1.07	0.04263
7	Albumin_PDTC	704	104.074	66	161	73268.1	28860.7	4341.388		0.58	0.828511
8	Albumin_PDTC	704	137.391	71	168	96723.26	52315.9	8046.112		1.07	0.204404
9	Albumin_PDTC	704	127.73	67	170	89921.92	45514.5	6645.521		0.88	0.102202
10	Albumin_PDTC	704	120.268	64	163	84668.67	40261.3	5943.166		0.79	
11	Albumin_PDTC	704	111.754	65	162	78674.82	34267.4	4943.94		0.66	0.568747
12	Albumin_PDTC	704	116.562	62	165	82059.65	37652.3	5528.188		0.73	0.218874
13	Albumin_PDTC	704	111.982	62	163	78835.33	34427.9	4817.226		0.64	0.109437
14	Albumin_PDTC	704	82.173	52	145	57849.79	13442.4	1856.02		0.25	
15	Albumin_PDTC	704	55.104	49	59	38793.22	44407.4				
16	Albumin_PDTC	704	66.891	61	76	47091.26					
17	Albumin_PDTC	704	67.241	62	80	47337.66					

Table D.24: Raw data for quantification of S6 western blots by Image J for the PDTC treated samples for Aim2

Sr No	Title	Area	Intensity	Min	Max	Pixels	Pixel - Bckgrd	Stats	B6 Normalized	STATS
1	PDTC_S6	544	151.096	84	216	82196.22	32492.39	28616.76	1.14	1
2	PDTC_S6	544	118.938	84	186	64702.27	14998.44	12153.16	0.52	0.424687
3	PDTC_S6	544	161.881	88	216	88063.26	38359.43	7016.63	1.34	0.245193
4	PDTC_S6	544	189.675	108	219	103183.2	53479.37	56578.36	1.87	1.977106
5	PDTC_S6	544	201.71	128	220	109730.2	60026.41	3287.45	2.10	0.114878
6	PDTC_S6	544	194.73	105	220	105933.1	56229.29	1898.01	1.96	0.066325
7	PDTC_S6	544	147.217	87	211	80086.05	30382.22	21615.11	1.06	0.755331
8	PDTC_S6	544	133.415	84	205	72577.76	22873.93	11848.22	0.80	0.414031
9	PDTC_S6	544	99.658	82	139	54213.95	4510.12	5924.11	0.16	0.207015
10	PDTC_S6	544	144.114	86	213	78398.02	28694.19		1.00	
11	PDTC_S6	544	96.079	86	120	52266.98	2563.15	27379.75	0.09	0.956773
12	PDTC_S6	544	168.061	97	223	91425.18	41721.35	17417.06	1.46	0.608631
13	PDTC_S6	544	158.866	92	216	86423.1	36719.27	8708.53	1.28	0.304316
14	PDTC_S6	544	143.785	88	212	78219.04	28515.21		1.00	
15	PDTC_S6	544	96.11	87	151	52283.84	49703.83		1.74	
16	PDTC_S6	544	89.031	83	121	48432.86				
17	PDTC_S6	544	88.961	83	108	48394.78				

Table D.25: Raw data for quantification of p-65 western blots by Image J for the PDTC treated samples for Aim2

Sr No	Title	Area	Intensity	Min	Max	Pixels	Pixel - Bckgrd	phospho:total	Stats	Normalize	STATS
1	PDTC - p-p65	112	92.366	79	118	10344.99	1475.488	982.4994451	2023.342	0.485582	1
2	PDTC - p-p65	112	112.589	80	162	12609.97	3740.464	2432.703055		1.202319	0.448867
3	PDTC - p-p65	112	116.321	81	181	13027.95	4158.448	2654.824953		1.312099	0.259154
4	PDTC - p-p65	112	106.438	82	147	11921.06	3051.552	2060.38116		1.018306	1.13497
5	PDTC - p-p65	112	109.152	83	161	12225.02	3355.52	2169.164905		1.07207	0.157814
6	PDTC - p-p65	112	117.107	83	164	13115.98	4246.48	2659.753933		1.314535	0.091114
7	PDTC - p-p65	112	102.83	81	142	11516.96	2647.456	1313.088599		0.64897	0.553641
8	PDTC - p-p65	112	89.5	80	104	10024	1154.496	595.235492		0.294184	0.392024
9	PDTC - p-p65	112	86.536	80	103	9692.032	822.528	414.5958411		0.204906	0.196012
10	PDTC - p-p65	112	119.33	82	175	13364.96	4495.456	2157.902016		1.066504	
11	PDTC - p-p65	112	95.723	79	119	10720.98	1851.472	965.641671		0.477251	0.509753
12	PDTC - p-p65	112	110.054	79	169	12326.05	3456.544	1732.600372		0.856306	0.400151
13	PDTC - p-p65	112	103.036	77	156	11540.03	2670.528	1510.141103		0.74636	0.200075
14	PDTC - p-p65	112	78.152	77	79	8753.024	-116.48	-82.76441281		-0.0409	
15	PDTC - p-p65	112	78.714	77	80	8815.968	8869.504				
16	PDTC - p-p65	112	79.67	78	82	8923.04					

Sr No	Title	Area	Intensity	Min	Max	Pixels	Pixel - Bckgrd
1	PDTC - t-p65	4320	124.737	68	187	538863.8	1.501769805
2	PDTC - t-p65	4320	127.711	83	199	551711.5	1.537575247
3	PDTC - t-p65	4320	130.103	83	193	562045	1.566373706
4	PDTC - t-p65	4320	123.017	83	193	531433.4	1.481061883
5	PDTC - t-p65	4320	128.487	83	198	555063.8	1.546917891
6	PDTC - t-p65	4320	132.611	82	203	572879.5	1.596568745
7	PDTC - t-p65	4320	167.466	86	215	723453.1	2.016205153
8	PDTC - t-p65	4320	161.1	70	214	695952	1.939561763
9	PDTC - t-p65	4320	164.785	86	223	711871.2	1.983927281
10	PDTC - t-p65	4320	173.035	90	215	747511.2	2.08325307
11	PDTC - t-p65	4320	159.255	85	215	687981.6	1.917348904
12	PDTC - t-p65	4320	165.705	86	215	715845.6	1.995003612
13	PDTC - t-p65	4320	146.883	85	209	634534.6	1.76839634
14	PDTC - t-p65	4320	116.896	80	175	504990.7	1.407368168
15	PDTC - t-p65	4320	83.149	76	90	359203.7	358819.2
16	PDTC - t-p65	4320	82.604	70	93	356849.3	
17	PDTC - t-p65	4320	83.427	77	92	360404.6	

Table D.26: Raw data for quantification of STAT-3 western blots by Image J for the gp130 fusion protein treated samples for Aim2

Sr. No	title	Area	Mean	min	Max		Pixels	Pixel - Bkgrd	phospho:total	Stats	B6 Normalized	STATS
1	p-STAT3_FP	153	80.085	76	80	100	12253.01	33.507	38.5706738	56.51494	0.682486343	1
2	p-STAT3_FP	153	80.307	76	80	100	12286.97	67.473	88.1275396	27.46067	1.559367165	0.485901
3	p-STAT3_FP	153	80.137	76	80	100	12260.96	41.463	42.8466025	15.85442	0.758146493	0.280535
4	p-STAT3_FP	153	85.307	78	97	100	13051.97	832.473	858.81899	2909.96	15.1963182	51.49011
5	p-STAT3_FP	153	93.085	81	124	100	14242.01	2022.507	4102.73122	1784.192	72.59551764	31.57027
6	p-STAT3_FP	153	98.693	80	135	100	15100.03	2880.531	3768.33092	1030.104	66.67849274	18.22711
7	p-STAT3_FP	153	180.046	89	212	100	27547.04	15327.54	17147.5846	17248.22	303.4168497	305.1975
8	p-STAT3_FP	153	175.229	91	213	100	26810.04	14590.539	13383.4459	2890.111	236.8125348	51.13888
9	p-STAT3_FP	153	185.111	92	214	100	28321.98	16102.485	18170.4042	1445.055	321.5150655	25.56944
10	p-STAT3_FP	153	176.451	95	214	100	26997	14777.505	20291.44		359.0456	
11	p-STAT3_FP	153	182.444	91	217	100	27913.93	15694.434	13098.7798	20277.71	231.7755291	358.8026
12	p-STAT3_FP	153	160.778	86	214	100	24599.03	12379.536	15066.788	13049.81	266.5983264	230.9091
13	p-STAT3_FP	153	161.641	86	213	100	24731.07	12511.575	39803.9481	6524.906	704.308437	115.4545
14	p-STAT3_FP	153	146.693	83	206	100	22444.03	10224.531	13141.3162		232.5281872	
15	p-STAT3_FP	153	80.085	78	83	100	12253.01	12219.498				
16	p-STAT3_FP	153	79.647	77	84	100	12185.99					
1	t-STAT3	0.017	149.09	90	211	0	2.53453	0.868717				
2	03-26-2014	0.017	143.026	94	212	0	2.431442	0.765629				
3	03-26-2014	0.017	154.913	97	210	0	2.633521	0.967708				
4	03-26-2014	0.017	155.008	89	210	0	2.635136	0.969323				
5	03-26-2014	0.017	126.987	94	173	0	2.158779	0.492966				
6	03-26-2014	0.017	142.954	94	201	0	2.430218	0.764405				
7	03-26-2014	0.017	150.569	98	212	0	2.559673	0.89386				
8	03-26-2014	0.017	162.118	98	214	0	2.756006	1.090193				
9	03-26-2014	0.017	150.118	98	204	0	2.552006	0.886193				
10	03-26-2014	0.017	140.828	97	206	0	2.394076	0.728263				
11	03-26-2014	0.017	168.469	100	213	0	2.863973	1.19816				
12	03-26-2014	0.017	146.321	96	209	0	2.487457	0.821644				
13	03-26-2014	0.017	116.479	94	169	0	1.980143	0.31433				
14	03-26-2014	0.017	97.518	89	106	0	1.657806	0.7780447				
15	03-26-2014	0.017	98.777	92	104	0	1.679209	1.665813				
16	03-26-2014	0.017	97.672	91	104	0	1.660424					

Table D.27: Raw data for quantification of mTOR western blots by Image J for the gp130 fusion protein treated samples for Aim2

Serial No	Title	Area	Intensity	Min	Max	Pixels	Pixels - Bckgrd	Average	Phospho: total	Average	B6 Normalized	Stats
1	p_mTOR_F	0.01	154.406	120	202	1.54	0.300	0.164273	0.395	0.189933	2.079	1
2	p_mTOR_F	0.01	135.91	120	193	1.36	0.115		0.098		0.518	0.936417
3	p_mTOR_F	0.01	132.188	119	181	1.32	0.078		0.076		0.402	0.540641
4	p_mTOR_F	0.01	152.269	120	193	1.52	0.279		0.170		0.897	0.399148
5	p_mTOR_F	0.01	132.705	120	171	1.33	0.083		0.042		0.222	0.436645
6	p_mTOR_F	0.01	127.205	117	157	1.27	0.028		0.015		0.079	0.252097
7	p_mTOR_F	0.01	143.291	117	194	1.43	0.189		0.103		0.544	
8	p_mTOR_F	0.01	156.389	123	199	1.56	0.320		0.165		0.871	0.750031
9	p_mTOR_F	0.01	150.927	116	199	1.51	0.265		0.129		0.679	0.169715
10	p_mTOR_F	0.01	158.103	120	199	1.58	0.337		0.172		0.906	0.084858
11	p_mTOR_F	0.01	147.269	121	196	1.47	0.229		0.123		0.648	
12	p_mTOR_F	0.01	163.791	122	199	1.64	0.394		0.220		1.160	1.251784
13	p_mTOR_F	0.01	171.098	121	198	1.71	0.467		0.243		1.280	0.522578
14	p_mTOR_F	0.01	157.603	120	190	1.58	0.332		0.364		1.919	0.261289
15	p_mTOR_F	0.01	123.654	118	128	1.24	1.244					
16	p_mTOR_F	0.01	124.568	121	128	1.25						
17	p_mTOR_F	0.01	125	120	138	1.25						

Serial No	Title	Area	Intensity	Min	Max	Pixels	Pixels - Bckgrd
1	tmTOR.tif	0.019	107.617	59	187	2.044723	0.759632667
2	tmTOR.tif	0.019	129.122	63	198	2.453318	1.168227667
3	tmTOR.tif	0.019	121.218	71	194	2.303142	1.018051667
4	tmTOR.tif	0.019	153.745	78	204	2.921155	1.636064667
5	tmTOR.tif	0.019	171.439	98	209	3.257341	1.972250667
6	tmTOR.tif	0.019	165.372	93	203	3.142068	1.856977667
7	tmTOR.tif	0.019	163.852	89	206	3.113188	1.828097667
8	tmTOR.tif	0.019	169.381	88	210	3.218239	1.933148667
9	tmTOR.tif	0.019	175.801	93	214	3.340219	2.055128667
10	tmTOR.tif	0.019	170.716	90	212	3.243604	1.958513667
11	tmTOR.tif	0.019	165.451	93	210	3.143569	1.858478667
12	tmTOR.tif	0.019	161.707	94	214	3.072433	1.787342667
13	tmTOR.tif	0.019	168.684	95	215	3.204996	1.919905667
14	tmTOR.tif	0.019	115.573	66	203	2.195887	0.910796667
15	tmTOR.tif	0.019	68.119	59	81	1.294261	1.285090333
16	tmTOR.tif	0.019	66.647	58	75	1.266293	
17	tmTOR.tif	0.019	68.143	59	78	1.294717	

Table D.28: Raw data for quantification of S6 western blots by Image J for the gp130 fusion protein treated samples for Aim2

Serial No	Title	Area	Intensity	Min	Max	Pixels	Pixels - Bckgrd	nospho: tot	Average	B6 Normalized
18	p-S6_FP	0.029	128.4	62	197	3.724	1.963	1.228	0.928	1.323
19	fusion prot	0.029	111.883	69	181	3.245	1.484	0.568		0.612
20	fusion prot	0.029	137.214	71	200	3.979	2.218	0.988		1.065
21	fusion prot	0.029	173.474	88	205	5.031	3.270	1.177		1.268
22	fusion prot	0.029	179.424	95	205	5.203	3.442	1.204		1.297
23	fusion prot	0.029	190.517	115	207	5.525	3.764	1.334		1.438
24	fusion prot	0.029	153.655	79	199	4.456	2.695	0.816		0.880
25	fusion prot	0.029	113.785	72	183	3.300	1.539	0.529		0.570
26	fusion prot	0.029	82.827	65	120	2.402	0.641	0.211		0.227
27	fusion prot	0.029	100.183	68	164	2.905	1.144	0.363		0.391
28	fusion prot	0.029	93.889	70	140	2.723	0.962	0.295		0.317
29	fusion prot	0.029	139.809	75	194	4.054	2.293	0.642		0.692
30	fusion prot	0.029	147.912	78	190	4.289	2.528	0.769		0.829
31	fusion prot	0.029	75.709	55	106	2.196	0.435	0.195		0.210
32	fusion prot	0.029	57.674	51	68	1.673	1.761			
33	fusion prot	0.029	63.774	57	82	1.849				

Serial No	Title	Area	Intensity	Min	Max	Pixels	Pixels - Bckgrd
34	t-S6	0.035	131.326	82	207	4.596	1.599
35	fusion prot	0.035	160.243	90	220	5.609	2.611
36	fusion prot	0.035	149.78	89	211	5.242	2.245
37	fusion prot	0.035	165.05	89	212	5.777	2.779
38	fusion prot	0.035	167.362	91	214	5.858	2.860
39	fusion prot	0.035	166.246	92	215	5.819	2.821
40	fusion prot	0.035	179.964	91	214	6.299	3.301
41	fusion prot	0.035	168.781	91	212	5.907	2.910
42	fusion prot	0.035	172.553	94	214	6.039	3.042
43	fusion prot	0.035	175.839	96	214	6.154	3.157
44	fusion prot	0.035	178.914	99	215	6.262	3.264
45	fusion prot	0.035	187.678	100	212	6.569	3.571
46	fusion prot	0.035	179.555	97	209	6.284	3.287
47	fusion prot	0.035	149.399	81	197	5.229	2.231
48	fusion prot	0.035	84.256	75	114	2.949	2.998
49	fusion prot	0.035	85.7	77	93	3.000	
50	fusion prot	0.035	86.99	79	98	3.045	

Table D.29: Raw data for quantification of Akt western blots by Image J for the gp130 fusion protein treated samples for Aim2

Serial No	Title	Area	Intensity	Min	Max	Pixels	Pixels - Bckgrd	nospho: tot	Average	B6 Normalized
1	fusion prot	0.023	114.527	59	190	2.634121	1.246945	0.423921	0.584959	0.724702192
2	fusion prot	0.023	156.276	88	198	3.594348	3.594348	0.670316		1.145919288
3	fusion prot	0.023	149.151	85	197	3.430473	3.430473	0.66064		1.12937852
4	fusion prot	0.023	153.363	89	197	3.527349	3.527349	0.57799		0.988085582
5	fusion prot	0.023	144.347	88	193	3.319981	3.319981	0.540666		0.924279771
6	fusion prot	0.023	142.941	81	192	3.287643	3.287643	0.533376		0.911817349
7	fusion prot	0.023	100.931	69	145	2.321413	2.321413	0.37161		0.635275847
8	fusion prot	0.023	70.027	60	80	1.610621	1.610621	0.257179		0.439653288
9	fusion prot	0.023	66.031	60	72	1.518713	1.518713	0.238269		0.407325448
10	fusion prot	0.023	68.943	58	79	1.585689	1.585689	0.245719		0.420062658
11	fusion prot	0.023	67.588	60	76	1.554524	1.554524	0.247107		0.422435001
12	fusion prot	0.023	154.912	84	183	3.562976	3.562976	0.558663		0.955046958
13	fusion prot	0.023	102.625	70	149	2.360375	2.360375	0.366114		0.625878948
14	fusion prot	0.023	72.065	54	96	1.657495	1.657495	0.323628		0.553249532
15	fusion prot	0.023	56.973	48	66	1.310379	1.387176	0.43951		
16	fusion prot	0.023	63.651	57	70	1.463973				

Serial No	Title	Area	Intensity	Min	Max	Pixels	Pixels - Bckgrd
1	t-Akt_02-0	0.033	184.777	116	212	6.10	2.94
2	t-Akt_02-0	0.033	162.49	102	209	5.36	5.36
3	t-Akt_02-0	0.033	157.353	101	207	5.19	5.19
4	t-Akt_02-0	0.033	184.933	120	208	6.10	6.10
5	t-Akt_02-0	0.033	186.077	132	204	6.14	6.14
6	t-Akt_02-0	0.033	186.783	118	206	6.16	6.16
7	t-Akt_02-0	0.033	189.3	116	207	6.25	6.25
8	t-Akt_02-0	0.033	189.777	144	209	6.26	6.26
9	t-Akt_02-0	0.033	193.15	129	206	6.37	6.37
10	t-Akt_02-0	0.033	195.553	149	207	6.45	6.45
11	t-Akt_02-0	0.033	190.633	114	210	6.29	6.29
12	t-Akt_02-0	0.033	193.263	113	210	6.38	6.38
13	t-Akt_02-0	0.033	195.367	145	215	6.45	6.45
14	t-Akt_02-0	0.033	155.2	89	211	5.12	5.12
15	t-Akt_02-0	0.033	95.277	89	103	3.14	3.16
16	t-Akt_02-0	0.033	96.007	91	102	3.17	

Table D.30: Raw data for quantification of p-65 western blots by Image J for the gp130 fusion protein treated samples for Aim2

Sr.No	Blot	Area	Intensity	Min	Max	Pixel	Pixel - Bckgrd	Normalized to t-p65	Average	Normalized to B6	Statistics
1	p-p65	0.013	115.212	84	199	1.498	0.274	1.275	2.475	0.515	1.000
2	p-p65	0.013	162.896	98	212	2.118	0.894	3.591		1.451	0.469
3	p-p65	0.013	156.084	95	209	2.029	0.805	2.560		1.034	0.271
4	p-p65	0.013	121.879	91	201	1.584	0.361	0.486	0.250	0.196	0.101
5	p-p65	0.013	104.512	85	177	1.359	0.135	0.154		0.062	0.083
6	p-p65	0.013	102.451	86	141	1.332	0.108	0.110		0.045	0.048
7	p-p65	0.013	99.582	85	141	1.295	0.071	0.072	0.179	0.029	0.072
8	p-p65	0.013	97.343	88	135	1.265	0.042	0.093		0.037	0.090
9	p-p65	0.013	94.939	87	108	1.234	0.010	0.041		0.016	0.045
10	p-p65	0.013	108.357	91	175	1.409	0.185	0.510		0.206	
11	p-p65	0.013	112.556	90	176	1.463	0.239	0.442	1.500	0.178	0.606
12	p-p65	0.013	127.03	92	203	1.651	0.428	1.758		0.710	0.513
13	p-p65	0.013	112.993	90	183	1.469	0.245	0.610		0.246	0.256
14	p-p65	0.013	103.364	91	163	1.344	0.120	3.189		1.288	
15	p-p65	0.013	94.902	89	104	1.234	1.224	0.665			
16	p-p65	0.013	93.875	89	101	1.220					
17	p-p65	0.013	93.633	86	101	1.217					

Sr.No	Blot	Area	Intensity	Min	Max	Pixel	Pixel - Bckgrd
1	t-p65	0.016	128.505	111	193	2.05608	0.214832
2	t-p65	0.016	130.637	109	196	2.090192	0.248944
3	t-p65	0.016	134.739	114	179	2.155824	0.314576
4	t-p65	0.016	161.503	123	205	2.584048	0.7428
5	t-p65	0.016	169.951	122	206	2.719216	0.877968
6	t-p65	0.016	176.349	131	210	2.821584	0.980336
7	t-p65	0.016	176.566	125	209	2.825056	0.983808
8	t-p65	0.016	143.234	113	191	2.291744	0.450496
9	t-p65	0.016	131.162	115	172	2.098592	0.257344
10	t-p65	0.016	137.755	115	182	2.20408	0.362832
11	t-p65	0.016	148.962	116	211	2.383392	0.542144
12	t-p65	0.016	130.28	110	186	2.08448	0.243232
13	t-p65	0.016	140.19	112	208	2.24304	0.401792
14	t-p65	0.016	117.429	110	136	1.878864	0.037616
15	t-p65	0.016	114.753	110	120	1.836048	1.841248
16	t-p65	0.016	114.753	110	120	1.836048	
17	t-p65	0.016	115.728	107	123	1.851648	

Table D.31: Raw data for quantification of MMP-2 western blots by Image J for the gp130 fusion protein treated samples for Aim2

Serial No	Title	Area	Intensity	Min	Max	Pixels	Pixels - Bckgrd	Average	B6 Normalized	Stats
1	MMP2_fus	0.023	117.19	63	190	2.69537	1.220694333	1.764146	0.69194632	1
2	MMP2_fus	0.023	155.571	84	200	3.578133	2.103457333		1.192337444	0.269519
3	MMP2_fus	0.023	149.694	84	198	3.442962	1.968286333		1.115716235	0.155607
4	MMP2_fus	0.023	153.469	89	200	3.529787	2.055111333		1.164932683	1.078303
5	MMP2_fus	0.023	144.092	81	195	3.314116	1.839440333		1.04268033	0.075417
6	MMP2_fus	0.023	142.912	82	194	3.286976	1.812300333		1.027296116	0.043542
7	MMP2_fus	0.023	102.202	71	144	2.350646	0.875970333		0.496540725	0.168717
8	MMP2_fus	0.023	70.269	60	80	1.616187	0.141511333		0.080215205	0.219882
9	MMP2_fus	0.023	66.076	58	76	1.519748	0.045072333		0.025549095	0.109941
10	MMP2_fus	0.023	69.682	59	79	1.602686	0.128010333		0.07256221	
11	MMP2_fus	0.023	69.945	58	93	1.608735	0.134059333		0.075991065	0.455121
12	MMP2_fus	0.023	153.971	73	183	3.541333	2.066657333		1.171477493	0.521388
13	MMP2_fus	0.023	103.394	71	148	2.378062	0.903386333		0.512081389	0.260694
14	MMP2_fus	0.023	68.79	51	95	1.58217	0.107494333		0.060932787	
15	MMP2_fus	0.023	61.894	51	76	1.423562	1.474675667			
16	MMP2_fus	0.023	64.296	57	72	1.478808				
17	MMP2_fus	0.023	66.159	60	71	1.521657				

RAW DATA FOR AIM 3:

Table D.32: Real time PCR data for the gene Haptaglobin for samples treated with the Antibiotics

	Haptaglobin	GAPDH				
Treatment	Ct	Ct	Dct	DDct	old change	Normalized
105	16.67	22.545	-5.875	0.092	0.938	0.931
106	16.955	23.01	-6.055	-0.088	1.063	1.055
108	16.47	22.38	-5.91	0.057	0.961	0.954
989	16.365	22.62	-6.255	-0.288	1.221	1.212
992	16.655	22.395	-5.74	0.227	0.854	0.848
435	14.275	22.825	-8.55	-2.583	5.992	5.947
436	12.965	22.43	-9.465	-3.498	11.298	11.213
438	22.875	23.035	-0.16	5.807	0.018	0.018
694	20.98	27.655	-6.675	-0.708	1.634	1.621
417	14.23	22.805	-8.575	-2.608	6.097	6.051
506	18.26	28.71	-10.45	-4.483	22.362	22.195
515	14.44	22.715	-8.275	-2.308	4.952	4.915
522	14.975	22.62	-7.645	-1.678	3.200	3.176
696	16.955	23.15	-6.195	-0.228	1.171	1.162
702	15.255	22.675	-7.42	-1.453	2.738	2.717
705	14.74	22.93	-8.19	-2.223	4.669	4.634
826	22.975	27.045	-4.07	1.897	0.269	0.266
827	15.19	22.855	-7.665	-1.698	3.245	3.220
832	15.065	22.62	-7.555	-1.588	3.006	2.984
833	14.625	22.77	-8.145	-2.178	4.525	4.491

	Dct	*DDct*	*old change*	*Norm*	
C57BL/6	-5.967	1.78E-16	1.007547	1.000	
(n=6)	0.19617	0.19617	0.140537	0.139484	
	0.08773	0.08773	0.06285	0.062379	
Apc Min	-6.2125	-0.2455	4.73532	4.700	
(n=6)	4.198783	4.198783	5.05053	5.0127	
	2.099391	2.099391	2.525265	2.50635	0.03511
Apc Min	-8.736	-2.769	9.153	9.084	
(n=4)	1.206444	1.206444	8.886647	8.820084	
Polymyxin	0.603222	0.603222	4.443324	4.410042	0.36089
Apc Min	-7.03429	-1.06729	2.803172	2.782175	
(n=7)	1.465064	1.465064	1.621404	1.609259	
Nor/Amp	0.553742	0.553742	0.612833	0.608243	0.10273
					0.07533
					0.42062

Table D.33: Real time PCR data for the gene PEPCK for samples treated with the Antibiotics

Treatment	PEPCK Ct	GAPDH Ct	Dct	DDct	fold change	Normalized
105	18.82	23.5	-4.68	0.734	0.601	0.564
106	18.39	23.95	-5.56	-0.146	1.107	1.037
108	18.35	23.63	-5.28	0.134	0.911	0.854
989	17.755	23.89	-6.135	-0.721	1.649	1.545
992						
435	19	23.44	-4.44	0.974	0.509	0.477
436	18.05	23.025	-4.975	0.439	0.738	0.691
438	26.32	24.515	1.805	7.219	0.007	0.006
694	24.84	28.755	-3.915	1.499	0.354	0.332
417	19.475	24.66	-5.185	0.229	0.853	0.800
506	20.915	29.2	-8.285	-2.871	7.317	6.857
515	18.67	23.305	-4.635	0.779	0.583	0.546
696						
702	17.915	23.255	-5.34	0.074	0.950	0.890
705	19.3	23.515	-4.215	1.199	0.436	0.408
826	18.37	23.565	-5.195	0.219	0.859	0.805

	Dct	*DDct*	*old change*	*Norm*	
C57BL/6	-5.41375	0	1.067024	1	
(n=6)	0.604943	0.604943	0.44003	0.41239	
	0.302472	0.302472	0.220015	0.206195	0.047850725
Apc Min	-2.88125	2.533	0.401882	0.376638	
(n=4)	3.153996	3.153996	0.307029	0.287743	
	1.576998	1.576998	0.153515	0.143872	0.325187831
Apc Min	-6.035	-0.621	2.918	2.734	
(n=4)	1.967867	1.967867	3.812257	3.572793	
Poly	0.983933	0.983933	1.906128	1.786397	0.184063746
Apc Min	-4.91667	0.497083	0.748376	0.701367	
(n=4)	0.611971	0.611971	0.27461	0.25736	
Nor/Amp	0.231303	0.231303	0.103793	0.097273	0.381227523

Table D.34: Real time PCR data for the gene PFK for samples treated with the Antibiotics

Treatment	PFK Ct	GAPDH Ct	Dct	DDct	fold change	Normalized
105	28.97	23.5	5.47	0.169	0.890	0.836
106	29.415	23.95	5.465	0.164	0.893	0.839
108	29.41	23.63	5.78	0.479	0.718	0.675
989	28.38	23.89	4.49	-0.811	1.755	1.650
435	26.38	23.44	2.94	-2.361	5.138	4.831
436	25.92	23.025	2.895	-2.406	5.301	4.984
438	29.285	24.515	4.77	-0.531	1.445	1.359
694	33.32	28.755	4.565	-0.736	1.666	1.566
417	25.76	24.66	1.1	-4.201	18.395	17.294
506	31.18	29.2	1.98	-3.321	9.995	9.397
515	26.44	23.305	3.135	-2.166	4.489	4.220
522						
696						
702	28.275	23.255	5.02	-0.281	1.215	1.143
705	28.71	23.515	5.195	-0.106	1.076	1.012
833	27.035	23.565	3.47	-1.831	3.558	3.345

	Dct	*DDct*	*old change*	*Norm*
C57BL/6	5.30125	0.000	1.064	1
(n=6)	0.560541	0.560541	0.467923	0.439918
	0.280271	0.280271	0.233962	0.219959
Apc Min	3.7925	-1.509	3.38753	3.185
(n=4)	1.01399	1.01399	2.118394	1.991606
	0.506995	0.506995	1.059197	0.995803
Apc Min	2.072	-3.230	10.960	10.304
(n=3)	1.020592	1.020592	7.003252	6.5841
Poly	0.510296	0.510296	3.501626	3.29205
Apc Min	4.561667	-0.73958	1.950042	1.83333
(n=3)	0.949452	0.949452	1.394653	1.311181
Nor/Amp	0.358859	0.358859	0.527129	0.49558

Table D.35: Raw data for quantification of STAT-3 western blots by Image J for for samples treated with the Antibiotics

Sr. No	Title	Area	Intensity	Min	Max	Pixels	Pixel - Bgkgrd	hospho:tot	Average	Normalize	STATS
1	p-STAT3-Poly	0.028	112.942	106	128	3.16	0.02	0.02	0.23	0.067578	1
2	03-28-2014 1	0.028	112.331	104	118	3.15	0.00	0.00		-0.00574	1.935644
3	03-28-2014 1	0.028	112.642	105	120	3.15	0.01	0.01		0.035044	
4	03-28-2014 1	0.028	135.104	110	192	3.78	0.64	0.89		3.903117	
5	03-28-2014 1	0.028	117.585	108	166	3.29	0.15	0.27		1.164279	2.311777
6	03-28-2014 1	0.028	133.773	108	194	3.75	0.60	0.80		3.489762	1.163041
7	03-28-2014 1	0.028	126.042	110	183	3.53	0.38	0.52		2.281292	
8	03-28-2014 1	0.028	164.923	109	212	4.62	1.47	1.90		8.318976	5.533622
9	03-28-2014 1	0.028	161.462	111	213	4.52	1.37	1.55		6.805359	2.731743
10	03-28-2014 1	0.028	159.119	113	208	4.46	1.31	1.29		5.649127	
11	03-28-2014 1	0.028	166.081	116	209	4.65	1.50	1.34		5.871738	
12	03-28-2014 1	0.028	129.715	108	181	3.63	0.49	0.23		1.022912	
13	03-28-2014 1	0.028	110.612	106	115	3.10	3.15	2.08			
14	03-28-2014 1	0.028	112.119	107	117	3.14					
15	03-28-2014 1	0.028	114.404	108	123	3.20					

Sr. No	Title	Area	Intensity	Min	Max	Pixels	Pixel - Bgkgrd
1	t-STAT3 - Poly	0.013	195.125	129	215	2.54	1.02
2	t-STAT3 - Poly	0.013	194.256	122	220	2.53	1.01
3	t-STAT3 - Poly	0.013	187.414	124	216	2.44	0.92
4	t-STAT3 - Poly	0.013	171.357	115	213	2.23	0.71
5	t-STAT3 - Poly	0.013	158.613	114	214	2.06	0.55
6	t-STAT3 - Poly	0.013	174.266	122	215	2.27	0.75
7	t-STAT3 - Poly	0.013	172.933	116	217	2.25	0.73
8	t-STAT3 - Poly	0.013	176.017	120	215	2.29	0.77
9	t-STAT3 - Poly	0.013	184.475	121	217	2.40	0.88
10	t-STAT3 - Poly	0.013	194.492	138	225	2.53	1.02
11	t-STAT3 - Poly	0.013	202.721	136	216	2.64	1.12
12	t-STAT3 - Poly	0.013	192.195	119	213	2.50	0.99
13	t-STAT3 - Poly	0.013	113.502	107	133	1.48	1.51
14	t-STAT3 - Poly	0.013	120.114	111	138	1.56	
15	t-STAT3 - Poly	0.013	115.616	110	123	1.50	

Table D.36: Raw data for quantification of p-65 western blots by Image J for for samples treated with the Antibiotics

Sr. No	Title	Area	Intensity	Min	Max	Pixels	Pixel - Bgkgrd	hospho:tota	Average	B6 Normalized	STATS
1	nor_Amp -	7380	113.836	78	215	840109.68	224942.40	219823.52	488974.11	0.449560647	1
2	p-NFkB Blo	7380	150.643	72	231	1111745.34	496578.06	490694.95		1.0035193	0.395294
3	p-NFkB Blo	7380	155.731	80	225	1149294.78	534127.50	578659.18		1.18341477	
4	p-NFkB Blo	7380	147.887	80	221	1091406.06	476238.78	666718.78		1.363505283	
5	p-NFkB Blo	7380	83.962	76	100	619639.56	4472.28	8151.72		0.016671064	0.570698
6	p-NFkB Blo	7380	133.825	78	219	987628.50	372461.22	495215.59		1.012764444	0.507397
7	p-NFkB Blo	7380	116.591	78	216	860441.58	245274.30	333801.75		0.682657314	
8	p-NFkB Blo	7380	127.761	38	216	942876.18	327708.90	422914.40		0.864901427	0.490562
9	p-NFkB Blo	7380	98.473	77	170	726730.74	111563.46	126083.72		0.257853579	0.283625
10	p-NFkB Blo	7380	118.999	79	214	878212.62	263045.34	259143.33		0.529973527	
11	p-NFkB Blo	7380	95.697	78	172	706243.86	91076.58	81170.94		0.166002529	
12	p-NFkB Blo	7380	124.746	79	215	920625.48	305458.20	310048.05		0.634078661	
13	p-NFkB Blo	7380	82.769	74	100	610835.22	615167.28	406496.77			
14	p-NFkB Blo	7380	83.774	67	117	618252.12					
15	p-NFkB Blo	7380	83.525	77	94	616414.50					

Sr. No	Title	Area	Intensity	Min	Max	Pixels	Pixel - Bgkgrd
1	nor_Amp0	0.013	195.125	129	215	2.536625	1.02
2	nor_Amp0	0.013	194.256	122	220	2.525328	1.01
3	nor_Amp0	0.013	187.414	124	216	2.436382	0.92
4	nor_Amp0	0.013	171.357	115	213	2.227641	0.71
5	nor_Amp0	0.013	158.613	114	214	2.061969	0.55
6	nor_Amp0	0.013	174.266	122	215	2.265458	0.75
7	nor_Amp0	0.013	172.933	116	217	2.248129	0.73
8	nor_Amp0	0.013	176.017	120	215	2.288221	0.77
9	nor_Amp0	0.013	184.475	121	217	2.398175	0.88
10	nor_Amp0	0.013	194.492	138	225	2.528396	1.02
11	nor_Amp0	0.013	202.721	136	216	2.635373	1.12
12	nor_Amp0	0.013	192.195	119	213	2.498535	0.99
13	nor_Amp0	0.013	113.502	107	133	1.475526	1.51
14	nor_Amp0	0.013	120.114	111	138	1.561482	
15	nor_Amp0	0.013	115.616	110	123	1.503008	

Table D.37: Raw data for quantification of STAT-3 western blots by Image J for for samples treated with the Antibiotics

Sr. No	Title	Area	Mean	Min	Max	Pixels	Pixel - Bgkgrd	otal:GAPDH	Average	Normalize	STATS
1	03-13-2014	0.053	174.742	109	223	9.261326	3.397052667	3.319748	4.146323	0.800649	1
2	03-13-2014	0.053	193.513	130	224	10.25619	4.391915667	4.339883		1.046682	0.140721
3	03-13-2014	0.053	184.471	125	219	9.776963	3.912689667	4.238901		1.022328	0.070361
4	03-13-2014	0.053	173.812	115	217	9.212036	3.347762667	4.686759		1.130341	
5	03-13-2014	0.053	117.46	108	144	6.22538	0.361106667	0.658197		0.158742	0.104871
6	03-13-2014	0.053	112.233	104	121	5.948349	0.084075667	0.111785		0.02696	0.069102
7	03-13-2014	0.053	118.057	104	134	6.257021	0.392747667	0.534503		0.12891	0.039896
8	03-13-2014	0.053	119.403	103	142	6.328359	0.464085667	0.598911		0.144444	0.013729
9	03-13-2014	0.053	109.423	98	132	5.799419	-0.064854333	-0.0733		-0.01768	0.094495
10	03-13-2014	0.053	111.096	97	153	5.888088	0.023814667	0.023461		0.005658	0.042259
11	03-13-2014	0.053	115.037	97	185	6.096961	0.232687667	0.20738		0.050015	
12	03-13-2014	0.053	101.876	94	116	5.399428	-0.464845333	-0.47183		-0.11379	
13	03-13-2014	0.053	103.722	91	112	5.497266	5.864273333	3.875057		0.934577	
14	03-13-2014	0.053	115.233	108	124	6.107349					
15	03-13-2014	0.053	112.985	104	125	5.988205					
Sr. No	Title	Area	Mean	Min	Max	Pixels	Pixel - Bgkgrd				
1	nor_Amp0	0.013	195.125	129	215	2.536625	1.023286333				
2	nor_Amp0	0.013	194.256	122	220	2.525328	1.011989333				
3	nor_Amp0	0.013	187.414	124	216	2.436382	0.923043333				
4	nor_Amp0	0.013	171.357	115	213	2.227641	0.714302333				
5	nor_Amp0	0.013	158.613	114	214	2.061969	0.548630333				
6	nor_Amp0	0.013	174.266	122	215	2.265458	0.752119333				
7	nor_Amp0	0.013	172.933	116	217	2.248129	0.734790333				
8	nor_Amp0	0.013	176.017	120	215	2.288221	0.774882333				
9	nor_Amp0	0.013	184.475	121	217	2.398175	0.884836333				
10	nor_Amp0	0.013	194.492	138	225	2.528396	1.015057333				
11	nor_Amp0	0.013	202.721	136	216	2.635373	1.122034333				
12	nor_Amp0	0.013	192.195	119	213	2.498535	0.985196333				
13	nor_Amp0	0.013	113.502	107	133	1.475526	1.513338667				
14	nor_Amp0	0.013	120.114	111	138	1.561482					
15	nor_Amp0	0.013	115.616	110	123	1.503008					

Table D.38: Raw data for quantification of Akt western blots by Image J for for samples treated with the Antibiotics in Aim 3

Sr. No	Title	Area	Mean	Min	Max	Pixels	Pixel - Bgkgrd	otal:GAPDH	Average	5 Normalize	STATS
1	p-AKT -Nor	0.025	130.065	108	210	3.251625	0.3548	0.346726	1.121776	0.309087	1
2	nor_Amp0	0.025	169.382	114	216	4.23455	1.337725	1.321877		1.178378	0.462082
3	nor_Amp0	0.025	168.072	119	215	4.2018	1.304975	1.413774		1.2603	0.231041
4	nor_Amp0	0.025	156.009	116	212	3.900225	1.0034	1.404727		1.252235	
5	nor_Amp0	0.025	120.581	111	133	3.014525	0.1177	0.214534		0.191245	0.110068
6	nor_Amp0	0.025	118.54	112	127	2.9635	0.066675	0.088649		0.079026	0.070947
7	nor_Amp0	0.025	117.849	110	136	2.946225	0.0494	0.06723		0.059932	0.040961
8	nor_Amp0	0.025	116.681	107	129	2.917025	0.0202	0.026068		0.023239	0.061541
9	nor_Amp0	0.025	117.779	108	133	2.944475	0.04765	0.053852		0.048006	0.027826
10	nor_Amp0	0.025	118.704	111	137	2.9676	0.070775	0.069725		0.062156	0.012444
11	nor_Amp0	0.025	120.674	111	141	3.01685	0.120025	0.106971		0.095358	
12	nor_Amp0	0.025	119.363	108	138	2.984075	0.08725	0.088561		0.078947	
13	nor_Amp0	0.025	115.94	110	125	2.8985	2.896825	1.914195			
14	nor_Amp0	0.025	115.391	108	122	2.884775					
15	nor_Amp0	0.025	116.288	110	124	2.9072					
Sr. No	Title	Area	Mean	Min	Max	Pixels	Pixel - Bgkgrd				
1	nor_Amp0	0.013	195.125	129	215	2.536625	1.023286333				
2	nor_Amp0	0.013	194.256	122	220	2.525328	1.011989333				
3	nor_Amp0	0.013	187.414	124	216	2.436382	0.923043333				
4	nor_Amp0	0.013	171.357	115	213	2.227641	0.714302333				
5	nor_Amp0	0.013	158.613	114	214	2.061969	0.548630333				
6	nor_Amp0	0.013	174.266	122	215	2.265458	0.752119333				
7	nor_Amp0	0.013	172.933	116	217	2.248129	0.734790333				
8	nor_Amp0	0.013	176.017	120	215	2.288221	0.774882333				
9	nor_Amp0	0.013	184.475	121	217	2.398175	0.884836333				
10	nor_Amp0	0.013	194.492	138	225	2.528396	1.015057333				
11	nor_Amp0	0.013	202.721	136	216	2.635373	1.122034333				
12	nor_Amp0	0.013	192.195	119	213	2.498535	0.985196333				
13	nor_Amp0	0.013	113.502	107	133	1.475526	1.513338667				
14	nor_Amp0	0.013	120.114	111	138	1.561482					
15	nor_Amp0	0.013	115.616	110	123	1.503008					

Table D.39: Raw data for quantification of mTOR western blots by Image J for for samples treated with the Antibiotics in Aim 3

mTOR											
Sr. No	Title	Area	Mean	Min	Max	Pixels	ixel - Bgkgr	otal:GAPDH	Average	B6 Normalized	STATS
1	p-mTOR	0.026	127.998	115	166	3.327948	0.145349	0.267841	0.170099	1.574617564	1
2	Nor_Amp0	0.026	128.339	119	178	3.336814	0.154215	0.187445		1.101973541	0.441891
3	Nor_Amp0	0.026	126.894	118	168	3.299244	0.116645	0.097184		0.571338729	0.220946
4	Nor_Amp0	0.026	126.528	115	137	3.289728	0.107129	0.127927		0.752070166	
5	Nor_Amp0	0.026	166.92	124	210	4.33992	1.157321	1.174974		6.907582372	5.741512
6	Nor_Amp0	0.026	144.821	118	195	3.765346	0.582747	0.522379		3.071027282	2.318887
7	Nor_Amp0	0.026	154.715	122	212	4.02259	0.839991	1.232527		7.24592774	1.33881
8	Nor_Amp0	0.026	131.939	118	180	3.430414	0.247815	0.374982		2.204488364	3.734892
9	Nor_Amp0	0.026	149.609	117	202	3.889834	0.707235	0.784825		4.613927419	3.215765
10	Nor_Amp0	0.026	172.266	125	208	4.478916	1.296317	1.452843		8.54114832	1.438134
11	Nor_Amp0	0.026	154.306	119	209	4.011956	0.829357	0.589008		3.462733179	
12	Nor_Amp0	0.026	120.958	114	129	3.144908	-0.03769	-0.02515		-0.147835761	
13	Nor_Amp0	0.026	120.583	91	133	3.135158	3.182599	2.445803			
14	Nor_Amp0	0.026	122.859	114	133	3.194334					
15	Nor_Amp0	0.026	123.781	118	133	3.218306					
Sr. No	Title	Area	Mean	Min	Max	Pixels	ixel - Bgkgr				
1	Nor_Amp0	0.029	129.558	106	211	3.757182	0.542667				
2	Nor_Amp0	0.029	139.215	106	213	4.037235	0.82272				
3	Nor_Amp0	0.029	152.233	107	218	4.414757	1.200242				
4	Nor_Amp0	0.029	139.722	105	210	4.051938	0.837423				
5	Nor_Amp0	0.029	144.81	108	215	4.19949	0.984975				
6	Nor_Amp0	0.029	149.313	108	211	4.330077	1.115562				
7	Nor_Amp0	0.029	134.346	105	213	3.896034	0.681519				
8	Nor_Amp0	0.029	133.634	107	210	3.875386	0.660871				
9	Nor_Amp0	0.029	141.919	106	210	4.115651	0.901136				
10	Nor_Amp0	0.029	141.613	108	212	4.106777	0.892262				
11	Nor_Amp0	0.029	159.399	109	211	4.622571	1.408056				
12	Nor_Amp0	0.029	162.53	110	213	4.71337	1.498855				
13	Nor_Amp0	0.029	155.716	111	213	4.515764	1.301249				
14	Nor_Amp0	0.029	111.719	104	118	3.239851	3.214515				
15	Nor_Amp0	0.029	111.252	106	119	3.226308					
16	Nor_Amp0	0.029	109.565	101	117	3.177385					

Table D.40: Raw data for quantification of S6 western blots by Image J for for samples treated with the Antibiotics in Aim 3

S6											
Sr. No	Title	Area	Mean	Min	Max	Pixels	ixel - Bgkgr	otal:GAPDH	Average	6 Normalize	STATS
1	p-S6 Nor/a	0.032	110.701	85	136	3.542432	0.582603	1.821726	1.109793	1.6415	1
2	02-22-201	0.032	102.785	85	136	3.28912	0.329291	0.438562		0.395174	0.634949
3	02-22-201	0.032	100.684	85	136	3.221888	0.262059	0.573973		0.517189	0.317475
4	02-22-201	0.032	113.233	85	136	3.623456	0.663627	1.604913		1.446137	
5	02-22-201	0.032	122.152	85	153	3.908864	0.949035	1.651158		1.487807	0.996238
6	02-22-201	0.032	112.666	85	136	3.605312	0.645483	1.114154		1.003929	0.495459
7	02-22-201	0.032	96.28	85	119	3.08096	0.121131	0.551544		0.496979	0.286053
8	02-22-201	0.032	96.345	85	119	3.08304	0.123211	0.225549		0.203236	0.172685
9	02-22-201	0.032	94.751	85	119	3.032032	0.072203	0.091755		0.082678	0.063508
10	02-22-201	0.032	98.736	85	136	3.159552	0.199723	0.282345		0.254413	0.028402
11	02-22-201	0.032	95.064	85	119	3.042048	0.082219	0.189544		0.170792	
12	02-22-201	0.032	93.535	85	119	2.99312	0.033291	0.169028		0.152305	
13	02-22-201	0.032	91.635	85	102	2.93232	2.959829	13.22415			
14	02-22-201	0.032	93.671	85	102	2.997472					
15	02-22-201	0.032	92.178	85	102	2.949696					
1	t-S6 Nor/A	0.019	127.871	102	205	2.429549	0.319808				
2	nor_Amp0	0.019	150.557	107	209	2.860583	0.750842				
3	nor_Amp0	0.019	135.069	104	204	2.566311	0.45657				
4	nor_Amp0	0.019	132.802	103	204	2.523238	0.413497				
5	nor_Amp0	0.019	141.29	106	211	2.68451	0.574769				
6	nor_Amp0	0.019	141.531	105	203	2.689089	0.579348				
7	nor_Amp0	0.019	122.598	106	182	2.329362	0.219621				
8	nor_Amp0	0.019	139.79	106	196	2.65601	0.546269				
9	nor_Amp0	0.019	152.455	112	203	2.896645	0.786904				
10	nor_Amp0	0.019	148.269	107	208	2.817111	0.70737				
11	nor_Amp0	0.019	133.869	106	191	2.543511	0.43377				
12	nor_Amp0	0.019	121.405	108	177	2.306695	0.196954				
13	nor_Amp0	0.019	122.819	108	185	2.333561	0.22382				
14	nor_Amp0	0.019	110.138	103	117	2.092622	2.109741				
15	nor_Amp0	0.019	111.94	105	121	2.12686					